Elucidating the Specificity of Membrane Interactions of Synaptotagmin-1 in Synchronous Neurotransmitter Release

Sarah Bentley Nyenhuis
Reston, Virginia

Bachelor of Science in Chemistry, University of Virginia, 2013

A Dissertation presented to the Graduate Faculty of the University of Virginia in Candidacy for the Degree of Doctor of Philosophy

Department of Chemistry

University of Virginia
July, 2018

Abstract

Neurotransmission involves Ca^{2+} dependent fusion of a neurotransmitter containing vesicle to the presynaptic plasma membrane to release the vesicle contents into the synaptic cleft. Soluble N-ethylmaleimide sensitive factor attachment protein receptors drive membrane fusion. The SNARE complex is not sensitive to Ca^{2+}, however, and thus the Ca^{2+} sensor Synaptotagmin-1 couples the depolarization and fusion events during synchronous neurotransmitter release. Synaptotagmin-1 is a vesicular-tethered membrane protein, with two homologous C2A and C2B domains attached through a flexible linker which extend outward on the cytoplasmic face of the synaptic vesicle. Upon Ca^{2+} influx, the hydrophobic loops of the two domains bind Ca^{2+} and insert into the membrane. The C2B domain contains several other regions capable of membrane interaction including a lysine rich polybasic face and the arginine apex. Some combination of these elements initiates the bridging of the Synaptotagmin-1 bound vesicle to the presynaptic membrane. Once this occurs, the SNARE complex drives the fusion and pore opening processes that lead to neurotransmitter release. This membrane interaction and insertion is lipid specific with certain head groups required to drive membrane bridging. This body of work focuses on further understanding the lipid specific interactions between Synaptotagmin-1 and the vesicle and plasma membranes. First, through mapping of the soluble C2AB domains insertion and orientation differences under different membrane compositions, highlighting differences in binding when PIP_2 is present. Next, through moving to more physiologically similar work on the full-length version of Synaptotagmin-1. Initial purification optimization, characterization, and comparison to the soluble domains will be shown to validate purification choice. This is followed by work on the driving forces for membrane insertion for full-length Synaptotagmin-1, determining coordination and electrostatic forces drive membrane interactions. Finally, an

examination of the mechanism for Synaptotagmin-1 will be explored through a series of measurements to determine if the calcium sensor may act as a distance regulator for SNARE-dependent fusion. Overall, the goal is to further understanding of Synaptotagmin-1 interactions with different lipids and its contribution to fusion by use of structural and functional studies using CW-EPR, pulsed-EPR, NMR, fluorescent techniques, TIRF and FLIC.

Table of Contents

List of Figures

Chapter 1

Chapter 2

Chapter 3

Chapter 4

Chapter 5

Chapter 6

Chapter 7

List of Tables

Chapter 3

Chapter 4

Chapter 5

Chapter 6

Abbreviations

Proteins:

Synaptotagmin:

Syt1	Synaptotagmin 1
Syt2(3,4,5…14)	Other Synaptotagmins by number

Cytosolic Syt1 constructs:

C2A	Residues 96-265 of Synaptotagmin1
shortC2A	Residues 136-260 of Synaptotagmin1
C2B	Residues 249-421 of Synaptotagmin1
shortC2B	Residues 271-429 of Synaptotagmin1
C2AB	Residues 136-421 of Synaptotagmin1
longC2AB	Residues 96-421 of Synaptotagmin 1

Membrane tethered:

FL SYT	Residues 1-421 of Synaptotagmin 1
ΔC2B	Residues 1-266 of Synaptotagmin 1

Other Proteins:

SNAREs:

SNARE	Soluble N-ethylmaleimide–sensitive factor attachment protein receptors

Syn (Syx)	Syntaxin-1A
Syb	Synaptobrevin 2
VAMP	Vesicle Associated Membrane Protein

Other regulatory proteins:

Cpx	Complexin-1
Munc-13	Mammalian Unc-13
CAPs	Calcium-dependent Activator Protein for Secretion, Unc31

Neuronal System:

SV	Synaptic Vesicle
PM	Plasma Membrane
RRP	Readily Releasable Pool

Lipids:

POPC (or PC)	1-palmitoyl-2-oleoyl-*sn*-glycero-3-phosphocholine
POPE	1-palmitoyl-2-oleoyl-*sn*-glycero-3-phosphoethanolamine
POPS (or PS)	1-palmitoyl-2-oleoyl-*sn*-glycero-3-phospho-L-serine
POPG	1-palmitoyl-2-oleoyl-*sn*-glycero-3-phospho-(glycerol)
DDAB	dimethyl dioctadecyl ammonium bromide salt
brain PC	porcine brain L-α-phosphatidylcholine
brain PE	porcine brain L-α-phosphatidylethanolamine
brain PS	porcine brain L-α-phosphatidylserine
PIP_2	phosphatidylinositol 4,5-bisphosphate
DPPC	1,2-dipalmitoyl-*sn*-glycero-3-phosphocholine
DPPE	1,2-dipalmitoyl-*sn*-glycero-3-phosphoethanolamine
DPPS	1,2-dipalmitoyl-*sn*-glycero-3-phospho-L-serine
DOPC	1,2-dioleoyl-*sn*-glycero-3-phosphocholine
DOPE	1,2-dioleoyl-*sn*-glycero-3-phosphoethanolamine
DOPS	1,2-dioleoyl-*sn*-glycero-3-phospho-L-serine
rhodaminePE	1,2-dioleoyl-*sn*-glycero-3-phosphoethanolamine-*N*-(lissamine-rhodamine-B-sulfonyl)
LUV	Large Unilamellar Vesicles

Detergents:

CHAPS	3-[(3-cholamidopropyl)dimethylammonio]-1-propanesulfonate
OG	n-Octyl-β-D-Glucopyranoside, Anagrade

Labels:

MTSL (*S*-(1-oxyl-2,2,5,5–tetramethyl-2,5–dihydro-1H–pyrrol–3-yl)methylmethanethiosulfonate)	
Alexa-546	Alexa Fluor 546 C5-maleimide
Alexa-488	Alexa Fluor 488 C5-maleimide
Bodipy	bodipy fl maleimide (bodipy fl *n*-(2-aminoethyl))maleimide)

Techniques:

PIPE	polymerase incomplete primer extension
PCR	polymerase chain reaction
EPR	Electron Paramagnetic Resonance
CW	Continuous Wave
SDSL	Site-directed spin-labeled
DEER	Double Electron-Electron Resonance
HSQC	Proton-Nitrogen heteronuclear single quantum coherence
NMR	Nuclear Magnetic Resonance
TIRF	Total internal reflection fluorescence
FLIC	Fluorescence Interference Contrast

Materials:

EDTA	2,2',2'',2'''-(ethane-1,2-diyldinitrilo)tetraacetic acid
Ca^{2+}	calcium chloride
Cd^{2+}	cadmium chloride
Pb^{2+}	lead acetate
ATP	Adenosine-5'-Triphosphate Disodium trihydrate
IP_3	D-myo-Inositol-1,4,5-triphosphate, sodium salt
NH_4Cl	Ammonium Chloride
NiEDDA	Nickel(II)-ethylenediamine-N,N'-diacetic acid
NaCl	sodium chloride
KCl	potassium chloride
MOPS	sucrose, 3-(N-Morpholino)propanesulfonic acid
Tris	Tris(hydroxymethyl)aminomethane hydrochlorid
HEPES	2-[4-(2-hydroxyethyl)piperazin-1-yl]ethanesulfonic acid
AEBSF	4-(2-aminoethyl)benzenesulfonyl fluoride hydrochloride
IPTG	Isopropyl-β-D-thiogalacto-pyranoside
dNTP	dinucleotidetriphosphate
DTT	Dithiothreitol

Amino Acids:

Single-Letter	*Three-Letter*	*Full Name*
A	Ala	Alanine
C	Cys	Cysteine
D	Asp	Aspartic Acid
E	Glu	Glutamic Acid
F	Phe	Phenylalanine
G	Gly	Glycine
H	His	Histidine
I	Ile	Isoleucine
K	Lys	Lysine
L	Leu	Leucine
M	Met	Methionine
P	Pro	Proline
Q	Gln	Glutamine
R	Arg	Arginine
S	Ser	Serine
T	Thr	Threonine
V	Val	Valine
W	Trp	Tryptophan
Y	Tyr	Tyrosine

Acknowledgements

The conclusion (and initiation) of this graduate degree would not have been possible without the strong influence, encouragement, and support of many people along this journey. To each of you, I am very grateful.

First and foremost, I want to thank my advisor Dr. David Cafiso for providing me with the opportunity to work and explore any idea freely in the lab. I did not fully understand what an important fit this group would be when I joined, but from this research I have learned far more than I was expecting about how to be a scientist, the art of troubleshooting, and about my own neurological condition. Thank you for being understanding when times were hard and encouraging me when I had my frequent doubts about being suited for the program. Your example and line of research has taught me to explore any question more deeply and to be more tolerant in a field full of so many unanswered questions.

I also want to thank our collaborators and friends in the Tamm lab and Jahn Labs. The insightful conversation and depth of questioning from our meetings together was very inspiring and eye opening. Thank you particularly to, Dr. Volker Kiessling and Dr. Binyong Liang for always offering advice and training for any questions or protocols, however simple.

Dr. Jeff Ellena, I also want to thank you for your constant support in the lab, group meetings, and through a very long, and somewhat turbulent NMR experience.

My lab members support, past and present, really made this experience more enjoyable. Whether it was through good times or bad, surprise birthday parties, pie, too many lab floods, or seemingly endless nights in the lab thank you for standing by me and for always making sure it was a “good time”. An extra thank you is deserved for Dr. Anusa Thapa, for training me and

preparing me for the lab experience. Your example and openness about your own health struggles and future success in the lab really showed me that with enough effort this would be possible. To other lab members, particularly Rafal, Damian, Vanessa, Jake, and Qian, and all others who were always there to lend a hand in a moment's notice thank you. To my wonderful undergrad, Nakul Karandikar, thank you for working harder and more independently than was expected of you through this final stretch. I look forward to working with you through the next year as well.

An additional acknowledgement is well deserved for two of my lab members Thushani Nilaweera and David Nyenhuis. Thank you both for standing by me from the very start of the program and still being right here at the end. Thushani the lab really changed when you joined, you added that enjoyable spark and push to do something fun that had been missing through previous years. Your kind words during our many discussions were always exactly what I needed to hear. David of course, thank you for your endless support, beyond the call of duty in the lab and at home. You have worn far more hats than you intended, whether it was husband, nurse, master French-presser, or copy-editor; you handled all of your roles far better than any of the rest of us could. I hope I can provide the same support through both of your final months as graduate students as you have for mine.

Of course, thank you to other friends and family who accepted early on that I am always in the lab, but happy. Especially those that went out of their way to visit us in Charlottesville.

Finally, where this all began, I want to thank the Biochem Lab team, Dr. Linda Columbus, Dr. Carol Price and Dr. Cameron Mura for unlocking the doors to your lab, beyond scheduled class periods, and allowing those in your course to freely investigate a question on our own time. Before this point I did not think it would be a possibility to perform research in a lab and I really did not realize how much I would enjoy it. Thank you as well for introducing me to David, it really was

the perfect randomly assigned lab group. An extra thank you is deserved to Linda Columbus who encouraged and sat with me through a less-than traditional application process to the PhD program at UVA.

Thank you as well to all of my committee members, Dr. Linda Columbus, Dr. Lukas Tamm, Dr. Jill Venton, and Dr. Ken Hsu for all of your work and time toward making this thesis the best it can be. Susie Marshall, I also want to thank you for all of the help with scheduling my defense, any question along the way, and for always offering a kind smile on my frequent trips in and out of Dave's office.

Dedication

This work is dedicated to all others who are battling a chronic neurological condition and in constant pain. I hope, with time, this work can contribute to the answers and words you seek to better understand and communicate your illness.

CHAPTER 1: Introduction to Neuronal Exocytosis

1.1 General Vesicle Trafficking and Exocytosis

Exocytosis is defined as the process by which secretory or signaling molecules, hormones, neurotransmitters, etc., are released through the fusion of vesicles carrying these signaling molecules to a membrane[1]. This process occurs in nearly every tissue and cell in the body (endocrine pituitary and pancreatic cells, rod photoreceptors, astrocytes, bipolar neurons, and calyx of held neurons to name a few) within signaling pathways, as a means of transporting messages and information[1]. Generally, vesicle trafficking and fusion can occur within a cell, as in a vesicle budding from the rough endoplasmic reticulum to attach to the Golgi body[1]. It can also occur from cell to cell, including the fusion and transfer of neurotransmitters between neurons that involves transport to the plasma membrane, fusion, and finally release through the synaptic cleft. Without this process signaling pathways would rely on diffusion of secretory molecules to transfer information, which is slow and unregulated. This would cause signaling processes to be unspecific, undirected, and require many signaling molecules to transfer sufficient amounts of information[1]. Pre-accumulating signaling molecules within a secretory vesicle concentrates and isolates them, which along with regulatory proteins and pathways, helps prevent unspecific signaling and can accelerate the time required for sending a signal[1]. The process follows a secretory vesicle through its lifetime: starting at budding, following to trafficking, tethering, docking, priming, and finally

fusion and release[1]. These vesicles fuse very quickly (on the sub-millisecond timescale for neurons, up to 6000 events/second in a calyx of held neuron) and carry molecules which propagate a large-scale response in the host, and thus must be tightly regulated[1]. One example regulatory pathway for exocytosis is calcium mediated: Ca^{2+}-dependent, regulated exocytosis. This occurs in both endocrine and neuronal systems[1]. The focus of this work is research in the neuronal system, but the endocrine and other systems are equally important.

1.2 Neurons, the Nervous Systems, and the Brain

The central and peripheral nervous systems control messaging between (*to* and *from*) the brain and the body. Sensory and motor inputs control how a person perceives and interacts with the world (emotions, senses, thought, movement, etc.)[2]. The central nervous system is composed of neurons in the brain and spinal cord (with roughly 86 billion neurons in the brain alone) and is also known as the control center of the body[2]. The peripheral nervous system controls communication to and from the brain to the rest of the body[2]. Within the peripheral nervous system there are two ways to communicate with the central nervous system: *to* (directed at the central nervous system) or *from* (central nervous system directed to the peripheral nervous system. Afferent (sensory) neurons achieve the *to* function, sending signals from the rest of the body (skin, internal organs, muscles, etc.) to the brain and efferent (motor) neurons perform the *from* function, commanding the rest of the body from the brain[2]. Motor neurons within the peripheral nervous system are working constantly throughout the body, whether perceived or not, as there are

voluntary (somatic nervous system) and involuntary (autonomic) pathways[2]. Meaning, systems which a person can intentionally control (i.e. movement) and ones which happen subconsciously in the background (i.e. a heart beating). Within the autonomic system there are also excitatory (sympathetic- fight-or-slight) and inhibitory (parasympathetic, relaxing) pathways[2].

These complex systems of communicating pathways are highly differentiated within each system. This controls the type, rate, and repetitiveness of information passed. Nerves (which are diverse themselves) are not the only components within these systems, many other cells are packed densely within these tissues with roles in aiding and supporting neuronal communication[2]. One type which is commonly known in the peripheral nervous system is Schwann cells, which control myelination around nerve fibers (often highlighted as a key factor in multiple sclerosis)[3]. It is important to understand the diverse function, anatomy, and pathways that the neurons in the central and peripheral nervous system perform to better understand the causes of diseases and neurological disorders that appear when something within these pathways goes awry. Since these systems are the main communication pathways in the body small alterations in any stage of the process causes major changes in mind and body function, a few general examples include: sleep disorders, psychiatric disorders, mood disorders, impaired learning/thinking/memory, impaired motor capacity, and chronic pain[4,5,6,7]. These diseases and conditions are tied to changes in various states including: proteins expression, point mutations within proteins, lipid and cholesterol regulation to name a few, but many neurological diseases and conditions are very poorly understood on the neuronal and particularly on the molecular level[5,6,7].

1.2.1 Anatomy and Classification of Different Neurons

As there are a variety of cells which play supporting roles for neurons in these systems, there is also diversity within nerve tissues. These are usually classified either structurally or functionally, and each is specialized to communicate differently as needed within the body and various regions of the brain[2]. The functional divisions include the previously mentioned afferent and efferent neurons within the peripheral nervous system and interneurons within the central nervous system[2]. Interneurons communicate only within the central nervous system[2]. Structural divisions are usually categorized by process or function (addressed below). Some major structural differences in neurons and neuronal connections include: differences in myelination (gray vs. white matter), the presence or absence of an axon (neurons without an axon are called anaxonic and are found in some regions of the brain), the number of branching points which extend from the cell body (unipolar, bipolar, multipolar), and the type of connectivity between neurons (presence or absence of a synaptic cleft)[2]. Each unique neuronal anatomy is specialized to fulfill the requirements of the tissue or tissues which it communicates with: some to function very quickly, some to work over long distances, and others to branch out and connect huge networks of other neurons for signal propagation. Neuronal systems are complex circuits and combinations of all these factors combine to send the desired signal, whether it is to excite or to suppress. To understand these structural divisions and diversity, one must look closer at the general anatomy of a neuron.

1.2.1.1 Neural Anatomy and Function can be broken down into four main parts: the cell body, the dendrites, the axon, and the axon terminals/boutons (*Figure 1.1*)[8]. The cell body, or

soma, contains the cell nucleus and the majority of the synthesis machinery (for example ribosomes)[8]. These proteins and lipids are shuttled throughout the rest of the nerve mainly through a process called anterograde transport (and shuttled back if damaged through retrograde transport), tethered to structural elements of the neuron to reach their destination[8].

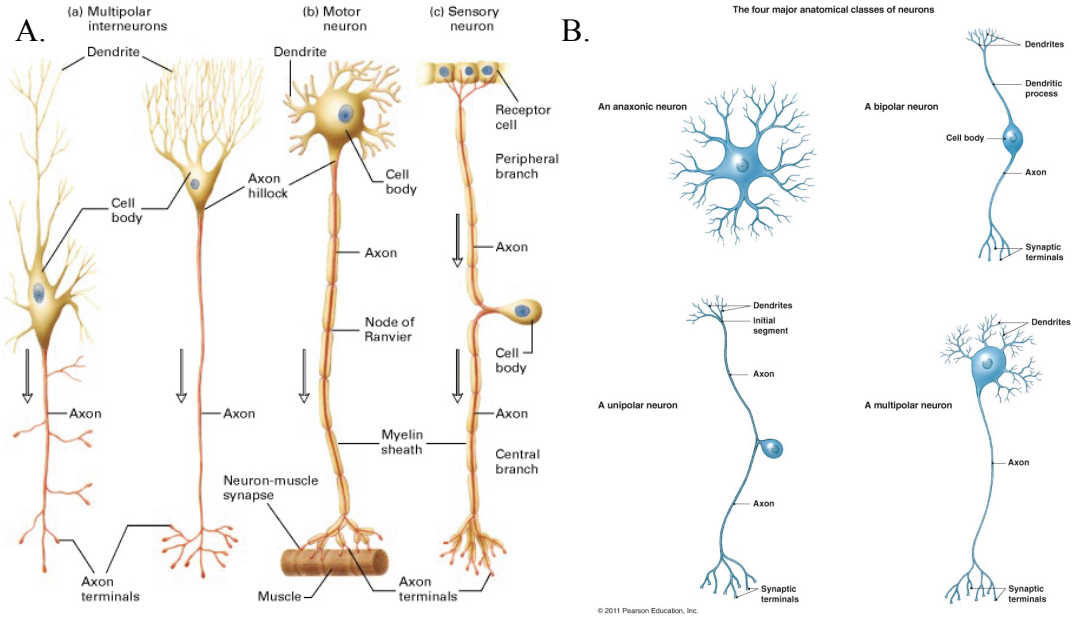

Figure 1.1: Neuronal diversity and makeup. Figures are from Lodish et al.

If the nerve (and sequence of nerves) is simplified and thought of as a vertical chain, dendrites would sit above the cell body. Dendrites are, relative to the rest of the neuron, small branched spindles (of variable length and branching), which receive the signals from a preceding neuron's axon terminal[8]. Branching increases the dendritic surface area and contacts with other neurons. The neuron's axon is a thin (μm to mm diameter and variable in length) extension downward from the cell body. An axon attaches to the cell body at a site called the axon hillock which carries an action potential from this junction to the branched axon termini[8].

1.2.1.2 An Action Potential is a very fast (up to 100 m/s) electrical impulse down the axon caused by a change in potential (measured in voltage) between the plasma membrane of the axon between the inside the of the cell vs. outside the cell[8]. This is unidirectional toward the axon termini and unstoppable once it has been initiated[8]. Before the action potential, dendrites receive the chemical messengers (signaling molecules, such as neurotransmitters) from the preceding synapse, these molecules then bind to chemically/ligand-gated ion-channels on the membrane surface of the dendrites[4]. If the ligands are inhibitory, the ion-channels will flux positive ions out of the cell to decrease the membrane potential in a process called hyperpolarization[4]. If the ligands are excitatory, there will instead by an influx of ions into the cell body, which increases the membrane potential[4]. This influx of ions travels to the cell body and collects until concentrations are high enough to overcome the threshold for the action potential to trigger an event down the axon from the axon hillock. The action potentials are caused by the rapid electrochemical gradient created by the sequential opening of voltage gated channels down the axon, with the influx of ions upstream of a particular channel causing it to open in turn, and so on down the neuron[4]. This leads to a large influx of either sodium of calcium ions depending on the tissue/neuron (sodium channels fluxes are usually faster or priming potentials)[8]. Preceding an action potential, the difference in membrane potential in the axon between the plasma membrane is about -70 mV at resting potential[8]. During an action potential event (depolarization) the inside of the axon fills with ions, altering its potential difference to values as high as 55 mV[4,8].

After the rapid depolarization and potential spike the axon must equally as quickly repolarize the cell. This occurs by a rapid outward flux of potassium ions[4]. This process is followed by a short refractory period before the nerve is ready to signal again. Different types of neurons, typically with longer axons, will have a myelin sheath (an extra insulative layer of myelin) which

adds additional insulation, preventing any leakiness of the ions during the action potential between the inside and outside of the cell to aid in and accelerate transmission of the potential over longer distances[8]. Myelination is a mixture of lipids, proteins, and high concentrations of cholesterol[8]. These regions do not have voltage gated channels[8]. The channels in a myelinated neuron are located in-between bundles of myelin at the nodes of Ranvier[8]. A myelinated neuron is classified as white matter, because of its appearance under a microscope[8]. A neuron which does not have a myelin sheath is classified as gray matter.

At the end of the action potential the signal must be passed to the next neuron (or tissue, i.e. muscle). When the action potential reaches the synapse (axon termini/presynaptic clefts), if it is an electrical synapse, the next neuron's dendrites are in contact with the presynaptic membrane. The flow of ions continues directly through pores between the two membranes called connexons. There is no need for neurotransmitters or signaling molecules in electrical synapses. This transfer of nerve impulses is very rapid, as it does not rely on diffusion of chemical signals from the presynaptic cell to the next. When the action potential reaches the synapse, if it is instead a chemical synapse, L-type voltage-gated calcium channels are opened which cause a calcium influx[6]. This influx triggers neuronal exocytosis (addressed in more detail below), which releases the messenger signals (such as neurotransmitters) through the synaptic cleft which are then detected by receptors on the membranes of the post synaptic cells. This causes the signal to be passed to the next neuron in the line, creating a signaling train[9].

1.2.1.3 Signaling molecules which function at chemical synapses are another major point of diversification for communication within the body. Some signaling molecules play roles in enhancing a signal cascade while others suppress an event. How each molecule communicates

with the post synaptic neuron after exocytosis is also a varied event with equally varied outcomes. Signaling molecules are typically low molecular weight neuro-transmitters or peptide-transmitters[9]. Some neurotransmitters include: monoamines, acetylcholine, glutamate, gama-aminoburtirc acid (GABA), glutamate, dopamine, epinephrine, serotonin, histamine, norepinephrine/noradrenaline, and adenosine-5-triphosphate (ATP)[9]. Some specifically peptide-based transmitters include: substance P, brain-derived neurotrophic factor (BDNF), oxytocin (and other endorphins), and statins[9].

A few example signaling molecules can highlight the different mechanisms for activating or suppressing a signaling cascade.

1.2.1.3.1 The monoamine Serotonin is known to regulate sleep cycles, hormone secretion, respiratory patterns, learning, and digestion among many others. Disruption in any part of this signaling pathway has been highlighted in conditions such as: schizophrenia, sleep disorders, depression, and anxiety[9]. In serotonin signaling networks, neurons are bundled tightly and have G protein-coupled receptors that are specific serotonin receptors[9].

Serotonin release and receptors can have both excitatory and inhibitory functions (feedback loops) depending on the neuron and the other neurotransmitters released alongside it, with an overall inhibitory effect on the body (calms)[9]. If released in large quantities serotonin has a somewhat biphasic activation[9].

1.2.1.3.2 GABA and Noradrenaline are known to regulate excitatory serotonin pathways as well as serotonin itself. GABA is the main inhibitory neurotransmitter in the entire nervous system, it is thought to work through sheer quantity/volume released at a time[9]. Noradrenaline is a stimulatory neurotransmitter (also called a stress-hormone) which activates fight-or-flight cascades[9]. These three neurotransmitters in combination with dopamine work to maintain a

balance within the brain and central nervous system. These neurotransmitters together act in a checks-and-balancing system, both signaling and regulating over-signaling other neurotransmitters, which overall controls a person's mood[9].

1.2.1.3.3 Dopamine is another excitatory and inhibitory pathway which works only with G-protein-coupled receptors to activate reward centers in the brain[9].

1.2.1.3.4 Glutamate is also an excitatory neurotransmitter and is associated with learning[9]. When glutamate levels are not regulated properly the observed effects include: chronic pain, autism, depression, Huntington's and Parkinson's degenerative diseases, as well as Alzheimer's disease[9]. Like other neurotransmitters, glutamate has a peripheral back-regulation effect on presynaptic neurons after exocytosis, where in high concentrations it will inhibit additional calcium influx into the cell[9]. This is important to emphasize as flow of transmitters in the synaptic cleft is not unidirectional; transmitters can diffuse freely in this small 20-40 nanometer distance to the postsynaptic neuron or back onto the presynaptic neuron where they can regulate additional impulses by binding to ion channels to prevent further calcium and current flux[4]. ATP is often released alongside glutamate, and functions as a way of spreading the molecular energy source throughout the body[9]. ATP will be addressed again below.

1.2.1.3.5 Acetylcholine is an example of a signaling molecule in the peripheral nervous system. It is not always used for communication between neurons, but also between muscle tissue and neurons at smooth muscle junctions. It has a mainly excitatory pathway, but it can self-regulate if found in high concentrations. Misfunction of acetylcholine pathways can lead to conditions such as myasthenia gravis[9].

1.2.1.3.6 Peptide transmitters, such as oxytocin are found to play roles in both the central and peripheral nervous systems, controlling pathways such as hormone regulation. In neurons these peptides work more by local and size effects rather than bulk/volume pathways[9].

1.3 A Closer look at the Presynaptic Cleft and Neuronal Exocytosis

The terminal region of a neuron functions to release these signaling molecules through a complex combination of function and regulation between ion channels, ion fluxes, molecular machinery, and lipid interactions[4]. These interactions and eventual fusion and release is the fastest known membrane fusion event that occurs in cells, on the sub-millisecond timescale[10].

1.3.1 Initial Anatomy and Cycling within a Synapse

1.3.1.1 Ion channels control the electrical signals passed throughout a neuron and between them. The axon terminal (presynaptic clef) is the final destination of an action potential, which is propagated through sodium channels in the axon into the cleft[4]. Arrival of this current triggers a calcium influx into the presynaptic cleft, through calcium-specific voltage gated ion channels that are localized within 100 nm of each site of fusion[4]. This calcium influx is on the order of a 16-fold increase in the concentration of calcium (Ca^{2+}): from 0.1 μM resting levels to 1.5-10 μM (this number can be higher depending on how it is estimated) post influx[4]. The presence of additional calcium then causes proteins to trigger a rapid, regulated fusion process[4]. Calcium then must

dissipate to signal the end of the fusion event. For nerve signaling to be a tight on-and-off triggered process, the removal of calcium from the site of fusion must also be regulated[4]. This regulation is through current control of sodium (Na^+) and potassium (K^+) channels and local ion concentrations at the synaptic cleft[4]. One way this occurs is upon calcium triggering, potassium channels are also activated, some by voltage changes and others through the binding of calcium or neurotransmitters, which drives K^+ out of the cell to restore resting currents (repolarization)[4]. Calcium channels can also be regulated directly by the inhibitory neurotransmitters and hormones mentioned above[4].

In order to sense an action potential and end a triggering event, baseline Na^+ and K^+ levels in a synapse must be tightly regulated. These concentrations sit around roughly 10 mM and 135-140 mM resting concentrations in the cell, respectively[4]. Na^+, K^+-ATPase's play a large role in this regulation[4]. There are also many ATP-dependent Ca^{2+} uptake systems in the synapse to aid in rapid calcium removal[4]. This highlights ATP and other polyvalent ions' importance in regulating signal transduction (this will be discussed in more detail below). Smaller fluxes in concentrations in sodium and potassium ions may also contribute to voltage and pH driven uptake of neurotransmitters into synaptic vesicles as well as cycling of lipids and protein throughout the synapse[4].

1.3.1.2 The Synaptic Vesicle Cycle occurs within the presynaptic cleft. Here, there are a large collection of synaptic vesicles (30-40 nm in size) which uptake and carry signaling molecules[10]. These vesicles travel to the plasma membrane and, through a series of steps after calcium influx (synchronous release), fuse and release their contents into the synaptic cleft[8]. For proper function of the nervous system, these vesicles must be present and ready to fuse every time a signal is required without delay[11]. This means there must be a readily releasable pool of vesicles

at all times[11]. These vesicles must also cycle rapidly to achieve this task. At the beginning stage of the synaptic vesicle's lifecycle, an empty synaptic vesicle is formed by budding, which is a two-step process involving invagination of and subsequent fission from the early endosome (*Figure 1.2)*[11,12]. While these vesicles are empty, they are still highly complex, being a mixture of the over 20 protein families and lipids required for regulating fusion (*Figure 1.3*)[13]. Empty vesicles sit in a reserve pool until a signal is received to fill the vesicle[14]. A synaptic vesicle is filled with transmitters upon acidification of the synaptic lumen, which creates a pH gradient that drives the transmitters into each vesicle[12]. Potentially through initial diffusion and some form of restricted/assisted movement, these vesicles travel toward the plasma membrane[11]. When they reach the plasma membrane region they concentrate into a readily releasable pool within the active zone[11-15].

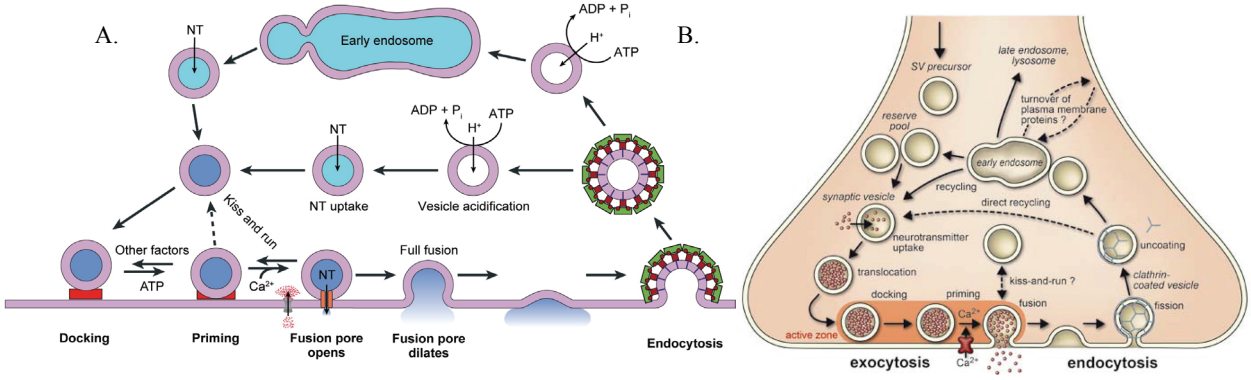

Figure 1.2: Representations of the Synaptic Vesicle cycle. A. is from Chapman. (2008). *Annu Rev Biochem.* **77:** 615-641. B. is from Jahn and Fasshauer. (2012). *Nature.* **490:** 201-207.

1.3.1.4 The Active Zone(s) encompasses the plasma membrane of the presynaptic cleft where the active parts of fusion occur. There are a variable number of active zones per synapse, ranging from 1 to upwards of 1000 depending on the tissue being studied[16]. When transmitter filled synaptic vesicles reach the active zone they dock and prime, which holds the vesicles in the releasable pool so that fusion is not limited by diffusion of vesicles. This pool size regulates each

synapses individual firing capacity and signal size, direct quantification of pool size (anywhere from 2 to ~6000) is complicated and easily over or underestimated depending on the technique used[15-18]. The holding/scaffolding process is thought to occur through large multidomain proteins (potentially involving: Synaptotagmins, Munc13, RIMs)[12,14]. There is strong evidence for the involvements of Synaptotagmin 1 and 7 in this process, as knockout neurons show a significant decrease in pool size[15]. Once a vesicle is primed for fusion, it will likely proceed through the fusion cycle (discussed below)[12]. When a vesicle fuses with the membrane it then goes through a series of intermediates: stalk formation, hemi-fusion, and finally opening of either a full or transient fusion pore for releasing transmitter[14]. What happens to the vesicle at this point could be a mix of transitions, potentially depending on the tissue[11,14].

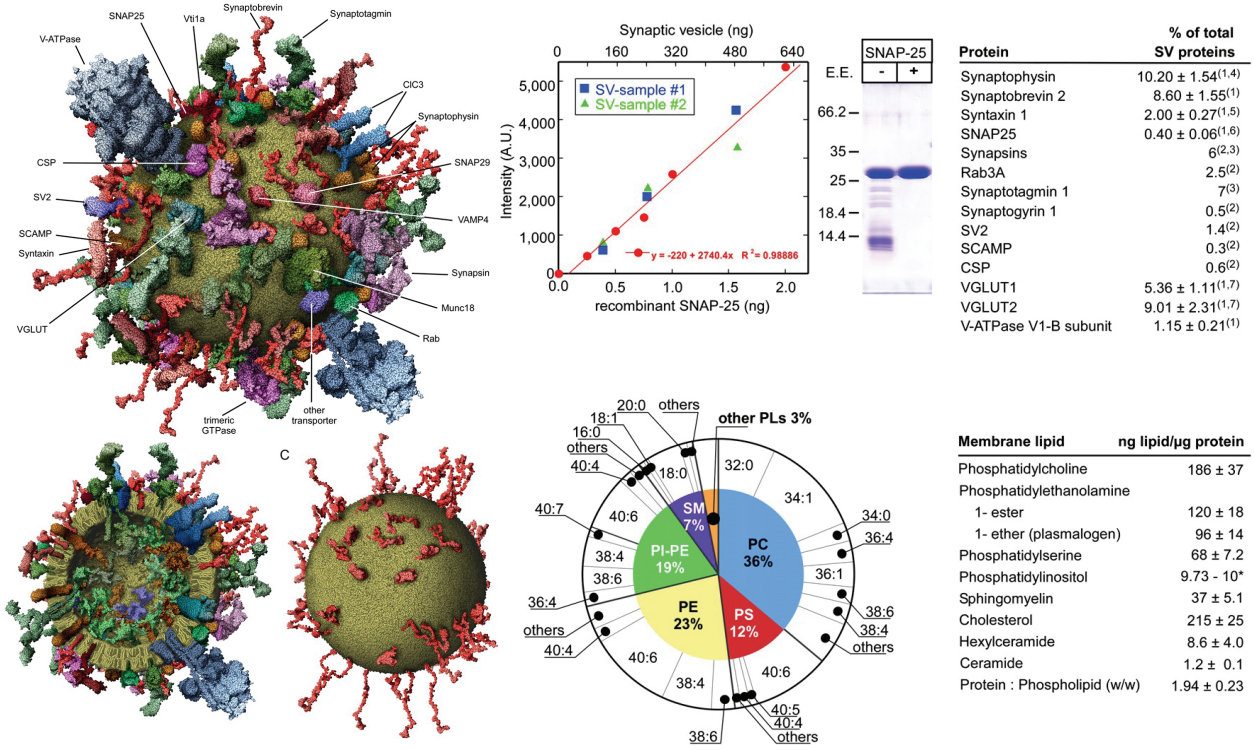

Protein	% of total SV proteins
Synaptophysin	10.20 ± 1.54[1,4]
Synaptobrevin 2	8.60 ± 1.55[1]
Syntaxin 1	2.00 ± 0.27[1,5]
SNAP25	0.40 ± 0.06[1,6]
Synapsins	6[2,3]
Rab3A	2.5[2]
Synaptotagmin 1	7[3]
Synaptogyrin 1	0.5[2]
SV2	1.4[2]
SCAMP	0.3[2]
CSP	0.6[2]
VGLUT1	5.36 ± 1.11[1,7]
VGLUT2	9.01 ± 2.31[1,7]
V-ATPase V1-B subunit	1.15 ± 0.21[1]

Membrane lipid	ng lipid/µg protein
Phosphatidylcholine	186 ± 37
Phosphatidylethanolamine	
1- ester	120 ± 18
1- ether (plasmalogen)	96 ± 14
Phosphatidylserine	68 ± 7.2
Phosphatidylinositol	9.73 - 10*
Sphingomyelin	37 ± 5.1
Cholesterol	215 ± 25
Hexylceramide	8.6 ± 4.0
Ceramide	1.2 ± 0.1
Protein : Phospholipid (w/w)	1.94 ± 0.23

Figure 1.3: Representation of the Synaptic Vesicle. Images from from Takamori et al. (2006). *Cell.* **127:** 831-846.

1.3.1.5 Vesicle Recycling and general Exocytotic mechanisms are heavily debated. Generally, a filled synaptic vesicle is known to come down to the plasma membrane and release its contents, but how this occurs and what happens to the empty synaptic vesicle could involve a mix of different processes. In one type of event, the vesicle must come down to the plasma membrane, dock and prime then release its contents through a transient fusion pore before disengaging from the membrane empty, this is called kiss-and-run (kiss-and-run also sometimes refers to a primed vesicle being removed from the readily releasable pool without releasing neurotransmitter as a way to regulate pool density)[11,12]. Kiss-and-run events are better established in an equivalent system in neuroendocrine cells with the transport of dense core vesicles[7.8,19]. Whether transmitter release in a kiss-and-run event involves protein mediated fusion is debated. If it is free of protein then it is a type of unregulated fusion called spontaneous mini-release[8,10]. These events happen rarely, likely involving one vesicle at a time unlike coordinated synchronous and uncoordinated (without instant calcium trigger) asynchronous release which will involve a large pool of vesicles. If a vesicle does not kiss-and-run the vesicle is said to undergo full fusion (also called kiss-and-stay) and merge with the plasma membrane[11,12,14,19]. This cannot occur in rapid succession without recovery of the vesicles however as the plasma membrane would quickly start to expand after every fusion event.

Recovery of lipid and protein from fused synaptic vesicles is called neuronal endocytosis[11,12,14]. There is not a full consensus over the mechanism and proteins involved in this event, but many studies lead to the idea that endocytosis is clathrin-mediated[11,12,14]. Clathrin coating is a two-protein layered substance which identifies and retrieves synaptic vesicles from the membrane; the outer layer is composed of clathrin, the inner layer is composed of clathrin adaptors[11]. Clathrin-adaptors are a combination of proteins that identify and link to the membrane

and proteins of the synaptic vesicle[11]. The clathrin adaptors also act to connect the vesicle and clathrin layers by tethering clathrin[11]. Specific lipid and protein interactions or targets on the synaptic vesicle which are involved in endocytosis are still heavily studied, two examples would be Synaptotagmin (helical formation post fusion of the luminal domain could act as a target location) and highly acidic lipids on the plasma membrane (such as PIP_2, which varies in phosphorylation and charge throughout the PIP lifecycle, a synaptojanin mediated process)[11]. Clathrin coating does not appear to occur at random, but instead is constantly involved in recycling any asynchronous events. the calcium trigger also somehow regulates endocytotic triggering, potentially through the protein calmodulin[11]. After clathrin-coated vesicles are retrieved from the plasma membrane they are either returned and sorted in the endosome or mature separately, after which they lose their coating and enter the reserve pool, ready to be once again filled with signaling molecules[11]. These later recycling steps likely occur through tight regulation by GTPase proteins[11].

1.3.1.6 Synchronous and Asynchronous Release of transmitters occur when a neuron fires or signals initially through an action potential. There are typically two waves of kinetically unique calcium-dependent fusion and release following the action potential and calcium influx[18]. The first, occurring on the sub-millisecond timescale is called synchronous release. As the name implies synchronous release is a fast, large population of calcium-dependent synchronized (phasic) release[10,18]. Following the initial transmitter release, a slower and delayed asynchronous release of (usually) smaller populations of vesicles fuse and release over 10s of milliseconds[10].

Asynchronous release is not tightly coupled to the calcium influx but may use the remaining levels of calcium after the initial calcium influx and before baseline calcium levels are resored[18]. Another idea is that asynchronous release uses a unique calcium source of off target

locations (such as axon localized calcium), not the voltage-gated (P/Q type) calcium channels triggered from the action potential localized in the active zones[20]. Spontaneous mini-release in comparison is a calcium-independent release, which occurs rarely in comparison to synchronous and asynchronous release (with the exception of knockout conditions, such as Syt1 knockout or "unclamping", in mice, which are often fatal)[18-21]. Each of these types of fusion and release are tightly regulated, mainly by different Synaptotagmins (addressed in more detail below)[10,18,20]. In a lab, these events are measured mainly through electrical stimulation followed by measuring the excitatory postsynaptic currents, where each type of release displays a characteristic excitation intensity and duration[10,18].

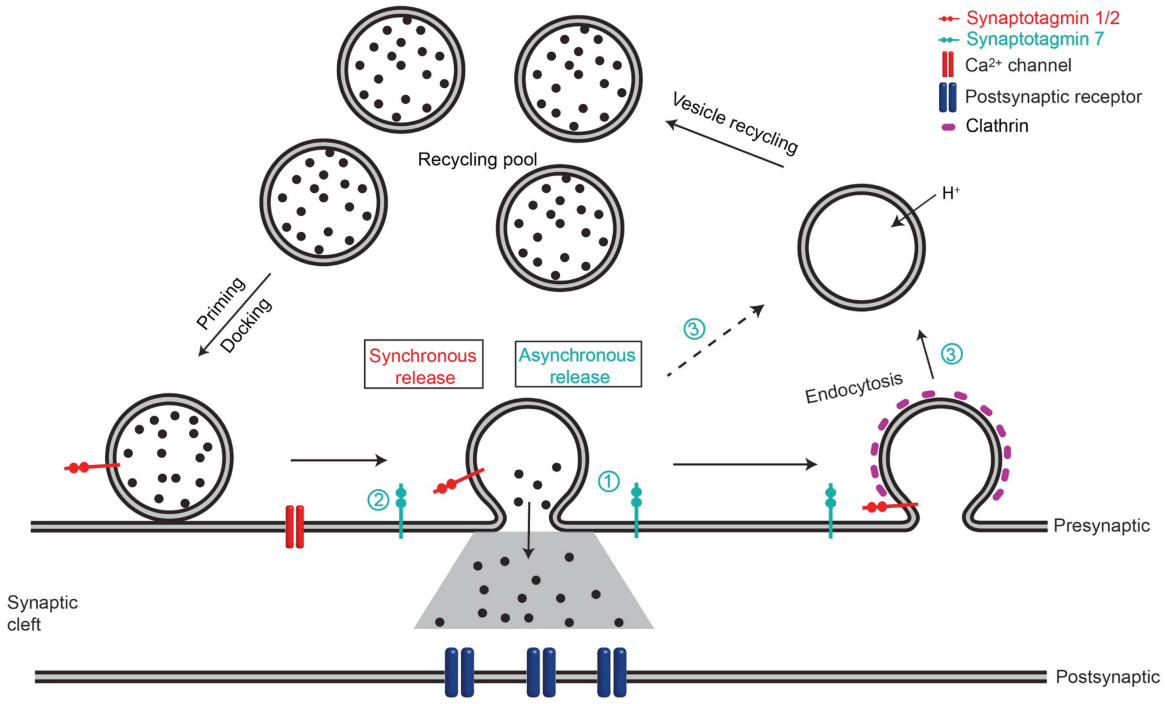

Figure 1.4: Synaptotagmins roles in Synchronous and Asynchronous release. Image from Chen and Jonas. (2017). *Neuron*. **94:** 694-696.

With few known exceptions, synchronous release dominates as the main mechanism that neurons use to communicate, as it is the fastest and most tightly regulated (driven by Syt1, Syt2,

and Syt9)[18,22]. However, when prolonged and continuous stimulation (prolonged stimulus trains resulting in pulse train depression and desensitization) of a neuron occurs the readily releasable pool becomes depleted, as endocytosis becomes rate limiting (likely driven by Syt7)[10,21]. In these cases, synchronous release slows, but asynchronous release persists and often increases in quantity (still on the slower timescale)[10]. It is theorized that this is because asynchronous release may have access to a larger subset of the readily releasable pool than synchronized release (*Figure 1.4*)[10].

1.3.2 A Molecular View of the Site of Fusion

1.3.2.1 The Core Fusion Complex is the driving force for neuronal exocytosis. This complex is also referred to as soluble N-ethylmaleimide-sensitive-factor (NSF) attachment protein receptors or SNAREs[12]. The SNARE complex is composed of three proteins: synaptic vesicle tethered synaptobrevin (Syb or VAMP, vesicle associated membrane protein), plasma membrane tethered syntaxin (Syn or Syx), and plasma membrane associated SNAP-25 (through palmytolation)[12]. Together these proteins form a four-helix bundle, of roughly 100 angstroms in length, consisting of a single helix from both Syb and Syn and two from SNAP-25[14]. Within the helical bundle these are often called Q and R SNAREs, where Qa, Qb, Qc, and R refer to the helices contributed from Syn, SNAP-25 (x2), and Syb respectively[12]. The Q and R designation refers to the residue at the central or zero layer of the helical bundle[12,14,23]. SNAREs are also often differentiated as v- or t-SNAREs which refer to vesicular (Syb) and target-membrane (Syn, SNAP-25) components[23]. Alone, Syb is a small unstructured or partially unstructured (before SNARE zippering) protein with a C-terminal transmembrane helix spanning the synaptic vesicle membrane[14]. SNAP-25 is a soluble protein (that likely becomes helical in the acceptor complex)

with a stretch of cysteines which are the palmitoylated attachment site to the plasma membrane[14,23]. Syn is more complex with a C-terminal transmembrane helix, then a SNARE forming helix (again forming either in the acceptor complex or appearing as a broken helix at residues 225-226), and finally a flexibly linked regulatory Habc domain, which consists of an antiparallel three-helix bundle[10,23,24].

The SNARE complex was first identified as a target for botulinum and tetanus neurotoxins, which are known to block fusion without altering the structural elements of the terminal, which suggested that the SNARE proteins were essential for nervous system function[12]. The complex is also SDS resistant, highlighting stability which would be required to drive fusion[10]. The SNARE complex is named due to its assembly and disassembly being regulated and driven by energy sources from the AAA1-ATPase, NSF (N-ethylmaleimide sensitive factor). NSF dependent disassembly after fusion is aided by the α-SNAP (soluble NSF-attachment protein) cofactor, which helps separate the complex for endocytosis[12,14].

SNARE assembly, resulting in a fully zippered SNARE complex, is thought to go through a series of regulated steps. First Syn is itself regulated (by proteins discussed below); it is able to form an open or closed state, referring to its ability to back-bind the Habc domain to the SNARE helix, forming a stable four helix bundle mimicking the SNARE complex[14]. Syn is also likely associated or lying on the plasma membrane at this point through associations of charged lipid residues (PIP_2) with charged regions in Syn[24]. A driving force must occur to lift the complex off the plasma membrane to begin Syb assembly. This likely occurs through direct or indirect regulatory protein interactions with Syt1 or through contacts with SNAP-25[24]. Priming for fusion requires syntaxin to form an initial t-SNARE or acceptor complex with SNAP-25 in a 1:1 complex on the plasma membrane[23]. This complex formation will lift Syn off of the membrane surface,

making it ready to accept Syb to form the four-helix bundle and fuse. It is important to mention that experimentally forming a 1:1 complex with Syn and SNAP-25 is difficult to achieve and appears to be dependent on the regulatory proteins present and the detergent system the full-length proteins were purified in (to prevent aggregation of syntaxin)[23,24]. A 2:1 complex of Syn:SNAP-25 is energetically favorable *in vitro* because the complex forms a stable four helix bundle, but is off-pathway for *in vivo* fusion[25]. The 2:1 complex is a stable intermediate which is rate limiting and undesirable for physiologically relevant measurements, because it slows the rate of fusion to seconds or even minutes compared to the physiological sub millisecond timescale[25]. The 2:1 complex appears to be regulated in the lab and in neurons through various accessory proteins such as Munc18 (more below)[23]. After the 1:1 complex is formed, Syb needs to be within a certain distance and a certain amount of energy (~40 k_BT activation energy, probably from regulatory proteins and membrane rearrangement) is required to begin to zipper and form the trans SNARE complex[26]. Zippering of the bundle occurs from N to C-terminals and pulls the synaptic vesicle and the plasma membrane closer together[14]. It is unclear if the entire C-terminus zippers through the transmembrane domains to form tighter fusion or if the SNARE bundle (or SNAREpin) is attached through a flexible linker for both Syb and Syn[26]. Assembly itself is a large energy release, upward of 110 kcal/mol, which helps drive fusion[26,27]. The SNARE complex alone is actually able to fuse the two membranes together (and often called the minimal protein machinery for fusion), but not fuse alone on the timescale required for neurotransmission, and if unregulated this would be dangerous in a neuron[26,27]. After fusion, the complex sits together on the plasma membrane as a cis-SNARE complex in a low energy state where it is disassembled by NSF and endocytosed (*Figure 1.5*)[14].

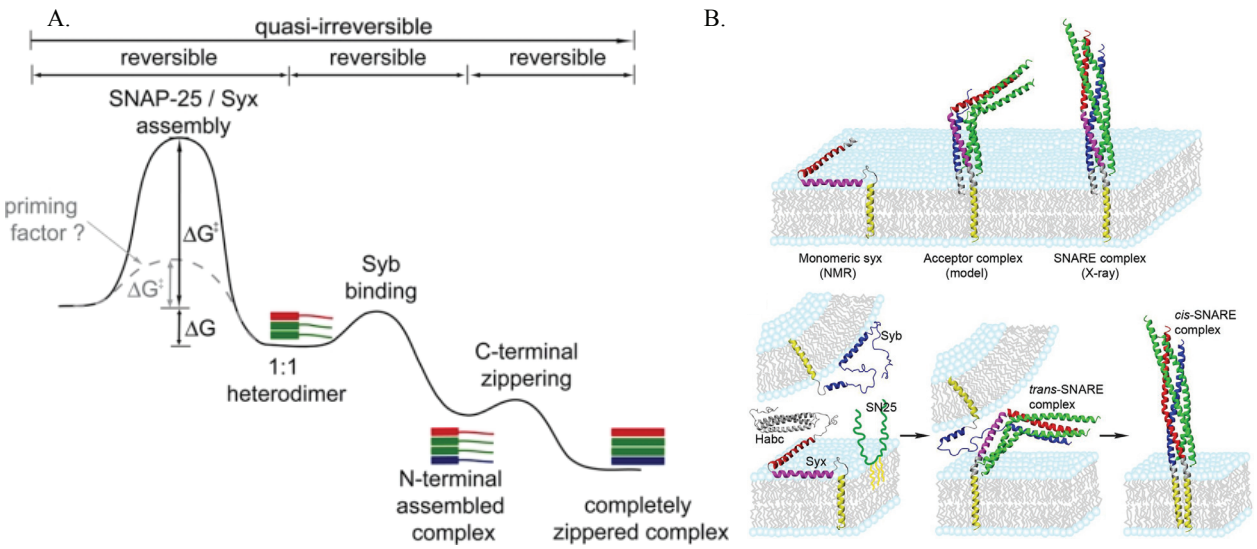

Figure 1.5: Energetics of SNARE mediated fusion and representation of the SNARE complex. A. is from Wiederhold K, Fasshauer D. (2009) *J. Biol. Chem.* **284**:13143–13152. B. is from Laing et al. (2013). *PNAS.* **10:** 19384-19389.

1.3.2.2 Intermediate States for Fusion Pore Opening from the synaptic vesicle membrane and plasma membrane perspective also progress rapidly through a series of intermediate steps. These steps follow: stalk formation, hemifusion, partial fusion pore opening, and full fusion pore opening, which results in release of neurotransmitters into the synaptic cleft[12,14]. Stalk formation involves initial lipid mixing between the synaptic vesicle and the plasma membrane bilayers[14]. Curvature stress of the membranes, potential linker stiffness of the SNARE complex, water removal between the bilayers, hydrophobicity changes within the bilayers, and lipid rearrangements/flipping all contribute to the energy barrier to undergo this step and the following steps[14]. After a lipid and protein stalk is formed, the bilayers between the synaptic vesicle and the plasma membrane merge into a single bilayer interface between the neurotransmitter filled lumen and the synaptic cleft[14]. Next comes partial or full opening of the fusion pore, this stage could be dependent on the number of SNARE complexes involved in each synaptic vesicle fusion[14,28]. It has been proposed that only a single SNARE complex is required for fusion, but for synchronous

fusion more are required to act in unison to open a full fusion pore[28]. The exact number of SNAREs for each fusion pore is not fully known and estimates depend on the study (3-9, 5-11, 5-8, 10-15, overall 3-15 copies per pore)[28]. These copies are also likely tissue specific, as the expression level of SNARE complexes in a synapse with a 40 nm synaptic vesicle and 50 nm active zones places 70-75 copies of SNAREs within the synaptic cleft whereas endosomal or chromaffin cell expression can be up to 100-fold lower[28,29]. The fusion pore makeup is also somewhat up for debate, as it is unclear if this is a pure lipid pore, protein transmembrane domain and lipid pore, or pure protein walled pore[30]. After fusion and release of neurotransmitter the synaptic vesicle merges bilayers completely and is then targeted for endocytosis (*Figure 1.6*)[14].

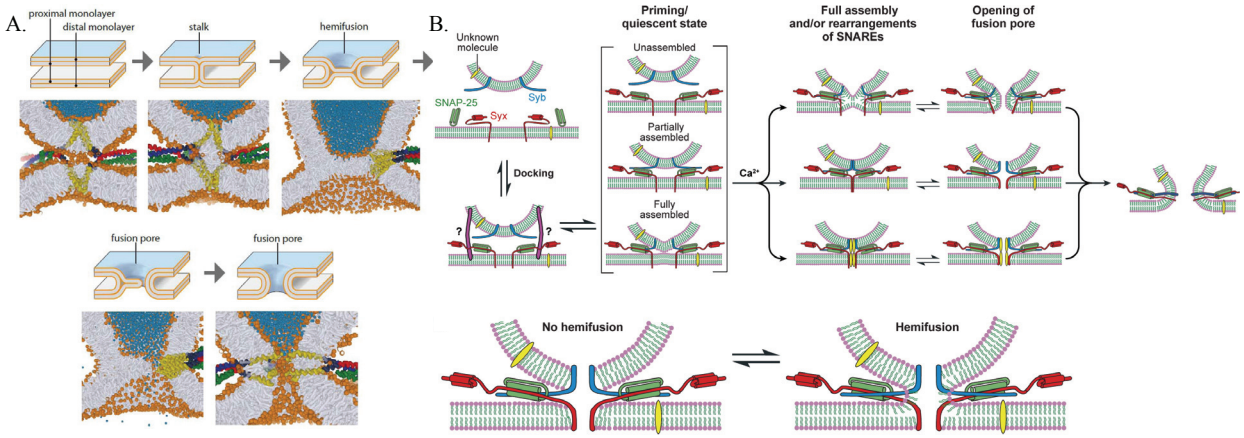

Figure 1.6: Representations of the Intermediates for SNARE-dependent fusion. A. is from Jahn and Fasshauer. (2012). *Nature.* **490:** 201-207. B. is from Chapman. (2008). *Annu Rev Biochem.* **77:** 615-641.

1.3.2.3 Regulatory Proteins play an equally significant role in fusion as the SNARE complex. Without regulatory proteins neuronal fusion (and any other fusion site) would not be a controlled event which occurred through a system of on and off signaling. Small mini-release would be present above baseline levels and the human body would not function regularly. Defects in regulation contribute to diseases and conditions such as chronic pain (most of which are in just

the beginning stages of research) (*Figure 1.7*)[2,9]. A description of various regulatory proteins follow below.

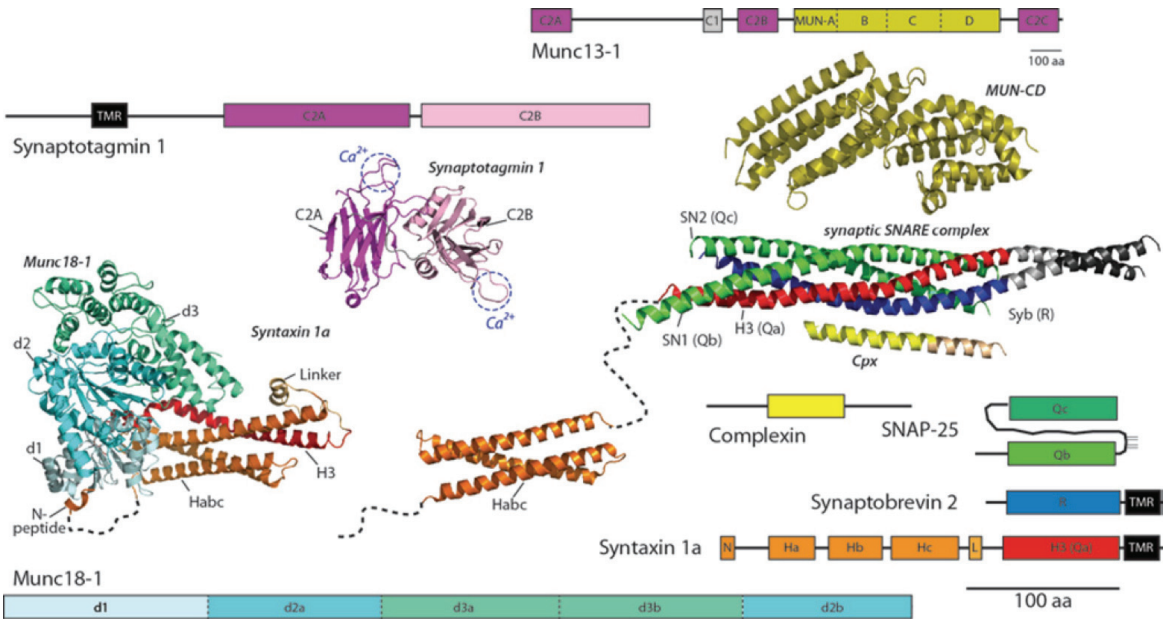

Figure 1.7: Representations of the SNAREs and key Regulatory proteins involved in Fusion. Image is from is from Jahn and Fasshauer. (2012). *Nature.* **490:** 201-207.

1.3.2.3.1 Munc18 is a member of the Sec1 family which acts by regulating syntaxin function[8]. It appears to play a role in inhibiting fusion[10,11]. Munc18 can regulate the equilibrium between the open and closed states of syntaxin[10,11,23,31]. Munc18 is an arched or bean-shaped protein, with a central cavity which has grooves capable of accommodating Syn in the closed state[14,32]. It can hold the Habc domain closed in these grooves until SNAP-25 is present where Munc18 then shifts to accommodate SNAP-25 while opening Syn[23]. It has been debated if Munc18 must be removed before or after addition of SNAP-25, but it appears that a SNAP-25:Syn:Munc18 complex is a better representation of the acceptor complex for fusion[23]. An additional region of Munc18 has also been highlighted to interact with the SNARE complex[33]. This region is a bent extended hairpin in the D3a domain of Munc18 which could act as a scaffold for efficient Syb

structuring (into a helix) and aid in getting Syb into the proximity of the acceptor complex[33]. Munc18 is also capable of disassembling/preventing the off target 2:1 complex of Syn and SNAP-25 for *in vitro* studies (*Figure 1.8*)[23].

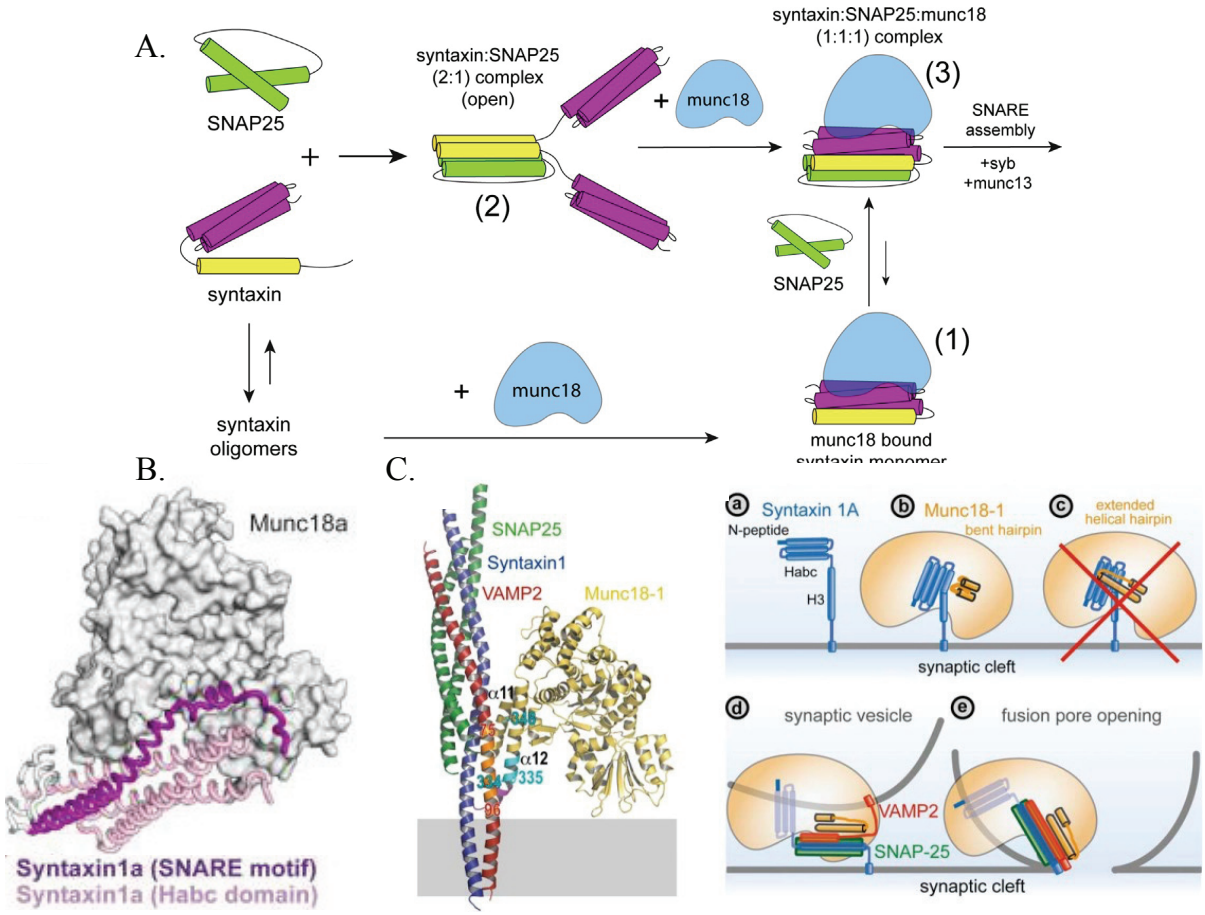

Figure 1.8: Representative Collection of Munc18 Mechanisms. A. is from Dawidowski and Cafiso. (2013). *Biophys J.* **104:** 1585-94. B. is from Baker et al. (2015). *Science.* **349:** 1111-4. and C is from Parisotto et al. *J Biol Chem.* **289:** 9639-9450.

1.3.2.3.2 Munc13 (Mammalian Unc-13) is a member of the CATCHR (Complex Associated with Tethering and Containing Helical Rods) protein family[14,34]. Munc13 is known to act as a regulatory protein in the early and later stages of exocytosis[14]. Munc13s are large, multidomain proteins with domains consisting of: one C1 domain, two C2 domains, and a MUN domain[14]. The C1 domain is a phorbol-ester-binding domain regulated by diacylglycerol, the C2

domains are calcium binding domains, and the MUN domain is conserved throughout the CATCHR family[10,14]. A related protein in the CATCHR family which has a MUN domain and regulates fusion is CAPs (Calcium-dependent Activator Protein for Secretion, Unc31)[34]. The MUN domain within these proteins and alone *in vitro* is known to promote assembly of the SNARE complex for vesicle priming[10,14]. However, the long and flexibly linked domains of Munc13 (and other CATCHR proteins) suggest it likely acts as a scaffold with each C2 domain tethered to the membrane of either the synaptic vesicle or plasma membrane (like synaptotagmins) and the MUN domain in the middle available to act as a binding platform for the SNARE complex[14,35]. Munc13 first appears in the synaptic vesicle cycle as early as the readily releasable pool, regulating its size and population potentially through calcium dependent replenishment and trafficking vesicles from reserved to releasable pools[36]. The role of Munc13 also highlights varying differences in the definition of the readily releasable pool and when a vesicle is in this category[36]. Munc13 is activated by first breaking the regulated heterodimerized form and then recruited by RIM (Rab3-interacting molecules) proteins, which are known as central organizers of the active zone[10]. Once at the active zone, Munc13 is thought to open the acceptor complex, potentially by displacing Munc18 (*Figure 1.9*)[10,14].

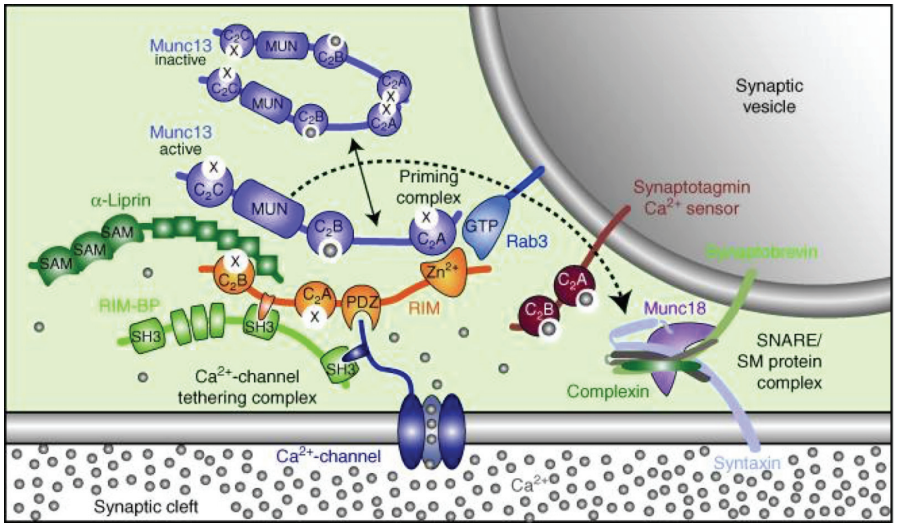

Figure 1.9: Representative Collection of Munc13 Mechanisms. Image from Sudhof and Rizo. (2011). *Cold Spring Harb Perspect Biol 2011;3:a005637.*

1.3.2.3.3 Complexin is a small cytoplasmic regulatory protein thought to both inhibit and activate fusion[14]. In solution complexin (Cpx) is unstructured and is known to bind to the SNARE complex through formation of a small SNARE binding helix. It also has two terminal lipid binding domains which are thought to form helices on the membrane[14]. The dual role complexin plays is thought to work in combination with the calcium sensor for activating and inhibiting fusion[14]. The activating role is localized to the SNARE helix domain, where complexin is thought to stabilize an intermediate state of SNARE formation, by binding to the partially zippered SNARE complex (super-priming)[14,37]. In the inhibitory role, complexin acts as a clamp for SNARE-zippering. The clamp is supposed to be release by Synaptotagmin upon calcium triggering (either due to a direct interaction with SNAREs or a peripheral lipid disruption)[14]. Another inhibitory role has been proposed where Cpx interacts with the acceptor complex, blocking the zippering of Syb and thus fusion[37]. The C and N-terminal domains are also known to bind to membrane (more work has been performed on the C-terminal)[37-39]. This membrane binding is weak and curvature sensitive[37-39]. Binding to the acceptor complex can enhance membrane binding as well as higher degrees of

membrane curvature[37]. This sensitivity could be mediated by Synaptotagmin binding to membrane, which also induces curvature strain (*Figure 1.10*).

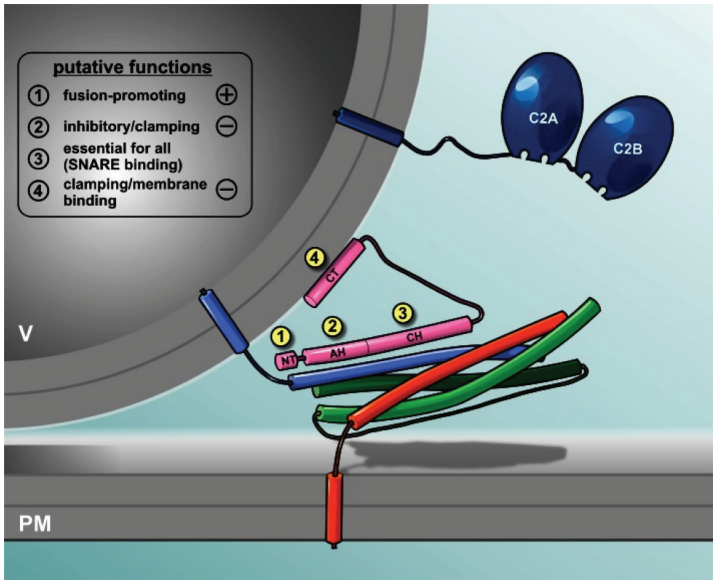

Figure 1.10: Representative Collection of Complexin Function. Image from Mohromann et al. (2015). *Cell Mol Life Sci.* doi: 10.1007/s00018-015-1998-8.

1.3.2.3.4 Additional Regulatory Proteins in addition to those mentioned above include RIMs and Rabs[4]. Rab3 is a vesicle GTP-binding protein[10]. RIM is a large protein consisting of two nested domains which can interact with Rab3[10]. RIM also has a zinc finger which interacts with the C2A domain of Munc13, converting Munc13 to its active monomer form[10]. RIMs are thought to tether Calcium channels to the active zone[10]. A final regulatory protein to mention is the calcium sensor for fusion: Synaptotagmin.

1.3.2.4 The Calcium Sensor for synchronous release is Synaptotagmin-1 (Syt1). Like many of the other regulatory proteins, there are many homologs of Synaptotagmin[40,41]. The first identified was Syt1. At its discovery it was called p65, but soon after 12 other Synaptotagmins were identified[40]. There are now 17 synaptotagmins identified in the mammalian genome[40].

Synaptotagmins are membrane proteins, tethered through a transmembrane helix followed by a flexible linker of variable lengths that connects to, usually two, flexibly linked C2 domains. A short luminal domain is also identified in some of the Synaptotagmin homologs, which is likely unstructured during exocytosis and forms a helix which could cluster Synaptotagmin as a targeting region for endocytosis[42]. C2 domains are conserved domains first identified in protein kinase C[43]. The C2 domain, which is approximately 50 angstroms in length and 25 angstroms in width, is composed of eight antiparallel beta-sheets (beta-sandwich) attached by flexible loops length-wise[40,44,45]. On one side of the domain, the loops are called calcium binding loops on account of their ability to bind calcium and other divalent ions[38,40]. On the opposite end of the domain, there is usually one or two conserved helixes[40,44,45]. The amino acid sequence of the domains often displays conserved lysine rich stretches in one of the beta-sheets (in Syt1 C2B, the polybasic face)[40,44,45].

1.3.2.4.1 Other Synaptotagmins and Proteins with C2 domains are expressed differentially in various tissues and neuron types throughout the nervous systems[40]. Highlighting a few Synaptotagmins: Syt1, Syt2 and Syt9 have been identified as the calcium sensors in synchronous release (*Figure 1.11*)[40,41]. Syt1 is found in many excitatory synapses throughout the brain and body[41]. It is synaptic membrane tethered and contributes to 7% of the protein found on the synaptic vesicle, with ~ 15 Syt1/vesicle (see *Figure 1.3*)[13]. Syt2 is also synaptic vesicle tethered, but it is expressed mostly within Calyx of Held neurons and within either cerebellar basket cells or Purkinje cells[41]. Syt9, which is also called Syt5, is vesicle tethered and localized to striatal synapses and within the olfactory bulb[41]. Syt7 has been identified as the calcium sensor in asynchronous release and is localized to the plasma membrane[20,40].

Not all Synaptotagmins bind calcium, however, as only Syt1, 2, 3, 5, 6, 7, 9, and 10 are calcium binders. Each has a C2A domain which typically binds three calcium ions and a C2B domain which binds two calcium ions[45]. These ions are coordinated mainly through the longer first and third loops of each domain and in solution the calcium affinity of each domain is low (for Syt1, the C2A affinities are roughly 54-75 μM, 530 μM and 20 mM, and the C2B binds at 300-400 to 500-600 μM when measured for soluble constructs)[46,47]. In the presence of charged phospholipid lipid membranes these affinities increase 100-10,000-fold to 1-20 μM calcium (but this is still a measurement of soluble domains *Figure 1.12*)[40]. The domains' affinity for calcium varies among the Synaptotagmins. Syt3, 5, 6, and 10 are located on the plasma membrane and have 10-fold higher calcium affinities than Syt1 and Syt2[40]. These differences in affinities could act as redundant regulators within a hierarchy where if one fails others can substitute in its place[47].

A.

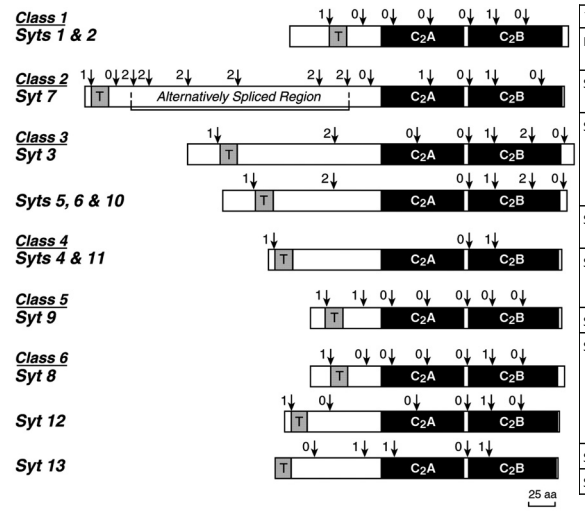

B.

Table 1Localization and Function of Ca2+-Binding Synaptotagmins at Central Synapses

Isoform	Localization	Function	Reference	mRNA Database Entry (Mouse)[a]	Chromosome
Syt1	Many excitatory synapses	Fast Ca^{2+} sensor	Kerr et al., 2008	NM_001252341.1	10
Syt2	Calyx of Held, cerebellar basket cell–Purkinje cell synapse	Fast Ca^{2+} sensor	–	NM_009307.3	1
Syt3	–	Unknown	–	NM_001114116.1	7
Syt5/9[b]	Striatal synapses, olfactory bulb	–	Xu et al., 2007		7
Syt6	–	Unknown	–	NM_018800.4	3
Syt7	–	Asynchronous release, facilitation, replenishment; Ca^{2+} sensor at chromaffin cells	Liu et al., 2014, Jackman et al., 2016, Luo and Südhof, 2017	NM_018801.3	19
Syt9[b]	–	Unknown	–	NM_021889.4	7
Syt10	Olfactory bulb	IGF-1 release	–	NM_018803.2	15

Figure 1.11: Synaptotagmins classes, structure, and localization comparison. A. is from Sudhof. (2002). *JBC.* **277:** 7629-7632. B. Is from Chen and Jonas. (2017). *Neuron.* **94:** 694-696.

There are also other C2 domain proteins which do not fully fit the Synaptotagmin sub-type such as: extended Synaptotagmins, rabphillins, DOC2B, Munc13, and ferlins[44-51]. Extended Synaptotagmins are found in yeast and partake in trafficking of glycerolipid within the endoplasmic reticulum[48]. Rabphillins are neuronal proteins which interact with the actin cytoskeleton and endocytosis, potentially through in PIP_2 binding[49]. DOC2B is involved in diacylglcerol and Munc13 binding and translocation[50]. Ferlins, including: dysferlin, myoferlin, and otoferlin, have ~ 6 C2 domains and are involved in membrane fusion and trafficking involved in either muscle development or hearing[51]. Ferlins are suspected to function similarly to Syts, being involved in lipid specific interactions, but potentially have more C2 domains since the signaling events need to occur faster than neuronal signaling[51]. While not all of these C2 domain proteins are involved directly in fusion events, each seems to act in some way with its environment, specifically with lipids.

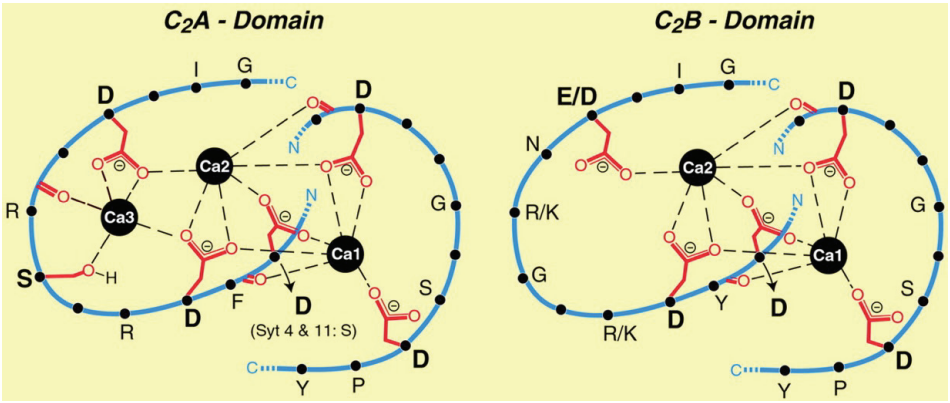

Figure 1.12: Synaptotagmins C2 domains Calcium Binding Loops Coordination to Calcium. Image is from Sudhof. (2002). *JBC.* **277:** 7629-7632.

1.3.2.5 Lipids and Ions are as important as the molecular machinery within the synaptic cleft. Lipid and ionic components of the aqueous solution play important roles in exocytosis, whether it is a direct interaction with proteins (like Syn and Syt1 with charged ions and lipids), or more indirect (like changes in fluidity and curvature).

The synaptic vesicle membrane is ~50% lipid (roughly 6992 lipids total) and is composed of a mixture of: 36% (2524 molecules of) phosphatidylcholine (PC), 41% (1621 C1-ester and 1311 C2-ether molecules of) physphatidylethanolamine (PE), 12% (857 molecules of) physphotidylserine (PS), 2% (132 molecules of) phosphatidylinositol (PI), 7% (516 molecules of) sphingomyelin, and 1.5% (108 molecules of) hexosylceramide[13]. The surface is also composed of 5663 molecules of cholesterol within this bilayer[13]. According to early studies the plasma membrane surface is composed of: ~34% PC, ~28% PE, ~11-15% PS and PI, ~1% phosphatidylinositol 4,5-bisphosphonate (PIP_2), ~20-21% cholesterol, and 1-6% of ceramide, glycolipids and sphingomyelin[52]. The acyl chain composition of these lipids is diverse covering 16:0 to 22:6 saturation of chains, the highest percent being 18:0 and 22:6 chains[52]. The exact distribution of lipid content on the plasma membrane is slightly more variable, but 36% PC, 30% PE, 15%, PS, 1% PIP_2, and 20% cholesterol is often used to mimic physiological conditions[24]. The plasma membrane bilayer is also asymmetrically distributed between the cytosolic and exofacial (synaptic cleft side) leaflets[53]. One large asymmetric distribution is of cholesterol, which is biased toward the cytosolic leaflet[53,54]. PIP_2 is also particularly interesting because of its large bulky headgroup that could sit up to 5.5 angstroms above the bilayer headgroups, and its high charge concentration (-4)[55,56]. PIP_2 may be capable of charge clustering, which would provide targets for membrane binding proteins such as synaptotagmin[56]. PIP_2 is also a second messenger in the cell and is cycled through its charge (and naming) depending on the stage in exocytosis and endocytosis (*Figure 1.13*)[55]. All of these lipid types/makeups including cholesterol create two surfaces which themselves can vary characteristics such as: fluidity (cholesterol, acyl chain packing), curvature (lipid head and asymmetric distribution of leaflets), distribution/packing (lipid sequestration or lipid mediated protein sequestration), and charge (headgroup charges)[10,14,53,54].

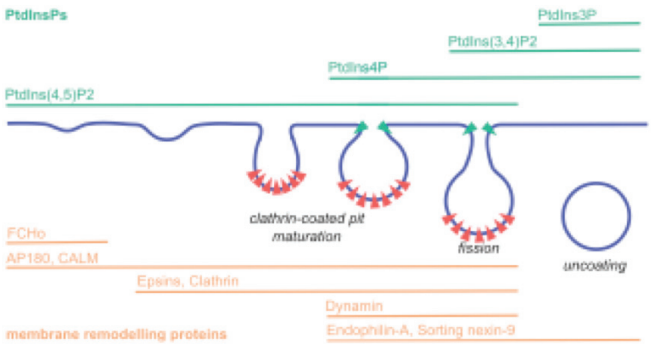

Figure 1.13: PIP Cycling throughout Exocytosis and Endocytosis. Image is from Lauwers et al. (2016). *Neuron.* **90:** 11-25.

The cytosolic composition at the synaptic cleft is also composed of a diverse set of ions in flux which work between and against each other to maintain balance in the cell and to signal events. The salt makeup of the aqueous solution around the synaptic cleft is ~140 mM KCl and ~10 mM NaCl, but this changes throughout an action potential event[4]. Calcium influx which signals fusion causes a ~16-fold increase in the concentration of resting calcium concentrations (0.1 μM resting levels to a 1.5-10 μM)[4]. ~1.4 mM (or higher depending on estimations and the stage in vesicle cycling) ATP and magnesium are also present in the cell acting as an energy source for neuronal exocytosis and endocytosis (such as to ATPases)[57,58]. ATP levels are known to cycle throughout signaling events, likely through release from reserve pools at times of energy strain[57,58]. While these ions have direct roles for maintaining concentration gradients inside and outside the cell and providing energy to molecular machines, they also have indirect (and regulatory) effects on the lipids and proteins around them. Lipids adsorb ions at specific concentrations creating an ionic double layer and altering local concentrations of ions, like calcium on the surface which could enhance Syt1 binding[58]. Charge variations whether through salt or polyvalent ions in the aqueous environment can also shield different protein interactions[59,60]. ATP in particular has been a highlight in unexpected regulation of the SNARE complex and Syt1[59,60].

1.4 Proposed Synaptotagmin-1 Mechanisms

Synaptotagmin 1 is an extensively studied protein, but how it fulfills its role as the calcium sensor and contributes to the energy required for SNARE dependent fusion is still unclear. Again, Syt1 is a membrane tethered protein with two flexibly linked C2 domains. Within these domains both C2A and C2B bind to calcium and insert into membrane[62]. When studied in the soluble constructs alone as C2A and C2B the calcium binding loops insert to membrane at affinities which vary according to the lipid composition present[62,63]. When the C2A and C2B domains are tethered their affinities are not additive suggesting they act cooperatively or synergistically to promote into mutual membrane insertion[62,63]. Aside from the calcium binding loops, two additional regions have been highlighted as critical regions in the C2B domain: the arginine apex and the polybasic face[64-67]. The arginine apex is composed of two arginine residues, R398 and R399 which are proposed to interact with either SNAREs or membrane[64]. When these residues are mutated to glutamate synchronous release is inhibited[64]. The polybasic face is a positively charged poly-lysine stretch (often focused around K326, K327) on C2B known to interact with negatively charged complexes, whether they are: DNA, SNAREs, or lipid[65,66]. DNA is an off-target contaminant (through unsuccessful purification) with the polybasic face which blocks other charged interactions and must be avoided to ensure binding effects are physiologically relevant[67]. C2A also has a smaller

lysine rich region, but it is not highlighted in any key interactions during fusion. The C-terminal amphipathic helix of C2B has also been highlighted for potential interactions with membrane[68]. Regions that are less studied are the luminal domain and juxtamembrane linker of Syt1, because very little research has been performed on the Full-length Syt1[11,42]. The luminal domain is likely unstructured during exocytosis[11,42]. The linker region consists of a cysteine populated region after the transmembrane domain, with the cysteines likely palmitoylated (with additional post translational modifications throughout the linker)[69]. The linker also has two large regions of positive and negative charge and a glycine zipper, but any structuring or function during fusion is unclear[69,70]. While the functional role of Syt1 has yet to be solidified one trend emerges, Syt1 triggers and regulates fusion through either direct contact with SNAREs or contact with lipid (or both) (*Figure 1.14*).

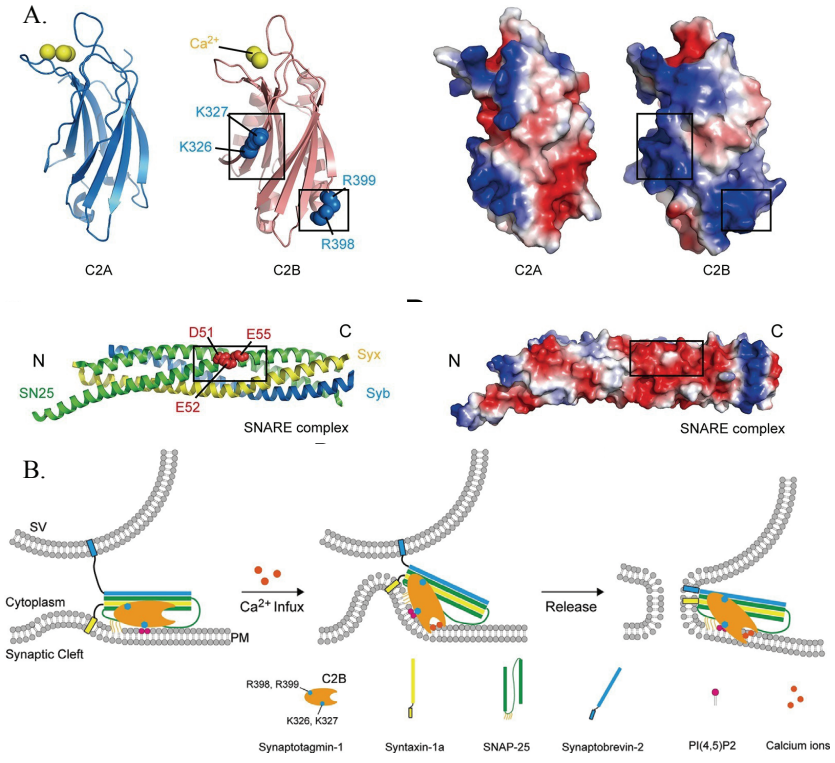

Figure 1.14: *Representation of Charged Surfaces on Syt1 and SNAREs and how they could interact through the Arginine Apex.* Images are from Wang et al. (2016). *eLife* 2016;5:e14211.

1.4.1 The "Protein-centric" and "Lipid-centric" approaches

In order to achieve fast and efficient fusion, the fusion machinery and regulatory proteins must be concentrated and within close proximity to each other all around the synaptic vesicle and plasma membranes. This leads to two main perspectives regarding synaptotagmin's regulatory function in the field: one where the direct interaction with SNAREs as molecular machines is the priority and lipid interactions are secondary calcium sensing effects (protein-centric) and one where the lipid interactions are the priority and indirectly regulate SNARE binding, with nonspecific SNARE interactions as secondary effects (lipid-centric). Each of these ideas involves the same key regions in Syt1: the calcium binding loops in the C2A and C2B domains, the arginine apex in the C2B domain, the polybasic face in the C2B domain, and the amphipathic helices in the C2B domain (though this one is far less common). The majority of these mechanisms and contacts are driven by basic principles: electrostatic interactions, coordination chemistry, hydrophobicity, and steric hinderance.

Early work highlighted Syt1 as a calcium binding protein, which interacts with the lipid membrane through calcium dependent insertion of the calcium binding loops[10,12,14,71]. Through this established function, there was an additional search for how Syt1 regulated the fusion machinery[10,14,71]. Early work using pull-down assays identified a direct interaction between Syt1 and Syn[71]. Another idea was that Syt1 and complexin must work against each other binding to the SNARE complex as an activator and inhibitor, respectively[12,14,19]. These ideas spurred a protein-centric race to determine the exact binding site between the SNARE complex and Syt1, a few example interactions follow.

The arginine apex focus: In one example, a combination of fluorescence techniques and pull-down assays highlight key interactions between the SNARE complex, which has a region of positive charge on SNAP-25 that interacts directly with the negatively charged region of the arginine apex[65]. Here, preceding calcium influx, the Syt1 polybasic face interacts with charged lipids on the plasma membrane (PIP_2) as well as the arginine apex-SNARE contact[65]. Upon calcium influx these contact sites remain, but the calcium-binding loops of the C2B domain also insert into the plasma membrane bilayer. This creates curvature strain and aids the SNAREs in creation of the fusion pore (see *Figure 1.14*)[65].

The polybasic face focus: In a few examples using a combination of crystallography, fluorescence techniques (such as FRET and lipid mixing experiments), and knockout studies using excitatory postsynaptic currents (EPCs), authors found the polybasic face from the synaptic vesicle can hold a contact with the charged region in SNAP-25, which is tethered to the plasma membrane in a calcium independent manner. This interaction would bridge the two bilayers and bring Syb into proximity to the t-SNAREs, priming them for fusion,[64,65,72]. Calcium influx would then bring the bilayers closer in proximity as Syt1 inserted into the plasma membrane and the SNAREs would zipper and fuse the bilayers[66]. This idea leaves the option for the additional interaction between the synaptic vesicle and the arginine apex to decrease the inter-bilayer distance, further aiding SNARE dependent fusion[64]. A third example assesses the idea that curvature strain by Syt1 could help disrupt the bilayers, assisting fusion (*Figure 1.15*)[72].

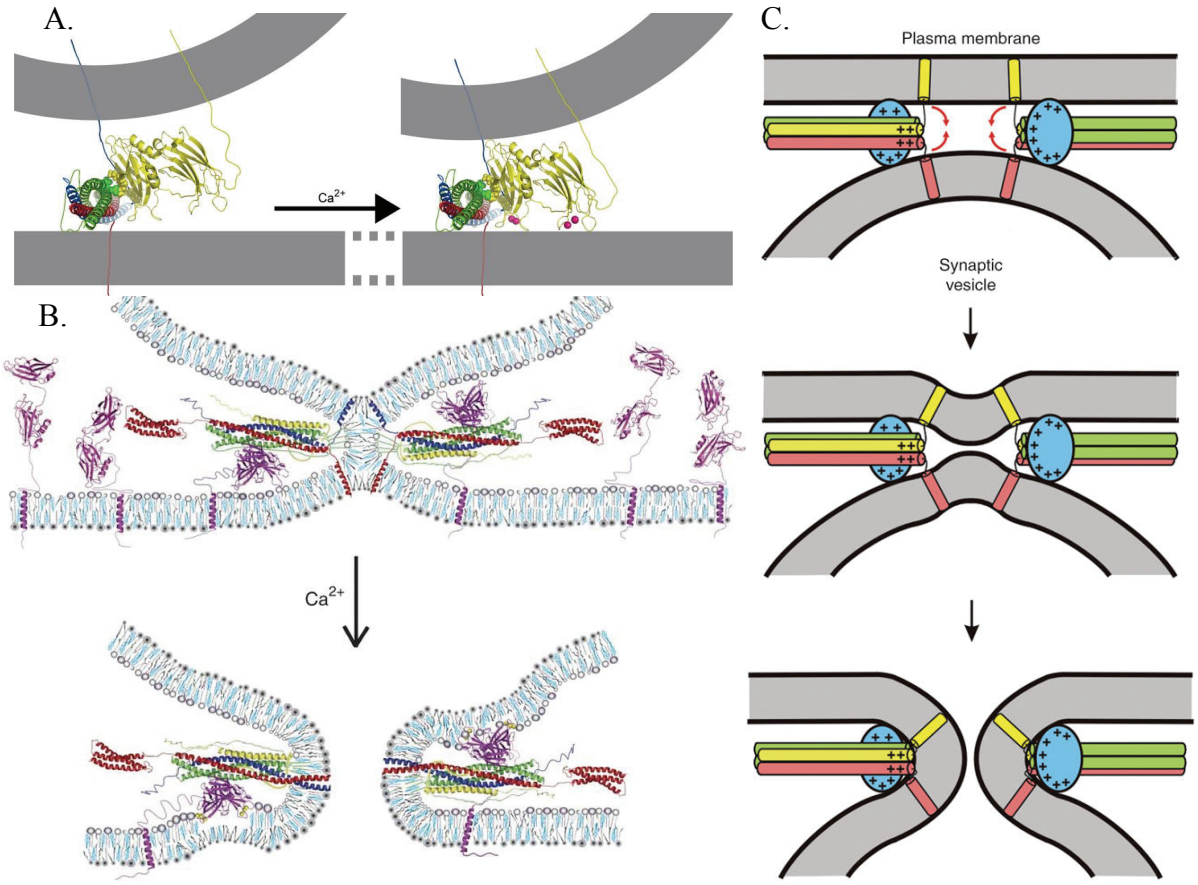

Figure 1.15: Representation of how Syt1 and SNAREs could interact through the polybasic face. A. is from Loewen et al. (2006). *Mol biol. Cell.* **17:** 5211-5266. B is from Vrljic M, et al. *Nature structural & molecular biology*. 2010; 17:325–331. C. is from Xue et al. (2008). *NSMB*. **15:** 1160-1168.

The C2B helix focus: Through work using crystallography, isothermal titration calorimetry, and EPCs, a mechanism is presented that highlights the interplay between Syt1 and complexin, after it was accepted that the two could bind to SNAREs simultaneously, rather than competitively in the same binding site[73]. Here, the amphipathic HA helix on the C2B domain contacts Syn in the SNARE bundle, and complexin binds Syb in the turn of the bundle[74]. There is also an additional C2B domain attached to SNAP-25 through the polybasic face[73]. The idea is that complexin and Syt1 form an additional, 5th, helix within the bundle[73]. This in combination with the additional

C2B domain on SNAP-25 locks the partially unzippered SNAREs apart. Upon calcium influx, the helix in Syt1 disconnects from the bundle, unlocking it (*Figure 1.16*)[74].

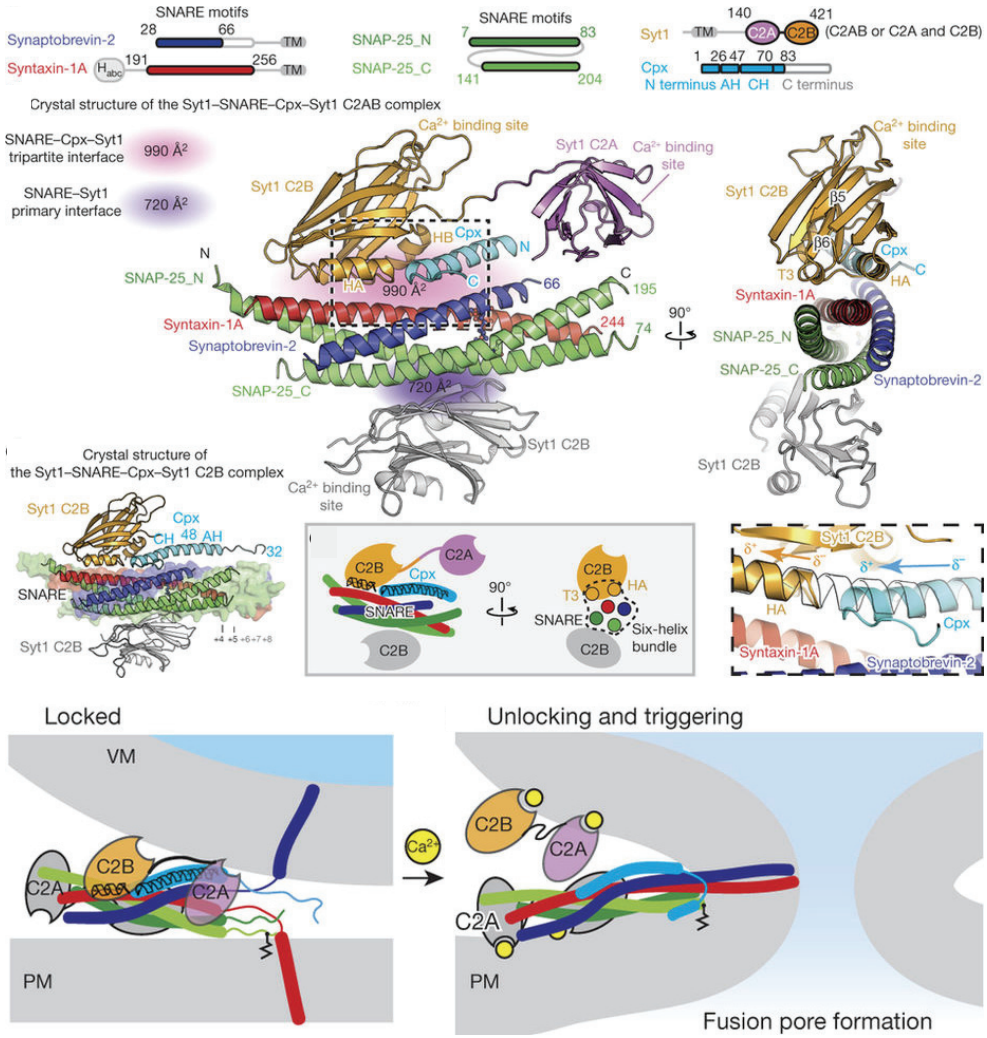

Figure 1.16: Representation of how Syt1 and SNAREs could interact through the Amphipathic Helix. Images from Zhou et al. (2017). *Nature.* **548:** 420-425.

Having observed such diversity of the proposed SNARE-Syt1 contacts, it seems that there is likely not a single contact site between the proteins. This heterogeneity between different sites on Syt1 and weak overall binding to the SNARE complex has been observed over a series of EPR and FRET measurements[74]. An additional observation is that many SNARE-Syt1 binding events are enhanced by binding at lower physiological salt, but when under physiological concentrations of salt, including ATP, the Syt1-SNARE interaction is abolished[74]. Only the Syt1-membrane

interaction, driven by PIP2, remains and is observed through a series of florescence, EPR, and *in vivo* amperometry (*Figure 1.17*)[61]. This transitions to a more lipid-centric focus.

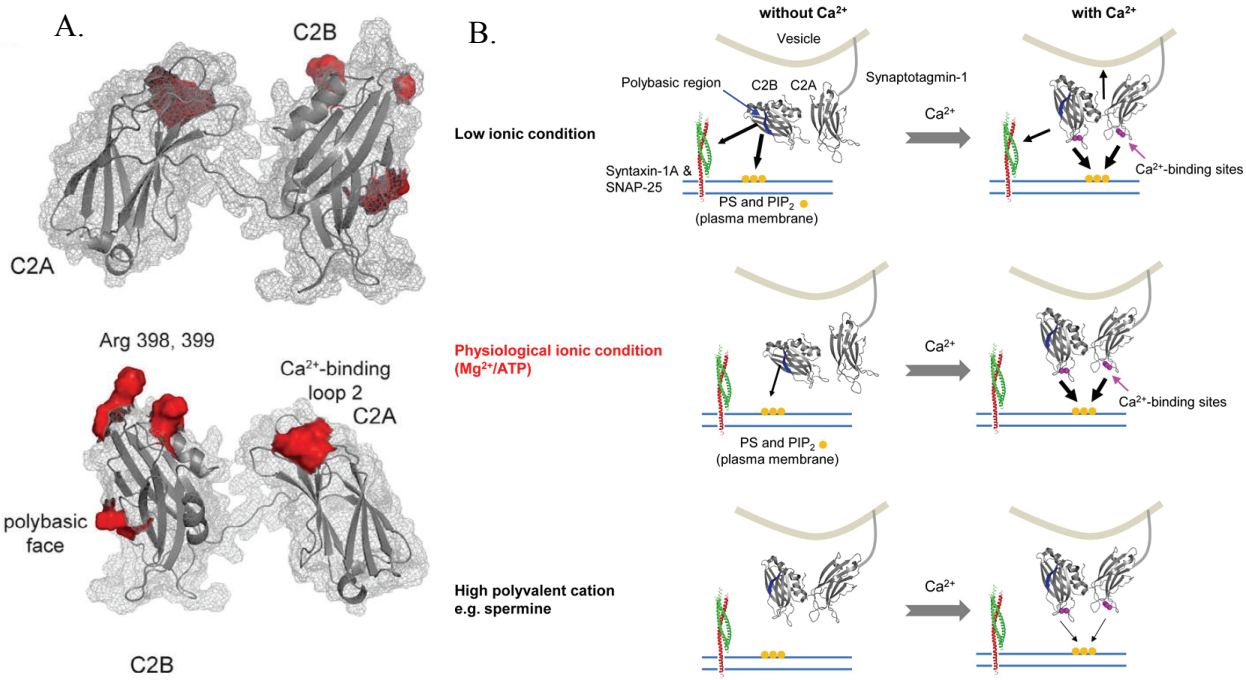

Figure 1.17: Representation of the Heterogeneous interaction between Syt1 and SNAREs. A. is from Lai et al. (2011). *J Mol Bio.* **405:** 696-706. B. is from Park et al. (2015). *NSMB.* **22:** 815-823.

The polybasic face focus: Syt1 is known to interact with negatively charged substances through the polybasic face on the C2B domain[62,63,65,75]. The polybasic face has been proposed to act in both calcium dependent and calcium independent lipid interactions to regulate the fusion process[62,63,65,75]. Calcium dependent and independent processes include: Syt1 forming oligomers, Syt1 binding to negatively charged phospholipids (like PS and PIP_2), and Syt1 simultaneously binding to the synaptic vesicle and plasma membranes[66]. Again, calcium dependent oligomerization and Syt1 negatively charged lipid binding have been proposed to regulate the opening, dilation, or stabilization of the fusion pore[66]. Simultaneously binding to both membranes should accelerate membrane fusion by bringing the synaptic vesicle and plasma membranes into close proximity[66]. Calcium independent interactions between the polybasic face and high

concentrations of charge on the plasma membrane (either PS clusters or PIP_2) would aid in initial docking of Syt1 tethered synaptic vesicles[62,63,66,75]. One proposed mechanism, from EPR and docking measurements, is that the C2B domain could act as an electrostatic switch, first priming the vesicles in a calcium independent manner through charge interactions between the polybasic face and the plasma membrane while also bringing the SNAREs into proximity[62,63]. Next, upon calcium influx the orientation of the domains switch, inserting the calcium binding loops into PS and other charged lipid, either through coordination or electrostatics, which would pull the synaptic vesicle closer to the plasma membrane in range for the SNAREs to fuse[62,63]. An additional interaction of the polybasic face with the plasma membrane containing PIP_2 has also been shown to tilt the C2B domain toward the membrane, which would drive the two membranes even closer[75]. An additional regulatory process, driven by ATP, between the polybasic face and the membrane has also been observed using cryo-EM and fluorescent techniques, wherein ATP can compete with the charge on the membrane to prevent calcium independent binding (*Figure 1.18*)[61].

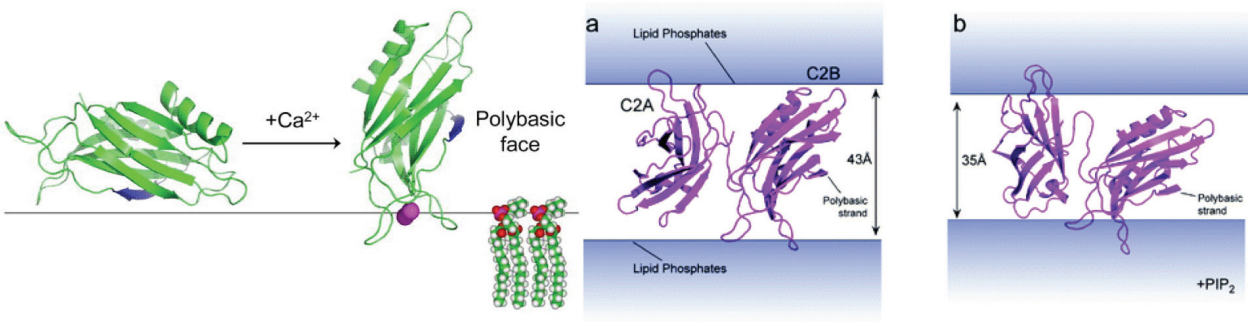

Figure 1.18: Representation of how Syt1 and lipid membrane could interact through the Polybasic Face. A. is from Kuo et al. (2010). *J Mol Bio.* **387:** 284-294. B. is from Kuo et al. (2011). *Biochemistry.* **50:** 2633-2641.

Soluble Syt1 fragments are also known to aggregate vesicles[76,77]. This aggregation is thought to be evidence that Syt1 can bring the two bilayers together for fusion and is frequently observed on an EM grid[66,77]. Vesicle aggregation and clustering of soluble Syt1 on a membrane

has been observed in many forms, such as: ring formation, box formation, tubule formation and other membrane defect causing formations (deemed clams and volcanos, similar to tubules)[76,77,78]. From these observations arises the idea that protein rings form around a fusion pore (and vesicle docking site), which is a common theme for Syt1 function. The idea of Syt1 rings has been presented in many different forms, initially as speculation that a protein like Syt1 could induce steric clash between membranes along with Munc18[78]. This progressed into a thorough investigation of C2B domain ring formation driven by the polybasic face. This theory was initially called the washer model because the C2B domain formed rings between the synaptic vesicle and the plasma membrane, which would block membrane binding until calcium influx[77]. Here the C2B domain would rearrange, inserting the calcium binding loops and thus breaking the washer, permitting fusion[79]. This theory progressed after observing rings from other C2B domain containing proteins to the idea that 'halos' can arise in solution; their formation driven by ATP dependent ring formation through binding to the polybasic face. This interaction is then out-competed by PIP_2 binding on the membrane surface[79-82]. The rings still break apart upon calcium influx[79-81]. This has also led to the hypothesis that these rings bind to SNAREs along the HA helix of C2B as mentioned above[82]. However, these observations are usually under low salt conditions with high charge densities of lipid on the membrane[79,80]. When salt and charge concentrations become more physiological, the number of rings observed decreases significantly[79,80]. The rings also conflict with the previously observed Syt1 rings which were formed upon calcium addition (*Figure 1.19*)[77].

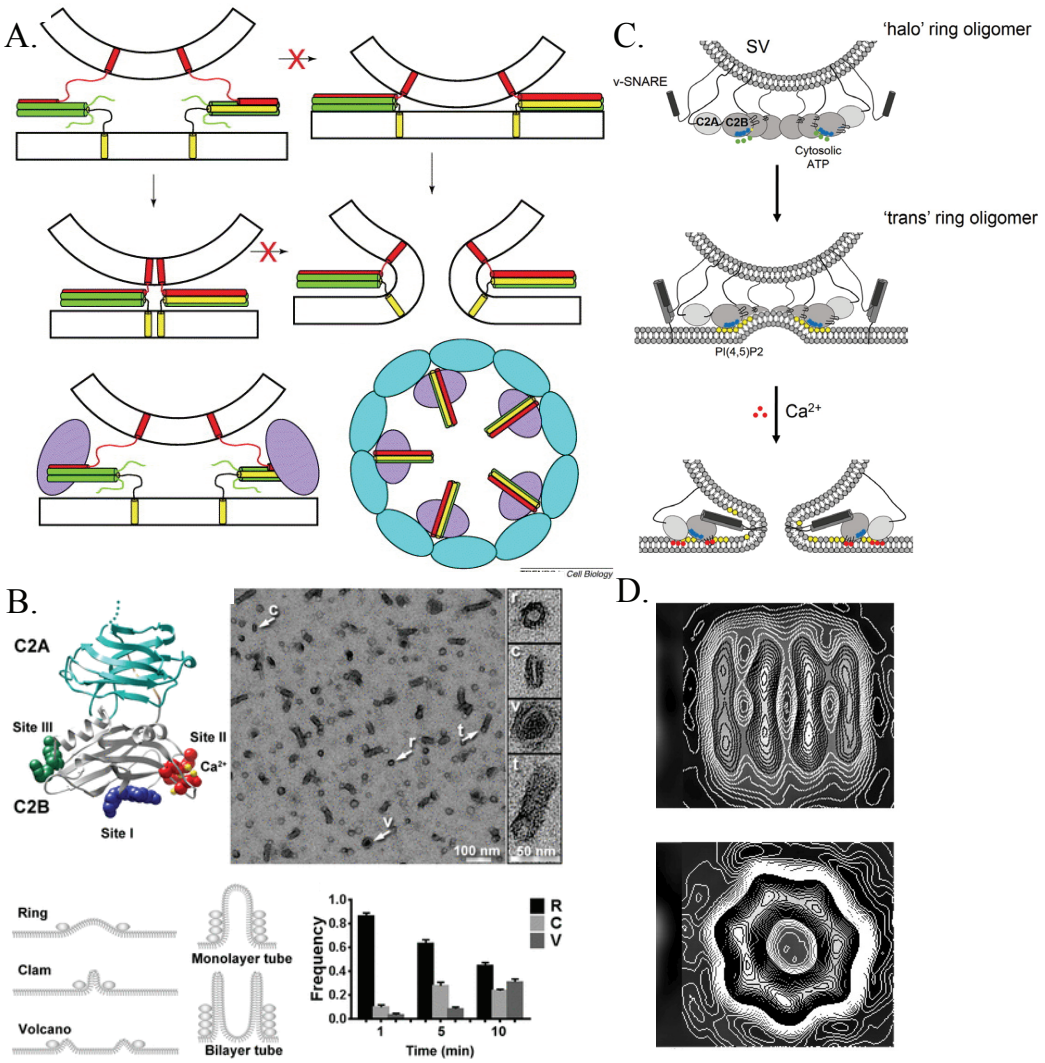

Figure 1.19: Representation of how Syt1 and lipid membrane could form Oligomers or Rings. A. is from Rizo J, Chen X, Arac D. *Trend Cell Biol*. 2006; 16:339–350. B. is from Wang et al. (2014). *PNAS.* **11:** 13996-13971. C. is from Wang et al. (2017). *Elife.* doi: 10.7554/eLife.27441. D. is from Wu et al. (2003). *Proc natl acd sci usa.* **100:** 2082-7.

The arginine apex focus: The arginine apex is located opposite the calcium binding loops in the C2B domain and has been observed to insert into lipid[64,75]. The idea is that the C2B domain can bridge bilayers[64,75]. When the arginine apex is mutated to glutamates in fluorescence, EPR, and *in vivo* studies, the soluble fragment of Syt1 also cannot aggregate vesicles, suggesting it is critical for the bridging process[64]. This proximity can be enhanced depending on the lipids present in the membrane. PIP_2 is known to interact with the polybasic face of C2B. If three points on the

C2B domain were interacting with opposing membranes, it would orient the domain such that the bilayers are very close together and place a large amount of strain on the bilayers, helping to accelerate SNARE dependent fusion (*Figure 1.20*)[75,83].

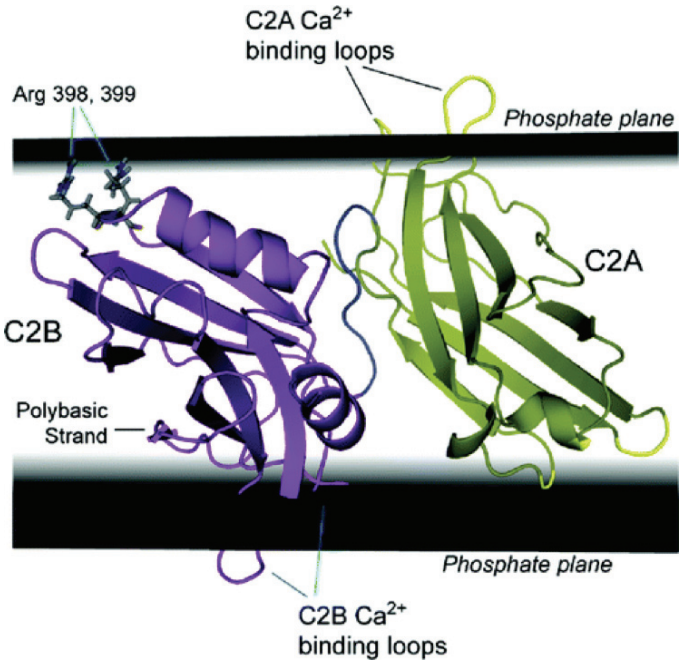

Figure 1.20: Representation of how Syt1 and lipid membrane could interact through the Arginine Apex. Image is from Kuo et al. (2011). *Biochemistry.* **50:** 2633-2641.

Curvature strain, the amphipathic helix, and lipid sequestration: Another frequent observation is that Syt1, along with vesicle aggregation and tabulation, can induce lipid defects which produce curvature strain on the membrane[76,83]. This curvature effect is calcium dependent and produces strain on the membrane which decreases the stability of the bilayer, which could promote fusion, also observed on EM grids[84]. The curvature defect itself creates a buckle in the membranes. This is closer (visually) to stalk formation, the first stage in fusion and the highest energy barrier to overcome (observed by promoting lipid mixing of the two bilayers). The buckling of the membrane is theorized to decrease the energy required for stalk formation by 20 k_BT, which would cut the stalk formation energy (40 k_BT) in half, where the remaining energy would come

from the bilayers themselves[76]. Syt1 is thought to drive this bilayer change by calcium dependent insertion of the calcium binding loops into one leaflet, of the bilayer[83]. It could also occur through insertion of the amphipathic C-terminal, HB-helix on the C2B domain, observed using simulation in NAMD[68]. Both would expand the area the lipid heads occupy, but the acyl chain packing would be unchanged. This would create an empty space below the calcium binding loops, filled by rearrangement and tilting of the acyl chains[83]. The bending and tilting effect appears to then propagate throughout neighboring lipids of the same leaflet and the opposite leaflet, creating local positive curvature and lipid disordering[83]. Syt1 is capable of binding to both the plasma membrane and the synaptic vesicle membrane, which could create counter buckling, which is very close to stalk formation itself[83]. This binding could be driven either by the loops or the arginine apex, or again by a conformational change/switching of the HB-helix in C2B[68,83]. After buckling of the two bilayers' adjacent leaflets, the outer leaflets are then under a high degree of stress which likely facilitates the hemifusion and fusion pore opening[83].

This theory, from work using EPR, FTIR, and fluorescence techniques, ties nicely into the observation that Syt1 C2A and C2B domains' calcium binding loops are known to preferentially bind to PS in the presence of calcium[84]. This is either through electrostatic interactions between the calcium binding loops and negatively charged PS or it is driven by coordination directly to the PS molecules (see *Figure 1.12*)[58,84,85,86]. Syt1 calcium is known to incorporate PS into open coordination sites when PS is present[58,85]. PS itself also induces positive curvature in membranes, and in a mixed lipid environment PS does not form ideal mixtures[84]. This creates a cycle where if Syt1 can sequester the PS in a membrane, this would induce a curvature effect and cluster the PS charges, both of which will enhance Syt1 binding, enhancing the curvature strain on the membrane and again promoting stalk formation[84]. The PS clustering also has the added benefit of sequestering

charge away from the SNARE complex, which may be inhibited by charge interactions on the membrane (*Figure 1.21*).

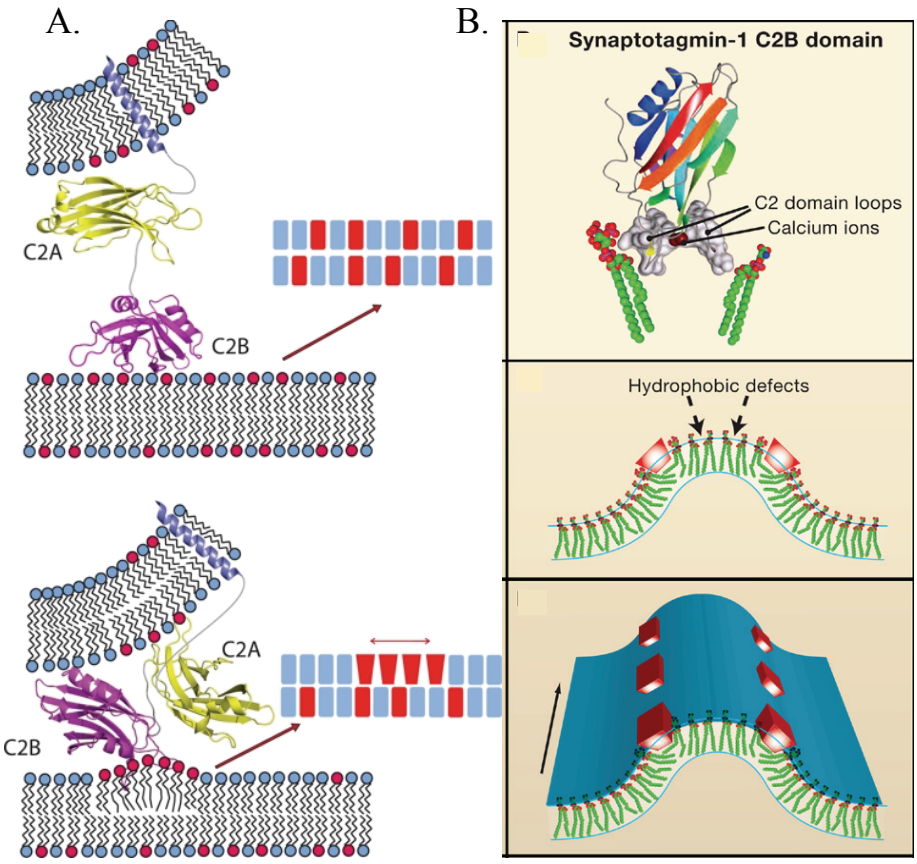

Figure 1.21: Representation of how Syt1 and lipid membrane could cause Curvature Strain. A. is from Lai et al. (2011). *JBC.* **286:** 25291-25300. B. is from McMahon et al. (2010). *Cell.* **140:** 601-605.

These theories all present compelling evidence that Syt1 bridges bilayers as a result of calcium influx and alters lipid composition and structure, peripherally enhancing SNARE dependent fusion. Syt1 also likely comes into occasional direct contact with the SNARE complex, enhancing localization in the fusion pore and potentially regulating the steps in fusion. The largest issue with these mechanisms however, is that very little work has been performed examining the full-length versions of these proteins. The soluble constructs are likely suitable substitutes but driving and regulating membrane fusion is probably enhanced when the domains are already

tethered to one of the two membranes. This could mean that subtle effects within these proposed mechanisms would be more obvious in the full-length protein.

1.5 Research Aims

Syt1 is well established as the calcium sensor in neuronal exocytosis. Syt1 binds to membrane and potentially the SNARE complex, but how these roles help trigger and drive SNARE dependent fusion on the sub-millisecond timescale is still unclear. The aims in this work will focus on gaining a deeper understanding of Syt1-membrane interactions at specific locations on the C2 domains, such as the calcium-binding loops and the polybasic face, and any effects these may have to help drive fusion. This membrane interaction and insertion is again lipid specific with certain head groups required to drive membrane insertion and bridging[76]. This headgroup specificity and varied lipid compositions in the plasma membrane vs. the vesicle membrane (mainly PIP_2 presence only on the plasma membrane) could play a key role in Syt1 activating fusion.

The Ca^{2+} binding loops located in both the C2A and C2B domains of Syt1 interact with PS headgroups located on both the vesicular and plasma membrane[75,85]. This interaction is potentially driven through coordination and/or electrostatic interactions, while the polybasic face is thought to interact electrostatically with PIP_2[85]. The C2A domains' Ca^{2+} binding loops show clear Ca^{2+} dependent binding to PS[87]. The C2B domain has been proposed to act as an electrostatic switch, with initial Ca^{2+} independent binding through its polybasic face[88]. Ca^{2+} influx switches the interaction mode and C2B domain orientation allowing insertion and burial of the Ca^{2+} binding

loops, potentially leading to a stronger and closer bridging interaction. The aim of this work is to further understand the lipid specific interactions between Synaptotagmin-1 and how this would drive the C2A and C2B domains either to the vesicular or plasma membranes.

The first major aim of this work focuses on the question: does Syt1 membrane insertion and orientation change in the presence of different lipids? In the Cafiso lab, this was approached through EPR CW and power saturation measurements in the calcium binding loops of the C2A and C2B domains and areas near the polybasic face on the soluble C2AB construct. The goal was to orient and map the domains insertion to the bilayer. This was achieved through docking of the soluble C2AB domains to look at insertion and orientation differences under different membrane compositions. This investigation, in collaboration with work from members in the Cafiso and the Jahn labs (Max Plank Institute for Biophysical Chemistry, Germany) uses a combination of different structural and functional techniques to reach the conclusion that PIP_2 and PS cooperate to trap Syt1 to the plasma membrane in the presence of calcium[88].

The second aim of this work focuses on moving to more physiologically similar work on the full-length version of Syt1. Initial purification optimizations were performed, with a series of CW EPR and pulsed-EPR measurements used to compare the result of purifying the full-length construct in either OG or CHAPs. This work highlights that differences in purification can result in different Syt1 protein states when reconstituted into membrane[89]. Additional characterization of the CHAPs procedure using CW EPR, power saturation EPR and TIRF, in comparison to the soluble domains, will be shown as validation for the choice to proceed with the CHAPs protocol[89].

The third aim of this work focuses on the driving forces for membrane insertion including work on the full-length Syt1. Previous work in only the soluble constructs of Syt1 and homologous C2 domains could not fully differentiate the electrostatic and coordination-based interactions of

the protein to the membrane[85,87,90]. To contribute to this investigation, experiments on the soluble constructs, including ultracentrifugation sedimentation assays, were combined with CW and power saturation experiments on the full-length Syt1. In collaboration with the Igumenova lab (Biochemistry and Biophysics, Texas A&M University) this work highlights the use of a non-native metal ion, cadmium, in revealing the dual roles of coordination and electrostatics in Syt1 membrane interactions[86].

The fourth aim of this work attempts to propose a mechanism for Syt1, the distance regulator. A series of CW EPR, power saturation EPR, pulsed-EPR, HSQC-NMR and other experiments explored vesicular (*cis*) and plasma membrane binding (*trans*) of Syt1 under various physiologically relevant lipid, salt, and ion composition to determine if Syt1 may act as a distance regulator between the vesicle and plasma membranes for SNARE-dependent fusion.

1.6 References

1. Thorn, et al. (2016). Exocytosis in non-neuronal cells. *Neurochemistry.* **137:** 849-859.
2. Gleitman, H., Gross, J., & Reisburg, D. (2011). Psychology, 8th edition. New York: W. W. Norton.
3. Milijkovic et al. (2013). Multiple Sclerosis: Molecular Mechanism and Therapeutic Opportunities. *Antioxidants and redox signaling.* **19:** 2286-2334.
4. Reichardt and Kelly. (1983). A molecular description of the nerve terminal function. *Annu Rev Biochem.* **52:** 871-926.
5. Lauwers et al. (2016). Membrane Lipids in Presynaptic Function and Disease. *Neuron.* **90:** 11-25.
6. Garland. (2012). Pain Processing in the Human Nervous System: A Selective Review of Nociceptive and Biobehavioral Pathways. *Prim Care.* **39:** 561-571.
7. Wang et al. (2015). SNAP25 is associated with schizophrenia and major depressive disorder in the Han Chinese population. *J clin psychiatry.* doi: 10.4088/JCP.13m08962.
8. Lodish et al. (2000). Molecular Cell Biology, 4th edition. New York. Editor W.H. Freeman.
9. Trueta and De-Miguel. (2012). Extrasynaptic exocytosis and its mechanisms: a source of molecules mediating volume transmission in the nervous system. *Frontiers in physiology.* **3:** 319. Doi: 10.3389/fphys.2012.00319.
10. Sudhof and Rizo. (2011). Synaptic Vesicle Exocytosis. *Cold Spring Harb Perspect Biol 2011;3:a005637.*
11. Chapman. (2008). How Does Synaptotagmin Trigger Neurotransmitter Release? *Annu Rev Biochem.* **77:** 615-641.
12. Murthy and De Camilli. (2003). Cell Biology of the presynaptic terminal. *Annu Rev Neuroscience.* **26:** 701-728.
13. Takamori et al. (2006). Molecular Anatomy of a Trafficking organelle. *Cell.* **127:** 831-846.
14. Jahn and Fasshauer. (2012). Molecular Machines governing exocytosis of synaptic vesicles. *Nature.* **490:** 201-207.
15. Kaeser and Regehr. (2017). The readily releasable pool of synaptic vesicles. *Current opinion in neurobiology.* **43:** 63-70.
16. Ruiz et al. (2011). Active Zones and the Readily releasable pool of synaptic vesicles at the neuromuscular junction of a mouse. *JNeurosci.* **6:** 2000-2008.
17. Reim, et al. (2001). Complexins regulate a Late Step in Calcium Dependent Neurotransmitter Release. *Cell.* **104:** 71-81.
18. Hagler and Goda. (2000). Properties of Synchronous and Asynchronous Release during Pulse train depression in cultured hippocampal neurons. *Journal of Physiology.* 199.111.227.090.
19. Sudhof. (2013). Neurotransmitter Release: The Last Millisecond in the life of a synaptic vesicle. *Neuron perspective, cell press.* **80:** 675-690.
20. Wen et al. (2013). Synchronous and asynchronous modes of synaptic transmission utilize different calcium stores. *eLife.* DOI: 10.7554/eLife.01206.
21. Bacaj et al. (2013). Synaototagmin-1 and -7 Trigger Synchronous and Asynchronous Phases of Neurotransmitter release. *Neuron.* **80:** 947-959.

22. Hestrin and Galarreta. (2005). Synchronous vs asynchronous release: a tale of two types of inhibitory neurons. *Nature Neuroscience.* **8:** 1283-1284.
23. Dawidowski and Cafiso. (2016). Munc18-1 and the Syntaxin-1 Terminus Regulate Open-Closed States in a t-SNARE complex. *Structure.* **24:** 392-400.
24. Laing et al. (2013). Prefusion structure for syntaxin-1a suggests pathway for folding into neuronal trans-SNARE complex intermediate. *PNAS.* **10:** 19384-19389.
25. Fasshauer et al. (1997). Structural Changes Are associated with soluble n-ethylmaleimide-sensitive fusion protein attachment protein receptor complex formation. *JBC.* **272:** 28036-28041.
26. Wiederhold K, Fasshauer D. (2009). Is assembly of the SNARE complex enough to fuel membrane fusion? *J. Biol. Chem*. **284:**13143–13152.
27. Weber T, et al. SNAREpins: minimal machinery for membrane fusion. Cell. 1998; 92:759–772.
28. Bogaart and Jahn. (2011). Counting the SNAREs needed for membrane fusion. *JMCB*. **3:** 204-205.
29. Bogaart et al. (2010). One SNARE complex is sufficient for membrane fusion. *NSMB*. **17:** 358-364.
30. Bao et al. (2016). Exocytotic fusion pores are composed of both lipids and proteins. *NSMB*. **23:** 67-73.
31. Dawidowski and Cafiso. (2013). Allosteric control of syntaxin 1a by munc18-1: characterization of the open and closed conformations of syntaxin. *Biophys J.* **104:** 1585-94.
32. Baker et al. (2015). A direct role for the Sec1/Munc19-family protein Vps33 as a template for SNARE assembly. *Science.* **349:** 1111-1114.
33. Parisotto et al. An extended helical conformation in Domain 3a of munc18-1 provides a template for SNARE complex assembly. *J Biol Chem.* **289:** 9639-9450.
34. James and Martin. (2013). CAPS and Munc13: CATCHRs that SNARE vesicles. *Front Endocrinol* **187:** 10.3389/fendo.2013.00187.
35. Ma et al. (2010). Munc13 mediates the transition from the closed syntaxin-Munc18 complex to the SNARE complex. *NSMB.* **18:** 542-549.
36. Chen et al. (2013). The Munc13 proteins differentially regulate readily releasable pool dynamics and calcium-dependent recovery at a central synapse. *J Neurosci.* **33:** 8336-8351.
37. Zdanowicz et al. (2017). Complexin Binding to Membranes and Acceptor t-SNAREs explain clamping effect on fusion. *Biophysical Journal.* **113:** 1235-1250.
38. Mohromann et al. (2015). Complexins: Small but capable. *Cell Mol Life Sci.* **doi:** 10.1007/s00018-015-1998-8.
39. Snead et al. (2014). Membrane Curvature sensing by the C-terminal domain of complexin. *Nature Communications.* **5:** doi: 10.1038/ncomms5955.
40. Sudhof. (2002). Synaptotagmins: Why so Many? *JBC.* **277:** 7629-7632.
41. Chen and Jonas. (2017). Synaptotagmins: That's why so many. *Neuron*. **94:** 694-696.
42. Bai et al. (2000). Membrane-embedded Synaptotagmin penetrates cis or trans target membranes and clusters via novel mechanism. *JBC.* **275:** 25427-25435.
43. Perin et al. (1990). Phospholipid binding by a synaptic vesicle protein homologous to the regulatory region of protein kinase C. *Nature.* **345:** 260-263.

44. Rizo and Sudhof. (1998). C2-domains Structure and function of a universal ca2+ binding domain. *JBC.* **273:** 15879-15882.
45. Zhang et al. (1998). Mechanism of phospholipid binding by the C2A domain of synaptotagmin 1. *Biochemistry.* **37:** 12395-403.
46. Fernandez et al. (2001). Three-dimensional structure of the C2B domain: Synaptotagmin 1 as a phospholipid binding machine. *Neuron.* **32:** 1057-1069.
47. Sugita et al. (2002). Synaptotagmins form a hierarchy of exocytotic Ca2+ sensors with distinct ca2+ affinities. *EMBO J.* **21:** 270-280.
48. Saheki and De Camilli. (2017). The Extended Synaptotagmins. *BBA-Molecular Cell Research.* **1864:** 1490-1493.
49. Montaville et al. (2008). The PIP2 binding mode of the C2 domains of rabphillin-3A. *Protein Science.* **17:** 1025-1034.
50. Groffen et al. (2004). Ca2+ induced recruitment of the Secretory vesicle protein DOC2B to the target membrane. *JBC.* **279:** 23740-23747.
51. Pangrsic et al. (2012). Otoferlin: a multi-C2 domain protein essential for hearing. *Cell Press.* **35:** 671-680.
52. Cotman et al. (1969). Lipid composition of synaptic plasma membrane isolated from rat brain by zonal centrifugation. *Biochemistry.* **8:** 4606-4612.
53. Wood et al. (2012). Cholesterol Asymmetry in Synaptic Plasma membranes. *J Neurochem*. **116:** 684-689.
54. Pfrieger. (2003). Role of cholesterol in synapse formation and function. *BBA-Biomembranes.* **1610:** 271-280.
55. McLaughlin et al. (2002). PIP2 and Proteins: Interactions, Organization and Information, Flow. *Annu. Rev. Biophys.* **31:** 151-175.
56. Li et al. (2009). Molecular Dynamics simulations of pip2 and pip3 in lipid bilayers determination of ring orientation and the effects of surface roughness on a Poisson-Boltzmann description. *Biophys J.* **97:** 155-163.
57. Sperlagh and Vizi. (1996). Neuronal Synthesis, storage, and release of ATP. *Seminars in neuroscience.* **8:** 175-186.
58. Rangaraju et al. (2014). Activity Driven local ATP synthesis is required for synaptic function. *Cell.* **156:** 825-835.
59. McLaughlin et al. (1981). Adsorption of Divalent Cations to Bilayer Membranes containing Phosphatidylserine. *J Gen. Physiol.* **77:** 445-473.
60. Park et al. (2015). Synaptotagmin-1 Binds to PIP2 containing membrane but not to SNAREs at physiological ionic strength. *NSMB.* **22:** 815-823.
61. Park Y, et al. (2012). Controlling synaptotagmin activity by electrostatic screening. *Nat Struct Mol Biol.* **19:** 991–997
62. Kuo et al. (2010). The calcium-dependent and calcium-independent membrane binding of synaptotagmin 1: 2 modes of C2B binding. *J Mol Bio.* **387:** 284-294.
63. Herrick et al. (2006). Positions of Synaptotagmin 1 and the membrane interface: cooperative interactions of tandem C2 domains. *Biochemistry*. **45:** 9668-9674.
64. Xue et al. (2008). The Janus-faced nature of the C2B domain is fundamental for synaptotagmin-1 function. *NSMB.* **15:** 1160-1168.
65. Wang et al. (2016). Synaptotagmin-1 C2B domain interacts simultaneously with SNAREs and membrane to promote membrane fusion. *eLife.*, eLife 2016;5:e14211.

66. Loewen et al. (2006). C2B polylysine motif of synaptotagmin facilitates a calcium independent stage of synaptic vesicle priming in vivo. *Mol biol. Cell.* **17:** 5211-5266.
67. Ubach et al. (2001). The C2B domains of Synapototagmin 1 is a ca2+-binding module. *Biohem.* **40:** 5854-5860.
68. Wu, Z. & Schulten, K. (2014). Synaptotagmin's Role in Neurotransmitter Release Likely Involves Ca (2+)-induced Conformational Transition. *Biophys J* **107**: 1156-66.
69. Vrljic et al. (2011). Post translational modifications and lipid binding profile of insect cell expressed full length mammalian synaptotagmin 1. *Biochem.* **50:** 9998-10012.
70. Lu et al. (2014). The Juxtamembrane linker of full length synaptotagmin 1 controls oligomerization and calcium dependent membrane binding. *JBC.* **32:** 22161-22171.
71. Kee and Scheller. (1996). Localization of synaptotagmin-binding domains to syntaxin. *J Neurosci.* **16:** 1975-1981.
72. Vrljic M, et al. Molecular mechanism of the synaptotagmin-SNARE interaction in Ca2+-triggered vesicle fusion. *Nature structural & molecular biology*. 2010; 17:325–331.
73. Zhou et al. (2017). The primed SNARE-complexin-synaptotagmin complex for neuronal exocytosis. *Nature.* **548:** 420-425.
74. Lai et al. (2011). Synaptotagmin 1 and SNAREs form a complex that is structurally heterogeneous. *J Mol Bio.* **405:** 696-706.
75. Kuo et al. (2011). Phosphatidylinositol 4,5-bisphospate alters synaptotagmin 1 membrane docking and drives opposing bilayer closer together. *Biochemistry.* **50:** 2633-2641.
76. Martens et al. (2007). How Synaptotagmin promotes membrane fusion. *Science.* **316:** 1205-1208.
77. Wu et al. (2003). Visualization of synaptotagmin 1 oligomers assembled onto lipid monolayers. *Proc natl acd sci usa.* **100:** 2082-2087.
78. Rizo J, Chen X, Arac D. (2006) Unraveling the mechanisms of synaptotagmin and SNARE function in neurotransmitter release. *Trends in cell biology*. **16:** 339–350.
79. Wang et al. (2014). Calcium sensitive ring-like oligomers forms by synaptotagmin. *PNAS.* **11:** 13996-13971.
80. Zanetti et al. (2016). Ring-like oligomers of Synaptotagmins and related C2 domain proteins. *Elife.* 2016;5:e17262 doi: 10.7554/eLife.17262.
81. Wang et al. (2017). Circular oligomerization is an intrinsic property of synaptotagmin. *Elife.* 2017;6:e27441 doi: 10.7554/eLife.27441.
82. Rothman et al. (2017). Hypothesis – buttressed rings assemble, clamp, and release SNAREpins for synaptic transmission. *FEBSPress.* **591:** doi: 10.1002/1873-3468.12874.
83. McMahon et al. (2010). Membrane curvature in synaptic vesicle fusion and beyond. *Cell.* **140:** 601-605.
84. Lai et al. (2011). Synaptotagmin 1 modulates lipid acyl chain order in lipid bilayers by demixing phoshatidylserine. *JBC.* **286:** 25291-25300.
85. Morales et al. (2016). Cd2+ as a Ca2+ surrogate in protein-membrane interactions: isostructural but not isofunctional. *J AM Chem Soc.***135:** 12980-12983.
86. Katti et al. (2017). Non-native metal ion reveals the role of electrostatics in synaptotagmin 1-membrane interactions. *Biochem.* **56:** 3283-3295.
87. Herrick et al. (2009). Solution and Membrane-Bound Conformations of the Tandem C2A and C2B Domains of Synaptotagmin 1: Evidence of Bilayer Bridging. *J. Mol. Bio.* **390:** 913-919.

88. Perez-Lara et al. (2016) PtdInsP_2 and PtdSer Cooperate to Trap Synaptotagmin-1 to the Plasma Membrane in the Presence of Calcium, *Elife*. doi: e15886.
89. Nyenhuis and Cafiso. (2018). Choice of reconstitution protocol modulates the aggregation state of full-length membrane-reconstituted Synaptotagmin-1. *Protein Science.* **27:** 1008-1012.
90. Morales and Igumenova. (2012). Synergistic effect of Pb2+ and PIP2 on C2 domain-membrane interactions. *Biochemistry.* **51:** 3349-3360.

CHAPTER 2: Materials, Methods, and Theory

2.1 Materials

2.1.1 Lipids and detergents

1-palmitoyl-2-oleoyl-*sn*-glycero-3-phosphocholine (POPC), 1-palmitoyl-2-oleoyl-*sn*-glycero-3-phosphoethanolamine (POPE), 1-palmitoyl-2-oleoyl-*sn*-glycero-3-phospho-L-serine (POPS), 1-palmitoyl-2-oleoyl-*sn*-glycero-3-phospho-(1′-rac-glycerol) (POPG), dimethyldioctadecylammonium bromide salt (DDAB), porcine brain L-α-phosphatidylcholine (brain PC), porcine brain L-α-phosphatidylethanolamine (brain PE), porcine brain L-α-phosphatidylserine (brain PS), phosphatidylinositol 4,5-bisphosphate (PIP_2), 1,2-dipalmitoyl-*sn*-glycero-3-phosphocholine (DPPC), 1,2-dipalmitoyl-*sn*-glycero-3-phosphoethanolamine (DPPE), 1,2-dipalmitoyl-*sn*-glycero-3-phospho-L-serine (DPPS), 1,2-dioleoyl-*sn*-glycero-3-phosphocholine (DOPC), 1,2-dioleoyl-*sn*-glycero-3-phosphoethanolamine (DOPE), 1,2-dioleoyl-*sn*-glycero-3-phospho-L-serine (DOPS), 1,2-dioleoyl-*sn*-glycero-3-phosphoethanolamine-*N*-(lissamine rhodamine B sulfonyl (rhodaminePE), were obtained from Avanti Polar Lipids Inc. (Alabaster, AL). 3-[(3-cholamidopropyl) dimethylammonio]-1-propanesulfonate (CHAPS), and n-Octyl-β-D-Glucopyranoside, Anagrade (OG) were from Anatrace (Maumee, OH). Sodium cholate and triton X-100 were from Sigma (St. Louis, MO) *(Figure 2.1)*.

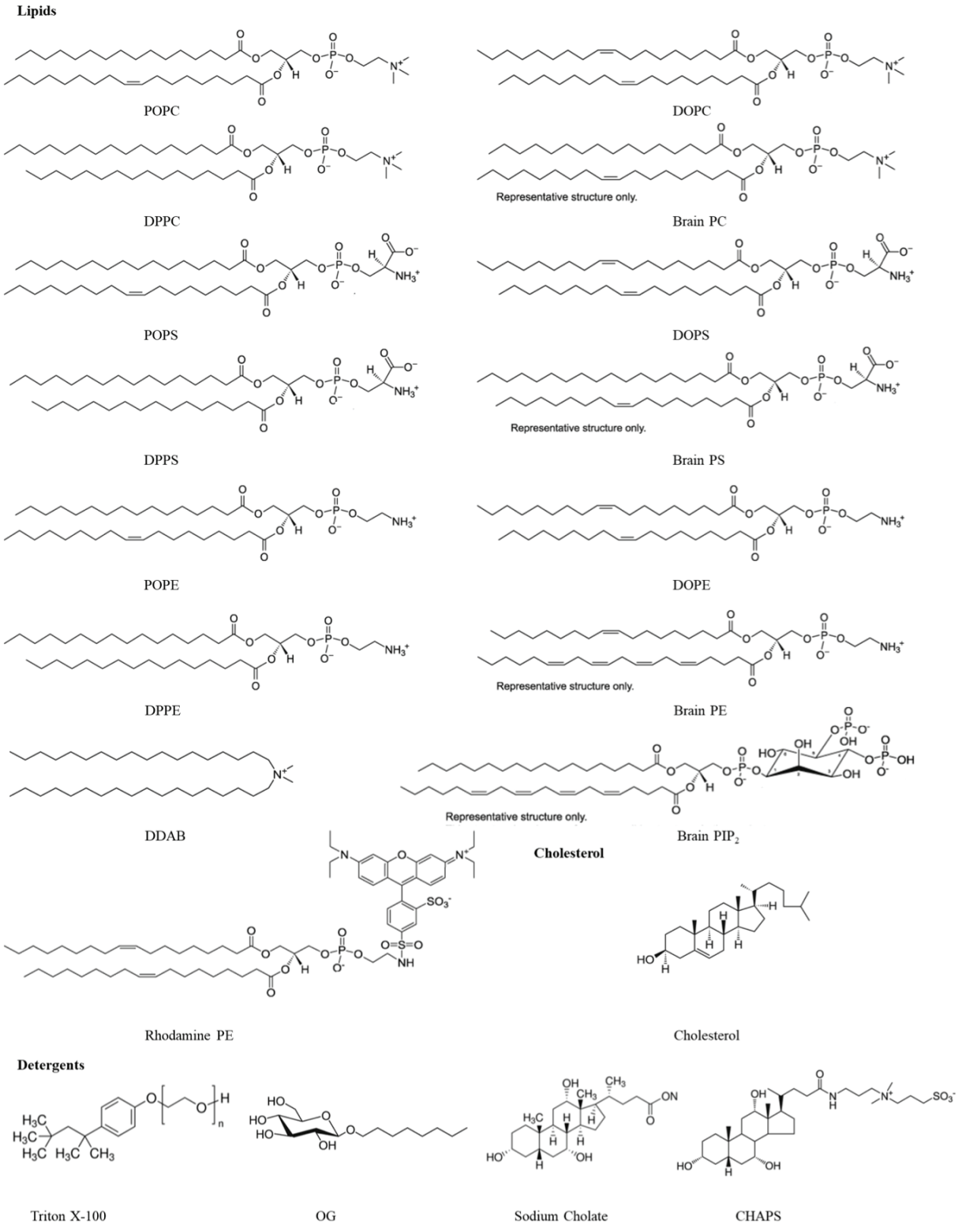

Figure 2.1: Collected Lipids and Detergents used in experiments. Structures from Avanti Polar Lipids. PO lipid are acyl chains with a *16:0-18:1* saturation, DO lipids are *di-18:1*, and DP lipids are *di-16:0*. Shown below are the detergents used in the Full-length purification for shape and structure comparison.

2.1.2 Buffers and Chemical Reagents

Cholesterol, 2,2',2'',2'''-(ethane-1,2-diyldinitrilo) tetraacetic acid (EDTA), calcium chloride (Ca^{2+}), sucrose, 3-(N-Morpholino) propanesulfonic acid (MOPS), nickel sulfate hexahydrate, potassium chromium (III) oxalate, glycerol, NaCl, KCl, cadmium chloride, lead acetate, yeast extracts, and tris(hydroxymethyl)aminomethane hydrochloride (Tris) were from EMD Millipore/Sigma (St. Louis, MO). 2-[4-(2-hydroxyethyl)piperazin-1-yl] ethanesulfonic acid (HEPES) and Adenosine-5'-Triphosphate Disodium trihydrate (ATP) were from Gold Biotechnologies (St Louis, MO). D-myo-Inositol-1,4,5-triphosphate (IP_3, sodium salt) was from Cayman chemical company (Ann Arbor, MI). Tryptone was from IBI Scientific (Dubuqe, IA). Bacto Agar was from BD (Franklin Lakes, NJ). Chloroform, acetic acid and all other inorganic acids, bases, and hydrogen peroxide were from Fisher Scientific (Fair Lawn, NJ). D_2O, deuterated glycerol, and deuterated NH_4Cl were from Cambridge Isotopes (Tewksbury, Ma). Nickel(II)-ethylenediamine-N,N'-diacetic acid (NiEDDA), was synthesized as described previously (Altenbach, Greenhalgh et al., 1994).

2.1.3 Antibiotics, Enzymes, Inhibitors, DNTPs, Primers

Benzonase Nuclease (25 KU), 4-(2-aminoethyl) benzenesulfonyl fluoride hydrochloride (AEBSF), chloramphenicol, were from EMD Millipore/Sigma (St. Louis, MO). Leupeptin, Aprotinin, Isopropyl-β-D-thiogalacto-pyranoside (IPTG), Ampicillin sodium salt, kanamycin, and dNTP Mixes were from Gold Biotechnologies (St Louis, MO). Thrombin was from MP Biomedicals (Santa Ana, CA). PfuUltra High-Fidelity DNA Polymerase was from Agilent (Santa Clara, CA). DPN1 restriction endonuclease was from New England Biolabs (Ipswich, MA). QIAprep spin miniprep kit was from Qiagen (Germantown, MD). Primers for PCR were from

Integrated IDT Technologies (Coralville, IA). Sequencing for PCR was from Genewiz (South Plainfield, NJ).

2.1.4 Cell Lines

BL21(DE3) cells, BL21(DE3)-pLys, BL21(DE3)-RIL, and Top10 competent cells were from Invitrogen (Waltham, MA).

2.1.5 EPR and Fluorescent Labels

MTSL (*S*-(1-oxyl-2,2,5,5 – tetramethyl - 2,5 – dihydro - 1H – pyrrol – 3 - yl) methyl methanethiosulfonate) was purchased either from Santa Cruz Biotech (Santa Cruz, CA) or Cayman Chemical company (Ann Arbor, MI). Alexa Fluor 546 C5-maleimide, Alexa Fluor 488 C5-maleimide, and BODIPY FL Maleimide (BODIPY FL *N*-(2-Aminoethyl)) Maleimide) were from Thermo Fisher Life technologies (Waltham, MA).

2.1.6 EPR Tubes

0.6IDx0.84OD-100 mm Borosilicate and 1.5IDx1.8OD-100 mm Quartz capillaries were purchased from VitroCom (Mountain Lakes, NJ). TPX capillaries were purchased from Molecular Specialties, Inc. (Milwaukee, WI).

2.1.7 Columns for Purification

GSTPrep FF 16/10, GSTrap FF, HiTrap Benzamidine FF, HiTrap SP, HiTrap Q HP, HiPrep 26/10 Desalting, HiTrap 16/60 Sephacryl S-100 HR pre-packed columns were from GE Healthcare (Piscataway, NJ). These columns were run using ÄKTA Prime and BioRad NGC

Systems. Nickel NTA and Nickel agarose high density beads were from Gold Biotechnologies (St Louis, MO).

2.1.8 Additional General Lab Equipment

Amicon Ultra Concentrators were from EMD Millipore/Sigma (St. Louis, MO). SDS-Page Gels, BioBeads, gel boxes, other components, and accessories were from BioRad (Hercules, CA). All syringes were from BD (Franklin Lakes, NJ). Syringe filters, dialysis tubing and cassettes, needles, borosilicate tubing and other glass and plasticware were mainly from Fisher Scientific (Pittsburg, PA). Extrusion was performed with a hand-held Mini extruder (Avanti Polar Lipids, Birmingham, AL). Water was purified with a Nanopure system from Barnstead (Dubuque, IA) to achieve a resistivity of 18.2 MΩ/cm. Shigemi tubes were from Sigma-Aldrich (St. Louis, MO).

2.2 Methods

2.2.1 Site-Directed Mutagenesis

Site-directed mutagenesis must first be used to remove any native cysteines from all protein constructs to perform EPR or certain site-specific labeled florescent techniques. Next, a cysteine is added to the desired location or locations for probing with these techniques. Other possible mutations (neutralizing charged amino acids) are also addressed in construct sections below. The method used for this mutagenesis was polymerase incomplete primer extension (PIPE) polymerase chain reaction (PCR)[1]. PIPE mutagenesis takes advantage of the ability of Pfu polymerase to synthesize complementary strands of template DNA when a primer complementary to the template

and dNTPs are present[1]. The process follows a series of varied temperature steps to anneal primers and extend the new product. The steps are: denaturation to activate Pfu polymerase, denaturation to melt the DNA, annealing to allow the primer to attach to the template strand, and elongation when Pfu runs along the primer and attaches free dNTPs complementary to the template[1]. This is repeated over many cycles allowing an exponential amplification of new DNA strands until free dNTPs are depleted from solution *(Figure 2.2)*[1]. DPN1 is then added to digest template or mother plasmid because template DNA is methylated or hemimethylated from the TOP10 cell line and the PCR product is not[1].

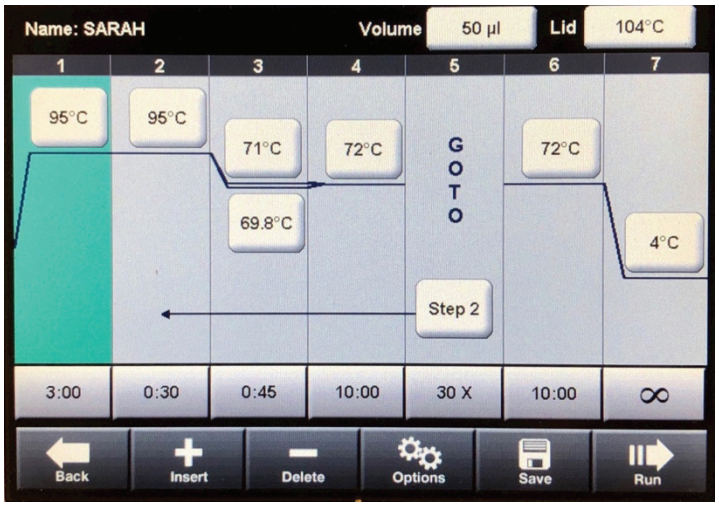

Figure 2.2: Example BioRad Thermocycler method used for PIPE Mutagenesis of Syt1. Steps 1 and 2 are denaturation steps, Step 3 is Annealing over a gradient according to the placement of the tube in the thermocycler, Step 4 is extension time and temperature, Step 5 lists the number of cycles performed, Step 6 is final extension, step 7 cools the reaction and holds temperature. The conditions in the image are optimized for the most difficult reactions for FL Syt. Most of the mutants' PCR reactions follow the temperatures, times and cycles listed in the methods.

2.2.1.1 Primer Design

Oligonucleotide primer design involves first choosing the desired amino acid to mutate (typically to a cysteine). Next, the amino acids need to be reverse translated to the codon level to

design the primers. The codon encoding the cysteine or other mutation that most closely resembles the existing amino acid (one or two nucleotides changed ideally) codon is selected for the primer. This will make primer annealing easier. Next, 20-30 nucleotides are selected on the forward template and reverse template strands attempting to center the mutation on the strand. The reverse and forward primers are designed to be complementary to the existing forward and reverse template DNA, only changing the complementary base pairs to match the desired mutant location. These primers are designed with blunt ends, meaning fully overlapping/complementary sequences. Once the initial primer is designed it is checked through a list of requirements before ordering from IDT Technologies. One, for temperature stability the primer GC content needs to be around 40-60%[2]. Two, check to see if the primer could adopt a secondary structure/hairpin, often due too many hairpin bases in a row or potential inter-primer interactions that would lead to structured, self-dimerized, or undesired cross-dimers. Both prevent annealing to the template[2]. Three, look for repeats or runs; this involves checking to ensure there are not any large strands of repeats (ATATAT) or runs of single bases that could lead to frame shifts or mis-priming in the PCR[1]. Four, check for cross homology, where large sections of the primer repeat because it can lead to mis-priming and potential frame shifts or deletions[2]. Five, the primers will ideally end in a G or a C in blunt primer design to act as a clamp and increase specific priming/binding on the 3' end[2]. Six, check the melting temperature (Tm) of the primers to ensure the primers match (to ensure they are complementary) and that they are within range to anneal and will not have any likely secondary annealing[2]. Online oligo-analyzers (such as geneinfinity.org) will direct the design through most of the above checks.

2.2.1.2 PCR Thermocycler Setup

Polymerase chain reaction (PCR) reactions were setup mixing: mother (WT or other mutant) plasmid/template, forward and reverse primers for the desired mutant, 10 mM DNTP mixture, Pfu Ultra polymerase, Pfu Ultra reaction buffer, and water. As needed DMSO or extra magnesium was added if mutants were particularly difficult. The sample was then placed in the thermocycler and the PCR was carried out with a lid temperature of 104°C. A temperature of 95°C was used for the first and second denaturation steps, which lasted for 3 minutes and 30 seconds, respectively. Next, 50-72°C annealing temperatures were used for 1 minute with the actual temperature depending on the melting temperature of the primers (annealing temperature is usually 5°C or more below the Tm of the primers). Finally, 68 or 72°C was used for the extension temperature with a time of 6.5 to 10 minutes depending on the plasmid template (usually 1 minute per kilobases of template plus 1 minute) and the difficulty of the mutation. These conditions were repeated for 20 cycles (30 cycles were run if incomplete extension was clear on DNA gels). After the cycles completed there is a final elongation step under the same conditions of the previous elongations and then the tube is moved to a final hold temperature of 4°C (the tube must cool to at least 37°C before addition of DPN1 to prevent temperature degradation of the enzyme, cooling completely to 4°C is safest). Next, DPN1 was added for 1 to 2 hours at 37°C to digest the methylated template plasmid. DNA gels were run to verify the existence of DNA product.

2.2.1.3 Transformation

PCR product was transformed into Top10 cells (Invitrogen, Waltham, MA) on ampicillin (soluble) or kanamycin (full length) containing plates according to the construct. Cells were first incubated on ice for 30 minutes with PCR product. The sample was then heat shocked for 45

seconds at 42°C and allowed to recover on ice for 2 more minutes. Next, SOC media was added to the sample and the cells were left to shake at 37°C from 45 minutes to 2 hours. After shaking the sample was plated using sterile technique, inverted and incubated overnight at 37°C.

2.2.1.4 Miniprep

A single colony was selected to inoculate 6-12 mL miniprep-cultures of standard LB or SOC media with 50 mg/mL ampicillin or kanamycin at 37°C and 200 rpm shaking overnight. Cells were then pelleted using a tabletop centrifuge at 3200xg. Miniprep was performed initially using the Qiagen QIAprep spin miniprep kit and procedure, but later supplemented by equivalent buffers from Thermo Scientific. The kit follows a standard "bind-wash-elute" procedure. Briefly, after cell pelleting resuspension buffer containing RNAse is added and cells are resuspended with light vortexing. Alkaline lysis buffer is added next and cells are inverted 3-6 times over a short period, upwards of 2 minutes. Acidic neutralization buffer is added and the sample is again inverted, denaturing proteins and other cell debris out of solution. The precipitate is then spun out of solution over 10 minutes on a tabletop centrifuge at max speed. The purified lysate is then transferred to a spin column and plasmid DNA is bound to a silica surface over a 1-minute spin allowing other DNA and cell contaminants to pass through the column. The column is next washed with either 1 or 2 ethanol containing buffers over 2 or 3 spins of 1-minute each to remove contaminating sugars and RNAs. The column is next spun for 1-minute to remove residual ethanol to prevent DNA precipitation. Finally, autoclaved DDH_2O is added over the column and allowed to sit for 1-2 minutes before spinning a final minute to elute the DNA plasmid.

2.2.1.5 Mutant Verification

Purified plasmid DNA is sent for standard sanger sequencing at Genewiz. Once the results come back the mutant is verified using comparison of the known Syt1 amino acid sequence (Uniprot ID: P21707), with the ExPASy translate tool used to convert nucleotide base sequences to amino acid sequence, and protein BLAST to align the mutant sequence with the wild-type. The Syt1 mutations in varying protein lengths and domains are listed below.

2.2.2 Syt1 Protein Constructs Produced from Mutagenesis

2.2.2.1 Cytosolic Syt1 constructs: C2A (96-265), shortC2A (136-260), C2B (249-421), shortC2B (271-429), and C2AB (136-421) were previously added to the pGEX-KG vector and purified using N-terminal GST tags. DNA of rat Syt1 (P12707) was provided by Dr Carl Cretz (Pharmacology, University of Virginia) and for the shortC2B plasmid was provided by Josep Rizo (Biophysics, Texas Southwestern Medical Center)[3]. Native constructs or mutations of the polybasic face sites: K326A:K327A or the arginine apex sites: R398Q:R399Q were used for many sedimentation, binding, and FLIC assays. For EPR and NMR measurements, the native cysteine at residue 277 was mutated to an alanine for each construct using standard PIPE site-directed mutagenesis. For EPR or FLIC measurements, single cysteine point mutations were then introduced into C2AB at sites M173C, F234C, T285C, V304C, T327C, F349C, E350C, G368C, S391C and into C2A at site M173C. Double or triple mutations for FLIC and EPR were also introduced into the C277A plasmids at R398Q:T285C and R398Q:R399Q:285C for probing the arginine apex. All mutations were verified by Genewiz DNA sequencing.

2.2.2.2 Full length Syt1 constructs: from rat (1-421) or ΔC2B (1-266) were previously cloned into a pET-28a vector with an N-terminal HIS6-tag, provided by Reinhard Jahn (Max Planck Institute for Biophysical Chemistry)[4]. Native cysteines (C73A, C74A, C76A, C78A, C82S, and C277S) were mutated using the standard PIPE site-directed mutagenesis[2]. For EPR and FLIC measurements, single cysteine point mutations were introduced into the cysteine-free constructs using the same method at positions: K86C, K90C, K95C, K104C, K114C, A123C, Q154C, M173C, D188C, F234C, E269C, V304C, L323C, R388C, A395C for FL SYT or positions: K95C, K104C, K114C, A123C, Q154C, M173C, D188C, F234C for ΔC2B. Double mutants in FL SYT K86C:P136C, P136C:L323C, P136C:T329C, M173C:V304C, M173C:L323C, M173C:A395C were also introduced for EPR DEER measurements. DNA sequencing for all mutations was verified by Genewiz DNA sequencing.

2.2.3 Protein Expression and Purification

After attaining the DNA plasmid for the desired protein construct the plasmid must be transformed into cell lines designed to grow and express the protein of interest. BL21 cells of varying specificity are designed to express soluble and full-length proteins and (depending on the vector and promoter being used) permit induction with IPTG (an equivalent to lactose which will not be metabolized and depleted by the cells), which allows for optimization of cell growth into the later log-phase before protein expression is induced[5]. Here, one can reach a desired density of cells before activating the lac operon/switching off the lac repressor[5]. In most cases the temperature of the incubator is then decreased to slow protein expression to prevent inclusion bodies and rapid consumption of nutrients in media which would accelerate cell toxicity and death[6]. Once protein

is expressed for an optimized time period, media is removed through cell pelleting, cells are resuspended in solution, and then cells are ruptured with mechanical force (using a French pressure cell) to access the desired protein. Detergents are often added to cell resuspension buffer to help denature cell membranes. For soluble proteins detergents are then removed in most cases. For membrane proteins detergent must be present in every buffer and dialysis step to create micelles which anchor the transmembrane regions of the membrane protein. Removal of these detergents will precipitate the protein.

For the Syt1 case, cell debris is pelleted away and cell lysate remains with the desired protein among many other cell contaminants. In order to work with Syt1 it must be purified to remove other proteins, lipids, DNA, and sugars. Syt1 is particularly sensitive to contamination by charged DNA/RNA and other charged molecules that can bind to the polybasic face of the protein, which significantly alter Syt1 function. Syt1 follows standard purifications where a specific tag (GST or NTA) is used first to perform affinity chromatography. Affinity chromatography beads allow specific binding of these tags (nickel for histidine tags, glutathione for glutathione-s-transferase) to resin so that other contaminants can be washed away through different buffer conditions[7]. The tag is then removed through thrombin cleavage (LVPRGS cleavage site) to prevent any effects of protein oligomerization, diffusion, or functionality. This usually occurs at high salt for optimal thrombin efficiency[7].

Affinity chromatography cannot fully separate the charged impurities from the protein so following a desalting (rapid gel filtration, separating by size) or dialysis step to move the protein into low salt (but not too low or too long for Syt1 as it rapidly precipitates), ion exchange chromatography is performed. Ion exchange chromatography uses either positive or negatively charged (anion typically a quaternary ammonium salt (Q) or cation for syt1 case a sulfopropyl

group (SP) exchange) resin to bind to the protein according to its pI[8,9]. Once bound to the column the protein is run through a salt gradient which washes away contaminants with different charge profiles than the protein, which can then be eluted depending on the buffer salt and pH. This type of exchange can be manipulated according to salt gradient concentrations, pH, and run times. In a standard purification, anion exchange (Q) would be used for proteins of higher pI and then run with a pH about 1 unit above the pI[8,9]. A cation exchange (SP) would typically be used with lower pIs and run with a pH 1 unit below the pI[8]. *(Figure 2.3)* Running for too long at extreme pH or too close to the pI typically precipitates the protein[8]. When these classic running conditions were run with the majority of the Syt1 constructs large salt gradients and varied pH values were not efficient enough to effectively separate Syt1 from DNA. Thus, the majority of the Syt1 constructs (pI about 8-9) are run on an SP column. This was selected to immediately pass negatively charged DNA impurities through the column and to then elute Syt1 through a gradient. Throughout the process multiple peaks with Syt1 will elute; earlier peaks are tightly bound with DNA and discarded, while the cleanest and largest peak is always eluted at the very end of the gradient. ΔC2B is also best separated from DNA under an untraditional use of a Q column and pH selected to allow the protein to flow through but leave DNA and any tightly contaminated Syt1 bound to the column since ΔC2B has a pI of 6.13 and is unstable for long periods at room temperature. The DNA and contaminants are then eluted through the gradient and discarded.

For Syt1, each peak of protein is checked for purity using SDS-page to look for protein contaminants and UV-Vis 260/280 ratios to check for DNA impurities, as DNA absorbs at 260 nm and protein (W, C, Y residues) at 280 nm[10]. The majority of the time the protein quantity and quality are high enough to proceed, if not gel filtration through differing resin sizes and packing is used depending on the size and type of remaining impurities. Once the protein is successfully

deemed pure, it is concentrated and then manipulated as needed for the desired experiments. Detailed steps for the different experiments and Syt1 constructs are shown below.

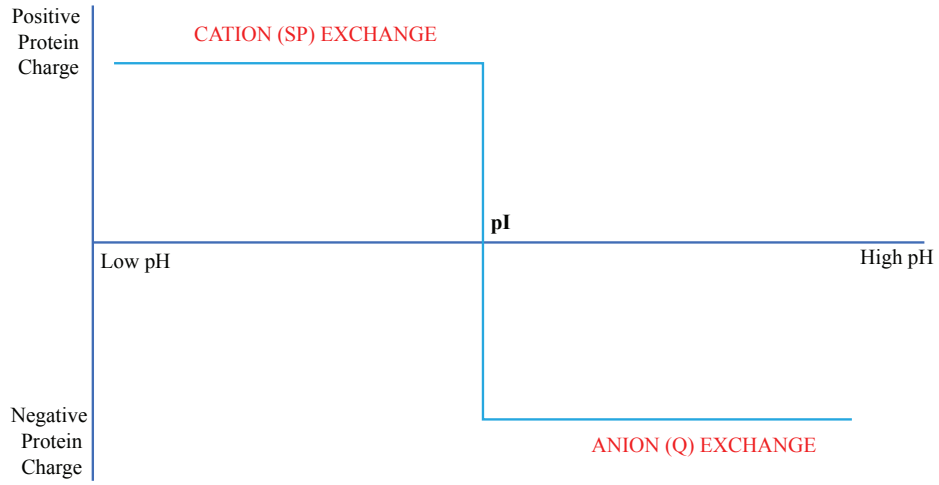

Figure 2.3: Representation of the standard use, or selection guide, for Ion Exchange Chromatography. A cation exchange is usually used with a pH lower than the pI of the protein and an anion exchange is usually used with a pH higher than the pI of the protein.

2.2.3.1 Soluble Cytosolic Proteins Expression and Purification

For sedimentation assays, CW EPR, DEER, and FLIC*: *C2A, shortC2A, C2B, shortC2B, and C2AB plasmids were transformed into BL21(DE3) cells on ampicillin containing plates. A single colony was selected to inoculate 50 mL precultures of standard LB media with 50 mg/mL ampicillin at 37°C and 200 rpm shaking for 6 hours to overnight. LB main cultures were then inoculated to 1 L in 2.8 L Fernbach flasks and grown at 37°C and 200 rpm shaking, until induction with 0.1 mM IPTG at an OD_{600} of 0.8-1.0. The cells were then left to grow at 20°C with 200 rpm shaking for up to 12 hours.

For HSQC NMR: C2A, C2B and shortC2B plasmids were transformed into BL21(DE3) cells on ampicillin containing plates. A single colony was selected to inoculate 5 mL pre-precultures of standard LB media with 50 mg/mL ampicillin at 37°C and 200 rpm shaking for 8 hours. 1 mL LB pre-precultures were then used to inoculate 50 mL precultures of standard M9

media containing deuterated NH_4Cl, these were grown overnight at 37°C with 200 rpm shaking. M9 main cultures with deuterated NH_4Cl were then inoculated with 12.5 mL precultures into 250 mL cultures in 2.8 L Fernbach flasks and grown at 37°C and 200 rpm shaking, until induction with 0.1 mM IPTG at an OD_{600} of 0.8-1.0. The cells were then left to grow at 20 degrees C with 200 rpm shaking for up to 6 hours[11].

All cells were pelleted at 12,000 rpm, 12 min, 4 degrees C then resuspended in PBS buffer containing 2 mM EGTA and 2% triton x-100. Protease inhibitors: 50 μM leupeptin, 20 units/mL aprotinin, and 0.8mM AEBSF were added along with 0.01% benzonase nuclease. The cells were lysed by French press and cell debris was pelleted by ultracentrifugation at 18,000 RPM, 30 min at 4 °C. The supernatant was collected and bound to a GSTPrep FF 16/10 column using the AKTA prime. The column was washed using Bead wash (PBS, 1% triton x-100, 2 mM EGTA), Prep (50 mM tris base, 150 mM NaCl, pH 8.4), and equilibrated into Cleavage (50 mM tris base, 150 mM NaCl, 4 mM $CaCl_2$, pH 8.4) buffers. Once washed, 5 mg thrombin per L of protein was manually injected into the column to cleave the GST tag. The column was left at room temperature overnight. The protein was then eluted from the GSTPrep column using the AKTA prime by attaching 3 GSTtrap FF and 1 HiTrap benzamidine FF(HS) columns attached in sequence to the GSTPrep column to separate the protein and thrombin from the GST tag. Protein was eluted with Elution buffer (50 mM tris, 750 mM NaCl, 25 mM EGTA).

For C2A, shortC2A, and C2AB, the samples were moved into a lower salt concentration by a HiPrep 26/10 desalting column using SPA buffer (50 mM MOPs, 1 mM $CaCl_2$, 150 mM NaCl, pH 7.2) to permit binding to the ion exchange column. The samples were then quickly loaded onto the ion exchange column, as the protein begins to precipitate after 30 minutes if not loaded onto the SP column. SPA and SPB (50 mM MOPs, 1 mM $CaCl_2$, 800 mM NaCl, pH 7.2)

buffers are used to run the HiTrap SP HP column. This step separates any remaining DNA contaminated protein from the pure samples.

For C2B and shortC2B, the ionic strength of the solution was then reduced by a HiPrep 26/10 desalting column using QA buffer (150 mM KCl, 50 mM MOPS, and 5 mM EDTA (pH 7.2)) to permit binding to the ion exchange column. Again, the samples were then quickly loaded onto the ion exchange column, to prevent precipitation. QA and QB (800 mM KCl, 50 mM MOPS, and 5 mM EDTA (pH 7.2) buffers are used to run the HiTrap Q HP column.

For each prep, every fraction was checked for DNA and protein contaminants on the NanoDrop (260/280 ratio are examined and no more than a 0.6 ratio is accepted (usually no more than 0.45 ratio appears)) and run on a 12% SDS-PAGE gel. Pure fractions were collected and quantified using a Bradford assay then dialyzed or exchanged by HiPrep 26/10 desalting column into the desired buffer.

For EPR, sedimentation assays, FLIC**,** Calcium or Metal free (excludes $CaCl_2$) buffer (150 mM KCl, 20 mM HEPES, 1 mM CaCl2, pH 7.4) depending on the desired experiment and to permit spin labeling.

For NMR*,* the protein was further purified and buffer was exchanged using a gel filtration column, HiPrep 16/60 Sephacryl S100-HR on the BioRad NGC Quest. NMR Buffer was: 50 mM MES, 150 mM NaCl, 3 mM $CaCl_2$, 10% D_2O, pH 6.3[11].

2.2.3.2 Full Length and ΔC2B Purification

FL Syt and ΔC2B constructs were transformed into BL21(DE3)-RIL cells onto Kanamycin and chloramphenicol containing plates, and a single colony was selected to inoculate 50 mL

precultures of standard TB medium containing 50 mg/L Kanamycin. These were grown for approximately 12-15 hours at 37 °C. The precultures were added to 950 mL culture of TB medium and 50 mg/L Kanamycin in a 2.8 L Fernbach flask and grown ~2 h at 37°C until an OD_{600} of 0.8−1. Expression was induced with 0.5 mM isopropyl β-d-thiogalactopyranoside (IPTG) and 50 mg/L chloramphenicol. The cells were then grown for 15-18 h at 22°C with 200 rpm shaking. The cells were pelleted by centrifugation at 12,000 rpm for 12 min at 4°C.

2.2.3.2.1 Chaps purification

The pellet was solubilized in extraction buffer 1 (20 mM HEPES, 500 mM NaCl, 8 mM imidazole, pH 7.4). Once resuspended a 1:1 volume of extraction 2 buffer (20 mM HEPES, 500 mM NaCl, 8 mM imidazole, 10% Na-Cholate, pH 7.4) was added (the cells will not resuspend in the cholate buffer if not first resuspended in cholate free buffer). Protease inhibitors (50 μM leupeptin, 20 units/mL aprotinin, and 0.8mM AEBSF were added along with 0.01% benzonase nuclease to the cell suspension. Cells were lysed using the French press. Cell debris was pelleted by ultracentrifugation at 18,000 rpm for 35 min at 4°C[12,13].

The supernatant was added to a pre-equilibrated Ni-NTA column and allowed to bind to the resin overnight at 4°C with shaking. The lysate was then allowed to flow through the column and the resin was washed with 3 column volumes of wash buffer (20 mM HEPEs, 300 mM NaCl, 40 mM imidazole, 1% CHAPs, pH 7.4). (*If spin labeling*: the column was left in a small volume of wash buffer and ~1 mg of MTSL was added (solubilized in ethanol) to the column which then labeled in the dark at 4°C overnight with shaking). The resin was then washed again with 3 column volumes of wash buffer, and subsequently eluted in excess elution buffer (20 mM Tris, 300 mM NaCl, 400 mM imidazole, 1% Chaps, pH 7.4) until no protein was detected in the flow through by

the NanoDrop. Lysate, flow through, wash, and elutions were all run on a 12% SDS-Page gel to check for protein purity. Clean fractions were collected and concentrated in 30 K amicon concentrators. 5 mg thrombin per L protein grown was then added to the protein which was then dialyzed (20 mM HEPEs, 150 mM NaCl, 1 mM EDTA, 1% Chaps, pH 7.4) overnight at 4°C. FL Syt and ΔC2B were further purified to remove DNA contaminants using the Atka prime. A HiTrap SP (HiTrap Q for ΔC2B**)** column was run using AktaA (20 mM HEPEs, 1% Chaps, pH 7.4) and AtkaB (20 mM HEPEs, 1000 mM Nacl, 1% Chaps, pH 7.4) and eluted over a 0-1 M salt gradient. Protein elutions were run on a 12% SDS-Page gel and checked on the NanoDrop to verify protein purity and DNA cleanliness with 260/280 ratios. Clean protein was then collected and concentrated in 30 K amicon concentrators. Protein concentration was measured by the Bradford assay to follow desired reconstitution[12,13].

2.2.3.2.2 OG purification

The FL Syt cell pellet was solubilized in resuspension buffer 1 (PBS buffer, 0.1% triton x-100, pH 7.4). Protease inhibitors (50 μM leupeptin, 20 units/mL aprotinin, and 0.8mM AEBSF were added along with 0.01% benzonase nuclease to the cell suspension. Cells were lysed using the French press. Cell debris was pelleted by ultracentrifugation at 18,000 rpm for 35 min at 4°C[4].

The supernatant was added to a pre-equilibrated Ni-NTA column and allowed to bind to the resin overnight at 4°C with shaking. The lysate was then allowed to flow through the column and the resin was washed with 3 column volumes of RNA/DNA wash buffer (25 mM HEPEs, 0.1% triton x-100, 20 mM $CaCl_2$, 150 mM NaCl, pH 7.4). The resin was then washed again with 3 column volumes of Wash2 buffer (25 mM HEPEs, 0.01% triton x-100, 20 mM imidizole, 150 mM NaCl, pH 7.4). Next, the column detergent was rapidly swapped with 3 column volumes of

Swap buffer (25 mM HEPEs, 20 mM imidazole, 150 mM NaCl, pH 7.4) and subsequently eluted in excess Elution buffer (25 mM HEPEs, 500 mM Imidazole, 150 mM NaCl 1% OG, pH 7.4) until no protein was detected in the flow through by the NanoDrop. Lysate, flow through, wash, and elutions were all run on a 12% SDS-Page gel to check for protein purity. Clean fractions were collected and concentrated in 30 K amicon concentrators. 5 mg thrombin per L protein grown was then added to the protein which was then dialyzed (25 mM HEPEs, 150 mM NaCl, 1 mM $CaCl_2$, 1% OG, pH 7.4) overnight at 4°C. The entire nickel column was run in the cold room as the protein is not stable throughout this purification.

The protein was further purified to remove DNA contaminants using the Atka prime. A HiTrap SP column was run using Akta A (25 mM HEPEs, 150 mM KCl, 1% OG, 1 mM $CaCl_2$ pH 6.3) and AtkaB (25 mM HEPEs, 800 mM KCl, 1% OG, 1 mM $CaCl_2$ pH 6.3) and eluted over the salt gradient. Protein elutions were run on a 12% SDS-Page gel and checked on the NanoDrop to verify protein purity and DNA cleanliness with 260/280 ratios. Clean protein was then collected and concentrated in 30 K amicon concentrators. Protein concentration was measured by the Bradford assay and spin labeled and reconstituted according to the following methods[4].

CD, FTIR, and terbium assays were performed previously to verify functionality and folding of the above constructs[3,4].

2.2.4 Site-Directed Spin-Labeling and Fluorophore Labeling

In order to perform EPR or site-specific fluorescent techniques a label must be attached to the protein at the desired location. The labels are attached covalently using cysteine chemistry (a sulfhydryl-specific label) following the mutagenesis steps. For EPR, a standard, and well-studied

MTSL label (*S*-(1-oxyl-2,2,5,5-tetramethyl-2,5-dihydro-1H-pyrrol-3-yl) methyl methanethiosulfonate) is used in most cases. This label is attached by creating a disulfide (S-S) bond between the MTSL sulfhydryl group and the existing cysteine[14,15]. The label itself has a stable free radical localized in the $2p_z$ π orbital of the ^{14}N-O bond[15]. The paramagnetic electron is stable and cannot distribute beyond these two atoms due to the stability, steric restraints, and sp^3 hybridization of the rest of the ring complex. The reaction for attaching the label is light sensitive and is reversible. MTSL is not soluble in buffer, so it must be solubilized in 100% ethanol first; this is best done fresh each time as MTSL can self-dimerize preventing the reaction with the protein[16]. After the label is attached to the protein, one must be very careful not to add any reducing agents to the mixture or the label will fall back off. The protein would then have the free radical available from the nitroxide for EPR detection[14,15]. Free-spin is very mobile and will be very noticeable on CW measurements so washing free label away and avoiding reducing agents is very important.

The use of MTSL (R_1 when attached to the protein) is advantageous compared to other labels, as it is already so well characterized using crystallographic analysis[17-20]. Between the pyrroline ring and the attachment to the protein backbone (C_α) there are five chemical bonds, X_1 to X_5. These bonds do not all freely rotate in space however, as each EPR spectra achieved would then just be very sharp averaged lines which do not give any insight into local structure or environment of the probe. Instead, the X_4 and X_5 bond (closest to the nitroxide ring) rotations dominate the spectra being observed. This is due to hydrogen bonding between the label S_δ and the C_α atom within the protein backbone (deemed the X_4/ X_5 model) *(Figure 2.4)*[17-19]. This additional backbone bond, which restricts the C_α- C_β-S_γ -S_δ (X_1, X_2, X_3) atoms dihedral angles, is the reason that anisotropic motion of the label can be observed on the EPR timescale[17-19]. For

example, the dihedral angles between the X_1, X_2, X_3 bonds have been analyzed and one can often predict both the solvent exposed angles for an α-helix, (X_1, $X_2 \approx -60°$, $X_3 \approx \pm 90°$) and angles under more restricted or tertiary contact ($X_1 \approx 180°$, $X_2 \approx 60°$ or $X_1 \approx -60°$, $X_2 \approx 180°$)[21]. The angles between these bonds are dependent on the location and accessibility of the label on each protein location as the R_1 label can adapt to packing or steric hindrance, so a sharp turn, mobile loop, β-sheet (internal, edge), or any differences in solvent accessibility/buried protein sites, will slightly influence the angle between these bonds[20].

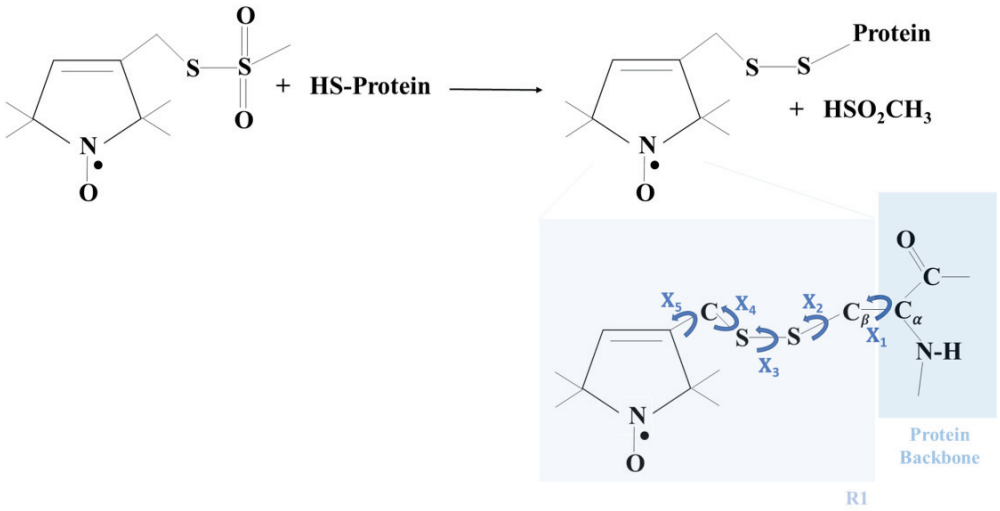

Figure 2.4: Spin-Labeling Reaction. MTSL attachment to a cysteine side chain, where the sulfhydryl-group of the MTSL covalently links to the cysteine forming a disulfide bone, producing R1 side chain (light blue). Methane sulfonic hydrate is a by-product of the reaction. Highlighted in the light blue box, are the dihedral angles of rotation throughout the sidechain when linked to the protein backbone (dark blue). Figure inspired by Langen, Biochemistry (2000).

For most of the fluorescent probe attachments the bond formed is an irreversible maleimide bond (C-S). This reaction is irreversible; however, it is more difficult to attach the label due to its light sensitivity and sensitivity to free oxygen species that may appear in the buffers. Extra degassing and no light exposure are thus required for these labels[22,23]. These labels are soluble in aqueous buffer, but should be solubilized fresh. Again, it is very important to avoid free label that

would appear as background and potentially adsorb to glass or membrane in solution, biasing measurements. The fluorescent labels used are selected according to the desired laser wavelength or excitation wavelength from a fluorimeter according to experimental design. The majority of the changes in label absorbance wavelengths are due to different degrees of aromaticity of the label, although this can be complicated by the fact that many structures are copyrighted[15].

Site-dependent labeling of this type is advantageous for high sensitivity localized structural study of local environments, dynamics, structures, and inter- or intra- molecular interactions/distances under controlled physiological conditions that can closely mimic native environments[14,15,22,23]. Labeling location (cysteine mutant) should be chosen with these considerations for each experiment. Planning the solvent accessibility of the label both for attaching the initial label and how tumbling and free or restricted rotation of the label are to be considered and will be reflected either in the error or the type of EPR spectrum which is produced (such as, restricted tumbling more immobile and broad). *(Figure 2.5)*

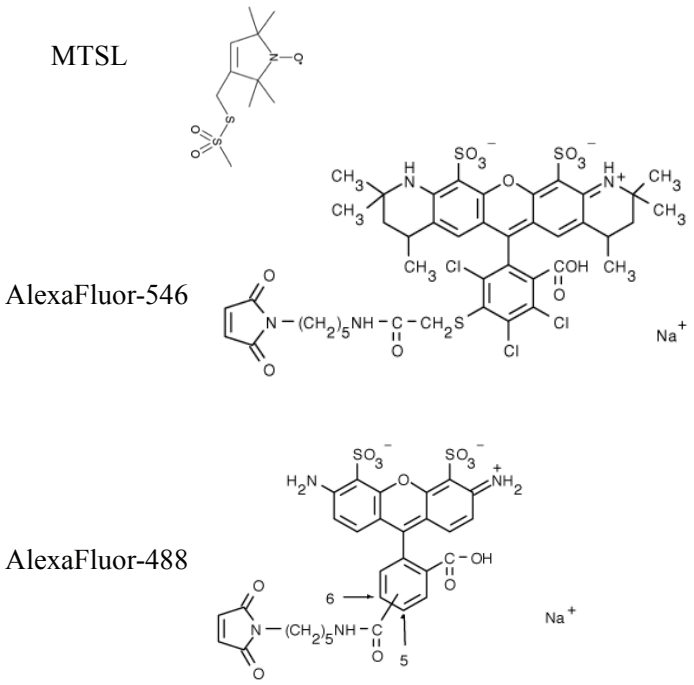

Figure 2.5: Structural Representation of different Probes used for Site-Directed Labeling. MTSL is used for EPR measurements. This probe has a clear size advantage for more closely mimicking proteins natural state and is less likely to interact with the local environment. AlexaFluor-546 and 488 are used in TIRF, FLIC, and other fluorescent measurements. Both fluoresce brightly and ideally have no impact on the proteins natural state and functionality. The AlexaFluor-546 label has a more flexible linker compared to the 488, which can influence the choice of label depending on experiments performed. There are slightly higher risks that these large labels with flexible linkers could form back-bonding interactions with the protein or interact preferentially with membrane, biasing measurements or errors predicted when compared to a freely rotating label.

2.2.4.1 C2A and C2AB were prepared for spin labeling by incubating the solution in DTT in a 1:2 ratio for 15 minutes. After incubation, the protein was spin labeled with MTSL in the dark, using a 1:10 protein to MTSL ratio. This labeling occurs for a minimum of 2 hours at room temperature or at 4 °C overnight with shaking[24]. The protein was then desalted on the Akta HiPrep 26/10 desalting column to remove any residual free label using metal free buffer (20 mM HEPEs, 150 mM KCl, pH 7.4) and concentrated to the desired volume to take EPR measurements using a 10K or 3K concentrator. If free label persists, the protein was washed while in the concentrator with excess metal free buffer[24].

2.2.4.2 Full length Syt1 or ΔC2B in Chaps were spin labeled on the Ni-NTA column in a small volume of wash buffer and allowed to bind with shaking in the cold room overnight- as mentioned in the Chaps purification section above.

2.2.4.3 Full length Syt1 in OG follows the fluorophore labeling, adding 1 mg MTSL rather than fluorophore label procedure below.

2.2.4.4 C2AB, FL SYT or ΔC2B in Chaps, and FL Syt in OG Fluorophore labeling: protein is prepared for labeling by washing into the desired Labeling buffer (25 mM HEPEs, 500 mM KCl, pH 7.4 and (1% detergent from above purifications for FL or ΔC2B) then incubating the solution in DTT in a 1:10 ratio for 2 hours at room temperature (4°C for 2 hours to overnight if the protein is unstable during purification)[25]. After incubation, the protein is run on a pre-equilibrated PD10 column (GE life sciences) in Labeling buffer and collected in half mL fractions. These fractions are run on the NanoDrop and protein fractions are collected and concentrated. The protein is then labeled with the desired label (0.5 mg to 1 mg Alexa-546, Alexa 488 (Invitrogen) or BODIPY Fl maleimide (Invitrogen)) or MTSL in foil a 1:10 protein to MTSL ratio). This labeling occurs for a minimum of 2 hours at room temperature or at 4°C overnight with shaking[24,25]. The protein is then run again down the pre-equilibrated PD10 column and fractions are checked on the Nanodrop. The labeled protein is then concentrated and washed thoroughly into Physiological buffer (25 mM HEPEs, 150 mM KCl, pH 7.4).

For MTSL labeling, the protein is washed on the concentrator until free spin is absent on the EMX.

For fluorophore labeling**,** the protein is then dialyzed through at least 12 L (4-6 swaps depending on timing) into physiological buffer over at least 2 days at 4°C[25].

2.2.5 Liposome LUV Extrusion:

Liposome extrusion allows for controlled addition of varied lipid mixtures and vesicle sizes depending on the desired physiological question being asked. This permits investigation with differing lipid charge compositions, membrane fluidity, vesicle curvature etc. Extrusion takes advantage of manually forcing clustered lipid components through a membrane of the desired liposome diameter. Before extrusion, the lipid is mixed in chloroform and methanol depending on lipid solubility then dried down either under nitrogen gas with vortexing or under vacuum with a rotary evaporator (RotaVap). It is very important with complex lipid mixtures to ensure that the lipid is properly mixed while drying, otherwise it is possible to produce heterogeneous liposomes (charge and distribution) within the solution. After evaporating all chloroform and methanol the dried lipid film is resuspended into the desired buffer and then freeze-thawed in liquid nitrogen. Freeze-thawing breaks up the largest lipid clusters, as initial resuspension produces large lipid leaflets, resembling layers in an onion[26]. After 5 or more freeze-thaw cycles the lipid is manually pushed through the membrane of selected pore diameter[26,27]. The lipid typically transitions from a white-opaque solution to an opalescent, nearly clear solution as it is successfully extruded. Sustained strong force produces the most uniform liposomes, but typically small distributions in size or multilamellar liposomes could appear[27]. Over time, in refrigerated storage the liposomes will eventually recluster into larger layers so samples are best used within days of extrusion (the lipid tails will also begin to oxidize more quickly once in aqueous solution) *(Figure 2.6)*[27].

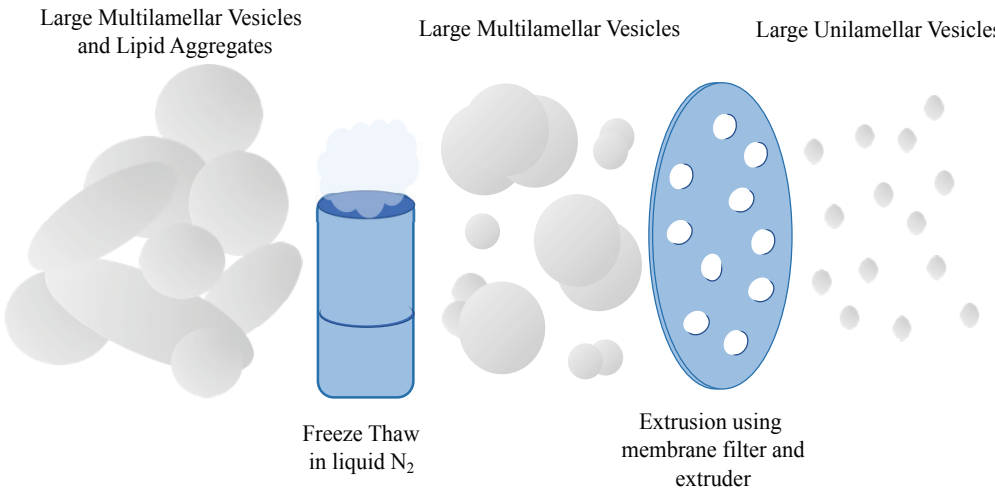

Figure 2.6: Lipid Freeze-Thaw and Extrusion. Initial resuspension of lipid into aqueous buffer produces large Multilamellar lipid aggregates which are difficult to push through an extruder membrane. Freeze thawing breaks up the largest of aggregates aiding in the extrusion process. Once the lipid has been freeze-thawed, the lipid is manually pushed through a membrane of chosen pore diameter.

2.2.5.1 For EPR measurements, varying lipid conditions: POPC:POPS, POPC:POPS:PIP_2, POPC:PIP_2 (at ratios dependent on experiment set-stated when used) were combined in chloroform and methanol in a round bottom flask and then dried under vacuum using a RotaVap for ~3 hours. The lipids were resuspended to the desired volume in Ca^{2+} buffer (20 mM HEPEs, 150 mM KCl, 1 mM Ca^{2+}, pH 7.4). The lipids were then freeze-thawed 5 times using liquid nitrogen. Lipids were extruded through a 100 nm pore diameter polycarbonate filter using a hand-held Mini extruder (Avanti Polar Lipids, Birmingham, AL)[4,28].

2.2.5.2 For sedimentation assays, POPC:POPS, POPC:PIP_2, POPC:POPG, POPC:POPS:DDAB, POPC:Cholesterol:POPS, POPC:Cholesterol:POPE:POPS:PIP_2, DOPC:Cholesterol:DOPE:DOPS:PIP_2, DPPC:Cholesterol:DPPE:DPPS:PIP_2, or brain PC:Cholesterol:PE:PS:PIP_2 (depending on experiment set ratios varied and are stated with data) were combined in chloroform and methanol in a round bottom flask and then dried under vacuum using a RotaVap for ~3 hours. Lipids were then resuspended in Sucrose buffer (20 mM HEPEs,

256 mM sucrose, pH 7 (sucrose concentrations were adjusted according to desired final salt buffer to maintain isosmotic pressure)) to permit ultracentrifugation sedimentation. The lipids were then freeze-thawed 5 times using liquid nitrogen. Lipids were extruded through a 100 nm pore diameter polycarbonate filter using a hand-held Mini extruder (Avanti Polar Lipids, Birmingham, AL)[4,28].

2.2.6 FL Syt1 Reconstitution

Reconstitution is another lipid technique used to control lipid composition, but here with protein included to form proteoliposomes. The desired lipid components are again mixed in chloroform and methanol depending on lipid solubility then dried down under nitrogen gas with vortexing. It is still very important with complex lipid mixtures to ensure that the lipid is properly mixed while drying, and that the lipid film is not too widely distributed in the tube being used as one is typically sample volume and concentration limited. After evaporation, the tubes are desiccated under vacuum for an extended period to remove any remaining reagent. The protein in detergent is then added to the lipid film while vortexing to resuspend the lipid. Depending on experimental design the detergent concentration is also adjusted to a value either slightly or well above the detergent's CMC to help incorporate the lipid into the micelle and prevent precipitation of the protein[29-31]. The resulting mixture is incubated at room temperature for an hour to an hour and a half with occasional vortexing to promote incorporation of lipid into the protein-containing micelles, forming mixed micelles. After sufficient time has been provided to form mixed micelles, again depending on experimental design, buffer without detergent is used to dilute the sample either just above or below the CMC to either slowly or quickly dissociate the detergent from the mixed micelles leaving proteoliposomes[29-31]. *(Figure 2.7)* The rate at which detergent is removed

from these mixtures can control the homogeneity of the resulting proteoliposomes[30]. To remove all free detergent from solution the solutions are dialyzed in excess buffer with the addition of BioBeads to enhance detergent absorption and removal. Unless additional steps are taken (electrical plating, etc) the initial micelle size and detergent dictate the size of the proteoliposome produced[31].

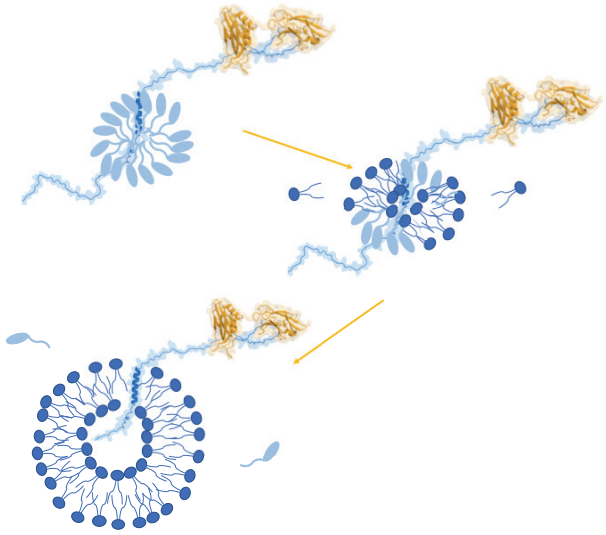

Figure 2.7: Representation of the reconstitution of Syt1. Syt1 starts in micelles, represented here as Chaps bean-like detergent. As lipid is added mixed micelles form as the detergent incorporates the lipid. After the sample is diluted below the detergent's CMC full liposomes form leaving detergent free in solution to dialyze away.

2.2.6.1 Fl Syt was reconstituted into either: POPC:Cholesterol (80:20), POPC:POPS (85:15), POPC:POPS:DDAB (70:15:15), POPC:POPS:PIP_2 (85:10:1.25), or PC:Cholesterol:PE:PS:PIP_2 (36:20:30:15:1). Lipid combinations were mixed in chloroform and methanol and evaporated under N_2 gas with vortexing[25]. The lipids were then put under vacuum overnight. Lipid films were dissolved in reconstitution buffer with 20 mM HEPEs, 150 mM KCL, 1% Chaps, pH 7.4 and the desired volume of protein to equal a 1:250 protein to lipid ratio with vortexing. The mixture was left to incubate for 1.5 hours at room temp with occasional vortexing[25]. The mixture was then diluted below the critical micellar concentration with addition of metal free

buffer (20 mM HEPEs, 150 KCl, pH 7.4). Protein was then dialyzed into metal free buffer to remove detergent in the presence of BioBeads. Desired divalent cations (Ca^{2+}, Cd^{2+}, Pb^{2+}) were added in separate buffers depending on desired EPR measurements.

2.2.7 Ultracentrifugation Sedimentation Assays

A vesicle sedimentation ultracentrifugation binding assay can be used to determine the binding affinity of proteins to lipid membranes[32]. In this experiment liposomes of a decided size are extruded in sucrose buffer to fill or load them, thus producing heavy liposomes that can pellet in an ultracentrifuge. They are then pelleted at a speed which does not also result in the pelleting of free-floating lipid. This removes lipid that would produce light scattering in the later fluorescent measurements. These pelleted liposomes will be clear if properly extruded and not largely clustered into membrane sheets. The pellet is then resuspended in a buffer with salt concentrations selected to be isosmotic to the sucrose concentration within the liposomes, to prevent bursting or rupture. Protein is then added at low concentrations to tubes and liposomes can be either titrated throughout the tubes or held constant depending on experimental setup (could vary another reagent, i.e. ATP) and allowed to incubate. This incubation will allow an equilibrium to be reached between protein bound to the lipid membrane and free in solution. After a short incubation period the series of tubes is then pelleted again for a period of time. A constant volume of aqueous solution is then carefully removed, avoiding any agitation or pipetting in proximity of the pellet which would result in free lipid and light scattering[32]. The unbound protein will be present in this aqueous solution at varying concentrations resulting in the titration. Unbound protein can be detected either

by intrinsic tryptophan emission or by emission from an attached label depending on the experiment design *(Figure 2.8)*.

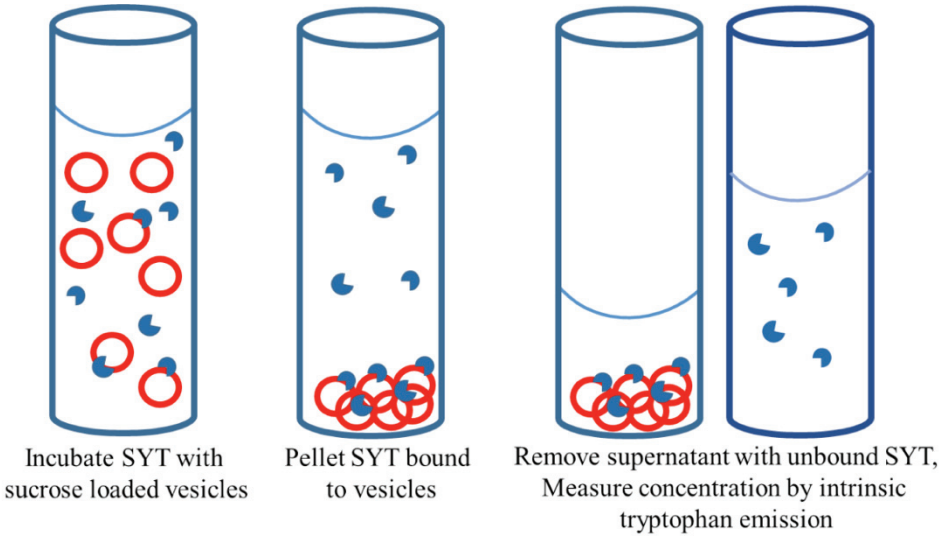

Figure 2.8: Ultracentrifugation sedimentation assay visualized over time. Through incubation, pelleting, then sample discarded (pellet) and sample for measurement (supernatant).

2.2.7.1 The ultracentrifugation assay was used to measure cytosolic protein (C2A, C2B, C2AB) binding affinity to LUVs of different lipid composition or protein mutants (KAKA, RQRQ) under varying salt, ATP, or metal conditions[32-35]. First, sucrose loaded LUVs were pelleted using a tabletop Ultracentrifuge at 100,000 xg, 20 degrees C for 1 hour to remove any free lipid that did not successfully extrude and to exchange the buffer. The pelted LUVs were then resuspended in the desired metal and salt buffers (20 mM MOPs, 100-300 mM KCl, pH 7 and either 1 mM $CaCl_2$, 1 mM $CdCl_2$, or 4 mM EGTA). An LUV titration was performed using constant 2 nM unlabeled protein, or with protein labeled Bodipy fl maleimide when working with ATP (ATP interferes with 285 nm excitation). After 10 minutes of incubation the LUVs and protein were again pelleted at 100,000 x g, 20 degrees C for 1 hour. The top free volume of each centrifuge tube was then removed to measure free protein concentration using intrinsic tryptophan

fluorescence or Bodipy emission (excitation 285 emission 342 or 480 nm excitation and 520 nm emission for Bodipy) using a FluorMax3 from Jobin Yvon (Edison, NJ). Removal of volume for measurements was well below the full sample volume to avoid light scattering due to free floating lipid near the LUV pellet. When binding was detected the fraction bound, f_b, and the molar partition coefficient, K (M^{-1}), were determined using $[P]_m/[L]=K[P]$, where $[P]_m$ is the protein bound to membrane (M), [L] is the accessible lipid concentration (M), and [P] is the concentration of protein in the bulk aqueous phase. Provided protein conditions are sufficiently dilute, $f_b=K[L]/(1+K[L])$. Lipid concentrations were verified using the phosphate assay[32-35].

2.2.8 Phosphate Assay

The phosphate assay is a colorimetric detection assay for determining concentration of lipid-phosphate present in a solution using UV-Vis[35]. Lipids are digested in acid and free phosphate is then bound to molybdate, producing a blue color depending on the phosphate concentrations present[35]. A standard curve of known free phosphate is used to determine unknown sample concentrations.

2.2.8.1 The phosphate assay performed is the modified version from Pokorny et al. of the Bartlett Assay[35,36]. To determine concentration of lipid phosphate in lipid extrusion and reconstitutions, standards were prepared to create a standard curve. Samples were heated to 200 degrees C in perchloric acid for 1 hour, 1% ammonium molybdate and 4% ascorbic acid was added and samples were left to incubate at 37 degrees C for 30 minutes. Sample absorbance was then measured on the UV-Vis at 800 nm.

2.2.9 Electron Paramagnetic Resonance Continuous Wave (EPR CW) measurements

Site-directed spin-labeling (SDSL) EPR is a high-resolution technique for examining local rather than global effects within a protein system. In combination with a more global technique (such as HSQC NMR or some fluorescent techniques) overall cause-and-effect of different experimental conditions can be fully localized within the protein of interest. SDSL EPR utilizes site-directed mutagenesis to introduce a cysteine to a site of interest and then attaches a paramagnetic spin-probe via spin-labeling. Using continuous wave (CW) EPR, this probe produces information regarding the site's dynamics, local environment (hindered/spatially restricted, unhindered, buried, free), the secondary structure within the protein (mobile/immobile-loop, helix sites, beta-sheets, sharp turns, etc.), and any tertiary contacts or structures. This technique can also be used to determine a proteins' membrane penetration depths, close distances (below 2 nm) within the protein, and even binding affinities with a few additional experimental probes or experimental steps. Pulsed EPR can also determine distances within the protein or proteins (between multiple probes) discussed below. This diversity of information acts as puzzle pieces within a structure mapping accessibility, mobility, conformational changes, interactions with other proteins or components in solution (membrane), oligomerization, tumbling, and stability to name a few, overall gaining a more intimate picture of the proteins structure and overall function.

EPR only requires the presence of an added small stable free radical (the paramagnetic spin probe) so samples can be prepared under a diverse range of solvents and components which can closely mimic physiological systems. It can also be run over a large range of protein sizes,

concentrations, and under very small sample volumes. The technique is also non-destructive, so samples can be reused if required. Systems can thus be studied where one is often sample limited or unstable at high concentrations. These are huge advantages over other structural techniques, which often rely on high (non-physiological) sample concentrations, introduction of very large labels or probes, or specific solution content (low or high salt, stabilizing agents, etc.). So, EPR compares favorably to some NMR techniques, crystallography, and fluorescent or electron microscopy, where there is often concern if effects being observed are physiologically relevant or artefactual due to the conditions used. EPR also does not have to be a "snapshot-in-time;" the solution can be active and unfrozen so it can be used to measure real-time dynamics, decay, transport, and flux of a label as different experimental components are varied.

EPR is a subset of spectroscopy, which is defined as the measurement of spectra produced when matter interacts with or emits electromagnetic radiation. Here, electromagnetic radiation is the coupling of electric and magnetic fields oscillating perpendicular to one another carrying with them electromagnetic energy[16]. Generally, spectroscopy measures resonance transitions and frequencies relative to an oscillatory source. For EPR, it measures quantized electron spin transitions relative to or induced by the oscillating magnetic field.

The technique works by measuring the interaction of the paramagnetic probe's unpaired electron (spin quantum number $s = 1/2$) with the magnetic field, this is called the Zeeman effect[16]. An unpaired electron has an intrinsic spin which produces a magnetic moment. This spin will experience torque when placed in an external magnetic field causing precession of the magnetic moment of the electron, this precession frequency is called the Larmor frequency (ω_L) where:

$$\omega_L = -\gamma B_0$$

Equation 2.1

Here, γ is the gyromagnetic ratio of the electron, a property of the electron (being the ratio of the electron's magnetic moment and the electron's angular momentum) and B_0 is the external magnetic field. This precession is often aligned along the magnetic field which is itself aligned along the z-axis. The electron can exist in two energy states, defined as allowed magnetic components m_s = -1/2 or +1/2 which are aligned along (parallel-lower energy) or against (perpendicular-higher energy) the magnetic field, respectively. These energy states are also the Zeeman levels of the spin system in a static external magnetic field[14]. Each level's energy of interaction is defined first by the Zeeman energy of interaction:

$$H_Z = g\beta S_z B_0 = g\beta S B_0$$

Equation 2.2

Where S is the electron spin angular momentum (S_z in the z direction), β is the Bohr magneton of the electron (9.2741×10^{-24} Joule/Tesla or 9.2741×10^{-21} erg/Gauss), B_0 is the external magnetic field of the magnet (Tesla or Gauss, where 1 G = 10^{-4} T), and g is the g-factor (Lande splitting factor) which defines the spectral absorption position of the paramagnetic species. g_e = 2.0023 for a free electron, when the electron is in an isotropic system and moving freely and rapidly[14,37]. The Hamiltonian can also be defined in terms of energy:

$$E = -\mu B_0 = g\beta S B_0$$

Equation 2.3

Where, the energy of interaction (E) is defined in terms of the unpaired electron's dipole moment (μ) within this magnetic field (B_0)[38]. This can also be expressed with the magnetic spin quantum number m_s as:

$$E = m_s g\beta S B_0$$

Equation 2.4

Where again, m_s = -1/2 or +1/2. These -1/2 and +1/2 states are low energy and high energy respectively[38]. At thermal equilibrium, there will be more spins in the -1/2 (parallel) state, according to the Boltzmann distribution. This is what produces the net magnetization in the z-axis, along the external magnetic field. The energy difference between the electrons low and high energy states (ΔE) is defined by:

$$\Delta E = h\nu = g\beta B_0$$

Equation 2.5

Where h is Plank's constant, 6.626×10^{-34} (Joule-second) and ν is the electromagnetic radiation's frequency[39]. This means, when resonance conditions are met and the microwave radiation ($h\nu$) applied matches the amount of energy between the electron's two states (ΔE) a transition between spin states can occur. This occurs only when $|\Delta m_s|$ states add to 1 and when the electromagnetic radiation is properly polarized[14]. To be polarized, one must be at a proper microwave frequency such that the fixed magnetic field's oscillation is directly perpendicular to the static magnetic field. This is achieved by holding the microwave frequency constant (fixed) and varying the magnetic field until it is at resonant absorption. Overall, this produces a single line for a CW EPR spectrum *(Figure 2.9).*

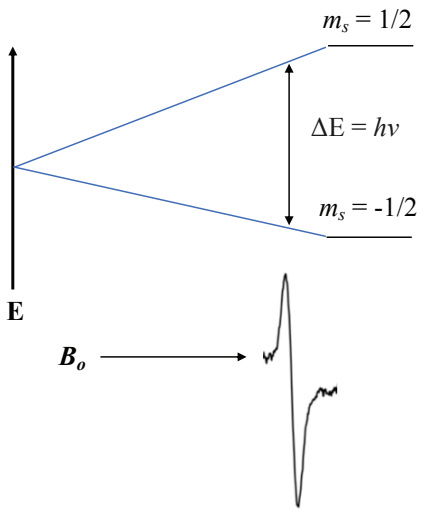

Figure 2.9: Zeeman Splitting. A single line is produced for a CW EPR spectrum when photons are absorbed and detected for a specific resonant frequency (v) and the overall microwave radiation (hv) matches the energy difference (ΔE) required to excite an electron from the ground to excited state *(m_s = - ½ to m_s = ½)*. E notes an increase in energy and H_0 the magnetic field.

However, there are typically three lines for a nitroxide label, this is due to interactions of the unpaired electron's magnetic moment with the nitrogen nucleus' magnetic moment which is in close proximity to the electron; this is called the hyperfine interaction (*Figure 2.10*)[39]. The hyperfine interaction arises because of the nearby nitrogen's ^{14}N isotope, which has a nuclear spin angular momentum of I=1. The other nearby nuclei are ^{12}O or ^{16}C which have 0 spin, and do not have rare isotopes present in sufficiently high quantity (above 1%) to contribute any additional spitting. The presence of the additional nuclear spin states allows the electron to experience an additional magnetic field which changes the allowed energy levels of the electron, according to $2I$ + 1 orientations, thus the single absorption line will split into three lines in the spectrum[14,37,38]. These three, allowed discrete electron spin orientations relative to the nitrogen's nuclear spin are defined as I_z = -1, 0, and +1 in the z-plane relative to the magnetic field[14,37,38]. On a CW EPR spectrum these are frequently referred to as the low field, center field, and high field lines from

left to right. These spin orientations then produce hyperfine splitting energy levels defined as $1/2A_0$, where A_0 is the hyperfine coupling constant[14,16,37]. This produces an additional definition for the high and low energy state differences:

$$\Delta E = h\nu = g\beta B_0 + A_0 m_I$$

Equation 2.6

Where, m_I = *-I, -I+1, I-1, I,* Δm_I must equal 0. The hyperfine interaction can first be defined as a tensor, A[37]:

$$\mathrm{A} = \begin{bmatrix} A_{xx} & A_{xy} & A_{xz} \\ A_{yx} & A_{yy} & A_{yz} \\ A_{zx} & A_{zy} & A_{zz} \end{bmatrix} \rightarrow \mathrm{A_{pc}} = \begin{bmatrix} A_{xx} & & \\ & A_{yy} & \\ & & A_{zz} \end{bmatrix} \rightarrow \mathrm{A_0} = \frac{(A_{xx}+A_{yy}+A_{zz})}{3}$$

Equation 2.7

In the principal axis system of the molecule, the tensor A reduces to just its principal components, or diagonal (A_{pc}). For a rapidly tumbling isotropic system the diagonal components are further averaged into the single quantity, A_0 in equation 2.6. In an anisotropic system, where the label has direction dependent properties and is not freely moving in any direction, the hyperfine constant will have a greater effect on the width of the spectra and the hyperfine contribution can be expressed using the three diagonal components[14,39].

Similarly, in an anisotropic system, the g-factor can be expressed as a tensor, g[37]:

$$\mathrm{g} = \begin{bmatrix} g_{xx} & g_{xy} & g_{xz} \\ g_{yx} & g_{yy} & g_{yz} \\ g_{zx} & g_{zy} & g_{zz} \end{bmatrix} \rightarrow \mathrm{g_{pc}} = \begin{bmatrix} g_{xx} & & \\ & g_{yy} & \\ & & g_{zz} \end{bmatrix} \rightarrow g^2 = g_x^2 l_x^2 + g_y^2 l_y^2 + g_z^2 l_z^2$$

Equation 2.8

Where the matrix is reduced to its principal components, g_{pc} in the principal axis system. For the g tensor, this corresponds to the axis of molecular symmetry[37].The final relation then gives

the effective g factor for an arbitrary cosine directionality away from the molecular symmetry axis[37].

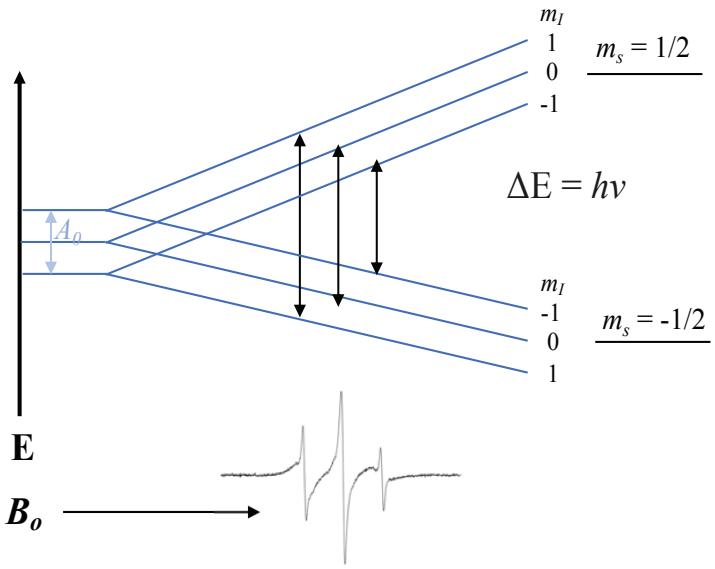

Figure 2.10: The hyperfine interaction. Energy (E) level diagram for a single electron, $m_s = 1/2$, interacting with a nuclear spin $I = 1$ ($m_I = -1, 0, 1$) at constant frequency with swept magnetic field (B_0). There are three possible energy transitions shown by black arrows which will produce CW EPR peaks (low field, center field, high field, from left to right).

For a nitroxide in aqueous solution, the resulting CW spectrum consists of three sharp, narrow lines due to high motional averaging. In practice, however, spectra of R1 on proteins often display a varying degree of broadening and a variety of lineshapes. There are several factors that contribute to broadening and observed lineshape. The first is orientationally averaging, which practically takes the form of label and/or protein tumbling and motion. As described above, the A and G tensors are dependent on the anisotropy of the label[37]. A label placed on a surface exposed site with few nearby sidechains, such as a loop within a protein, will tumble rapidly, resulting in highly averaged, narrow lines. A label buried in a protein or membrane, however, will have very restricted mobility that results in more anisotropic motion and a very broad spectrum, which is composed of contributions from only a few, defined label orientations. Spectra which appear fully

immobilized within the timescale of a CW experiment are termed powder patterns, and are frequently seen for powder and crystalline samples, or protein sites with only a particular allowed label conformation[37].

The spectrum is not always broadened purely due to restriction of the label's rotation/tumbling, however, as the protein being labeled can also tumble on the EPR timescale if it is small enough (less than 15 kDa). The local protein backbone mobility can have an effect as well. These tumbling effects can be defined in terms of the label's rotational correlation time (τ_c) which represent the length of time a label rotates or stays in a single orientation[14,37,38]. EPR is sensitive throughout the range of 0.1 to 100 ns[14,16,37,38]. While fast tumbling of the label causes a loss of detail in the spectrum due to averaging, it is not always disadvantageous. As an example, a small protein complexing with a larger protein or membrane surface would reduce overall tumbling, which allows verification of binding.

In addition to the environment around the label and the protein size, the correlation time is also sensitive to temperature and the sample viscosity. The addition of ~30% or more of viscous reagents or ozmolites to a solution, including: glycerol, sucrose, or PEGs, will further reduce the tumbling rates of the overall protein and result in a more anisotropic spectra[37,38]. Overall, linewidths of the EPR spectrum broaden with decreasing motion. The rotational correlation time can be defined in terms of temperature, viscosity and radius (where the sample is approximated to a sphere) by:

$$\tau_c = (6\left(\frac{kT}{8\pi\eta R^3}\right))^{-1}$$

Equation 2.9

where, *k*T account for temperature dependence, *k* is the Boltzmann constant, T is temperature, η represents viscosity, and R is the radius of the sphere in the model[37]. This rotation time then

represents the time required for a single radian rotation[14]. Rotational correlation time can also be defined in terms of the CW spectrum's peak heights and widths:

$$\tau_c = 6.5 \cdot 10^{-10} \cdot \Delta H_{p\text{-}p}(0) \cdot \left(\frac{A(0)}{\sqrt{A(-1)}} - 1\right)$$

Equation 2.10

here, the notation refers to peaks (low field, center field, high field) in terms of their m_I, being 1, 0, and -1 respectively[14,39]. So, here $\Delta H_{p\text{-}p}(0)$ refers to the peak to peak width of the central line and A(0) and A(1) are the peak-to-peak amplitudes (heights) of the center and high field lines respectively[14]. This treatment of rotational correlation time is valid for the fast-motional regime[39]. This relationship can alternatively be expressed with the addition of constants in relation to each peak-to peak width ($\Delta H_{p\text{-}p}(m_I)$) of the lines in the CW spectra[14,37,39]:

$$\Delta H_{p\text{-}p}(m_I) = [A + Bm_I + Cm_I^2]\tau_c + X$$

Equation 2.11

where, the peak-to-peak width is dependent again on the magnetic spin quantum number or spin state (m_I). This dependence is why each line will broaden at a different rate when tumbling changes. A, B, and C are linewidth parameters, which depend on the magnitude of the magnetic anisotropies (g and A_0) and the rate or molecular reorientations in the liquid[37,39]. τ_c is again the rotational correlation time (typical range for low viscosity samples is 10^{-10} to 10^{-11} seconds) and X, is motion independent contributions to the linewidth[14,37]. For the CW spectrum, the A term broadens all lines equally[14]. The B term is negative for nitroxide spin labels at 3400 G, this leads to broadening of the high field ($m_I = -1$) line and narrowing of the low field ($m_I = 1$) line[14,37]. Here, C ≈ -B so the C term is positive. The C term contributes to broadening of the low and high field lines but does not affect the center line ($m_I = 0$)[14,37]. These various terms explain the overall

asymmetry in a line shape undergoing intermediate motion[14]. Again, for fast exchange these terms average to give fairly symmetric, sharp lines[39].

Another reason for spectral broadening is saturation. Above, ΔE was defined between a low and a high energy state for the free electron. When photons of microwave energy/radiation (*hv*) are absorbed by a low energy spin state (aligned with the magnetic field), they jump to the higher energy level (aligned against the magnetic field)[14]. These spins must then in some way relax, or decay, back down to the ground state by emitting an equivalent photon of energy. Being able to observe these absorbance events is dependent on there being more spins in the ground state than in the excited sate. At room temperature, the difference is very small, and can be defined using the Boltzmann distribution:

$$\frac{n_{excited}}{n_{ground}} = e^{\frac{\Delta E}{kT}} = e^{\frac{g\beta H}{kT}}$$

Equation 2.12

where, $n_{excited}/n_{ground}$ are the ratio between the populations of spins in the excited and ground state, *k* is the Boltzmann constant (1.3807 x 10^{-16} erg/K or 1.3807 x 10^{-23} J/K, and T is the absolute temperature[37]. The Boltzmann constant and temperature together represent the average thermal energy. Again $\Delta E = g\beta H$ gives the energy difference between the two states. If the ratio between these states ever reaches full equilibrium ($n_{excited}/n_{ground} = 1$) or the levels of the excited state exceed the ground ($n_{excited}/n_{ground} > 1$) the system becomes saturated and the observed spectrum disappears[37,40]. In practice, this is only seen when excess microwave power is applied to the sample for a long period (see EPR power saturation below) due to the various pathways through which the excited spin state can relax.

The two main relaxation processes are spin-lattice relaxation, and spin-spin relaxation. Spin-lattice relaxation describes the transition back down to the ground state, through emission or

transfer of thermal energy to the environment (lattice)[41]. This relaxation rate and restoration of thermal equilibrium is defined as T_1, deemed either spin-lattice relaxation or longitudinal relaxation time[37,41]. Spin-lattice relaxation changes the overall Zeeman energy in the system. This relaxation is utilized in EPR power saturation, where additional paramagnetic reagents are added to the system, and energy is transferred first to these reagents through Heisenberg exchange and then to the environment (lattice), to accelerate relaxation and determine a spin label's location. For Heisenberg exchange to occur physical contacts and orbital overlap between the two species (the label and a relaxing agent) must be present to allow the excited spins to relax and exchange between orbitals[42,43]. As increasing degrees of Heisenberg exchange are observed in a spectrum, the lines continue to broaden, until they finally merge into a single peak[42].

In contrast to spin-lattice relaxation, spin-spin relaxation involves other spins in the system which cause mutual spin flips and do not affect the total number of spins in the excited or ground state, but only the lifetime for the excited state[37,41]. In a sense, this is because many spins in close proximity produce small magnetic fields themselves, with each spin experiencing a different frequency leading them to fall out of phase. The rate at which spins relax through this method is called T_2, or alternately either spin-spin relaxation or the transverse relaxation time[41]. This method does not change the overall Zeeman energy in the system and dominates the spin relaxation at low microwave power. For nitroxides, T_2 is normally much shorter than T_1, and so CW spectra are mostly dominated by T_2 related effects[42,43].

The relaxation processes that affect the observed CW spectrum can also be classified depending on whether they produce homogeneous broadening or inhomogeneous broadening. Homogeneous broadening occurs due to other electrons or nuclei in proximity to the free electron causing their own instantaneous magnetic fields. In relation to T_2 effects, homogeneous

broadening can be the result of dipolar interactions (through space interactions), where similar spins appear at high concentrations in solution and can exchange readily[42,43]. This type of broadening can be used for the determination of distances within ~8-20 angstroms[16]. Homogeneous broadening is also observed for T_1 relaxation due to Heisenberg-spin exchange, and for the motional narrowing / broadening effects described above (*Figure 2.11*)[42,44]. Homogeneous broadening results in Lorentzian shaped lines of averages of many uniform dipoles.

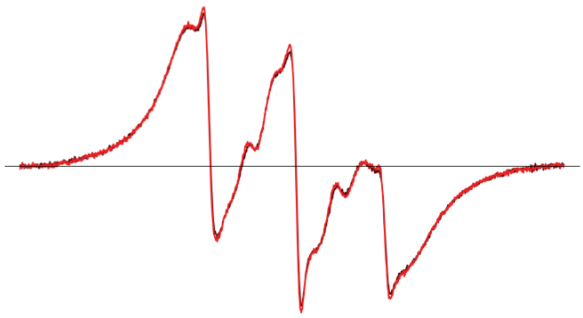

Figure 2.11: Broadening Effects on a CW Spectrum. This causes a loss of symmetry of the three peaks due to a negative slope or sliding baseline toward the high-field line. The resulting spectra shows a higher low field line than central line.

Inhomogeneous broadening is the result of spin-packets experiencing different effective magnetic fields. This type of broadening results in a more Gaussian type shape due to non-uniform dipole averaging of different spin packets which are shifted in frequency from each other and excited in different groups only when in resonance with the magnetic field sweep. Again, in most cases for CW EPR, broadening is a contribution of both homogeneous and inhomogeneous components, thus being both Lorentzian and Gaussian distributions, also known as a Voight shape[42].

A combination of these different broadening and relaxation pathways produce the information filled CW EPR spectra. To fully interpret this information the practical aspects of setting up a CW instrument should first be addressed. The main components of the machinery are:

the magnet (which produces the magnetic field), the microwave source, a resonator (to hold and amplify the sample), and a computer for detection and analysis[16].

Continuous wave EPR spectra are typically recorded at constant microwave frequency (X band is about 9.5 GHz) while sweeping the magnetic field (for MTSL often 100 Gauss sweeps centered around 3509 G, unless sites are particularly inhibited and the spectra is broad, then usually 150 Gauss). Resonators are designed to resonate or store microwave energy. This aids in sensitivity, since magnetic resonance transitions have a much smaller moment than in other forms of spectroscopy (eg optical) and also involve much smaller population differences[38]. Resonators work by orienting the electric and magnetic fields directly out of phase, creating "standing waves." The sample is then placed in a location with maximized magnetic field and minimized electric field[38]. Microwaves first enter the resonator through a passage of controlled size, dictated by the iris screw. The iris screw is adjusted to control the number of microwaves that enter and are reflected back from the sample cavity until critical coupling is achieved for the resonator. In this condition, absorption is maximized and there is no reflection out of the resonator. During the field sweep experiment, the sample becomes excited and the resulting absorption causes a loss of critical coupling, resulting in observable reflections[38]. A proper resonator must be chosen for desired experiments depending on sample size/volume and concentration limitations.

The spectra are observed through the detection diode and displayed as the first derivative of the absorbance spectra, because the spectrometer uses phase sensitive detection to enhance the signal-to-noise ratio and filter out electrical interference[38]. Phase sensitive detection requires modulation of the magnetic field at the site of the sample (sinusoidally) at a set modulation frequency (of 100 kHz, around 1 G amplitude for X-band). These values are chosen so that, the amplitude is ~10% of the peak-to-peak width of the each of the CW spectrum peaks. If the chosen

value is too high or low broadening, increased noise, and distortion of the lineshape will occur and information will be lost[38]. The phase sensitive detector then filters out all signals which are not modulated at 100 kHz, by comparing the phase of the signal amplitude to the modulating source. Signals that are the product of noise and electrical interference are not amplitude modulated and are thus suppressed[16,38]. EPR signals are approximately linear over the modulation amplitude, so when the signal is transformed into a sine wave, the amplitude of the signal is proportional to the signal's slope, resulting in a first derivative appearance for the output *(Figure 2.12)*[38].

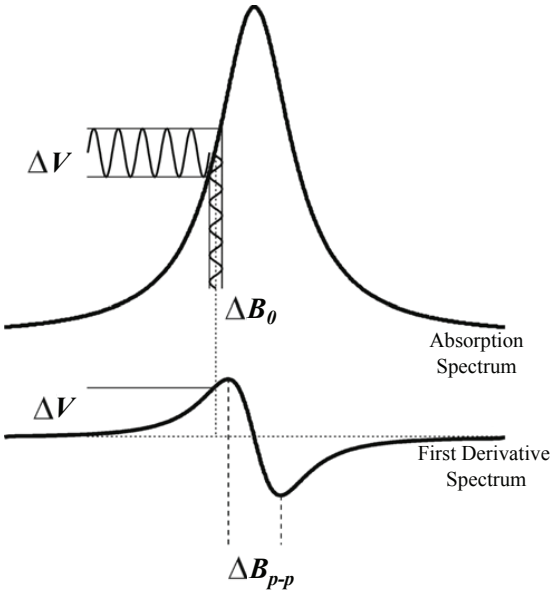

Figure 2.12: Field Modulation and Phase Sensitive Detection. To improve the signal-to-noise of a CW spectrum, a small (1G) 100 kHz modulation of the magnetic field is applied. A phase sensitive detector filters out all signals which are not modulated at 100 kHz, by comparing the phase of the signal with that of the modulating source. Detection is then displayed as the first derivative of the absorption line by field modulation with an amplitude, ΔB_0. The signal after the MW diode oscillates with the frequency of the field modulation (with amplitude ΔV). The signal after the phase-sensitive detector is a DC signal with that amplitude ΔV. The field difference between the inflexion points of the absorption line-shape is the peak-to-peak line width, $\Delta Bp\text{-}p$ of the derivative line-shape. Figure modified from Jeschke. 2007. ISBN: 978-0-387-25066-3.

Other parameters that will be set during a CW experiment should be briefly addressed. The receiver gain controls the magnitude of the signals received in the analog-digital converter[38]. Gain

set too high will cut off the tops and bottoms of peaks, gain set too low will result in digital noise. Microwave power is the power irradiating the sample. The observed signal increases linearly with the square root of power until saturation occurs[38,45]. When not performing power saturation experiments, the power should be in the linear range and will in part depend on the resonator chosen (dielectric vs. high power cavity resonators). The power is usually controlled by varying the attenuation, which is measured in log decibels. Samples in the dielectric resonators are typically run with an attenuation of 20 dB, whereas the cavity resonator can be run at 13 or 11 dB (addressed in more detail below). Next, there is the conversion time, which varies the amount of time the analog to digital converter spends at each point[45]. This effectively controls the rate at which the magnetic field is swept. Similarly, the Time Constant sets a delay, or slows detection to filter out high frequency noise[45]. A higher time constant can thus further decrease detected noise, but too long will decrease or eliminate detected signal. Changing the conversion time also can reduce noise, so long as it is short relative to the time constant chosen. For practical measurements, it has been found that shorter time constants and conversion times with larger numbers of signal averages (the signal/noise increases during additive averaging proportional to the square root of scans taken) results in the highest quality spectra. The effect of too many scans should also be considered, however, as resonators may not absorb perfectly, with a non-zero baseline that can be detected in the spectra of dilute samples or when very large numbers of scans are taken. These baseline deviations will need to be corrected / removed in later processing[38].

Experimental setup conditions will not be the only factors that may affect a CW spectrum. Sample concentrations and volumes need to be considered before running the instrument. Dilute samples, often resulting from an inability of the protein to concentrate due to instability, can be run more easily in the higher volume of a flat cell in a high-powered resonator.

Finally, processing a CW spectrum for use should be addressed. A CW spectrum usually needs to be baseline corrected, phased, and normalized when being used to compare different conditions and changes in lineshape. If the baseline appears distorted due to amplification of the resonator background this can be corrected by using a spline function (tools addressed in methods below). Phasing a spectrum maximizes the second derivative of the sample, by first transforming the signal into a complex representation by the Hilbert transform, and then attempting to move the entire detected signal into the real rather than the imaginary component by complex multiplications with a series of phase values[45]. Next, the spectra are usually normalized (as the number of scans performed increases the signal intensity in an additive form) by dividing all values of the spectra by the value of the second derivative so that intensities and broad components of the spectrum are highlighted against each other and due to changes in spin label mobility and environment. This could also be performed by scaling the height of all the central lines to the same intensity (height scaling) to compare shapes; the choice depends on user preferences. Not all experiments should be normalized. If the same numbers of scans are performed for a set of experiments or intensities are adjusted relative to each data set, the detected intensity of the spin label is proportional to the concentration of the sample. It can then be utilized in assays to determine population distributions by shifts in mobility and immobility, for kinetic-label decays, or for affinity-based assays. In comparison-based line-shape analysis, the many reasons for differences in mobility, immobility and broadening that are described above will be translated into potential physical explanations based on the experimental setup and the known environment and structure of the labeled site. (*Figure 2.13*) Shown below is a grouping of typical lineshapes produced from a C2 domain, which depend on local secondary structure and environment. These will be addressed more closely in future chapters.

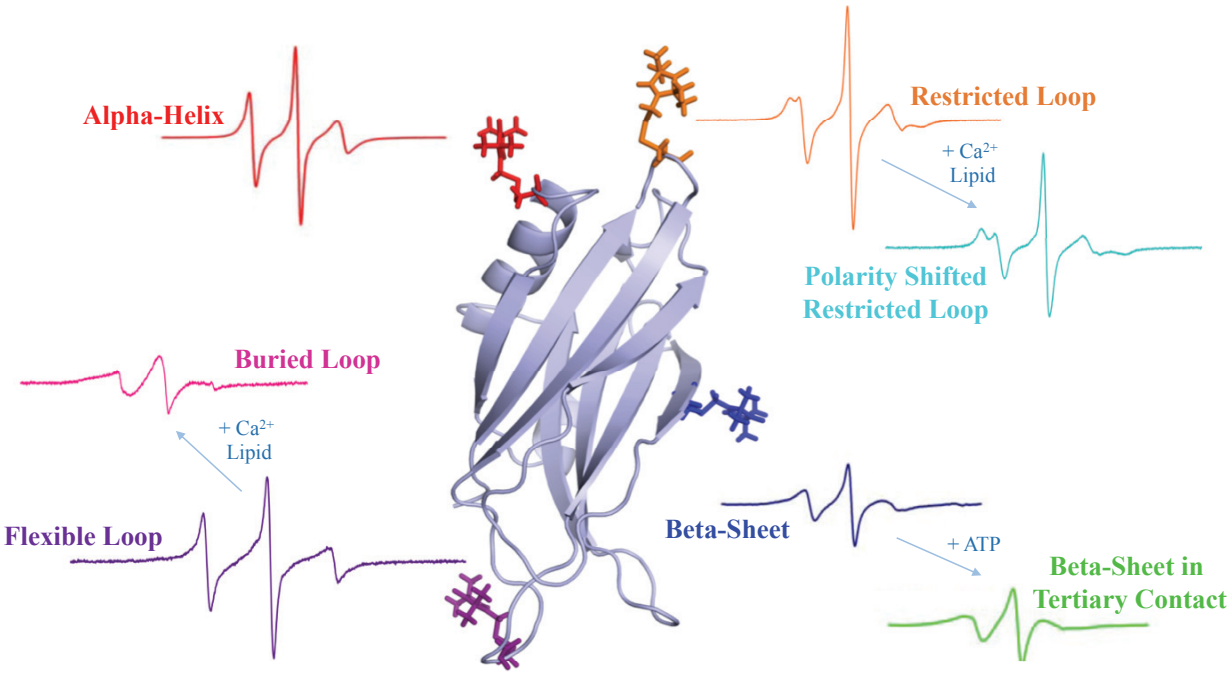

Figure 2.13: Example CW-EPR spectra highlight differences in lineshape for different spin-labeled locations on the C2B domain of Syt1 and under different conditions.

2.2.9.1 CW EPR was performed on a CW X-Band EMX spectrometer (Bruker Biospin, Billerica, MA) equipped with an ER 4123D dielectric resonator[4]. All EPR spectra were recorded with 100-G magnetic field sweep, 1-G modulation, and 2.0-milliwatt (mW) incident microwave power at room temperature. The measurements were performed on 6 µl samples in glass capillary tubes (0.60 mm inner diameter × 0.84 mm outer diameter round capillary; VitroCom, Mountain Lakes, NJ). The phasing, normalization, and subtraction of EPR spectra were performed using LabVIEW software provided by Dr. Christian Altenbach (UCLA, Los Angeles, CA) or with lab-made software from David Nyenhuis.

2.2.9.2 Cytosolic C2AB or C2A measurements were taken with a minimum of 75 µM protein. First, measurements were taken of the aqueous phase in Ca^{2+} buffer (metal free buffer with 1 mM $CaCl_2$ added). Next, LUVs in Ca^{2+} buffer were added to protein at a minimum of a 1:250

protein to lipid ratio and incubated 5-10 minutes before recording the spectra. After addition of LUVs, 4 mM EGTA was then added to chelate the Ca^{2+} to recover the aqueous spectra, verifying calcium-dependent lipid binding.

2.2.9.3 FL SYT and ΔC2B cis binding measurements were taken in reconstituted proteoliposomes of either charge or charge free compositions depending on experiment design. Measurements were first taken in the unbound aqueous phase with proteoliposomes in metal free buffer. The desired metal (to total 1 mM Ca^{2+}, Cd^{2+}, or Pb^{2+}) was then added and incubated 5-10 minutes before recording the next measurement. If any additional ions were to be included, mainly ATP and Mg^{2+}, they were added next and the measurement was repeated. Next, 4 mM EGTA was added to each sample and incubated 5-10 minutes before measuring again, to ensure binding was metal dependent. Charge free (PC and PC:Chol) measurements were taken with and without metal to ensure binding was metal dependent and verified by power saturation.

2.2.9.4 FL SYT and ΔC2B trans binding measurements were taken in reconstituted proteoliposomes of either charge or charge free compositions depending on experiment design. Measurements were first taken in the unbound aqueous phase with proteoliposomes in metal free buffer. Extruded LUVs of varying charge compositions were then added to the reconstituted mixture and allowed to incubate 5-10 minutes. The calcium-free spectra were then taken to look for metal free binding. The desired metal (to total 1 mM Ca^{2+} or Cd^{2+}) was then added and incubated 5-10 minutes before recording the next measurement. At this point, any additional ions could be added (ATP, Mg^{2+}) depending on desired experiment. Finally, 4 mM EGTA was added to each sample and incubated 5-10 minutes before measuring again, to differentiate metal and metal free binding.

2.2.10 EPR Power Saturation Experiments

EPR power saturation measures the relative location (depth measurement) of any spin-labeled position on a protein into and near the lipid membrane. With a collection of these measurements at different sites on the protein it is possible to dock and orient it relative to the lipid's acyl chains, head groups, interphase region, and the surrounding aqueous phase. Two fast relaxing paramagnetic reagents, oxygen and Nickel (II) ethylenediaminediacetic acid (NiEDDA), are used to determine the location of the spin label relative to the lipid membrane[40,46]. Other paramagnetic reagents can be used in place of NiEDDA, but its size and polarity make it ideal for creating an optimized opposing gradient and thus exchange rate compared with oxygen (*Figure 2.14*)[40,46]. NiEDDA reagent is run in the presence of N_2 gas to remove any O_2 in the air which would expose the label to multiple reagents at once. These paramagnetic reagents create opposing partitioned gradients into and out of the hydrophobic membrane and hydrophilic aqueous environment for oxygen and NiEDDA, respectively. Due to solvent accessibility of apolar or polar molecules, oxygen is most concentrated in the lipid acyl chains and NiEDDA is most concentrated in the aqueous phase[46]. When the spin-label is exposed to one of these species, it can collide and relax at a rate dominated by Heisenberg-Spin exchange, proportional to T_1[40,47]. The label's relaxation rate depends on the concentration of reagent in the vicinity of the label, more concentrated paramagnetic reagent leads to more collisions and thus a higher rate of relaxation[46]. Conveniently, this relaxation rate is also proportional to an increase in saturating power when the sample is stepped through a series of increasing microwave powers (power saturation

measurements). This permits direct measurement and localization of the label to the membrane according to the label's accessibility to these gradients using CW EPR[46].

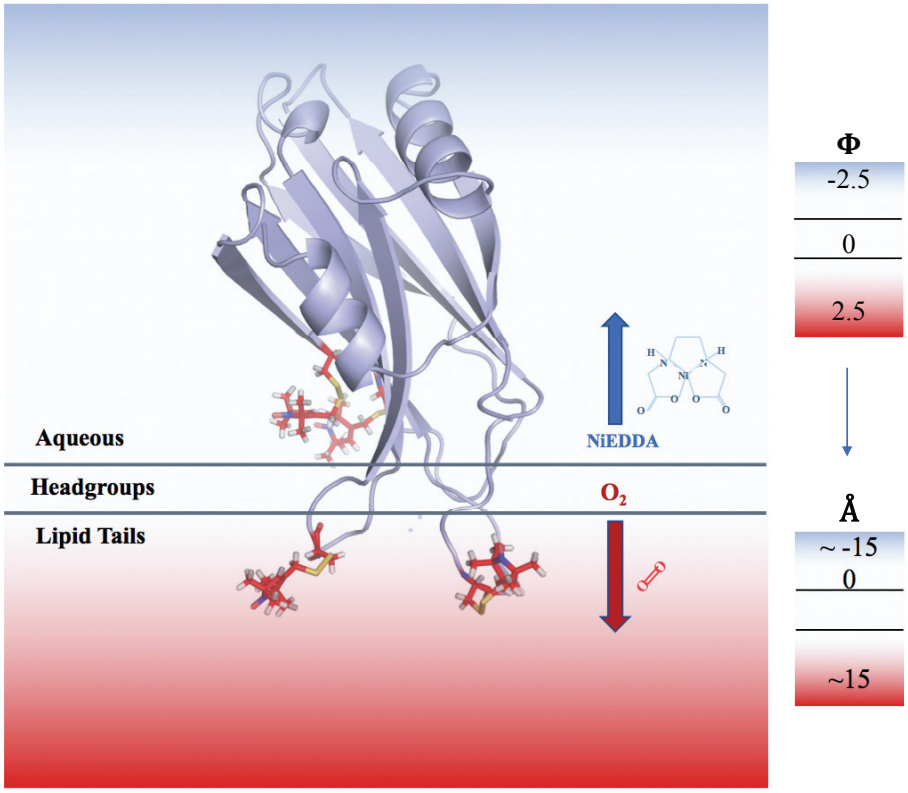

Figure 2.14: Power Saturation Representation. Opposing NiEDDA and O_2 gradients are shown in blue and red respectively. At the headgroup-lipid tail interface, depth measurements. are equal to zero.

Power saturation measurements look at the spin-label's signal intensity (amplitude of the central line of a CW spectra) measured at increasing levels of power. As the power is increased, the intensity of the central line increases linearly until it reaches saturating levels, where the number of spins in excited state approaches the number in the ground state, resulting in a decreased signal intensity[46]. Saturation can also be defined as disturbance of excited state equilibrium with the low energy electrons, where the spins in the excited state cannot relax back to the ground state at a high enough rate to compensate for the increased energy that the electron is being subjected

to. If there are fewer ground to excited state transitions, there is less for the instrument to detect and the apparent signal will decrease. This fits to the equation:

$$A = IP_{1/2}[1 + \left(2^{1/\varepsilon} - 1\right)\frac{P}{P_{1/2}}]^{-\varepsilon}$$

Equation 2.13

The initial linear increase in amplitude (A) is relative to the square root of incident power (P) applied. The inflection point then occurs at the $P_{1/2,}$ which is the power at which the first derivative line amplitude is half of the unsaturated value (half maximal saturation). This is again proportional to the longitudinal relaxation rate (T_1) of the label[40,46]. In a hydrophobic environment the $P_{1/2}$ of the label under oxygen is greater than the $P_{1/2}$ under NiEDDA *(Figure 2.15)*. ε is an adjustable parameter set at either 1.5 or 0.5 according to the limits of homogeneous and inhomogeneous saturation, respectively. The nitrogen control, with no paramagnetic relaxing agent, is often well represented by the homogeneous saturating 1.5 value[40,46]. These values, with the addition of a paramagnetic free control (N_2) allow one to define the relative accessibly ($\Delta P_{1/2}$) of the label to the two paramagnetic gradients:

$$\Delta P_{1/2\ O2\ or\ Ni} = P_{1/2}{}'_{O2\ or\ Ni} - P_{1/2}{}'_{N2}$$

Equation 2.14

Where $P_{1/2}{}'_{O2\ or\ Ni}$ is adjusted to correct for spin-spin relaxation time, $T_{2,}$ effects for comparing saturation curves when line-shapes are slightly variable[46]. This follows the equation:

$$P_{1/2}{}'_{O2\ or\ Ni} = \left(\frac{P_{1/2}}{\Delta H_{p-p}}\right)_{O2\ or\ Ni}$$

Equation 2.15

Where $\Delta H_{p\text{-}p}$ is the peak to peak width in G of the central line. Division of the peak to peak width corrects for any T_2 effects ($\Delta H_{p\text{-}p}$ is proportional to $1/T_2$) that would show up as Lorentzian broadening, directly detectable as increases in width of the central line. From the accessibilities of the two paramagnetic conditions the depth parameter (Φ) is defined as the natural log between the ratio of the two accessibilities[46]:

$$\Phi = \ln\left(\frac{\Delta P_{1/2\ O2}}{\Delta P_{1/2\ N2}}\right)$$

Equation 2.16

Depth parameter values define 0 as the interface between the bottom of the lipid headgroup and the start of the lipid acyl chains. Positive values are then in the acyl chains and negative values up to ~-1.5 are usually in the head-groups and the ionic double layer interfacial to the protein, while more negative values are in the aqueous phase. To determine exact angstrom measurements into or out of the membrane plane a series of power saturation measurements are performed on control lipid membranes with lipid probes containing spin labels positioned throughout the acyl chains in the lipid membrane. Each label position orients the depth of the membrane to the known acyl chain position, creating a standard curve:

$$\Phi = \mathrm{A}\,[\tanh(\mathrm{B}(\mathrm{x}\text{-}\mathrm{C}))] + \mathrm{D}$$

Equation 2.17

Where A is the bulk value of Φ in aqueous/water[40]. B represents the slope of the linear region of the equation[40]. C is the intercept of the linear region of the equation[16]. D is the bulk value of Φ in hydrocarbon[40]. X is then the distance from the plane oriented at the top of the lipid headgroups[40,47]. After determining the A, B, C, and D constants, experimental depth parameters of

protein spin-labels are then used to determine the depths around the membrane where the headgroup-aqueous interface equals 0[47]. Numbers here are again typically defined as positive into the membrane and negative out of the membrane. This curve fits well within the membrane and lipid interface, but the error begins to increase rapidly as samples become more aqueous.

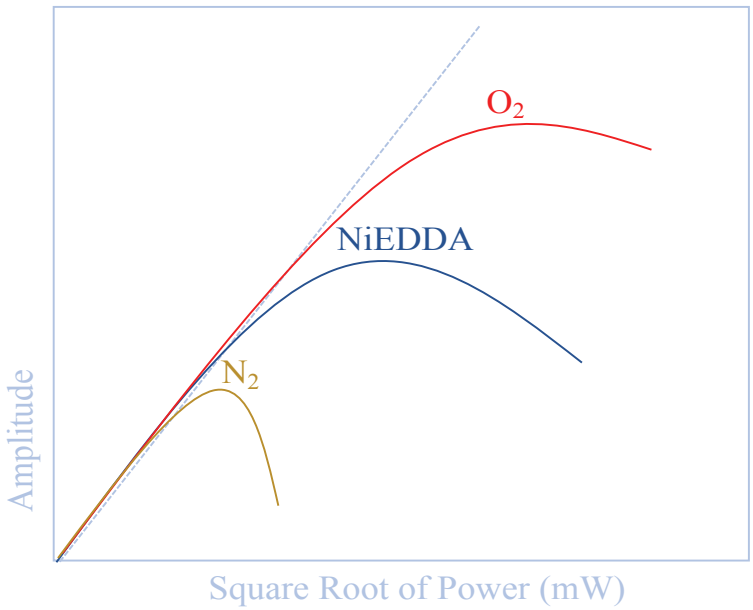

Figure 2.15: $P_{1/2}$ Curves. These representative saturation curves are in a membrane hydrophilic environment where that $P_{1/2}$ O_2 is greater than $P_{1/2}$ NiEDDA (and the N_2 control is small). The dashed line highlights the curves divergence from linearity when saturation is reached. The x-axis is the square root of the incident microwave power and the y-axis is the peak-to-peak amplitude of the first derivative of the central line.

2.2.10.1 CW Power Saturation EPR was performed on a CW X-Band EMX spectrometer (Bruker Biospin, Billerica, MA) equipped with an ER 4123D dielectric resonator[4]. All EPR spectra were recorded with 1-G modulation at room temperature. The measurements were performed on 10 µl samples in a gas-permeable TPX-2 tube. The $P_{1/2}$ curves were fit using PSE LabVIEW software provided by Dr. Christian Altenbach (UCLA, Los Angeles, CA).

2.2.10.2 Power saturation experimental design followed three power saturation stages under varied conditions: 20% O_2 gas, N_2 gas, 10 mM NiEDDA and N_2 gas. Samples were prepared by mixing desired protein samples, ions and cations, and membranes together with a short incubation. The sample was then placed in a the TPX-2 tube in the spectrometer and a gas line was attached to the bottom of the resonator. The samples were equilibrated under gas for 15 minutes before running the CW. For each stage, an initial 20 dB (2 mW), 100 G CW was taken to determine the peak-to-peak width of the central line. Next, power saturation was run under decreasing attenuation (increasing power) starting at 29 dB then increasing at 2 dB per step for 13 to 15 stages (up to 1 dB) over 10 G scans centered around the central line until complete saturation of the central line occurred. For each attenuation stage the corresponding microwave power steps were: 29 dB:0.25 mW, 27dB:0.398 mW, 25 dB:0.632 mW, 23 dB:1.001 mW, 21 dB:1.586 mW, 19 dB:2.514 mW, 17 dB:3.985 mW, 15 dB:6.315 mW, 13 dB:10.01 mW, 11 dB:15.86 mW, 9 dB:25.14 mW, 7 dB:25.14 mW, 5 dB:39.85 mW, 3 dB:100.1 mW, 1 dB:159 mW.

2.2.10.3 Power saturation analysis was performed through a series of steps. First, CW spectra for each of the 3 stages (20% O_2 gas, N_2 gas, NiEDDA and N_2 gas) were used to determine the peak-to-peak width ($\Delta H_{p\text{-}p}$) in gauss using WinEPR (Dr. Christian Altenbach (UCLA, Los Angeles, CA)). Next, the power saturation incremental CWs for each stage were analyzed in WinEPR to determine the maximum and minimum peak intensities (*A*) of the central line for each power step. For each stage, the *A* values were then entered with corresponding power into PSE to calculate a $P_{1/2}$ value. Each stage's $P_{1/2}$ value was divided by the $\Delta H_{p\text{-}p}$, providing an adjusted $P_{1/2}$'. Next the control/reference N_2 $P_{1/2}$', was subtracted from the two paramagnetic reagent stages $P_{1/2}$' for O_2 and NiEDDA, producing corresponding accessibility or collisional parameters for both reagents ($\Delta P_{1/2\ O2}$, $\Delta P_{1/2\ Ni}$). $\Delta P_{1/2\ Ni}$ was then adjusted, by 2, to correspond to 20 mM NiEDDA

rather than 10 mM (used due to difficulty saturating curves with nickel) for depth parameter calculations. Next, the natural log of $\Delta P_{1/2\ O2}$ divided by $\Delta P_{1/2\ Ni}$ produced a depth parameter (Φ). These values were fit to the curve: $\Phi = A\ [\tanh(B(x-C))]+D$, producing A, B C, D factors. Each depth parameter was then added to this equation to determine the x value, being the depth in angstroms. Depth values again, were deemed positive into the membrane, zero right at the top of the lipid headgroups, then negative into the ionic double layer and aqueous phase.

2.2.11 Pulsed Double Electron-Electron Resonance (DEER)

Double electron-electron resonance (DEER) measures the long-range dipole-dipole interaction (dipolar coupling) between two paramagnetic spins (here R1 labels again), separated by a distance of ~1.6 to 8 nm (or up to 10 in exceptional cases)[48,49]. This technique is in a valuable range for observing and quantifying distributions of physiological interactions within and between proteins, aggregation or ordering of proteins and complexes, and detecting conformational changes within a single protein depending on the experimental design[49]. Like CW EPR, it is not limited by protein size, structure, or buffer conditions. Samples are often frozen, and currently run at higher concentrations than CW requires (~50 μM -300 μM) and small volumes (~15 uL range), but advances in the technique's instrumentation would permit even smaller concentrations and volumes.

The method functions by separating coupling between the electron spin pairs of interest from other electron spin interactions (usually intramolecular interactions versus intermolecular background)[48,50]. DEER is a pulsed EPR technique, using two frequencies to allow pulses to manipulate two different populations of spins in the sample. The coupling between these two spin

populations then gives a time-resolved dataset from which distance measurements can eventually be extracted.

More generally, pulsed EPR measurements again utilize the inherent spin of an electron and its precession about a magnetic field in the z-axis[51]. This results from the net magnetization (sum of the magnetic moments) of the sample aligning with the external magnetic field (defined as the z-axis, the x-y plane magnetic moments usually cancel in large enough sample sizes). In addition to the static external magnetic field (B_0), the pulses are delivered by a perpendicular, oscillating magnetic field (B_1), where B_1 is much less than B_0. B_1 pulses control the experiment through manipulation of the magnetization of the sample. These pulses are applied to "tip" the sample magnetization out of the z-axis and are defined by the tip-angle applied, in this case they will be either a π (180°) pulse or a π/2 (90°) pulse[50]. A π pulse is also called an inversion pulse as it flips (or reverses) the populations of spins in the z-axis away from thermal equilibrium[50].
A π/2 pulse is also called a saturating pulse, as it tips the magnetization into the x-y plane and the z-axis magnetization thus goes to zero. Here the spins are phase coherent[50]. After a π/2 pulse the spins will decay back to thermal equilibrium in the z-plane through transverse (T_1) relaxation with the environment[50]. While the magnetization relaxes back to equilibrium it will also rotate (and eventually dissipate through T_2) throughout the x-y plane (again dictated by the Larmor frequency). The signal detection coils on a pulsed EPR instrument detect the signal in the x-y plane, and so the tip into the x-y plane followed by relaxation back to the z-axis will appear as a decay in the apparent signal, often referred to as a free induction decay (FID)[51].

As in CW experiments, relaxation effects also dictate how the experiment is designed and setup. T_1 relaxation describes the rate at which the sample magnetization returns to equilibrium (the z-axis aligned with the external field) by interactions with the environment/lattice[51]. Since

pulsed EPR experiments are detected in the x-y plane, this movement out of the x-y plane and back towards the z-axis as a result of T_1 relaxation is the main source of decay in a FID. T_2 instead describes the rate at which spins interact with each other, causing changes in the Larmor frequency of individual spin packets[51]. This causes the packets to begin to precess at different rates, eventually causing the signal to fan out in the x-y plane and apparent signal intensity in a single channel (x or y) to be lost. In a pulsed experiment, T_2 is frequently represented by T_2' or T_M, which includes this effect as well as a description of inhomogeneous broadening effects, described below. For pulsed experiments at cryogenic temperatures (78 K) with nitroxide labels, T_2 is usually >> T_1, and so T_1 sets the repetition time for pulsed experiments[50]. This is because repeating a pulsed experiment too quickly does not allow the spins to relax back to equilibrium/the z-axis, and so with every repetition fewer and fewer spins will be available to be flipped by the applied pulse, leading to reduced signal intensity.

Like CW EPR, these relaxation pathways can be described in terms of spectral broadening. For pulsed experiments, as in CW ones, there are both homogeneous and inhomogeneous broadening effects. Both T_1 and T_2 processes cause homogeneous broadening effects[51]. This broadening results in a sum of Lorentzian linewidths and the events are irreversible (depending on pulse sequences and any dead-time information will be lost). Inhomogeneous broadening, in contrast, is not the entire spin system, just the product of individual spin packets coupling to each other that are then shifted in relative frequency[50]. This loss of resonance results in more than one magnetic component which will overlap and cancel out, decreasing the overall transverse magnetization[50]. It is the product of many different homogeneously broadened lines in a Gaussian curve. Inhomogeneous broadening will affect the shape of the EPR signal/spectrum, rather than the decay as in homogeneous broadening[50]. Inhomogeneous broadening is a reversible event (the

spin packets are just out of phase in the x-y plane), so no overall signal/energy is lost depending on the experimental design[51]. Usually the energy in a free induction decay with contributions from inhomogeneous broadening can be refocused with an additional π pulse, this pulse inverts spins that have fanned out so that they fan together, this contributes to the echo, the actual signal measured. Other contributions to the echo decay are, T_2 effects, and different diffusion (spectral, spin, instantaneous) all of which can be classified again as a more general, T_M (phase memory time) to incorporate these effects[48,51].

While these broadening effects would usually shield observation of dipolar interactions at distances longer than ~1.6 nm (they are observable in shorter distances with CW EPR with a r^3 dependence on distance), proper experimental design can obtain a resolved observation of the dipolar interaction between paramagnetic centers[48]. This dipolar coupling was previously defined by a Pake pattern, which is a Fourier transform of the sample signal[48]. From a Pake pattern the components of dipolar coupling, frequency and inter-spin distance could separate[48]. Currently, DEER data can be converted to distance distributions by fitting to model based approached (gaussian fits) or model free assumptions (Tikhonov regularization)[48,50].

Currently, experiments performed in the lab are collected using a dead-time free four-pulse sequence with 16-step phase cycling at Q-band (~34 GHz with a higher power amplifier, though measurements can also be performed at X-band) (*Figure 2.16*)[48,50]. During the experiment, in the observe frequency channel a π/2 pulse is first applied for 16 ns which will tip the spins at the observe frequency into the x-y plane, where they will precess during the pulse[48,50]. After this pulse ends the spins will de-phase or lose coherence due to the different relaxation effects addressed above[50]. A π pulse is then applied for 32 ns to refocus the spins, which produces an initial undetected echo[48,50]. These spins will again begin to relax so a π pulse is then applied for 32 ns in

the pump frequency (75 MHz different resonance frequency from the observe pulse) to invert the spins at the pump frequency, this in turn affects the observe spins by changing the angular frequency they experience (dipolar effects/phase-lag)[48,50]. Note here, either the observe or pump pulse should be placed at the peak of the nitroxide spectrum, while the other is offset at a local maximum sufficiently far enough away to avoid cross excitation[50]. Finally, another π pulse is applied in the observe channel for 32 ns to refocus the spins in the observe, this will produce an observed echo that was affected by the pump pulse[48,50]. These phase-lag effects depend on the dipolar frequency of the spins and when the pulses were applied[50]. Cycling through the time that the pump pulse is applied can separate out the dipolar frequency, which will then be observed as an aggregate of the echo which will vary with the phase-lag (a cosine dependence)[48-51].

Again, the instrument is run at 80 K because relaxation rates slow at lower temperatures and the signal-to-noise ratio of the sample increases (based on an inverse relationship between temperature and the distribution of spin packets transitions)[50]. These temperatures need to be in a balance for cost efficiency and time efficiency. In a set period of time, the signal-to-noise will get better with lower temperature, but relaxation effects can actually become very slow, which will draw out each phase cycle time (T_1 dependence on pump cycle repetition rate), this decreases the number of cycles/scans one can perform in this period and then will actually lead to a decreased signal-to-noise (because of its square root dependence on the number of scans)[50]. An optimal temperature range to maximize both relaxation and signal-to-noise is 50 K, but that is not currently cost-effective due to cryogen costs[50]. Recent equipment advances however, could negate this consideration as there are development in cryogen-free (and contained cryogen) systems that can be run at 50 K for less continuous expense.

Sample preparation can also have an effect on the signal produced, while in most cases more concentrated samples lead to an increase in signal, in this case DEER experiments have an upper limit where too many spins will diffuse too fast (instantaneously) relative to the pulse lengths which will have large negative (decreasing) effects on the T_M (time one can observe the signal)[48,50]. The T_M affects the time to which the dipolar correlation can be followed, which must be maximized as the confidence (over even ability to observe) in longer distances is dependent on the amount of the corresponding oscillation that can be observed, and so is also dependent on time.. Membrane proteins have particular difficulty with this because a reconstituted protein, while not showing a beneficial gain in signal, will usually have shortened T_M relative to the protein concentration[48]. This is because spins end up confined and appear in higher local concentrations because they are tethered, increasing the protein-to-lipid ratio or running in detergent can extend the T_M but potentially at the cost of a physiological measurement (high ratios or no lipids in general can change the behavior of the protein[48]. A way to extend/maximize the T_M of a sample would be to put the sample in deuterated buffer[50]. This reduces any hyperfine field interactions with protons in the solution matrix[48,50]. The gain in phase-memory time length upon deuteration is usually ~30 percent, but this appears to be sample dependent. Labeling efficiency of a sample should also be considered in the analysis as the protein concentration does not always equal the number of spins (or double spins for a double labeled sample). If a sample is poorly labeled it results in a somewhat spin-dilute sample which can affect the populations of interacting spins or reduced the observed modulation depth.

A final consideration is data analysis, DEER data will produce varying distance distributions depending on background subtraction and dimensionality (if there is not a homogeneous background, assumptions for Tikhonov regularization will not be met), start-times

(where the decay begins), end-times (removing any artifacts from pulse overlap in imaginary channel data), population groupings of spins, and the type of fitting procedure used (Gaussian, Tikhonov, etc.)[50]. After considering all analysis factors interpreting distance distributions (depending on experimental design) should consider the available rotamers and any possible distances at that site. This can be modeled and fit to experimental data using tools like MMM[52,53].

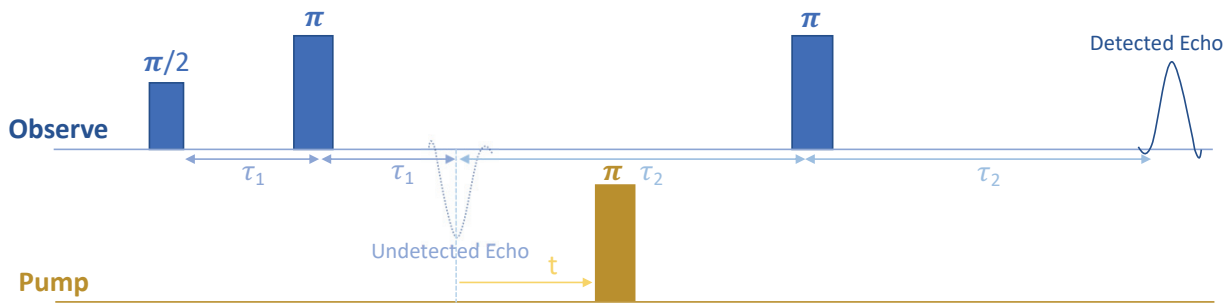

Figure 2.16: Four Pulse DEER pulse sequence. Time t is varied, and variation of the echo is recorded. Figure inspired by Jeschke. 2012. Annu. Rev. Phys. Chem.

2.2.11.1 Pulsed EPR was performed on a Bruker Elexsys E580 EPR spectrometer running at Q-band using an EN5107D2 dielectric resonator. Measurements were performed using a 12 µL sample volume of about 100-200 µM single or double spin-labeled Syt1 plus 3 uL deuterated glycerol. Samples were loaded into quartz capillaries of 1.5 ID x 1.8 OD 100 mm length and flash frozen in liquid nitrogen then run at 80 K. DEER data were collected using a dead-time free four-pulse sequence with 16-step phase cycling (one 16 ns π/2 and two 32 ns π observe pulses separated by a 32 ns π pump pulse)[54,55]. Pump and observe pulses were separated by 75 MHz. DeerAnalysis2015 or DD was used for the removal of background functions from initial dipolar evolution, V(t)/V(0) data[49,50,56,57]. Tikhonov regularization was used to extract distance distributions from the resulting F(t)/F(0) form factors[52,54].

2.2.12 Proton-Nitrogen heteronuclear single quantum coherence (HSQC) nuclear magnetic resonance (NMR)

Unlike EPR, where electrons are the focus, two-dimensional NMR spectroscopy measures the transfer of magnetization between nearby nuclei[58]. This transfer is categorized as either through-space (nuclear Overhauser effect-NOE) or through-bond (J-coupling) (Figure 2.17)[59]. J-coupling can be broken down into two different through bond interactions depending on the nuclei involved: either like, being the same type (correlated spectroscopy-COSY), or unlike, being different kinds (heteronuclear single quantum coherence -HSQC), nuclei[59].

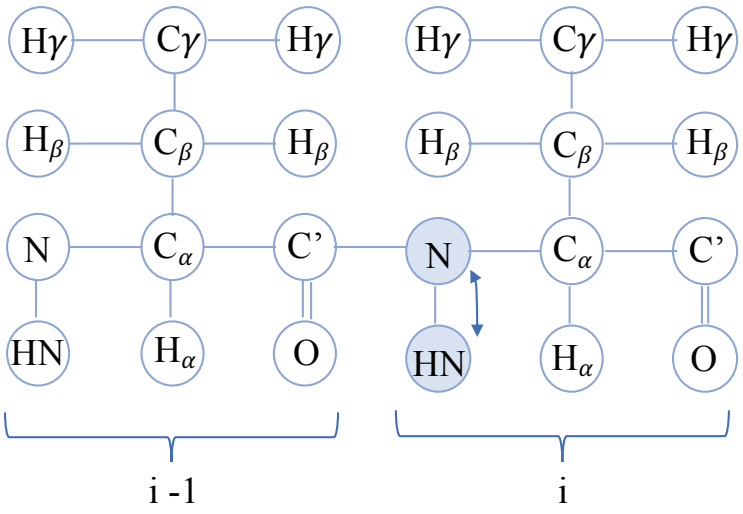

Figure 2.17: J-Coupling. Magnetization is transferred from the hydrogen to the attached ^{15}N nuclei, next the chemical shift is evolved on the N and the magnetization is then transferred back to the H for detection. Image inspired by: Cavanagh et al. Protein NMR Spectroscopy – Principles and Practice by J. (Academic Press).

HSQC measurements utilize inverse detection of an insensitive nucleus (^{15}N) coupled and polarized to a sensitive ^{1}H proton. A spectrum thus consists of a 2D map of ^{15}N-^{1}H cross-peaks or

resonances of (for a proteins case) amide bonds throughout the amino acid backbones and any amide bonds which appear in sidechains. This means all residues in a protein except for proline are in theory visible as a single signal with this technique as well as a few amide side chains from Asn, Gln, Trp, and sometimes Arg (depending on buffer conditions)[60]. These sidechain signals are very sensitive to hydrogen bonding with nearby or adjacent carbonyl backbones, so shifts on these sidechains when ligands are added are also peripherally indicative of backbone interactions[60]. Each type of amino acid bond has particular local electronic and magnetic environments and classically specific types of residues bonds will map to specific regions of the 2D spectrum. ^{15}N shifts will be sensitive both to direct hydrogen bonding and hydrogen bonding to preceding carbonyls (ring currents), as well as conformational changes (*Figure 2.18*)[60]. This technique does, however, downplay any effects due to interactions with prolines as they are undetectable, or any additional hydrophobic interactions occurring (which may be extrapolated later in analysis of shifts as a whole on the protein surface)[60].

This environmental sensitivity allows for global detection of changes (chemical shifts) in the protein structure when experimental changes are made. Here, this sensitivity was used for affinity titrations of a ligand (ATP or IP_3) to the protein (C2B), which is categorized under chemical shift perturbation[65]. For affinity-based titrations peak assignment must be determined for residues in the protein (for this set of data, 3D NMR- ^{1}H, ^{15}N, ^{13}C was performed by Rizo Group, PDB: 1k5w)[61]. Once the peaks are mapped and assigned the shifting of individual peaks can be tracked and fit to determine the affinities of the ligands to individual residues. For HSQC spectra, the geometric distance moved by each peak is calculated, where ^{15}N shifts are weighted by 0.14 relative to ^{1}H shits (0.2 is often used for glycine)[60]. This adjustment occurs as most ^{15}N backbone shifts are 130.8-108.8 Hz (depending on the spectrometer magnet size used) or 22 ppm and ^{1}HN

shifts are 10.04-6.92 Hz or 3.12 ppm so 3.12/22 equals 0.14[58,60]. Chemical shifts are usually reported in ppm to correct for any differences in raw frequency (Hz), which changes depending on the spectrometer frequency/magnet size[58].

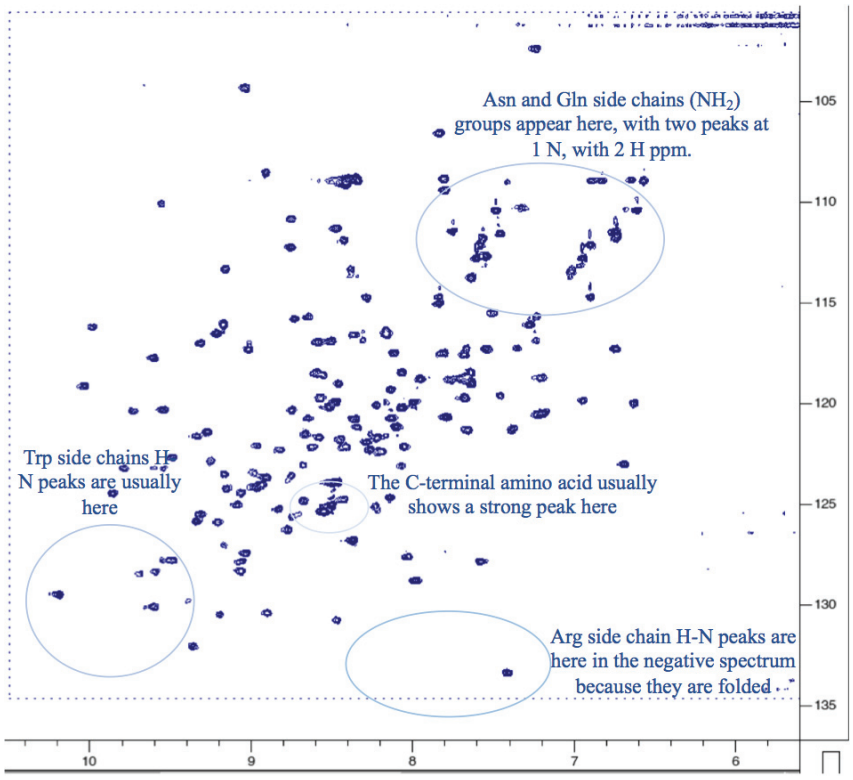

Figure 2.18: Characteristic Chemical Shift Locations of Side-Chains. Most peaks appear from the amide backbone of the residues throughout the protein, but some amino acid sidechains also have amide bonds. These typically appear in certain regions of the spectrum. Image inspired by: Cavanagh et al. Protein NMR Spectroscopy, Principles and Practice by J. (Academic Press).

These chemical shifts will appear differently depending on the exchange rate of the ligand at each site. The exchange rate is a direct observation of the rate of exchange between free and bound ligand (or the off-rate constant, k_{off}). Exchange rates can fall under fast, intermediate, or slow categories relative to the chemical shift timescale (the difference in Hz between chemical shifts of free and fully bound protein)[60]. Fast exchange appears as a progressive movement of proteins peaks between the free-state and fully-bound peaks. This occurs when the k_{off} is greater

than the difference between the fully-bound and unbound shifts and usually represents weaker affinity binding at that position. Slow exchange will not show a progressive movement between fully bound and unbound states, only broadened peaks appearing either at one or both peak locations, but in differing ratios, as the signals are broadening and shifting at the same time[60]. Slow exchange occurs when the k_{off} is greater than the difference between the two states, and correlates to very high affinity binding[60]. Intermediate exchange falls in-between the two other exchange rates and is observed as broadening at the peak location of the bound or unbound state, or as broadening between nearly merging the peaks. These peaks may also often disappear or become undetectable in the spectrum[60].

In a more complicated titration, amide ^{1}H resonances on a protein can be in slow exchange while ^{15}N resonances are in fast exchange, this results in a complicated shift pattern, which can look like fast exchange, but with peaks that grow and shrink as they do in slow exchange[60]. In another case, if steric hinderance is occurring at a ligand binding site even at concentrations in the fast exchange regime, slow exchange will begin to appear as the on- and off- rates of the ligand binding are no longer dependent only on diffusion[60]. When this occurs, there will be both shifting and broadening of the lines, where the maximal broadening will occur at the 1/3 protein-ligand bound state[60].

Broadening of chemical shift peaks is also not always due to exchange rate. It is usually caused by either slow tumbling or exchange[58,60]. These occur first by tumbling effects if the ligand titrated is very large in size or if the protein aggregates upon ligand addition, as both of these will slow the overall tumbling of the protein and thus broaden all (or the vast majority of) peak signals[58,60]. Exchange effects occur for many reasons such as conformational changes before equilibria is reached or structural rearrangements after ligand binding[60]. Broadening due to these

exchange effects is difficult to differentiate from broadening due slow or intermediate binding effects, but often these shifts will be non-linear[60]. Curving of shifts plots can also occur if there is more than one binding site for the ligand on the protein, which leads to secondary effects on each site, and potentially two-state backbone shifts[60].

Intermediate exchange is not quantifiable in terms of K_d, as the observed shifts diverge from that predicted based on the population-weighted average. This leads to easily mis-interpretable data where binding curves are sigmoidal in shape, but not due to cooperative binding[60]. In slow exchange, the appearance or disappearance of the fully bound or unbound signals/peaks is proportional to the concentrations of free and bound protein (conventionally the bound state is more often used)[60]. Fast exchange is directly quantifiable using affinity-based calculations, as it does shift relative to the population-weighted average as predicted, with dissociation constants as strong as 10 nM and as weak as 10 mM[60]. The pattern of shifting (linear/curved) can also hint at any changes in protein backbone/allosteric changes from the ligand vs. ligand binding contacts at these sites. Intermediate and slow exchange do not show tracking of the peaks throughout different ligand concentrations and are difficult to quantify beyond relative comparisons of binding affinity. The fact that a single series of measurements produces both a binding affinity (or a dissociation constant, K_d) and the location of the ligand binding-site makes this technique very powerful and appealing compared to other methods that would require a different set of experiments to determine these observations (*Figure 2.19*)[60].

In order to perform these measurements, ^{15}N must be introduced into the protein for detection. This occurs by growing in nitrogen free media (M9) and adding in ^{15}N as the sole nitrogen source so that the entire protein is labeled. For well-defined peaks and low noise, the samples must also be run at very high volumes and concentrations relative to EPR (ideally ~400

μM or more, though they can be run at lower concentrations for longer time). The concentration a protein can reach while remaining in solution (stable) will often be a limiting factor. Sample size can vary depending on the tube used, but volumes between half a milliliter and 250 uL are often required for the titration or for each point of the titration depending on experimental design and protein stability[59]. Usually, smaller proteins are best for solution NMR (up to 50-65 kDa but can be pushed to a few 100 kDa) and this technique is not optimal for large full-length membrane proteins due to overall tumbling of the sample[58,59]. Membrane proteins can be run with effort, but usually in a membrane-memetic, rather than a lipid sample[58]. The samples are also usually run at higher temperatures to optimize signal-to-noise, since increasing the tumbling of the sample narrows linewidths and enhances proton exchange with buffer, which needs to be considered if the protein being run is not stable at high temperatures[58]. A balance between concentration and time spent at the required temperature can often establish the values to be used. NMR is very sensitive to changes in environment so sample conditions: length of time run, temperature, exact buffer conditions (salt, pH, buffering agent), D_2O content, and protein concentrations, need to be kept as constant as possible throughout the series of measurements to guarantee all shifting is from the ligand being added and not due to other variables[59,60]. For a titration, the concentrations of ligand used also need to be considered, as it ideally will fall within the entire weak binding and full saturation range of the affinity curve, with enough points at low and intermediate concentration to appropriately fit the inflection of the curve, otherwise error in the K_d will be high.

NMR instruments for 2D NMR experiments are typically run between 300 and 800 MHz. These frequencies (Larmor frequencies) correlate (nuclei dependent) to the magnetic field applied by the spectrometer magnet, where for a ^1H atom: 300 MHz equals 7 T field, 400 MHz equals 9.3 T field, 500 MHz equals a 11.7 T field, 600 MHz equals a 14 T field, and 800 MHz equals a 10.8

T field (All information from Bruker and Varian instruments, Tesla instead of Gauss are more frequently used for NMR experiments)[58]. These resonant frequencies (ν) or precession (transition) frequencies are directly proportional to the magnetic field applied:

$$\nu = (B_o\text{-}B_c)\gamma$$

Equation 2.18

where B_o is the applied magnetic field, B_e is a correction for small magnetic field effects generated by electrons circulating the molecule which can shield the nucleus from the applied magnetic field, and γ is the gyromagnetic ratio, a constant dependent on the nucleus ^1H which has a value of 42.58 MHz/T)[58,59,62]. The gyromagnetic ratio again represents the ratio of a nuclei's magnetic moment and it's angular momentum. The strength of the magnetic field applied directly affects the sensitivity and resolution of the sample, the higher the field the higher sensitivity, but running samples at higher fields is often more expensive[58].

The overall experimental setup of NMR experiments first aligns or polarizes the nuclear magnetic spins' dipoles to the constant magnetic field, and then a perpendicular frequency pulse is applied to disrupt this alignment to watch the spins precess and realign following principles already introduced in the EPR section, such as Zeeman and relaxation effects[59]. This pulse's resonant frequency, must be equivalent in energy to the difference between the excited and ground state of the nuclear spins[58]. An advantage for NMR is the long (ms) timescale for excited nuclei, this allows for the manipulation or passing of excitation (magnetization) to different nuclei (J-coupling, NOEs above)[58,62]. This allows one to measure the frequency of the passed magnetization (energy between states), or of multiple passes between many nuclei (1D, 2D, 3D NMR), from the signal produced. This leads into multi-dimensional experiments (^1H, ^{15}N, etc.), where each frequency overlap is the correlated peak or signal observed[58].

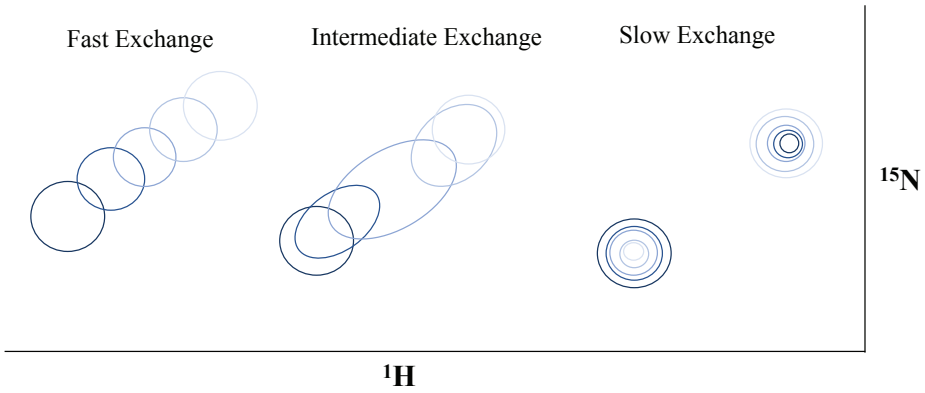

Figure 2.19: Collection of Chemical Shift Types. Chemical shifts in fast (left), intermediate (middle), and slow exchange. Fast exchange is shown as a continuous shifting from starting unbound state (dark blue) to fully bound ligand (light blue). Intermediate exchange shows broadening and blurring of shifts. Slow exchange shows progressive appearance and disappearance of the bound and unbound shift position.

2.2.12.1 Two-dimensional ^{15}N HSQC NMR C2B experiments were conducted on a Bruker 600 MHz NMR spectrometer, under initial instruction and troubleshooting of Dr. Jeff Ellena. A progressive titration of either IP_3 or ATP/Mg^{2+} to C2B was performed in 400 μM samples of 250 μL volume in NMR buffer 50 mM MES, 150 mM NaCl, 3 mM $CaCl_2$, 10% D_2O, pH 6.3). Samples were run in Shigemi tubes at a temperature of 27°C for 2 hours. Depending on stability of the protein, samples were changed every step of the titration or every two steps of the titration, as C2B precipitates at higher temperature (this is accelerated in the presence of ATP). A DDS (4,4-dimethyl-4-silapentane-1-sulfonic acid) NMR buffer was used as a chemical shift standard. The NMR data were processed in NMRPipe[63]. The residue assignments were matched in Sparky from the PDB NMR resonance assignments of C2B (PDB 1K5W)[64,65]. Chemical shift analysis was performed using CCPN NMR Analysis V2[66]. ATP and IP_3 titrations chemical shifts for each residue were fit to the equation: $y = A\frac{B+4x-\sqrt{(B+4x)^2-4x^2}}{4x-C}$, where y is the chemical shift, x is the ligand concentration, and A, B, and C are fitting factors to determine each dissociation constant[66].

Images were generated of the chemical shift intensities and dissociation constant intensities plotted onto the C2B domain in Pymol[67].

2.2.13 Total internal reflection fluorescence (TIRF) microscopy

2.2.13.1 TIRF microscopy was used to determine the vesicle capture rate and affinities of the full length Syt1 to verify functionality of the construct. All work was performed either with instruction or by Dr. Volker Kiessling. A Zeiss Axiovert 35 fluorescence microscope (Carl Zeiss), equipped with a ×40 water immersion objective (Carl Zeiss; numeric aperture = 0.7) and prism-based TIRF illumination was used to detect rhodamine B-labeled liposomes (mimicking the plasma membrane), which fluoresce close to the surface of the microscope[4]. An argon ion laser (Innova 300C; Coherent, Palo Alto, CA) light source was tuned to 514 nm[68]. Fluorescence was observed through a 610-nm band pass filter (D610/60, Chroma, Brattleboro, VT) by electron-multiplying CCDs (DU-860E or DV887ESC-BV, Andor Technologies)[4,68]. The beam was totally internally reflected at an angle of 72° from the surface normal, resulting in an evanescent wave that decays exponentially with a characteristic penetration depth of ∼100 nm[4]. An elliptical area of 250 × 65 μm was illuminated. The laser intensity, shutter, and camera were controlled by Volker's homemade program written in LabVIEW (National Instruments, Austin, TX)[68].

Wild-type Syt1 or ΔC2B were placed in a supported bilayer of a 1:1500 protein to lipid ratio. Supported bilayers were formed first by forming the initial layer of lipid (PC:Chol:PEG) using a Langmir-Blogett technique[4]. The Syt1 containing layer was then formed by incubating the chamber with reconstituted (PC:cholesterol, 4:1) Syt1 for 1-1.5 hours. This formed the outer leaflet. Free protein and lipid was initially washed away from the chamber once it was loaded onto

the microscope. Rhodamine labeled liposomes (target membrane) were added to these bilayers to observe capture. These contained brain PC: brain PE: brain PS: cholesterol: brain PIP_2: rhodaminePE (1,2-dioleoyl-*sn*-glycero-3-phosphoethanolamine-*N*-(lissamine rhodamine B sulfonyl)) in 32:30:15:2-:3:1 ratios. The fluorescence intensity on the supported bilayer was then followed using TIRF microscopy.

Experiments were performed by titrating the vesicles at increasing concentrations into the sample chamber at a fixed Ca^{2+}concentration. Between titration steps, the reaction was monitored for ~20-40 min to allow the system to approach equilibrium. The average fluorescence intensity of all camera pixels was recorded every 30 s[4]. The fluorescence changes between titration steps were fit to first order kinetics to extract saturation intensities and initial rates[4].

2.2.14 Site-directed Fluorescence Interference Contrast (FLIC) Microscopy

2.2.14.1 Site-directed fluorescence interference contrast (FLIC) microscopy allows for measurements relative to the membrane surface, much like power saturation, however here the measurements are focused away from the membrane. In combination, these techniques are powerful tools for mapping the distances and orientations of Syt1 domains under varying conditions. From these measurements "snapshots" or pictures of exactly what is happening during different stages of fusion can be assembled.

FLIC measures membrane proteins, or proteins tethered to the membrane otherwise, with specifically labeled cysteines supported on a patterned silicon chip with microscopic steps of silicon dioxide[69]. The fluorescence intensity depends on the position of the dye with respect to the standing modes of the exciting and emitting light in front of the reflecting silicon surface[69,70]. The

position is determined by the variable-height 16 oxide steps and the constant average distance between dye and silicon oxide[70].

~28 different label positions of Syt1 and ΔC2B were provided to Dr. Volker Kiessling to perform all of the FLIC measurements. Images were acquired on a Zeiss Axiovert 200 or Axio Observer 7 fluorescence microscope (Carl Zeiss) with a mercury lamp as a light source and a 40Å~ water immersion objective (Zeiss; N.A. = 0.7)[69]. Fluorescence was observed through a 610-nm band-pass filter (D610/60; Chroma) by a CCD camera (DV-887ESC-BV; Andor-Technologies). Exposure times for imaging were set between 40 and 80 ms, and the excitation light was filtered by a neutral density filter (ND 1.0, Chroma) to avoid photobleaching[69].

For a FLIC experiment, an image is acquired for every desired membrane condition of one supported membrane, across many repetitions. From each image, ~100 sets of 16 fluorescence intensities are fit with the fluorophore-membrane distance as a free parameter. The standard deviations of these results are usually on the order of 1 nm. The optical model consists of 5 layers of different thickness and refractive indices (bulk silicon, variable silicon oxide, 4 nm water, 4 nm membrane, bulk water), which we kept constant for all conditions[70]. The reported errors for the absolute membrane distance of each protein and lipid condition in EDTA are the standard errors from at least 3 repeats (see Supplemental Tables 1 - 2 for statistics). Not included in these errors are systematic errors that might originate in different membrane thicknesses or membrane-substrate distances between different lipid conditions and a systematic underestimation of the residue to membrane distance from the 10-20% of protein that is trapped on the substrate proximal side of the supported bilayer. The reported errors after buffer changes or the addition of C2AB are the standard errors of the detected distance changes from at least 3 repeats for each condition. Based on previous experiments with polymer supported bilayers we estimate the systematic

uncertainty for the measured absolute distance to be ~1-2 nm[8]. The systematic underestimation of the real distance caused by protein trapped on the substrate side of the supported membrane can be estimated if we assume that 10% of fluorophores reside at an average position between oxide surface and membrane i.e. at -6 nm from the distal membrane surface[68]. With this assumption measured FLIC distances of 0 nm, 5 nm and 10 nm would originate from 90 % fluorophores at 0.7 nm, 6.2 nm and 11.8 nm.

2.2.15 Membrane docking of Syt1

2.2.15.1 Membrane depth data were obtained from EPR power saturation then used to generate models for the position of Syt1 in bilayers of varying lipid conditions. Docking was performed by David Nyenhuis. Briefly, this approach utilized a version of Xplor-NIH that included a plane distance potential, and followed the general procedure described previously[24,71]. PBD structures were loaded in MMM and the site-scan feature of the software was used in conjunction with the Warsh rotameric library to determine possible rotamers for the positions of interest[52,72]. The most probable rotamer was then attached to each site *in silico*. The depth parameters for each data set were used as point-to-plane distance restraints and the labeled structure was subjected to simulated annealing and energy minimization to dock the domain to the membrane interface. The spin label atoms and all protein backbone atoms were fixed for the duration of the early simulated annealing runs. For these point-to-plane restraints, the distance range was set to the uncertainty in the label position, which was determined from the experimental error in the membrane depth parameter and the empirically derived calibration curve[11]. Approximately 100 structures were

generated from each simulated annealing run. The structures were analyzed and figures were generated using the program PyMOL (Schrödinger, Cambridge, MA).

2.3 References

1. Lesley et al. (2009). The polymerase incomplete primer extension (PIPE) method applied to high-throughput cloning and site-directed mutagenesis. *Methods Mol Bio.* **498:** 91-103.
2. Dodev et al. (2014). A tool kit for rapid cloning and expression of recombinant antibodies. *Nature scientific reports.* **4:** 5885.
3. Kuo, W. et al. (2011). Phosphatidylinositol 4,5-Bisphosphate Alters Synaptotagmin 1 Membrane Docking and Drives Opposing Bilayers Closer Together. *Biochemistry.* **50:** 2633-2641.
4. Lu, B. (2014). The Juxta-Membrane Linker of Full-Length Synaptotagmin 1 Controls Oligomerization and Calcium-Dependent Membrane Binding. *Journal of Biological Chemistry.* **289:** 22161-22171.
5. Rosano et al. (2014). Recombinant protein expression in Escherichia coli: advances and challenges. *Frontiers in Microbiology.* **5:**172.
6. Papaneophytou et al. (2013). Statistical approaches to maximize recombinant protein expression in Escherichia coli: A general review. *Protein expression and purification.* **94:** 22-32.
7. Kimple et al. (2015). Overview of Affinity tags for protein purification. *Curr Protoc Protein Sci.* **73:** doi: 10.1002/0471140864.ps0909s73.
8. Nachod. (1949). Ion Exchange: Theory and Application. *Academic Press Inc.* 125 East 23rd street, New York, NY.
9. Ge lifesciences. Ion Exchange Chromatography: Principles and Methods Handbook.
10. Porterfield at al. (2010). A Simple and General method for determining the protein and nucleic constant of viruses by UV absorbance. *Virology.* **407:** 281-288.
11. Perez-Lara et al. (2016). PtdInsP_2 and PtdSer Cooperate to Trap Synaptotagmin-1 to the Plasma Membrane in the Presence of Calcium, *Elife*. e15886.
12. Stein, A. Radhakrishnan, D. Riedel, D. Fasshauer, R. Jahn. 2007. Synaptotagmin activates membrane fusion through a Ca2+-dependent trans interaction with phospholipids. *Nat. Struct. Mol. Biol.* doi: 14:904–911. doi:10.1038/nsmb130.
13. Lin et al. (2014). Control of membrane gaps by Synaptotagmin-Ca2+ measured with a novel distance ruler. *Nature Communication.* doi:10.1038/ncomms6859.
14. Klug et al. (2008). Methods and Applications of Site-Directed Spin Labeling EPR Spectroscopy. *Methods in cell biology.* **84:** 617-658.
15. Kim et al. (2008). Efficient site-specific labeling of proteins vis cysteines. *Bioconjug. chem.* **19:** 786-791.
16. Klug and Felix. (2008). Methods and Applications of Site-directed Spin Labeling EPR Spectroscopy. *Methods in cell biology.* **84:** 617-658.
17. Columbus, L., Kalai, T., Jeko, J., Hideg, K., and Hubbell, W. L. (2001). Molecular motion of spin labeled side chains in alpha-helices: Analysis by variation of side chain structure. *Biochemistry* **40:** 3828–3846.
18. Columbus, L., and Hubbell, W. L. (2002). A new spin on protein dynamics. Trends Biochem. Sci. **27:** 288–295.
19. Columbus, L., and Hubbell, W. L. (2004). Mapping backbone dynamics in solution with site-directed spin labeling: GCN4–58 bZip free and bound to DNA. *Biochemistry* **43:** 7273–7287.

20. Lietzow, M. A., and Hubbell, W. L. (2004). Motion of spin label side chains in cellular retinol-binding protein: Correlation with structure and nearest-neighbor interactions in an antiparallel b-sheet. *Biochemistry* **43** 3137–3151.
21. Langen, R., Oh, K. J., Cascio, D., and Hubbell, W. L. (2000). Crystal structures of spin labeled T4 lysozyme mutants: Implications for the interpretation of EPR spectra in terms of structure. *Biochemistry* **39:** 8396–8405.
22. Toseland. (2013). Fluorescent labeling and modification of proteins. *J Chem Biol.* **6:** 85-95.
23. Hobbs et al. (2014). Biophysical and proteomic characterization strategies for cysteine modifications in ras GTPases. *Methods Mol Bio.* **1120:** 76-96.
24. Herrick et al. (2006) Position of Synaptotagmin 1 at the Membrane Interface: Cooperative Interactions of Tandem C2 Domains *Biochem.* **45:** 9668-9674.
25. Kiessling et al. (2013). Rapid Fusion of Synaptic Vesicles with Reconstituted Target SNARE Membranes. *Biophysical Journal.* **104:** 1950-1958.
26. Castle et al. (1999). Factors affecting the size distribution of liposomes produced by freeze-thaw extrusion. *International Journal of Pharmaceutics.* **188:** 87-95.
27. Lapinski et al. (2007). Comparison of Liposomes formed by sonication and extrusion: rotational and translational diffusion of an embedded chromophore. *Langmuir.* **23:** 11677-11683.
28. Rufener et al. (2005). Membrane-Bound Orientation and Position of the Synaptotagmin C2B Domain Determined by Site-Directed Spin Labeling. *Biochemistry.* **44:** 18-28.
29. Yan. (2003). Membrane Transporters: Methods and Protocols. *Methods in Molecular Biology*. 999 Riverview Drive, Totowa, NJ.
30. Philppot and Schuber. (1995). Liposomes as Tools in Basic Research and Industry. *CRC press Inc.*
31. Seddon et al. (2004). Membrane proteins, lipids and detergents: not just a soap opera. *BBA Biomembranes.* **1666:** 105-117.
32. Buser et al. (1998). Ultracentrifugation technique for measuring the binding of peptides and proteins to sucrose-loaded phospholipid vesicles. *Methods Mol. Bio.* **84:** 267-281.
33. Kuo, W., Herrick, D. Z., Ellena, J. F., & Cafiso, D. S. (2009). The Calcium-Dependent and Calcium-Independent Membrane Binding of Synaptotagmin 1: Two Modes of C2B Binding. *Journal of Molecular Biology*, *387*(2), 284–294. doi: 10.1016/j.jmb.2009.01.064.
34. Kuo et al. (2011). Phosphatidylinositol 4,5-bisphosphate alters synaptotagmin 1 membrane docking and drives opposing bilayers closer together. *Biochemistry,* **50:**2633-41.
35. Bartlett. (1959). Phosphorous Assay in Column Chromatography. *J. Biol. Chem.* **234:** 466-468.
36. Pokorny et al. (2002). Mechanism and Kinetics of d-Lysin Interaction with Phospholipid vesicles. *Biochem.* **41:** 11044-11056.
37. Berliner. (1976). Spin labeling Theory and Applications. *Molecular Biology. Academic press inc.*111 Fifth Avenue, New York, NY 10003.
38. Jeschke. (2007). ESR Spectroscopy in membrane biophysics. Chapter 2: Instrumentation and experimental setup. ISBN:978-0-387-25066-3.
39. Kivelson. (1960). Theory of ESR Linewidths of Free Radicals. *Journal of Chemical Physics.* **33:**1094-1116.

40. Malmberg and Falke. (2005). Use of EPR Power Saturation to analyze the Membrane-Docking Geometry of Peripheral Proteins: Applications to C2 Domains. *Annu. Rev. Biophys, Biomol. Struct.* **34:** 71-90.
41. Mitrikas et al. (2007). Electron spin-lattice and spin-spin relaxation study of a trinuclear iron (III) complex and its relevance in quantum computing. *Physical chemistry chemical physics.* **10:** 743-748.
42. Bales et al. (2009). EPR line shifts and line shape changes due to spin exchange of nitroxide free radicals in liquids 6. Separating line broadening due to spin exchange and dipolar interactions. *J phys chem.* **113:** 4930-4940.
43. Peric et al. (2012). EPR line shift and line shape changes due to Heisenberg spin exchange and dipole-dipole interactions of nitroxide free radicals in liquids: 8. Further experimental and theoretical efforts to separate the effects of the two interactions. *J phys chem.* **116:** 2855-2866.
44. Peric et al. (1997). EPR line shift and line shape changes due to Heisenberg spin exchange and dipole-dipole interactions of nitroxide free radicals in liquids. *J phys chem.* **101:** 8707-8716.
45. Weber et al. (1998) EMX User's Manual. Version 2. Bruker Instruments Inc. Billerica, MA USA.
46. Altenbach et al. (1994). A Collisional Gradient Method to determine the Immersion depth of nitroxides in lipid bilayers: Applications to spin-labeled mutants of bacteriorhodopsin. *Proc. Natl. Acad. Sci.* **91:** 1667-1671.
47. Frazier et al. (2002). Membrane-Bund Orientation and Position of the Synaptotagmin-1 C2A Domain by Site-Directed Spin Labeling. *Biochem.* **42:** 96-105.
48. Jeschke. (2012). DEER distance measurements on proteins. *Annu. Rev. Phys. Chem.* **63:** 419-446.
49. Stein et al. (2015). A straightforward approach to the analysis of DEER data. *Method. Enzym.* **563:** 531-67.
50. Jeschke et al. (2007). Distance measurements on spin-labelled biomacromolecules by pulsed electron paramagnetic resonance. *Phys Chem, Chem Phys* **9:**1895–1910.
51. Reginsson and Schiemann. (2011). Pulsed electron-electron double resonance: beyond nanometer distance measurements on biomacromolecules. *Biochem J.* **434:** 353-363.
52. Polyhach et al. (2011). Rotamer libraries of spin labelled cysteines for protein studies. *Physical Chemistry Chemical Physics* **13**:2356–2366.
53. Kiessling, V. & Tamm, L. (2003). Measuring distances in supported bilayers by fluorescence interference-contrast microscopy: Polymer supports and SNARE proteins. *Biophys J* **84**, 408-418.
54. Lee et al. (2017). Structure of the Ebola virus envelope protein MPER/TM domain and its interaction with the fusion loop explains their fusion activity. *PNAS.* **38:** E7987-E7996.
55. Pannier M et al(2000). Dead-time free measurement of dipole-dipole interactions between electron spins. *J Magn Reson* **142:**331–340.
56. Jeschke et al. (2006). DeerAnalysis2006-a comprehensive software package for analyzing pulsed ELDOR data *Appl. Magn. Reson.*. **30:** 473-498.
57. Brandon et al. (2012). The global analysis of DEER data. J. *Magn. Reson*. **218:** 93-104.
58. Kwan et al. (2010). Macromolecular NMR spectroscopy for the non-spectroscopist. *FEBS journal.* **278:** 687-703.

59. Feeny, J. (1999). Macromolecule-ligand interactions studied by NMR. *Encyclopedia of Spectroscopy and Spectrometer.* 1209-1216. doi: 1006/rwsp.2000.0163.
60. Williamson. (2013). Using chemical shift perturbation to characterize ligand binding. *Progress in nuclear magnetic resonance spectroscopy.* **73:** 1-16.
61. Ubach et al. (2001). The C2B domain of Synaptotagmin 1 is a $Ca2^{+}$ binding module. *Biochemistry.* **40:** 5854-5860.
62. Cavanagh et al. (2006). Protein NMR spectroscopy 2nd edition principles and practice. Academic Press.
63. Delaglio et al. (1995). NMRPipe: a multidimensional spectral processing system based on UNIX pipes. *Journal of Biomolecular NMR* **6**:277–293.
64. Goddard et al. (2008). SPARKY, NMR Assignment and Integration Software. SPARKY, NMR Assignment and Integration Software.
65. Fernandez et al. (2001). Three-dimensional structure of the Synaptotagmin 1 C2B-domain: synaptotagmin 1 as a phospholipid binding machine. *Neuron* **32**:1057–1069.
66. Vranken et al. (2005). The CCPN Data Model for NMR Spectroscopy: Development of a Software Pipeline. *Proteins*. **59:** 687 – 696.
67. DeLano, W. L. (2002). Pymol: An open-source molecular graphics tool. *CCP4 Newsletter On Protein Crystallography.* **40:** 82-92.
68. Domanska et al. (2009) Single vesicle millisecond fusion kinetics reveals number of SNARE complexes optimal for fast SNARE-mediated membrane fusion. J. Biol. Chem. **284**, 32158–32166.
69. Liang, B., Kiessling, V. & Tamm, L. K. (2013). Prefusion structure of syntaxin-1A suggests pathway for folding into neuronal trans-SNARE complex fusion intermediate. *Proc Natl Acad Sci U S A* **110**, 19384-19389.
70. Kiessling, V. & Tamm, L. (2003). Measuring distances in supported bilayers by fluorescence interference-contrast microscopy: Polymer supports and SNARE proteins. *Biophys J* **84**, 408-418
71. Schwieters et al. (2003). The Xplor-NIH NMR molecular structure determination package. *Journal of Magnetic Resonance* **160:**65–73.
72. Polyhach et al. (2010). Prediction of favorable sites for spin labelling of proteins. *Spectroscopy* **24**:651–659.

CHAPTER 3: Synaptotagmin-1 Membrane Insertion and Orientation depends on Lipid Compositions in the Bilayer

3.1 Introduction

While the details are still unclear, synaptotagmin-1 (Syt1) can be considered the trigger for neuronal exocytosis, potentially through binding to negatively charged lipids within either the plasma or vesicle membranes. The Syt1 calcium-dependent membrane interaction and insertion is lipid specific with certain head groups required to drive both insertion and bridging[1-5]. When studied in the soluble construct as C2AB the calcium binding loops of each domain insert into membrane at different affinities according to both the net charge on the surface and the specific type of lipid composition present[4-7]. Phosphatidylserine (PS) and phosphatidylinositol-4,5-bisphosphate (PIP_2) are highlighted as key charged lipid headgroups in this binding process[5-8].

The Ca^{2+} binding loops located in both the C2A and C2B domains of Syt1 interact with PS headgroups located on both the vesicular and plasma membrane[4,9,10]. The C2A domains' Ca^{2+} binding loops in particular have been shown to bind specifically to PS[9,11]. Calcium, when bound and coordinated to Syt1, is known to also incorporate PS into open coordination sites[10,12]. Syt1 can also sequester the PS in a membrane, which would increase local charge density and potentially enhance Syt1 binding affinity and depth of insertion into the membrane[13]. The PS clustering can also lead to curvature induction and may sequester charge away from the SNARE complex[13,14].

However, the C2A domain has also been observed to interact with PIP_2, which may either enhance or oppose PS binding[4,15,16]. The latter would occur because PIP_2 has been proposed to form dense charge clusters which may compete with the ability to coordinate PS on the membrane surface[16].

PIP_2 is particularly interesting as it differentiates the two membranes, being only located on the plasma membrane[4]. This lipid has a large and bulky headgroup with net negative four charge[6]. Due to its bulk, it has also been proposed through molecular modeling to sit above the rest of the bilayer headgroups, which could impact interactions and orientations between Syt1 and the plasma membrane[17]. Charge clustering would also impact binding with Syt1, particularly if it does sit above the membrane interface[15]. Interactions with the charged patch of lysine residues around K326, K327 on the C2B domain known as the polybasic face have been highlighted to potentially precede a calcium-trigger[4,7,18-21]. This interaction has been contested, however, by FRET measurements used to measure binding affinity on the soluble construct. In these experiments, it was found that while both the wild type C2AB construct and a mutant reducing the net charge at the polybasic face (KAKA mutant) had a large increase in calcium affinity to the calcium binding loops in the presence of PIP_2 containing vesicles (40 times for wild type), there was no significant difference between the mutant and the wild type[20,22]. This measurement was opposed by a series of other studies, however, which showed a significant decrease in calcium-dependent binding when PIP_2 is not present on the membrane[20,21]. Thus, as mentioned in the introduction, the polybasic face likely plays roles in both calcium- dependent and calcium-independent lipid interactions, which include: Syt1 oligomerizing, Syt1 binding to negatively charged phospholipids (like PS and PIP_2), and Syt1 simultaneously binding to the synaptic vesicle and plasma membranes[23]. Again, calcium dependent oligomerization and binding to negatively

charged lipids have been proposed to regulate the opening, dilation, or stability of the fusion pore[4,6,7,23].

Demonstrating and characterizing calcium-independent interactions between the polybasic face and high concentrations of charge on the plasma membrane, such as PIP_2 headgroups, would support the idea that Syt1 can dock synaptic vesicles[4,6,7,23]. Further investigation would also verify previous EPR and docking measurements where the C2B domain is proposed to act as an electrostatic switch. First, the vesicles are primed calcium-independently through charge interactions between the polybasic face and the plasma membrane, which also brings the SNAREs into close proximity. Then, the domains change orientation to insert the calcium binding loops into either the vesicle or plasma membranes in the presence of calcium, creating even closer proximity and tighter binding[7].

Previous EPR power saturation measurements in the lab, in PC:PS (75%:25%) containing bilayers (in the form of 100 nm vesicles) have been performed in an attempt to orient the insertion of the C2A and C2B calcium binding loops (mainly loop 1 and 3) into membranes with 25% negative charge[15,16,24-26]. EPR power saturation measurements have also been performed in PC:PS:PIP_2 (74%:25%:1%) vesicles with an overall negative charge of 29%, which demonstrated that the addition of PIP_2 drives the membranes closer together by changing the depth of insertion of the C2A and C2B domains (~6 Angstrom deeper insertion of the third calcium binding loop of C2B)[4]. However, these changes in insertion depth and orientation may be due to the lipid identity or simply the overall increase in charge on the membrane surface. Current CW and power saturation EPR measurements I performed were in PC:PIP_2 bilayers or in PC:PS:PIP_2 vesicles of the same net charge as the PC:PS vesicles. With this data, in collaboration with David Nyenhuis in the Cafiso lab, we were able to model the orientation changes of the C2B domain for PS or PIP_2

vesicles with net 20% negative charge[27]. Additionally, work by Ángel Pérez-Lara in the Jahn lab (Max Plank Institute for Biophysical Chemistry, Germany), and Anusa Thapa in Cafiso lab worked together using thermodynamic, kinetic, and various structural techniques to verify calcium-intendent binding of the C2B domain polybasic face to PIP_2 containing bilayers and to demonstrate affinity and dissociation rate changes between PS and PS:PIP_2 containing bilayers. Together, the aim is demonstrating the importance of the C2B domains' interaction with the plasma membrane, which would potentially drive membrane bridging by first initiating priming or docking of the synaptic vesicle, followed by calcium-dependent insertion, which is enhanced by electrostatic interactions of the polybasic face and PIP_2[27]. This work is published in *eLife* and titled, $PtdInsP_2$ and PtdSer Cooperate to Trap Synaptotagmin-1 to the Plasma Membrane in the Presence of Calcium[27].

3.2 Results

3.2.1 Synergy between PS and PIP_2 in Syt1 membrane binding

Using rapid mixing and Förster resonance energy transfer (FRET) between intrinsic tryptophan residues in the soluble C2AB construct of Syt1 and dansyl-labeled lipid headgroups within extruded liposomes, Ángel Pérez-Lara was able to monitor the kinetics of C2AB binding in the presence of calcium for various lipid conditions. These experiments were performed in dilute C2AB concentrations (0.25 μM) to minimize C2AB vesicle aggregation. This was verified through monitoring the turbidity by taking the absorbance at 450 nM for each concentration of C2AB and lipid. Liposomes were titrated in over a range of 0.3 nM to 3 nM of vesicles and with varying

charge distributions, starting with 0% net negative charge (PC vesicles), to verify that binding to vesicles was charge dependent. Combinations of charge were then compared first at 10% net negative charge (PC:PS 90:10%) or (PC:PIP_2 97.5:2.5%), then 20% net negative charge (PC:PS 80:20%) or (PC:PIP_2 95:5%) or (PC:PS:PIP_2 80:10:2.5%), next 30% net negative charge (PC:PS:PIP_2 70:20:2.5%) or (PC:PS:PIP_2 70:10:5%), and finally 40% net negative charge (PC:PS:PIP_2 60:20:5%). Binding at the lowest charge of 10% was not quantifiable through the experimental setup used, but higher charge densities yielded binding kinetics. Initial calculations yield the k_{obs} through monitoring the FRET over time of each lipid addition and fitting to a mono-exponential curve[27]. When the k_{obs} is plotted linearly as a function of vesicle concentration the k_{on} can be extracted as the slope of the line and the k_{off} the y-intercept[27,28]. Finally, the dissociation constant K_d is equivalent to the ratio k_{off}/k_{on}[27,28]. Interestingly, the K_d of either the PS alone or PIP_2 alone 20% net negative charge distribution were the only significant deviations from the set. This implies that when 20% net negative charge of both PS and PIP_2 are combined there is a synergy between the two lipid headgroups, increasing C2AB's affinity to membrane. The K_d was then separated into the k_{off} and k_{on} rates to attempt to isolate the effects contributing to this change in affinity. While there was a slight but significant decrease in the on-rate (association) of PS vesicles alone (potentially due to C2AB's lower calcium affinity relative to liposomes with PIP_2 present), the larger differences for just PS or PIP_2 liposomes were observed in the off-rate (dissociation)[21,27]. This implies that differences in affinity are purely due to the rate at which the C2AB dissociates from the membrane, and that when both PS and PIP_2 are present C2AB is far less likely to dissociate. To examine this more closely, the C2AB penetration and orientation within membrane was determined to isolate the effects of PS and PIP_2 calcium dependent binding.

Here, CW and power saturation EPR experiments were performed in the Cafiso lab to examine lineshape changes and the penetration depth of different sites on the C2AB construct in varying lipid compositions. The interactions of the Syt1 fragment (C2AB, residues 136-421, ~50 μM) with different lipid compositions, but conserved 20% net negative charge, were investigated for liposomes composed of: PC:PS (80:20%), PC:PIP_2 (95:5%), and PC:PS:PIP_2 (87.5:10:2.5%) (~25 mM samples). Experiments were performed in the presence of calcium (1 mM); EGTA (5-10 mM) was added to all liposome samples to ensure calcium-dependent binding was occurring (*Figure 3.1 and Table 3.1*). Measurements were taken at sites 173R1, 234R1, 304R1, 329R1, and 368R1 on the C2AB fragment. Anusa Thapa performed the 329R1 measurements. Insertion into membrane in the CW EPR lineshapes can be observed as broadening of the lines which results in a significant decrease in intensity relative to the aqueous, mobile loop measurements. The broadening is due to restriction of the label when inserted into membrane. Table 3.1 displays the resulting depth parameters and approximate distances. Positive distance values lie within the membrane relative to the phosphate headgroup-aqueous interface. Negative distance values lie in the aqueous phase. Distances were estimated using a calibration curve previously obtained[24]. Measurements were repeated 2-4 times and error was either the standard deviation or propagation from the $P_{1/2}$ fitting. The values for C2B measurements in PC:PS and PC:PIP_2 were then used as values for modeling/docking using Xplor-NIH, performed by David Nyenhuis (*Figure 3.2*).

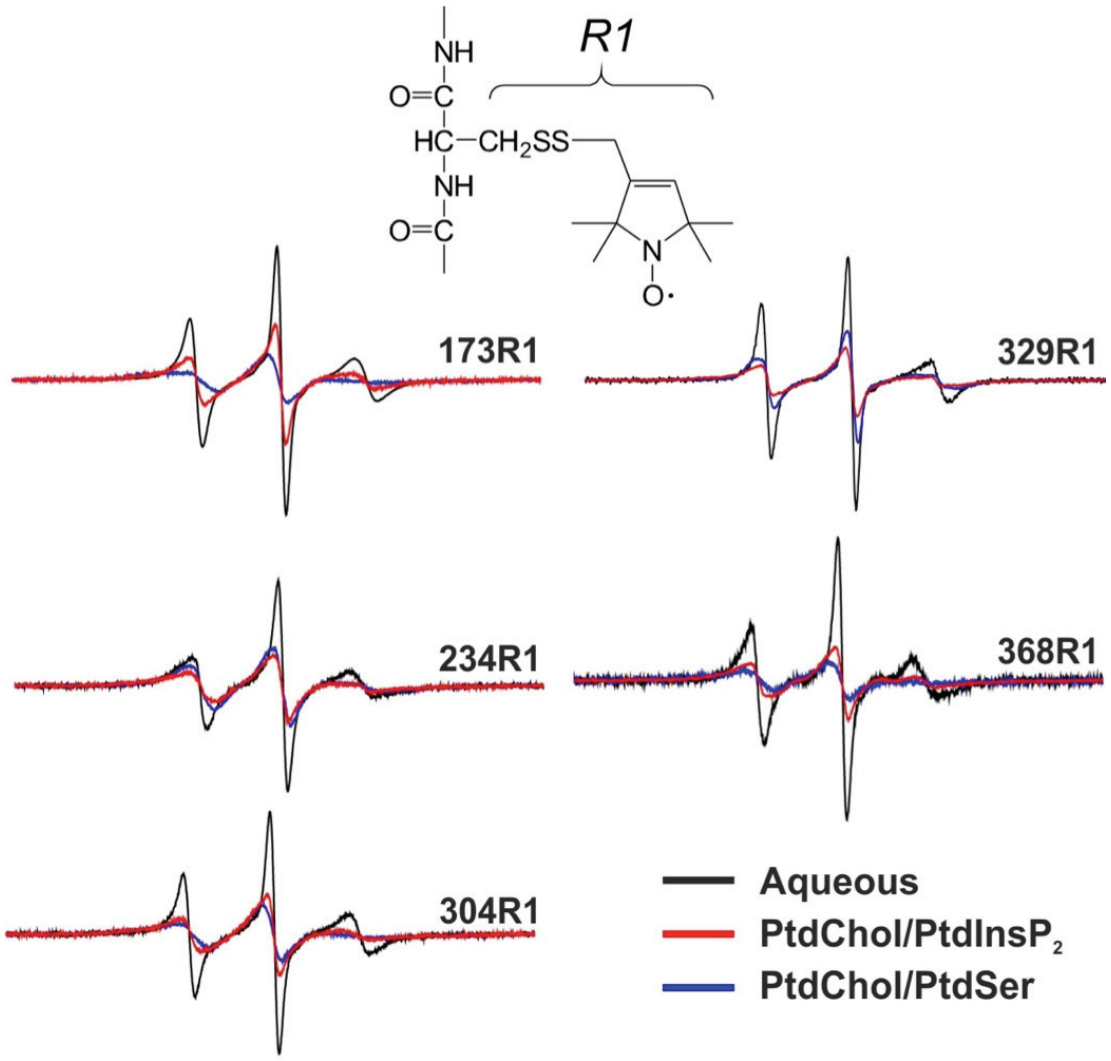

Figure 3.1: EPR spectra from sites 173R1, 234R1, 304R1, 329R1, and 368R1 on C2AB either in solution or bound to liposomes containing PC:PS (80:20) or PC:PIP₂ (95:5). The broader spectra are the result of membrane insertion which produces diminished signal amplitudes and slows the rate of R1 label motion when the C2AB fragment is bound to negatively charged liposomes (n = 2–3). PtdChol is PC, PtdInsP$_2$ is PIP$_2$ and PtdSer is PS. Image from Perez-Lara et al. (2016) *Elife*. e15886.

Mutant	Lipid composition	Depth parameter (Φ)	Approx. distance to phosphate plane (Å)*
M173R1	20% PS	+1.20 ± 0.10	+8.8
	5% PIP_2	−0.01 ± 0.20	+5.5
	10% PS + 2.5% PIP_2	+0.66 ± 0.10	+7.4
F234R1	20% PS	−0.10 ± 0.10	+5.2
	5% PIP_2	−1.50 ± 0.03	–0.6
	10% PS + 2.5% PIP_2	+0.00 ± 0.10	+5.5
V304R1	20% PS	−0.39 ± 0.20	+4.3
	5% PIP_2	−1.30 ± 0.10	+0.6
	10% PS + 2.5% PIP_2	−0.23 ± 0.10	+4.8
T329R1	20% PS	−2.00 ± 0.14	–5.4
	5% PIP_2	−0.80 ± 0.14	+2.8
	10% PS + 2.5% PIP_2	−2.10 ± 0.12	–7.3
G368R1	20% PS	+0.60 ± 0.10	+7.2
	5% PIP_2	−0.64 ± 0.05	+3.6
	10% PS + 2.5% PIP_2	+0.18 ± 0.10	+6.0

Table 3.1: Power saturation measurements for sites 173R1, 234R1, 304R1, 329R1, and 368R1 on C2AB in the presence of calcium and charged liposomes of varying conditions. Measurements of 329R1 were performed by Anusa Thapa. Positive distances lie on the hydrocarbon side of a plane defined by the lipid phosphates; negative distances reside on the aqueous side. Distances were estimated using a calibration curve empirically determined as described previously[88]. Depth parameters are typically the averages of two to four measurements and the error represents either standard deviations or errors propagated from the error in the measurement of $\Delta P^{1/2}$. These measurements were carried out at lipid concentrations high enough so that the C2AB fragment is completely membrane bound. Table from Perez-Lara et al. (2016) *Elife.* e15886.

Results from these measurements show for both the CW lineshapes and power saturation values that the lipid composition does alter the orientation of the C2B domain. For the C2A domain the first calcium binding loop, represented by 173R1, does not insert as deeply into PC:PIP_2 membranes. This is verified by power saturation, where in PS alone the loop is inserted 8.8 Angstroms into membrane and 5.5 Angstroms for PIP_2 alone. The third calcium-binding loop of C2A, represented by 234R1, is somewhat similar in lineshape, but the power saturation values

reveal again less insertion in the PIP_2 alone conditions, 5.2 Angstroms insertion for PS vs a somewhat interfacial 0.6 Angstroms out of the membrane for PIP_2. For each case PS:PIP_2 shows a slight deviation upward relative to the PS alone case, potentially due to PIP_2 headgroup height[17]. For the C2B domain, the first calcium binding loop, represented by 304R1, shows a slightly less mobile lineshape for PS alone, and power saturation measurements reveal a roughly 4 Angstrom lifting of the loop when comparing PIP_2 alone to the membranes with PS and PS:PIP_2. The third calcium binding loop in C2B is represented by 368R1, which displays the same lineshape and power saturation trend; lifting the loop about 3 Angstrom for PIP_2 alone compared to membranes with PS and PS:PIP_2. A final additional measurement in C2B at site 329R1 near the polybasic face highlights charged interactions with the charged lipid membranes. This location follows an opposite trend in lineshape and power saturation, revealing a preference to PIP_2 membranes and actually inserting when high concentrations of PIP_2 are present, with more aqueous, interfacial interactions for PS contributes. Docking was performed on the C2B domain to see if interactions of the polybasic face would change the orientation of the domain relative to membrane. This used only the PS and PIP_2 alone conditions since the combined case was similar to PS alone. The docking revealed significant tilting upward of the C2B domain due to the enhanced interaction of the polybasic face in the presence of bulky PIP_2, which agrees with previous observations at varying net negative charge[4].

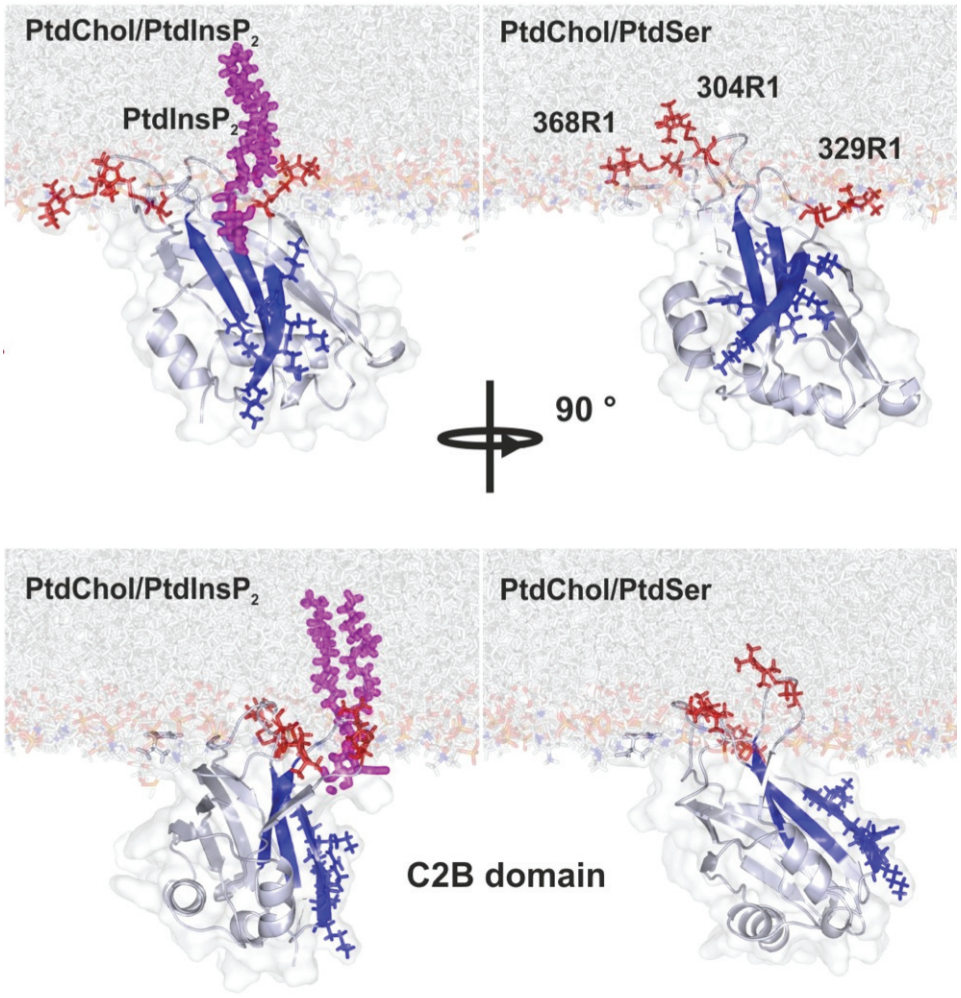

Figure 3.2: Docking orientation of the C2B domain (PDB ID: 1K5W) at the membrane interface. The polybasic face is colored in blue and shown in sticks. R1 labels are colored red and PIP_2 is colored pink to highlight potential proximity to the polybasic face. The figure was generating using Xplor-NIH and was aligned with a membrane simulation generated by CHARMM-GUI for a bilayer with PC:PIP_2 or PC:PS at a molar ratio of 97:3 or 80:20, respectively. PIP_2 was manually docked to the C2B domain. Image from Perez-Lara et al. (2016) *Elife.* e15886.

3.2.2 Interactions between PIP_2 and the polybasic face

Additional experimentation from Ángel Pérez-Lara (and collaborators) and Anusa Thapa using isothermal calorimetry (ITC), HSQC-NMR, and ultracentrifugation vesicle sedimentation assays sought to further characterize the interactions between the C2AB construct and either PS or PIP_2[27]. For ITC experiments PS and PIP_2 headgroups were mixed with the C2AB construct to

observe the thermodynamics of binding and isolate direct headgroup interactions from additional electrostatic and hydrophobic contributions within the liposome[27]. PS headgroups only demonstrated slight changed in enthalpy, but the PIP_2 headgroup IP_3 was very exothermic, binding to C2AB at a 1:1 ratio with an affinity of 14 ± 2 μM[27]. NMR experiments were then performed to determine potential locations for the interaction of IP_3 with the C2AB domains. These experiments were performed by Anusa Thapa on shortC2A and longC2B constructs (described in Methods) (*Figure 3.3*). NMR experiments revealed interactions in C2A in the charged (calcium bound) calcium binding loops and small chemical shifts in the loops of the C2B domain. The most significant chemical shifts, however, were observed at the polybasic face[27]. This confirmed previous proposals for an interaction between PIP_2 and the polybasic face[4,7,19,20,21,29]. (These measurements will be revisited using a shortC2B construct in a later chapter.) A series of follow up ITC measurements in the presence and absence of calcium was then used to monitor thermodynamic interactions between IP_3 and C2AB neutralization mutants: C2A calcium binding loops (D178A, D230A, D232A), C2B calcium binding loops (D309A, D363A, D365A) or both C2A and C2B calcium binding loops (D178A, D230A, D232A, D309A, D363A, D365A), which prevent coordination of calcium[27]. Wild-type C2AB constructs showed a reduction in binding affinity in the absence of calcium, which through work with the various neutralization mutants can be attributed to binding to the calcium-binding loops of the C2B domain (likely driven through electrostatic effects due to changes in enthalpy rather than entropy). ITC measurements on the C2A and C2B domains alone confirmed that C2B is the main binding site for IP_3 since C2B alone could recreate wild-type C2AB energy differences. Here, the authors also briefly examined IP_3-SNARE competition for binding to the C2B construct using ITC. At physiological salt and calcium conditions SNARE addition has no effect on C2B-IP_3 affinity. At low CA2B concentrations there

is a slight decrease in CA2B IP_3 affinity in the presence of SNAREs, but the overall affinity between Syt1 and SNAREs is lower than IP_3. This agrees with previous theories suggesting heterogeneity in Syt1 binding to the SNAREs under physiological conditions[5,30,31].

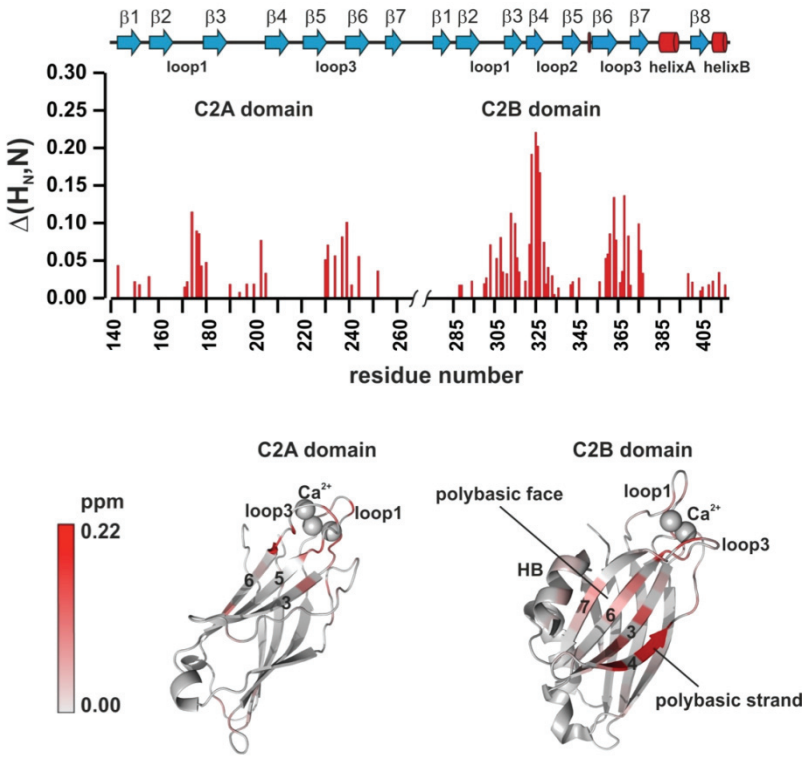

Figure 3.3: Averaged-weighted chemical shifts (ΔH_N, N) in ^{15}N-^{1}H correlated HSQC NMR spectra of C2A and longC2B in the presence of IP_3 and Ca^{2+}. Work performed by Anusa Thapa, repeated in a later chapter for a shorter fragment of the C2B domain. Top: Chemical shift changes are widely distributed in the polybasic region of C2B domain. Small chemical shift are also seen in the calcium-binding loops of the C2B and C2A domains. Measurements were made under normal ionic strength (150 mM NaCl, 50 mM MES, pH = 6.3, and 3 mM Ca^{2+}) at a frequency of 600 MHz for protons. Bottom: Chemical shifts are color coded and mapped onto the structures of C2B and C2A domains according to the color bar. Image from Perez-Lara et al. (2016) *Elife.* e15886.

The KAKA mutant of the polybasic face (which does not eliminate all of the lysine's on the polybasic face), mentioned above, was then used for additional ITC, FRET, and ultracentrifugation sedimentation assays to look at polybasic face binding to PIP_2. All of these experiments found that in the presence of calcium, the KAKA mutant binds with slightly less

affinity than the wild-type C2AB construct. In the absence of calcium, however, the KAKA construct does not bind to IP_3/PIP_2. Sedimentation assays were performed with charge contributions from PS, $PS:PIP_2$, or PIP_2 alone and a progressive mutation series: wild-type, KA, KAKA in the polybasic face (*Figure 3.4*). For PS in the presence of calcium, there is a slight relative reduction in affinity (shown as reciprocal molar partition coefficients of the KAKA mutant ($1x10^3$ M^{-1} WT to $3.4x10^2$ M^{-1} KAKA). When PS and PIP_2 are present binding affinity was reduced by a greater degree, ($5x10^4$ M^{-1} WT, $2.2x10^4$ M^{-1} KA, to $1x10^4$ M^{-1} KAKA), with the greatest reduction for PIP_2 alone ($2.2x10^4$ M^{-1} WT, $5.1x10^3$ M^{-1} KA, to $1.1x10^3$ M^{-1} KAKA). In liposomes with slightly higher charge and in the absence of calcium, the KAKA mutant cannot bind to either PS or PIP_2 bilayers alone, but still has a detectable binding affinity to $PS:PIP_2$. This again suggests synergy or cooperativity between PS and PIP_2. This also agrees with the increased affinity of the wild-type C2AB construct to $PS:PIP_2$ rather than either alone (20 μM lipid required for 50% binding relative to 45 μM for PIP_2 and 1 mM for PS). Overall, these measurements support the idea that PIP_2 is binding to the polybasic face preferentially over the calcium binding loops of the C2B domain.

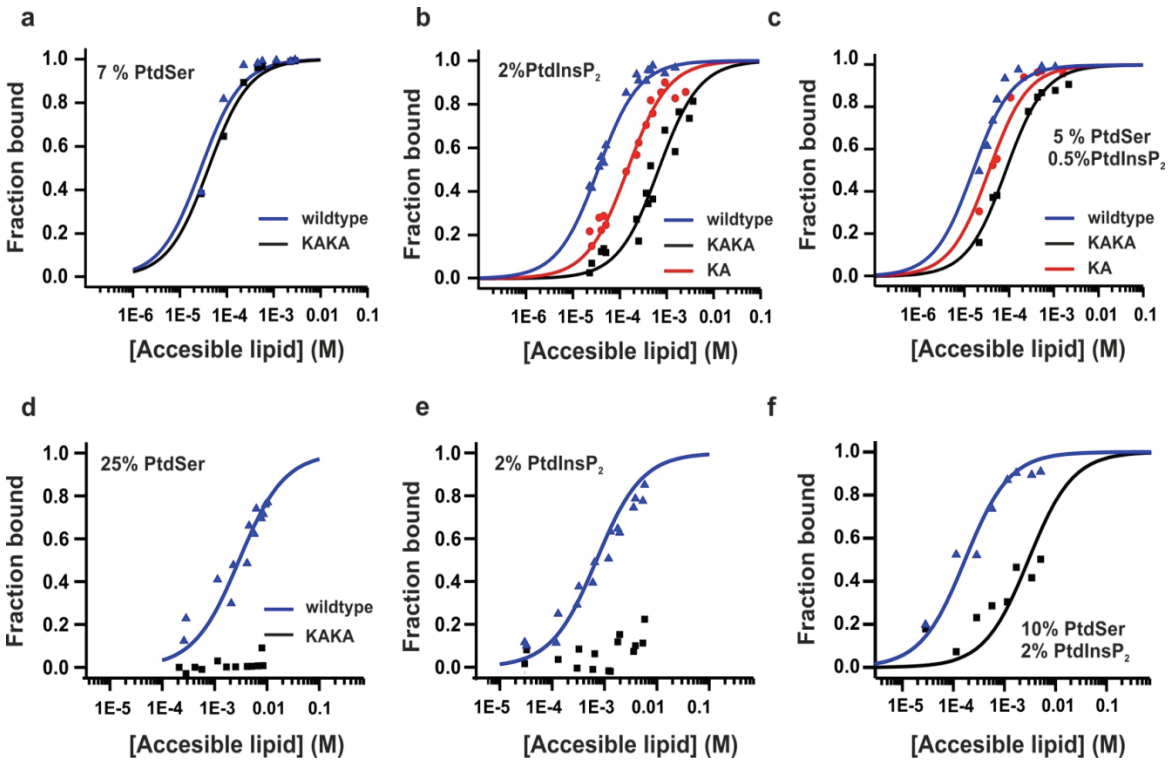

Figure 3.4 Equilibrium binding of the C2AB fragment and polybasic (KAKA) mutants to PC:PS, PC:PS:PIP_2 , and PC:PIP_2 bilayers. Data collected by Anusa Thapa. Shown first is Ca^{2+}-dependent (a,b,c) and then Ca^{2+}-independent partitioning (d,e,f) of a C2AB fragment into PC:PS in a and d, PC:PIP_2 in b and e, and PC:PS/:PIP_2 bilayers in c and f. (d,e) No binding of the KAKA mutant was observed in the presence of PS or PIP_2 alone in the absence of calcium . At equivalent charge densities, removal of lysine residues within the polybasic face reduced the membrane affinity in vesicles containing PS and PIP_2 (c) more than it did in vesicles containing either (a) PS or (b) PIP_2 in the presence of calcium. Image from Perez-Lara et al. (2016) *Elife.* e15886.

3.2.3 Phosphoinosites and Calcium decrease the dissociation rate of Syt1

The final experiments from Ángel Pérez-Lara and collaborators examined the specificity of PIP_2 binding to the polybasic face compared to other phosphatidylinositol derivatives of varying stereoisomers and charges using stopped flow and ITC experiments[27]. Their findings suggest that the kinetics of interaction with the C2AB construct are likely due to charge density of the headgroup. Bulk or steric hinderance may slightly hinder PIP_3 relative to PIP_2, however, which was observed with ITC. The last set of experiments attempted to determine if part of C2AB's

driving force (association rate) to the charged membrane is due to the available, local calcium concentrations. Varied calcium levels did not affect association but instead only dissociation rates, suggesting that initial interaction with the membrane is calcium-independent and that dissociation is due to decreased levels of accessible calcium. This observation fits nicely with the concepts involving calcium-independent priming of Syt1. Calcium flux and synchronous triggering would then cause Syt1 insertion into membrane, triggering SNARE dependent fusion. Finally, Syt1 would need to dissociate as calcium is depleted (controlled by ion channels to prepare for the next action potential). This dissociation could contribute to slower rates of asynchronous release (also mediated by Syt7) and fits with the observed drop in calcium concentrations after an action potential[32]. It could also imply that Syt1 dissociation from the membrane could promote conformational changes in the protein which act as signaling sites for endocytosis.

3.3 Discussion

Using a combination of quantitative thermodynamic, kinetic and structural methods, the Jahn and Cafiso labs were able to demonstrate PS and PIP_2 specific synergistic binding of the C2AB domains of Syt1. The combination of PS and PIP_2 increases binding affinity to the membrane, which are driven through additional electrostatic interactions, particularly of the C2B domain's polybasic face with PIP_2. This is apparent in the absence of calcium as well, which could assist in priming of the membrane prior to fusion. This polybasic face interaction alters and enhances the penetration depth and orientation of the C2 domains, helping to set the spacing

involved in potential bilayer bridging. As previously demonstrated, calcium increases the binding affinity of Syt1 to PIP_2 membranes, but the interaction is still mostly through the polybasic face and would not compete with PS for calcium binding loop insertion. Also, calcium coordination helps drive calcium binding loop penetration by preventing repulsion through neutralizing the negatively charged loops. Finally, phosphatidylinositol derivatives act with calcium to increase Syt1 binding affinity to the membrane by preventing Syt1 dissociation. Thus, time spent on the membrane, membrane penetration, and orientation must all contribute to Syt1 synchronous triggering.

Syt1 calcium-dependent (and independent) contact and insertion to membrane has previously been presented to be lipid specific with specific head groups required to drive membrane insertion and bridging[1-4]. When studied in the soluble construct C2AB, the calcium binding loops of each domain insert into membrane. PS and PIP_2 are highlighted as potential key charged lipid headgroups in membrane binding[4,6-8]. The Jahn and Cafiso labs agree with these findings, further indicating that an interplay, rather than a competition, is present between PS and PIP_2 headgroups. These lipids act at different regions of the protein, mainly at the calcium binding loops and polybasic face respectively, to bring Syt1's C2 domains into closer contact with the membrane surface.

The theory that the polybasic face interacts through electrostatic binding to PIP_2 headgroups was validated by quantifying the affinity of the previously identified KAKA mutation[4,18-21]. This work also characterized the calcium-independent interactions of the polybasic face with PIP_2, supporting the idea that Syt1 can dock synaptic vesicles[4,6,7,19]. This fits the notion that the C2B domain could act as an electrostatic switch by priming the vesicles calcium-independently through electrostatic interactions between the polybasic face and the plasma

membrane. Affinity measurements for Syt1 between the PIP_2 headgroup and SNARE complex also support the heterogeneity of SNARE binding and the potential competition between PIP_2 and SNARE binding to the polybasic face under physiological conditions[5,30,31]. This supports the idea that Syt1-membrane binding likely brings SNAREs into proximity for fusion, but that any direct interaction between Syt1 and the SNARE complex is beneficial, but unnecessary.

Before calcium influx, PIP_2 is actually somewhat repulsive toward the negatively charged C2B calcium binding loops, but that upon calcium addition PS will overcome this repulsion and also accommodate the PIP_2-polybasic face contact. This repulsion could explain the conflicting results observed in work with the KAKA mutation[21,22].

These findings agree that the C2A and C2B domains' calcium binding loops interact mainly with PS headgroups through coordination, but coordination to calcium and subsequently PS, as well as charge neutralization of the calcium binding loops through calcium addition, all collaborate to drive Syt1 membrane binding. This also explains why once calcium is bound to the binding loops, Syt1 affinity toward PIP_2 also increases[22]. Calcium coordination to the calcium binding loops, assisted by PS coordination, removes the repulsive effect between the calcium binding loops of the C2B domain and PIP_2.

In sum, these findings support the idea that Syt1 likely plays roles in both calcium-dependent and calcium-independent membrane interactions. A model is then proposed where: in the absence of Ca^{2+}, Syt1s are first tethered to synaptic vesicle and then each C2B domain adsorbs to the presynaptic plasma membrane interface. It then binds to PIP_2 through the polybasic face in a transient interaction, aiding in docking and priming of the synaptic vesicle. Here, the negative charges on the calcium binding loops of the C2A and C2B domains prevent penetration of the C2 domains into the presynaptic membrane through electrostatic repulsion. This promotes a high

dissociation rate of the C2B domain on the plasma membrane. Upon calcium influx and triggering, calcium binds to the calcium binding loops and neutralizes the negative charge and thus repulsion of the negatively charged membrane. Now, PS can bind to the calcium binding loops and complete calcium's coordination sphere, driving loop insertion (through permitting the hydrophobic residues insertion at the tips of the C2 domains). The presence of calcium now increases the C2B domain's affinity to PIP_2. This leads to deeper penetration of the C2B calcium binding loops into the bilayer and a tilting of the domain to accommodate the interaction of the polybasic face. Together, these events decrease Syt1s dissociation rate from the membrane and enhance its penetration into the plasma membrane core, which permits SNARE-dependent membrane fusion (*Figure 3.5*).

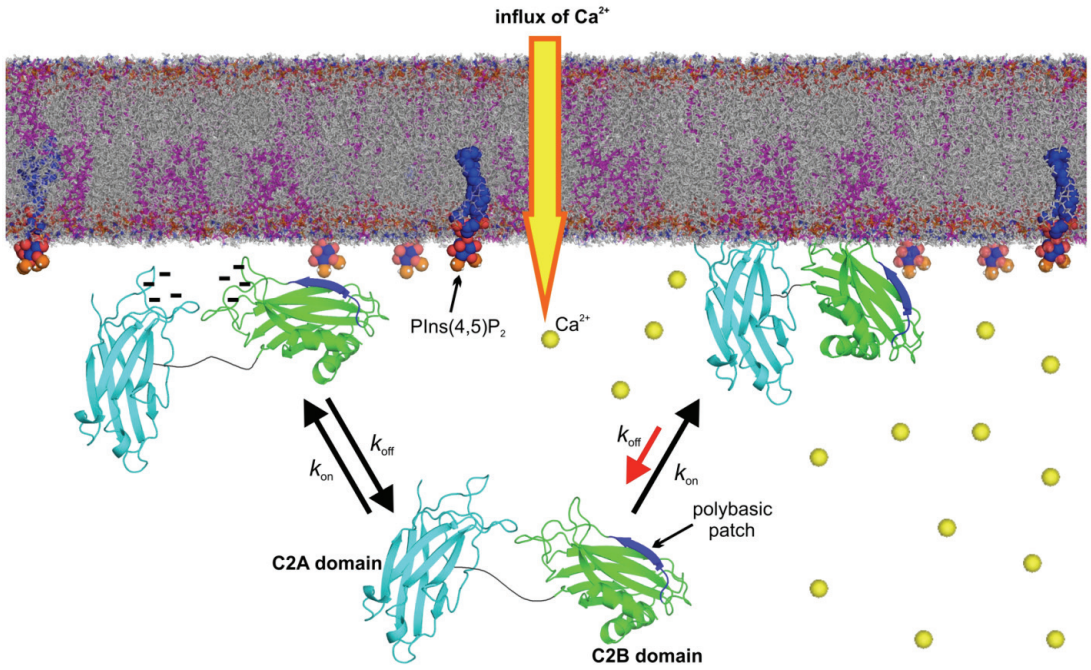

Figure 3.5 Model of the membrane-binding mechanism of Syt1. Figure generated by David Nyenhuis, Sarah Nyenhuis, and Angel Perez-Lara. NMR structures of the C2A domain (PDB ID: 1BYN) and the C2B domain (PDB ID_ 1K5W of Syt11 and a MD membrane simulation were rendered using PyMOL. The membrane used in this illustration was generated using the Membrane Builder input generator module in CHARMM-GUI of a bilayer with PC:Chol:PE:PS:PIP_2 at molar ratios of 55:11:22:11:1. Image from Perez-Lara et al. (2016) *Elife.* e15886.

3.4 References

1. Jahn and Fasshauer. (2012). Molecular Machines governing exocytosis of synaptic vesicles. *Nature.* **490:** 201-207.
2. Sudhof and Rizo. (2011). Synaptic Vesicle Exocytosis. *Cold Spring Harb Perspect Biol 2011;3:a005637.*
3. Kee and Scheller. (1996). Localization of synaptotagmin-binding domains to syntaxin. *J Neurosci.* **16:** 1975-1981.
4. Kuo et al. (2011). Phosphatidylinositol 4,5-bisphospate alters synaptotagmin 1 membrane docking and drives opposing bilayer closer together. *Biochemistry.* **50:** 2633-2641.
5. Lai et al. (2011). Synaptotagmin 1 modulates lipid acyl chain order in lipid bilayers by demixing phoshatidylserine. *JBC.* **286:** 25291-25300.
6. Kuo et al. (2010). The calcium-dependent and calcium-independent membrane binding of synaptotagmin 1: 2 modes of C2B binding. *J Mol Bio.* **387:** 284-294.
7. Herrick et al. (2006). Positions of Synaptotagmin 1 and the membrane interface: cooperative interactions of tandem C2 domains. *Biochemistry*. **45:** 9668-9674.
8. Vrljic M, et al. Molecular mechanism of the synaptotagmin-SNARE interaction in Ca2+-triggered vesicle fusion. *Nature structural & molecular biology*. 2010; 17:325–331.
9. Zhang et al. (1998). Mechanism of phospholipid binding by the C2A domain of synaptotagmin 1. *Biochemistry.* **37:** 12395-403.
10. Morales et al. (2016). Cd2+ as a Ca2+ surrogate in protein-membrane interactions: isostructural but not isofunctional. *J AM Chem Soc.***135:** 12980-12983.
11. Herrick et al. (2009). Solution and Membrane-Bound Conformations of the Tandem C2A and C2B Domains of Synaptotagmin 1: Evidence of Bilayer Bridging. *J. Mol. Bio.* **390:** 913-9.
12. Rangaraju et al. (2014). Activity Driven local ATP synthesis is required for synaptic function. *Cell.* **156:** 825-835.
13. Lai et al. (2011). Synaptotagmin 1 modulates lipid acyl chain order in lipid bilayers by demixing phoshatidylserine. *JBC.* **286:** 25291-25300.
14. Laing et al. (2013). Prefusion structure for syntaxin-1a suggests pathway for folding into neuronal trans-SNARE complex intermediate. *PNAS.* **10:** 19384-19389.
15. Guillen et al. (2013). Structural insights into the ca2+ and PI(4,5)P2 binding modes of the C2 domains of rabphillin 3A and Synaptotagmin 1. *PNAS.* **110:** 20503-20508.
16. Honigann et al. (2012). Phosphatidylinositol 4,5-bisphosphate clusters act as molecular beacons for vesicle recruitment. *NSMB.* **20:** 679-686.
17. Li et al. (2009). Molecular Dynamics simulations of pip2 and pip3 in lipid bilayers determination of ring orientation and the effects of surface roughness on a Poisson-Boltzmann description. *Biophys J.* **97:** 155-163.
18. Wang et al. (2016). Synaptotagmin-1 C2B domain interacts simultaneously with SNAREs and membrane to promote membrane fusion. *eLife.*, eLife 2016;5:e14211.
19. Loewen et al. (2006). C2B polylysine motif of synaptotagmin facilitates a calcium independent stage of synaptic vesicle priming in vivo. *Mol biol. Cell.* **17:** 5211-5266.
20. Li et al. (2006). Phosphatidylinositol bisphosphates as co-activators of Ca2+ binding to C2 domains of Synaptotagmin 1. *JBC.* **281:** 15845-15852.
21. Van den Bogaart et al. (2012). Phosphatidylinositol 4,5-bisphosphate increases Ca2+ affinity of Synaptotagmin-1 by 40-fold. *JBC.* **287:** 16447-16453.

22. Radhakrishnan et al. (2009). The Ca2+ affinity of Synaptotagmin 1 is markedly increased by a specific interaction of its C2B domain with phosphatidylinositol 4,5-bisphosphate. *JBC.* **284:** 25749-25760.
23. Loewen et al. (2006). C2B polylysine motif of synaptotagmin facilitates a calcium independent stage of synaptic vesicle priming in vivo. *Mol biol. Cell.* **17:** 5211-5266.
24. Herrick et al. (2009). Solution and Membrane-Bound Conformations of the Tandem C2A and C2B Domains of Synaptotagmin 1: Evidence of Bilayer Bridging. *J. Mol. Bio.* **390:** 913-9.
25. Frazier et al. (2003). Membrane-Bound orientation and position of the Synaptotagmin C2A domain by site-directed spin labeling. *Biochemistry.* **42:** 96-105.
26. Frazier et al. (2005). Membrane-Bound orientation and position of the Synaptotagmin C2B domain by site-directed spin labeling. *Biochemistry.* **44:** 18-28.
27. Perez-Lara et al. (2016). PtdInsP_2 and PtdSer Cooperate to Trap Synaptotagmin-1 to the Plasma Membrane in the Presence of Calcium. *Elife*. e15886.
28. Hui et al. (2005). Three distince kinetic grouping of the Synaptotagmin family: candidate sensors for rapid and delayed exocytosis. *PNAS.* **102:** 5210-5214.
29. Wang et al. (2016). Synaptotagmin-1 C2B domain interacts simultaneously with SNAREs and membrane to promote membrane fusion. *eLife.*, eLife 2016;5:e14211.
30. Park et al. (2015). Synaptotagmin-1 Binds to PIP2 containing membrane but not to SNAREs at physiological ionic strength. *NSMB*. **22:** 815-823.
31. Park Y, et al. (2012). Controlling synaptotagmin activity by electrostatic screening. *Nat Struct Mol Biol.* **19:** 991–997.
32. Bacaj et al. (2013). Synaototagmin-1 and -7 Trigger Synchronous and Asynchronous Phases of Neurotransmitter release. *Neuron.* **80:** 947-959.

CHAPTER 4: Full Length Synaptotagmin-1 Purification protocol modulates the Aggregation State of the Reconstituted protein

4.1 Introduction

Syt1 is the calcium sensor in neuronal exocytosis. There has been extensive research examining potential mechanisms by which Syt1 accomplishes this process using soluble constructs of Syt1, including the individual C2 domains, C2A and C2B, as well as a tandem construct, C2AB. This work highlights Syt1 as the calcium trigger, which binds to charged membranes in a calcium dependent manner, potentially acting as a bridge and priming source for SNARE-dependent fusion [1-5]. However, the soluble domains often exclude the first ~100-136 residues of Syt1, and eliminate the transmembrane tether, the first site for potential interactions with the synaptic vesicle. The transmembrane region is itself attached to a juxtamembrane-linker region which connects to the C2 domains. This linker has a cysteine rich region shortly after the transmembrane helix, with the cysteine residues likely to be palmitoylated[6]. The linker also has two large, highly charged regions and a glycine zipper, but any stable secondary structure or fusion function for this region of Syt1 is unknown[6,7].

If Syt1 acts as a bilayer bridge or primes fusion, tethering it to one of the two membranes reduces the energy required to initiate any binding and triggering events. Tethering also primes the C2 domains, bringing them into closer proximity to each membrane.C2AB fragments have been

shown to act as suitable substitutes for triggering fusion in rescue experiments, but the full-length construct would better mimic in *vivo* conditions[8]. Functional measurements of *in vitro* fusion involving various fluorescent techniques have been performed on purified full-length Syt1 (FL SYT), but very little structural work has been performed to characterize this full-length construct[3,9-21].

When the full-length construct is used, it is often purified in N-octyl-β-D-glucopyaranoside (OG), a nonionic detergent[3,10-19]. Another zwitterionic, bean-like detergent, 3-[(3-cholamidopropyl) dimethylammonio]-1-propanesulfonate (CHAPs) is used rarely (*Figure 4.1*)[20,21]. However, CHAPs is often used in brain extractions of the full-length constructs of Syt1 and SNARE proteins[22,23].

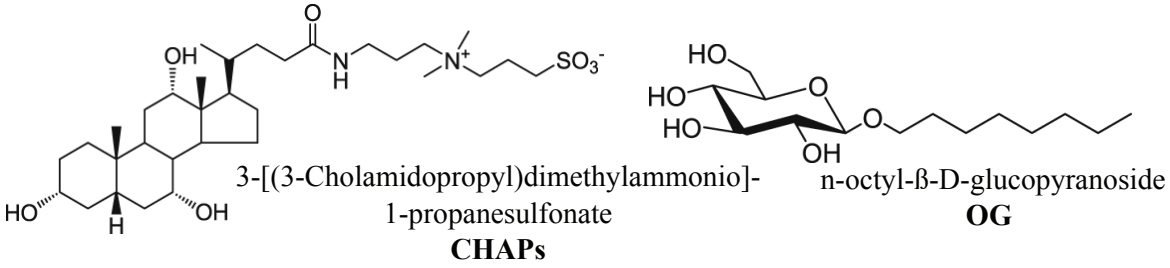

3-[(3-Cholamidopropyl)dimethylammonio]-1-propanesulfonate
CHAPs

n-octyl-ß-D-glucopyranoside
OG

Figure 4.1: Structures of CHAPs vs. OG. CHAPS is a larger zwitterionic, bean-like detergent. OG is neutral in charge. Images from Avanti Polar Lipids.

This work focuses on moving to more physiological experiments using the full-length version of Syt1. Initial purification and characterization of the two main purification schemes for FL SYT were examined using a series of CW EPR and pulsed-EPR measurements. Here, the full-length construct purified in either OG or CHAPs are compared to each other, and also to the soluble construct (as it has been shown to substitute for fusion). Differences in purification which result in different Syt1 protein states when reconstituted into membrane are then highlighted[24]. Due to the similarities between the CHAPs purification and the soluble construct, additional

characterization of the CHAPs procedure using CW EPR, power saturation EPR and TIRF will be shown in comparison to the soluble domains as the reason for choosing to proceed with the CHAPs protocol[24]. This work is published in *Protein Science* and titled, Choice of reconstitution protocol modulates the aggregation state of full-length membrane-reconstituted Synaptotagmin-1[24].

4.2 Results

Before examining structural data comparing the two FL SYT purifications the initial differences in the purification process should first be addressed (each protocol is detailed in the methods). Throughout the OG purification, Syt1 is unstable and actively precipitates over time due to small changes in ionic strength or temperature. The purification must be run in a cold room, with buffers kept at 4 °C to prevent precipitation, and flash frozen as quickly as possible. Even at 4 °C if protein yields are decent (for a membrane protein), FL SYT will eventually precipitate. Calcium slightly stabilizes the protein, as it does in the soluble constructs, but cannot prevent precipitation completely. It was also not possible to produce nucleotide-free protein, so an additional ion exchange step using cold buffers was added after affinity chromatography and before reconstitution[7]. However, the CHAPs purification produces a stable protein that (while it will eventually precipitate if it sits for an extended period at room temperature) can be purified at room temperature, in the absence of calcium, and tolerates the changes in ionic strength required for ion exchange chromatography. The CHAPs protein can also concentrate more easily but is yield limited.

Unexpectedly, once each preparation is reconstituted into lipid membranes the CW lineshapes of Syt1 linker and C2 domain mutants (90R1, 95R1, 173R1 and 304R1) in identical lipid mixes differ between each purification protocol. As EPR spectra are sensitive to the local structure around the labeled site as well as to changes in the environment, such as bilayer insertion, this would suggest a major change between the FL SYT proteins produced by the two methods.

4.2.1 FL SYT purified in OG yields different EPR spectra when compared to soluble C2AB

As shown in the previous chapter and the introduction, the calcium binding loops of the C2A and C2B domains (173R1 and 304R1 respectively) are known to insert into bilayers in the presence of calcium (sites shown in part A of *Figure 4.2*). This results in a broadening of the spectra as seen in part B of the figure, where soluble C2AB 173R1 and 304R1 in the presence of PC:PS vesicles transition from mobile aqueous loops in the absence of calcium (black) to broadened inserted loops in the presence of calcium (red). (*Figure 4.2*). Here, C2AB was purified as mentioned in the methods, briefly through solubilization of the membrane with triton x-100 and purification through a GST-tag and ion exchange chromatography.

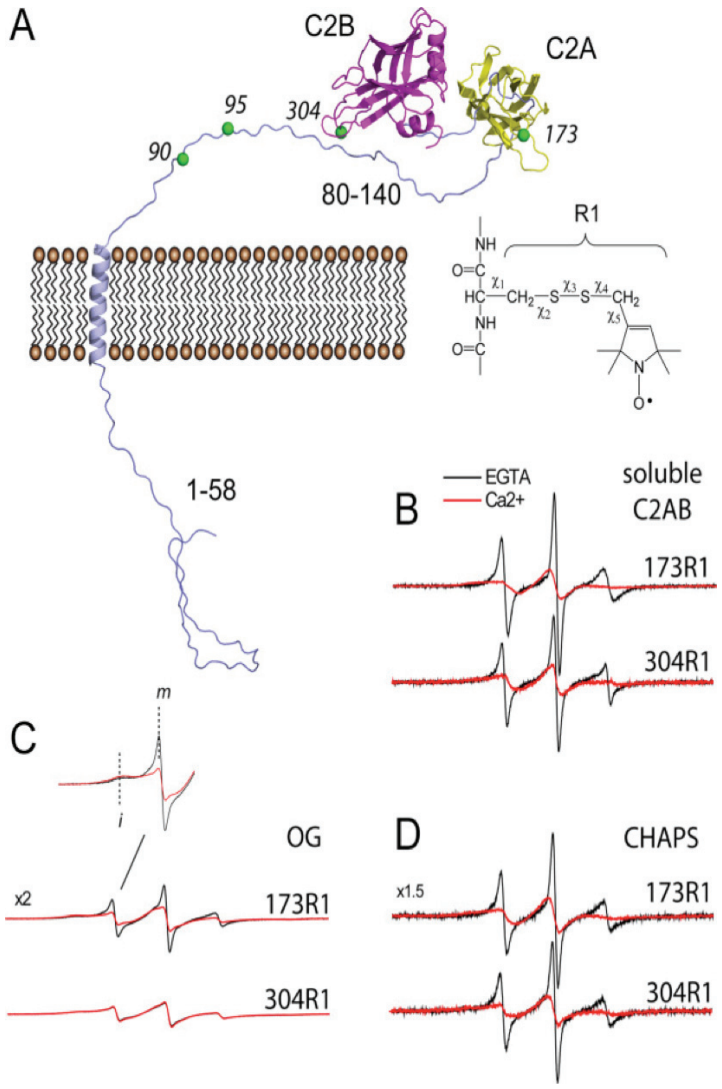

Figure 4.2: CW EPR Spectra comparing OG, CHAPS, and soluble proteins. A. A Full-length Syt1 model. Highlighting four sites labeled with the R1 nitroxide side chain: C2A (173), C2B (304) and two sites in the linker (90 and 95). B. Spectra from the soluble Syt1 C2AB construct, Syt1 (136–421), in the presence of 10 mM lipid vesicles composed of PC:PS at an 85:15 ratio C. Spectra from full-length Syt1 reconstituted into PC:PS (85:15) vesicles using Triton X-100 for solubilization and OG for reconstitution. D. Spectra from full-length Syt1 isolated using sodium cholate and reconstituted into PC:PS (85:15) using CHAPS. Red traces are spectra in the presence of 1 mM Ca^{2+}, and protein to lipid ratios in (C) and (D) are 1:200. The EPR spectra were recorded on samples where the total Syt1 concentration was approximately 50 μM. Image is from Nyenhuis and Cafiso. (2018). *Protein Science.* **27:** 1008-1012.

Moving to the full-length construct, purified in OG, reconstitution of 173R1 and 304R1 into PC:PS proteoliposomes is shown in part C of the figure (*Figure 4.2*). For the C2A domain of

FL SYT, EPR spectra are different than those obtained from the soluble construct. The spectrum preceding calcium addition is broadened and two motional components are apparent[24]. The more mobile component (*m*) resembles a lineshape expected for a label at an aqueous loop site and is comparable to C2AB, while the immobilized component (*i*) resembles a lineshape for a label that is membrane inserted or in tertiary contact[24]. Calcium addition produces a broadening of the spectra consistent with membrane insertion, but the changes in normalized amplitude are diminished compared to the spectra from the soluble C2AB construct[24]. For site 304R1 on the C2B domain, the spectra are broadened both with or without calcium addition and they do not undergo the transition seen using C2AB[24]. Thus, in the reconstituted system produced using OG, there is no evidence that the C2B domain moves from an aqueous to a membrane-inserted state[24].

Mutant Location	Depth	stdev	Distance (A)
FL SYT 173	1.0		8.0
C2AB 173	1.2	0.1	8.8
FL SYT 304	-0.54	0.05	3.5
C2AB 304	-0.39	0.2	4.3

Table 4.1: Representative Power Saturation comparing depths in the FL SYT vs. soluble C2AB in PC:PS. Shown above is a comparison of depth measurements between the full-length protein purified in CHAPS and the soluble construct. Depth measurements are similar indicating, calcium dependent insertion into membrane to a similar degree. Negative depths are positioned on the aqueous side of the membrane phosphate plane; positive values are positioned toward the hydrocarbon interior.

4.2.2 FL SYT purified in CHAPS yields similar EPR spectra when compared to soluble C2AB

One could initially argue that the difference in results observed for C2AB and FL SYT purified in OG could be due to the higher effective lipid concentration experienced by the C2 domains in the full-length protein. However, when FL SYT is purified and reconstituted using CHAPS, the CW lineshapes do not resemble the OG purification. Here, the EPR spectra obtained for 173R1 in the C2A domain and 304R1 in the C2B domain are virtually identical to those of the

soluble protein and show a clear indication of calcium-dependent insertion of the C2 domains, shown in part D of the figure (*Figure 4.2*)[24]. The slight differences in normalized amplitude between FL SYT from CHAPs and C2AB are likely due to a reduction in rotational correlation time for C2A and C2B in the tethered full-length protein[24]. Power saturation depth measurements within the CHAPs purified FL SYT also closely resemble those from the soluble constructs[24].

4.2.3 FL SYT is aggregated through the linker in the OG Preparation

Next, the juxtamembrane linker was compared between the FL SYT CHAPs and OG preparations. The juxtamembrane-linker on Syt1 has previously been reported to aggregate[7,23,25]. So, measurements at different locations on the linker were examined using EPR spectra and spin-spin dipolar coupling for two sites, 90 and 95, in the long juxta-membrane linker segment[24]. Unexpectedly, the EPR spectra from 90R1 and 95R1 are dramatically different when purified in CHAPs vs OG (*Figure 4.3*). In CHAPS, the linker yields lineshapes that are expected for a flexible protein segment, shown in blue in A and B of the figure (*Figure.4.3*). However, there is a distinct broadening of the spectra taken from the OG purification, indicating direct overlap of the R1 labels, which prevents observation of the expected characteristic flexible loop lineshape shown in red in A and B of the figure (*Figure.4.3*). This is clear evidence for spin-exchange, particularly for site 90R1. Spin-exchange results from collisions between labels and produces an obvious broadened lineshape and sloping intensities within the EPR spectrum from 90R1[26]. This broadening persists when reconstituted into different membrane compositions (PC, PC:Chol, PC:PS with and without Ca^{2+}) (*Figure 4.3.2*). The broadening persists even if the protein to lipid ratio is diluted from 1:200 to 1:1000 (*Figure 4.4*).

Next, DEER experiments were used to determine whether differences in dipolar coupling could be observed between the CHAPs and OG preparations for the single labeled mutants on the linker[24,27]. The OG and CHAPs preparations yield DEER traces that have dramatically different modulation depths (Δ) seen on the right of A and B in the figure (*Figure 4.3*). The modulation depth is a reflection of the number of spin pairs that are excited in the DEER experiment[24]. In this case it directly reflects differences in aggregation state[24,27]. For CHAPS, there is little or no modulation depth for the measurements (Δ was typically 2% or less); however, for samples prepared from OG, values of Δ were on the order of 7 to 10%[24]. Thus, the DEER data are consistent with the EPR spectra and indicate that there is a greater extent of aggregation when Syt1 is reconstituted using OG than CHAPS.

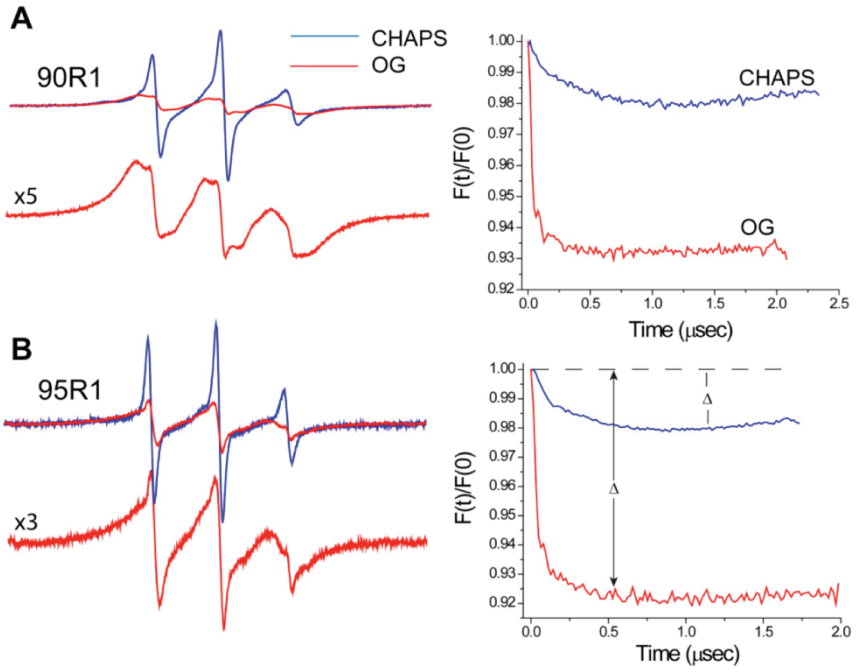

Figure 4.3: A comparison of CW EPR spectra and DEER traces from the juxta-membrane linker region. A. Left Site 90R1 and B. Left site 95R1. The corresponding background corrected DEER signals shown are on the right. Data are shown for reconstitution using CHAPS (blue spectra and DEER traces) and OG (red spectra and DEER traces). Because the spectra are broadened due to exchange interactions, the spectra from the OG preparation are expanded. The modulation depth, Δ, in the DEER data provides a relative measure of the oligomeric state of a protein. Image is from Nyenhuis and Cafiso. (2018). *Protein Science.* **27:** 1008-1012.

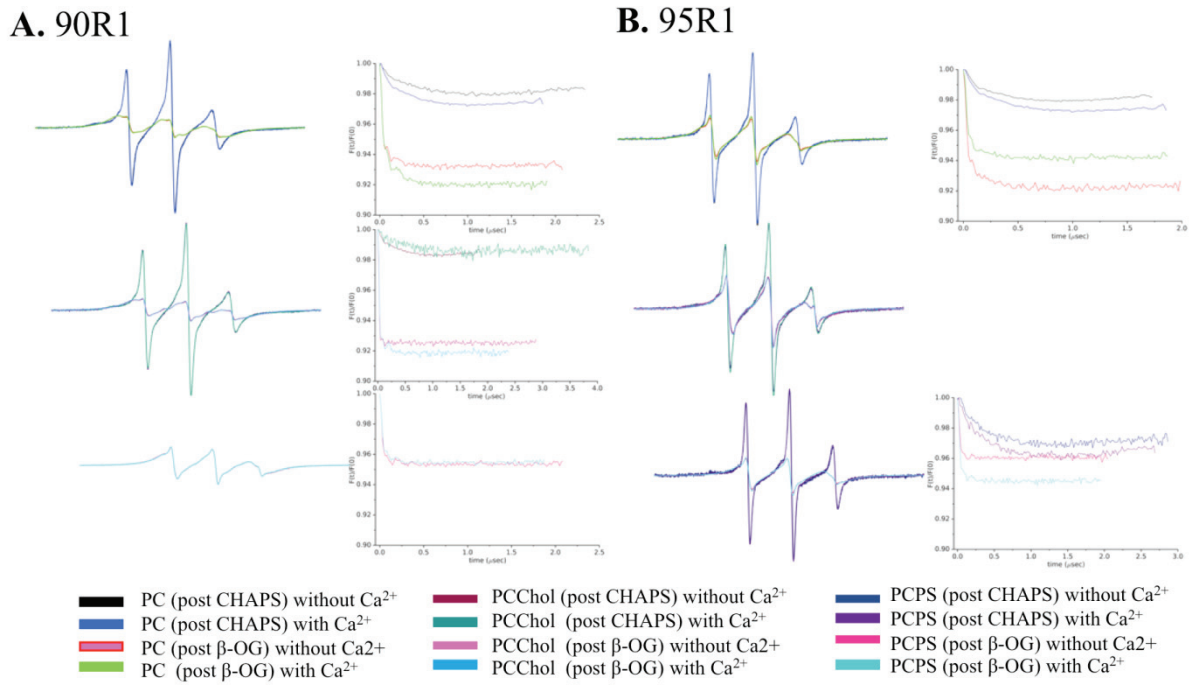

Figure 4.3.2: Additional CW EPR and DEER traces from the juxta-membrane linker region. A. Left 90R1 and B. Right 95R1. The corresponding background corrected DEER signals shown are on the right of each CW overlay. Data are shown first for reconstitution using CHAPS into PC without and with Calcium (Black and Blue spectra and DEER traces) and OG into PC without and with Calcium (Red and Green spectra and DEER traces). Second for reconstitution using CHAPS into PC:Chol without and with Calcium (Maroon and Teal spectra and DEER traces) and OG into PC:Chol without and with Calcium (Magenta and Skyblue spectra and DEER traces). Third for reconstitution using CHAPS into PCPS without and with Calcium (Navy and Purple spectra and DEER traces) and OG into PCPS without and with Calcium (Pink and Turquoise spectra and DEER traces). Each CW spectra is scaled to the same intensity to highlight exchange broadening. Like in Figure 4.3 Modulation depths in the DEER data provides a relative measure of the oligomeric state of a protein.

DEER experiments were also performed on single labeled sites in C2A and C2B and found that in both the OG and CHAPS preparations there was no evidence for self-association of the domains (*Figure 4.5*)[24]. These results and the juxtamembrane linker data suggest that Syt1 is more strongly aggregated in the OG preparation and that this aggregation is likely mediated by association within the linker domain[24]. Aggregation in the linker likely accounts for the different lineshapes and behavior of the C2 domains in these two preparations[24]. Since the C2B domain in

the OG preparation is not oligomerizing itself, the likely explanation for the broadened lineshape of 304R1 is that this domain is interacting with the membrane interface in the absence of calcium. In previous work, the Cafiso lab examined the linker using EPR spectroscopy on FL SYT that was purified and reconstituted from OG[7]. This preparation was different than the current OG preparation since it excluded ion exchange, but the juxtamembrane linker was also aggregated to a greater extent than observed here for Syt1 prepared from CHAPS.

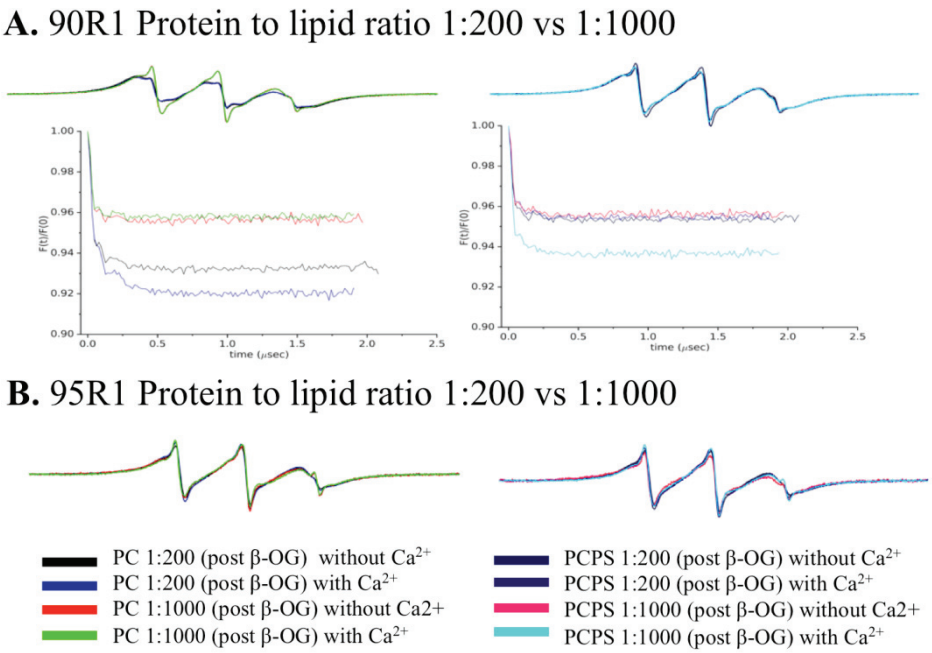

Figure 4.4: CW EPR and DEER traces from the linker region in lower protein to lipid ratios do not eliminate exchange broadening. A. Top 90R1 and B. Bottom 95R1. The corresponding background corrected DEER signals shown below of each CW overlay. Data are shown first OG reconstituted into PC without and with Calcium at a 1:200 protein to lipid ratio (Black and Blue spectra and DEER traces) then at a 1:1000 protein to lipid ratio (Red and Green spectra and DEER traces. Second for OG reconstituted into PCPS without and with Calcium at a 1:200 protein to lipid ratio (Navy and Purple spectra and DEER traces) and then into a 1:1000 protein to lipid ratio. (Pink and Turquoise spectra and DEER traces). Each CW spectra is scaled to the same intensity to highlight exchange broadening. Like in Figure 4.3 Modulation depths in the DEER data provides a relative measure of the oligomeric state of a protein.

4.2.4 Additional Characterization of FL SYT Purified in CHAPS

Due to the above observations, and particularly the similarity to the soluble constructs which are known to trigger fusion in functional assays, the CHAPs purification was selected for further work on FL SYT. From here, additional characterization of the construct was required to guarantee the effects observed within future experiments were not due to underlying issues with the FL SYT, itself.

Conveniently, the CHAPs purification behaves in a monomeric fashion, which is similar to the soluble constructs, and so any DEER experiments would be expected to reflect interaction due to conditions within the experiment and not from the protein's underlying tendency to aggregate (*Figure 4.5*).

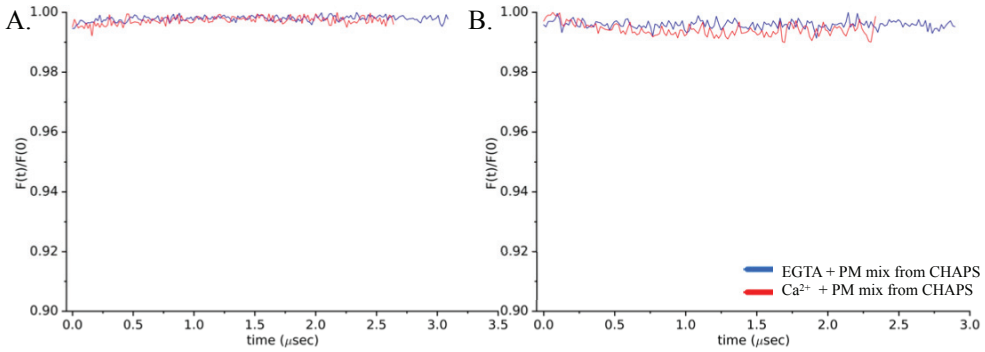

Figure 4.5: FL SYT 173R1 and 304R1 Purified in CHAPs does not aggregate the C2 domains. A. Left Site 173R1 and B. Right site 304R1. The corresponding background corrected DEER signals shown for a plasma membrane mix of lipids in EGTA (blue) or in calcium (red). The modulation depth in the DEER data provides a relative measure of the oligomeric state of a protein.

Next, looking into lineshape behavior, CW spectra were taken of each C2 domain in CHAPs before lipid reconstitution (*Figure 4.6*). The lineshape is very similar to the aqueous CW lineshape of the C2AB construct (in the OG prep, the labels are restricted even before reconstitution). Calcium was also added to the CHAPs protein, to check evidence for calcium dependent insertion into detergent. The CW lineshapes for both the C2A and C2B domains do not change significantly upon addition of calcium indicating it likely does not insert into the detergent, small changes seen in C2A, 173R1 could be due to coordination of the calcium to the calcium binding loops.

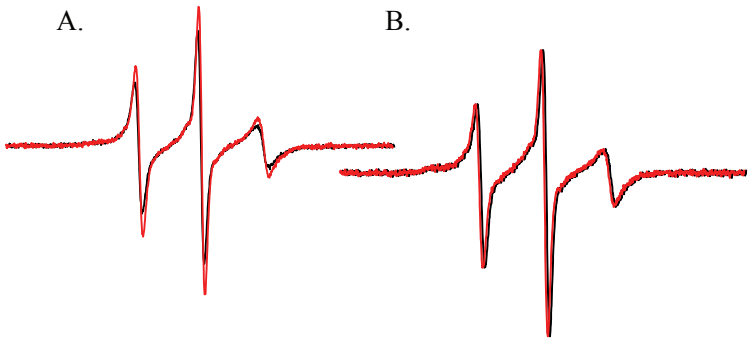

Figure 4.6: FL SYT 173R1 and 304R1 Purified in CHAPs shows no evidence of insertion into CHAPs upon addition of Calcium. A. FL SYT 173R1 in CHAPS, preceding reconstitution, without calcium in red and with calcium in black. Slight lineshape changes are likely due to calcium coordination. B. FL SYT 304R1 in CHAPS, preceding reconstitution, without calcium in red and with calcium in black.

The protein was then reconstituted into varying lipid conditions (PC:PS, PC:PS:PIP_2, PC:PIP_2, PC, PC:Chol, plasma membrane mix, etc.), Plasma membrane mix-in methods). First, a paramagnetic reducing agent, chromium (II) oxalate, was added to various lipid samples (in the absence of calcium) to look at the sidedness of FL SYT reconstitution within the proteoliposome bilayer (*Figure 4.7*). Chromium (II) oxalate is able to relax any spin probes it contacts in the aqueous phase, but it cannot penetrate a lipid bilayer to reach the inside of the proteoliposomes. Similar to probes for power saturation, broadening of the CW lineshapes is then observed if the

label comes into contact with the relaxing agent. The degree of broadening is then representative of the relative population of spins facing outward from the bilayer. Any remaining intensity in the CW spectra is then due to C2 domains facing the inside of the proteoliposomes. Measurements were made in the absence of calcium under different lipid conditions to ensure all probes were accessible, and not in contact with, or buried within the membrane (such as the polybasic face contact with PIP_2). Representative lineshapes from both 50 mM and 100 mM chromium (II) oxalate are shown to reduce the aqueous lineshape intensity for both C2 domains nearly to completion. This means that upon addition of calcium or other variables into solution, freeze-thaws are unnecessary for bilayer penetration, and that any changes in lineshape will be representative of changes occurring in the majority of proteins in the sample. Freeze-thawing was also attempted with the addition of calcium to charged lipid bilayers but this actually had a negative effect on the sample, leading to a free label population regardless of lipid conditions.

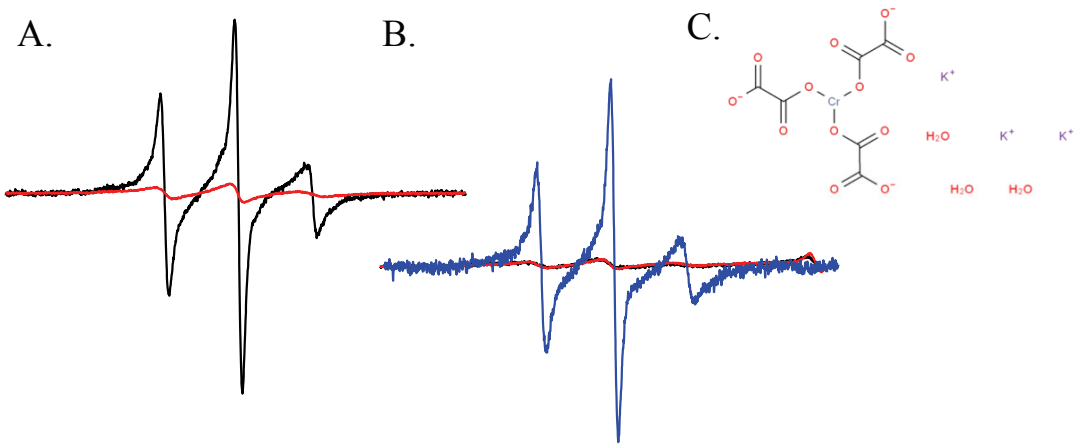

Figure 4.7: FL SYT 173R1 and 304R1 Purified in CHAPs is sided when reconstituted into Proteoliposomes. A. FL SYT 173R1 in Lipid and no Calcium (aqueous) in black and with addition of 50 mM Chromium (II) Oxalate B. FL SYT 173R1 in Lipid and no Calcium (aqueous) in blue and with addition of 50 mM Chromium (II) Oxalate (red) and 100 mM Chromium (II) Oxalate black. C. Structure of Chromium (II) Oxalate from Sigma. Chromium (II) oxalate is a broadening reagent, which relaxes spins that area accessible to reagent in the aqueous phase. It cannot penetrate the bilayer so any remaining spins from protein facing inward in the bilayer will not relax. The majority of the signal broadens for both the C2A and C2B domain under multiple types of lipid reconstructions, indicating a preference for the FL STY to face outward in the proteoliposomes.

Calcium dependent insertion into charged lipids was also examined in the CHAPs purification using PC and PC:Chol reconstitutions and measurements with CW EPR and power saturation (*Table 4.2, CWs are shown in chapter 6*). Previous lab members had demonstrated a calcium dependent membrane insertion in the OG purification without negatively lipid, which is not observed in the soluble construct. Calcium-dependent insertion is not observed in the CHAPs reconstitution, again agreeing with previous work with the soluble construct and verifying charge and coordination dependent insertion of the calcium binding loops. This led to the addition of charged lipid and the CW lineshapes for the CHAPs purification reconstituted into other lipid conditions, as represented above, are all very similar in lineshape and behavior to the soluble construct (performed in conditions such as: PC:PS, PC:PS:PIP_2, PC:PIP_2, PC).

Mutant Location	Depth	stdev	Distance (A)
FL SYT 173			
PC Ca	-1.9	0.05	Aqueous
PC no Ca	-2.0	0.1	Aqueous
PCChol Ca	-2.2	0.1	Aqueous
FL SYT 304			
PC Ca	-2.0	0.05	Aqueous
PC no Ca	-2.1	0.1	Aqueous
PCChol Ca	-2.2	0.05	Aqueous

Table 4.2: Power Saturation verifies that FL SYT membrane insertion is charge dependent. Shown above is a comparison of depth measurements between the full length protein purified in CHAPS reconstituted into uncharged, PC or PC:Chol bilayers. All measurements are aqueous, even after the addition of calcium, indicating, like the soluble protein, calcium binding loop insertion is charge dependent. Negative depths are positioned on the aqueous side of the membrane phosphate plane; positive values are positioned toward the hydrocarbon interior. Ca^{2+} addition is 1 mM. Aqueous measurements are 5 Å or further from the lipid phosphates.

Total internal reflection fluorescence (TIRF) experiments were performed to look into the functionality of the FL SYT construct purified in CHAPs. Previous work by Volker Kiessling in the Tamm lab using TIRF and fluorescence interference contrast microscopy (FLIC), with protein

purified from a previous lab member, Bin Lu, using the OG preparation suggested that in the full length construct the C2B domain was trapped on the tethered membrane (which agrees with CW lineshapes). Additionally, any activity in the form of membrane binding, observed through vesicle capture, was driven only through the C2A domain. This inhibitory role would be counter to expected behavior of the C2B domain seen in work with the soluble constructs (partially unpublished work)[7]. To examine the function of FL SYT purified in CHAPs, FL SYT and a ΔC2B construct were assayed using TIRF. Functional mutations deleting critical residues in the Ca^{2+} binding loops (D309A, D363A, D365A), polybasic face (K326AK327A), and arginine apex (R398QR399Q) of C2B were also created to examine the source of any potential C2B inhibition. if it was observed in the full-length CHAPs purification.

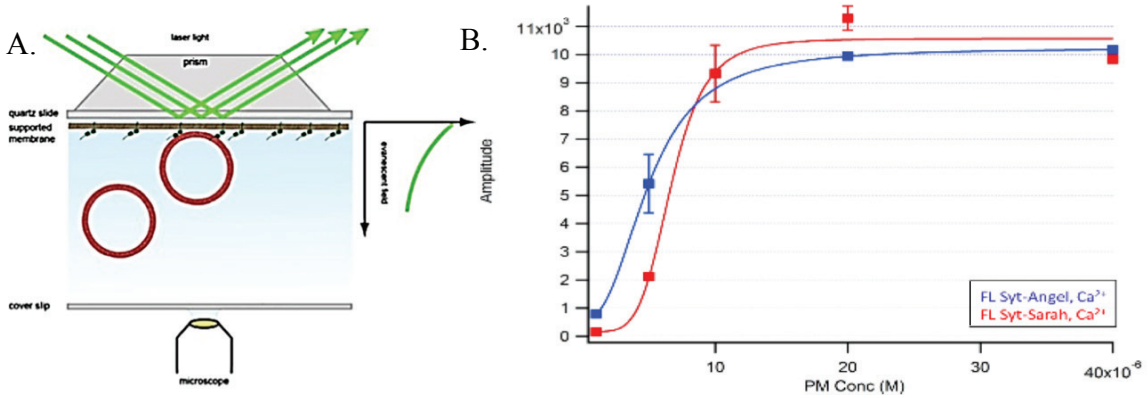

Figure 4.8: A comparison of function of FL SYT Purified in CHAPs between collaborators A. A graphic representation of TIRF, vesicle capture assay from Lu. B. Journal of Biological Chemistry. **289:** 22161-22171. 2014. Vesicles are observed only within in the evanescent field. B. FL SYT rates of vesicle capture of protein purified by Angel Perez-Lara in Jahn lab (blue) and in Cafiso lab (red) are within error. FL SYT within a supported bilayer of PC:Chol (80:20), vesicles mimicking the plasma membrane binding- a plasma membrane mix (32%PC:30% PE:15% PS:3% PIP_2:20% Chol:1% Rhod) were titrated in at varying concentrations. 100 μM calcium was present at all times.

Initially, the TIRF experiments focused on comparing the Cafiso lab CHAPS purified FL SYT to that produced by Angel in the Jahn lab. This followed from the previously mentioned result

that Bin Lu's OG purified protein did not have identical activity to Angel's. Both CHAPs preparations yield identical activity within error (*Figure 4.8*). Preliminary, TIRF measurements were then taken in different supported bilayer compositions to examine differences in activity of FL SYT and ΔC2B.

These measurements, detailed in the methods section, are titrations of liposomes with lipid compositions that mimic the plasma membrane surface. This liposome composition includes: 32% PC: 30% PE: 15% PS: 3% PIP2: 20% Chol: 1% rhodamine DPPE. The rhodamine is detectable within an evanescent field created by a 514 nm laser which is totally internally reflected at an angle of 72° from the surface normal. This results in an evanescent wave which decays exponentially with a characteristic penetration depth of ~100 nm and is detected by a camera with shutters controlled by Volker's in-house LabVIEW program[28]. These liposomes approach and bind to FL SYT which is tethered to a supported bilayer (mimicking the synaptic vesicle in the system). Liposomes are titrated in, with or without calcium to look at calcium-dependent and -independent binding. Samples were measured in 80% PC: 20% cholesterol and a more physiological: 35% PC: 20% Chol: 30% PE: 15% PS mixture (*Figures 4.9 and 4.9.2*). Upon saturation of each lipid titration point, the curve is fit exponentially then plotted as amplitude vs. concentration of PM lipid. These plots are fit to the Hill equation, but the shape and amplitude of the curves varies depending on the age of the prep and differences in sample preparation. Only curves acquired on the same day are equivalent without normalization. Protein free controls in supported bilayers with Ca^{2+} and EGTA have also been performed to guarantee the activity being observed is due to FL SYT function, and all controls are below the amplitudes observed when protein is present.

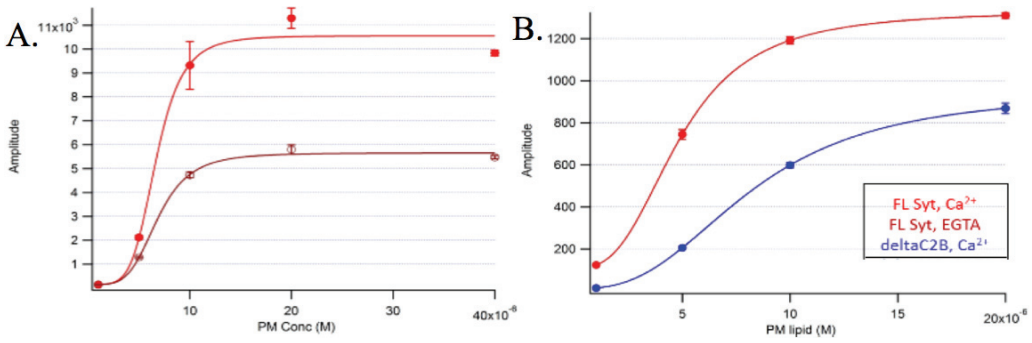

Figure 4.9: A comparison of function of FL SYT and ΔC2B Purified in CHAPs. A. FL SYT in Ca^{2+} (red) and EGTA (maroon) demonstrates a slight rate of vesicle capture before the addition of calcium, likely docking from the polybasic face then an increased rate of calcium dependent capture. B: FL Syt (red) and ΔC2B (blue) in the presence of calcium, show a drop, but not complete loss of activity upon deletion of the C2B domain, indicating both the C2A and C2B domains display the ability to capture when placed in a PC:Chol supported bilayer (80:20), vesicles are a plasma membrane mix-to mimic plasma membrane binding-(32%PC:30% PE:15% PS:3% PIP_2:20% Chol:1% Rhod) and titrated in at varying concentrations. 100 uM calcium was present for calcium cases, and chelated out for the EGTA, calcium free case. Intensities within plots are comparable, however A and B intensities are not relative, as they were not performed on the same day. Error bars are error within fitting to the Eq.

In the CHAPs purification the inhibition due to the C2B domain is no longer observed and the protein functions through calcium-independent binding at a lower rate than calcium-dependent. Deletion of the C2B domain also shows that both the C2A and the C2B domain likely contribute to vesicle capture. This negated the immediate need for functional mutants of the C2B domain, but they will be useful for future experimentation. Preliminary unpublished FLIC results by Volker Kiessling also show that the C2B domain in CHAPs is not trapped on the supported bilayer. A more thorough investigation using FLIC will be compiled in the future (using mutants listed in the methods section). Future, more detailed functional work using TIRF and FLIC under varying lipid and ion conditions to more quantitatively characterize FL SYT function and develop a better model may still be performed, but the preliminary results presented here were sufficient to proceed with the work which follows in future chapters.

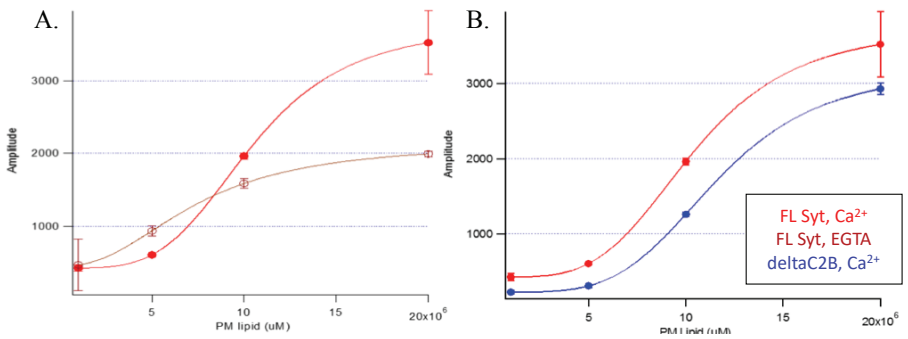

Figure 4.9.2: A comparison of function of FL SYT and ΔC2B Purified in CHAPs in a more physiological supported bilayer. A. FL SYT in Ca^{2+} (red) and EGTA (maroon) demonstrates a rate of vesicle capture before the addition of calcium, through docking from the polybasic face then an increased rate of calcium dependent capture, adding contribution from C2A and the calcium binding loops of C2B, here however calcium vs no calcium are more similar potentially indicating hinderance of C2A, potentially due to back-binding to the supported bilayer. B: FL Syt (red) and ΔC2B (blue) in the presence of calcium, show slight loss of activity upon deletion of the C2B domain, indicating both the C2A and C2B domains display the ability to capture when placed in a more physiological bilayer. The differences in capture again however are less significant (than 4.9) potentially due to additional charge interactions of the domains with the supported membrane. Supported bilayer mimicking the synaptic vesicle surface: 35% PC: 20% Chol, 30% PE, 15% PS. 100 uM calcium was present for calcium cases, and chelated out for the EGTA, calcium free case.

4.3 Discussion

4.3.1 Conclusions

To determine how Syt1 functions as the calcium sensor in neuronal exocytosis, experiments are performed that routinely incorporate Syt1 into systems including lipid bilayers and other components of the fusion machinery in order to reconstruct the *in vivo* fusion process[24]. Purifying and reconstituting the full-length Syt1 construct into these systems will better mimic *in* vivo fusion. Through CW EPR, power saturation, and DEER measurements it was demonstrated

that the detergent used to purify and reconstitute full-length Syt1 has a significant effect on the state of the protein in bilayers. When OG is used to reconstitute the protein, Syt1 is present in an aggregated state. This is mediated by the long juxtamembrane linker and alters the states and membrane binding of the tethered C2A and C2B domains relative to the soluble constructs. This is apparent particularly in the C2B domain, where EPR and FLIC data suggest C2B is tethered to the membrane and could not contribute to fusion. If this were the case there would be no priming by the polybasic face and no synergistic effects between lipids on the plasma membrane, such as PS and PIP_2, mentioned in the previous chapter. Here, any bilayer bridging would occur only through the C2A domain. In contrast, when purified and reconstituted using CHAPs, Syt1 is mostly monomeric and the EPR spectra from C2A and C2B resemble those of the soluble construct[24]. These results demonstrate that the choice of detergent used to purify and reconstitute Syt1 can modulate the state of the neuronal calcium-sensor[24].

At the present time, we do not know the degree to which differences in these reconstitution protocols modulate *in vitro* fusion assays, other than initial unpublished results using TIRF and FLIC. We also do not know whether Syt1 is monomeric or aggregated in the primed state at the focal site of fusion[24]. So, it is unknown which of these purifications better represents a native state[24]. However, it is easy to imagine that overexpression of Syt1 in *E. coli* produces locally high concentrations of protein that are not encountered in the native system, thereby facilitating aggregation[24]. Neutral detergents such as OG are also potentially not as efficient at solubilizing Syt1 as CHAPs[24]. Thus, when purified in OG the linker associates and the oligomer may become kinetically trapped during the membrane reconstitution procedure[24]. Here, similarities in function and response to environment and calcium were found between the soluble constructs and FL SYT purified in CHAPs. This agrees with previous work suggesting that CHAPS may produce the more

native-like state. In either case, structural studies are likely to be significantly affected by the procedure used to reconstitute Syt1.

Detergent choice has also been shown to be important in the reconstitution of other components of the fusion system. The choice of detergent was shown to alter the structure of syntaxin and SNAP25 in the acceptor complex, producing a sought after 1:1 complex, rather than the 2:1 complex, which have dramatic effects on the rate of SNARE assembly and membrane fusion[24,29]. Also, when reconstituting syntaxin with munc18, OG actually dissociates the complex[30].

Another interesting observation from this work (mentioned in more detail in Chapter 6), addresses the proposed mechanism that Syt1 functions as a washer or forms rings in the absence of calcium to prevent fusion then dissociates in the presence of calcium to permit fusion (detailed in the introduction)[31-34]. Looking at the model for how the C2B domain assembles into these rings, which involves interactions with PIP_2 on the plasma membrane with protein to protein links somewhere around the top and bottom of each C2B domain, distances on the order of ~40 Å should have been apparent in the C2B domain DEER data. The absence of any significant distance component around 4 nm and the absence of any calcium effect in the DEER traces indicates that these rings are not efficiently forming (at any detectable populations) in the reconstituted preparations (CHAPs is shown in *Figure 4.5*) of full-length[24]. While the DEER taken previously in the OG purification also showed no detectable indication of ring formation, it is appealing to think that aggregation through the linker could mediate ring formation. However, if the C2B domain is already trapped on the synaptic vesicle surface and insensitive to calcium activation, forming rings on the plasma membrane which dissociate in the presence of calcium is unlikely.

Overall, the results presented here provide clear evidence that the state of Syt1 is strongly influenced by the purification and reconstitution procedure employed[24]. Thus, caution should be used when reconstituting Syt1 and other components of the fusion system as the choice of detergent can modulate the membrane state of these proteins[24].

4.3.2 Future Directions

Briefly, an interesting set of experiments for future investigation of the full-length construct would be a more detailed quantification of the kinetics and initial rates of vesicle capture and other functional assays which mimic fusion. These can isolate effects based on different lipid compositions to observe changes in synergy between PS and PIP_2, calcium affinity, and membrane affinity in the presence of more physiological conditions, including the addition of ATP/Mg^{2+} which has been highlighted to hinder membrane binding[5,35,36]. The addition of SNARE complexes within the mix would also give further insight into Syt1 function. Here, the previously mentioned functional mutants, could be used to probe and localize any effects of varying lipid, ion, and protein compositions at regions already proposed to aid in calcium triggering.

4.4 References

1. Jahn and Fasshauer. (2012). Molecular Machines governing exocytosis of synaptic vesicles. *Nature.* **490:** 201-207.
2. Sudhof and Rizo. (2011). Synaptic Vesicle Exocytosis. *Cold Spring Harb Perspect Biol 2011;3:a005637.*
3. Kee and Scheller. (1996). Localization of synaptotagmin-binding domains to syntaxin. *J Neurosci.* **16:** 1975-1981.
4. Kuo et al. (2011). Phosphatidylinositol 4,5-bisphospate alters synaptotagmin 1 membrane docking and drives opposing bilayer closer together. *Biochemistry.* **50:** 2633-2641.
5. Perez-Lara et al. (2016) $PtdInsP_2$ and PtdSer Cooperate to Trap Synaptotagmin-1 to the Plasma Membrane in the Presence of Calcium, *Elife*. e15886.
6. Vrljic et al. (2011). Post translational modifications and lipid binding profile of insect cell expressed full length mammalian synaptotagmin 1. *Biochem.* **50:** 9998-10012.
7. Lu et al. (2014). The Juxtamembrane linker of full length synaptotagmin 1 controls oligomerization and calcium dependent membrane binding. *JBC.* **32:** 22161-22171.
8. Lynch et al (2007). Synaptotagmin C2A loop 2 mediated calcium-dependent snare interactions essential for ca2+-triggered vesicle exocytosis. *Mol Biol Cell.* **18:** 4957-4968.
9. Bai et al. (2000). Membrane-embedded Synaptotagmin penetrates cis or trans target membranes and clusters via novel mechanism. *JBC.* **275:** 25427-25435.
10. Lai et al. (2013). Fusion pore formation and expansion induced by a ca2+ and synaptotagmin1. *PNAS*. **110:** 1333-1338. (Ying Lai, 1333–1338, doi: 10.1073/pnas.1218818110.
11. Lou et al. (2015). Synaptotagmin-1 is an antagonist for Munc18-1 in SNARE zippering. *JBC*. **290:** 10535-10543.
12. Lee, et al. (2010). Dynamic Ca2+-dependent stimulation of vesicle fusion by membrane-anchored synaptotagmin 1. *Science*. **328:** 760–763. doi:10.1126/science.1187722.
13. Bai, J., Tucker, W.C. & Chapman, E.R. (2004). PIP2 increases the speed of response of synaptotagmin and steers its membrane-penetration activity toward the plasma membrane. *Nat. Struct. Mol. Biol*. **11**, 36–44.
14. Wang et al. (2011). Reconstituted Synaptotagmin 1 mediates vesicle docking, priming, and fusion. *JBC*. **195:** 115-9.
15. Gaffaney at al. (2008). Synaptotagmin C2B domain regulates Ca2+ triggered fusion in vitro. *JBC*. **283:** 31763-31775. 2008.
16. Diao et al. (2013). Complexin-1 Enhances the on-rate of vesicle docking via simultaneous SNARE and membrane interactions. *JACS*. **135:** 15274-15277.
17. Kyoung et al. (2011). In vitro system capable of differentiating fast Ca2+-triggered content mixing from lipid exchange for mechanistic studies of neurotransmitter release. *PNAS*. **108:** E304-E313.
18. Mahal, L.K., Sequeira, S.M., Gureasko, J.M. & Sollner, T.H.Calcium-independent stimulation of membrane fusion and SNAREpin formation by synaptotagmin I. *J. Cell Biol*. **158**, 273–282 (2002).
19. Stein, A. Radhakrishnan, D. Riedel, D. Fasshauer, R. Jahn. (2007). Synaptotagmin activates membrane fusion through a Ca2+-dependent trans interaction with phospholipids. *Nat. Struct. Mol. Biol.* 14:904–911. doi:10.1038/nsmb1305.

20. Jung et al. (2007). Molecular basis of synaptic vesicle cargo recognition by the endocytic sorting adaptor stoning 1. *JBC.* **179:** 1497-1510.
21. Grass et al. (2004). Recognition of a basic AP-2 binding motif within the c2b domain is dependent on multimerization. *JBC.* **279:** 54872-54880.
22. Baldwin and Barbieri. (2009). Association of Botulinum neurotoxin with synaptic vesicle protein complexes. *Toxicon.* **54:** 570-574.
23. Brose et al. (1992) Synaptotagmin: a calcium sensor on the synaptic vesicle surface. *Science* **256:** 1021-1025.
24. Nyenhuis and Cafiso. (2018). Choice of reconstitution protocol modulates the aggregation state of full-length membrane-reconstituted Synaptotagmin-1. *Protein Science.* **27:** 1008-1012.
25. Bai et al (2000) Membrane-embedded synaptotagmin penetrates cis or trans target membranes and clusters via a novel mechanism. *J Biol Chem.* **275:** 25427-25435.
26. Sachse and Marsh. (1986) Line-intensities in spin-exchanged nitroxide electron-spin-resonance spectra. *J Magn Reson.* **68:** 540-543.
27. Jeschke. (2012). DEER distance measurements on proteins. *Ann Rev Phys Chem.* **63:** 419-446.
28. Domanska et al. (2009) Single vesicle millisecond fusion kinetics reveals number of SNARE complexes optimal for fast SNARE-mediated membrane fusion. J. Biol. Chem. **284**, 32158–32166.
29. Kreutzberger et al. (2016). Assembly and comparison of plasma membrane SNARE acceptor complexes. *Biophys J.* **110:**2147-2150.
30. Ma et al. (2013). Reconstitution of the vital functions of Munc18 and Munc13 in neurotransmitter release. *Science.* **339:** 421-425.
31. Wang et al. (2014). Calcium sensitive ring-like oligomers forms by synaptotagmin. *PNAS.* **11:** 13996-13971.
32. Zanetti et al. (2016). Ring-like oligomers of Synaptotagmins and related C2 domain proteins. *Elife.* 2016;5:e17262 doi: 10.7554/eLife.17262
33. Wang et al. (2017). Circular oligomerization is an intrinsic property of synaptotagmin. *Elife.* 2017;6:e27441 doi: 10.7554/eLife.27441
34. Rothman et al. (2017). Hypothesis – buttressed rings assemble, clamp, and release SNAREpins for synaptic transmission. *FEBSPress.* **591:** doi: 10.1002/1873-3468.12874.
35. Park et al. (2015). Synaptotagmin-1 Binds to PIP2 containing membrane but not to SNAREs at physiological ionic strength. *NSMB.* **22:** 815-823.
36. Park Y, et al. (2012). Controlling synaptotagmin activity by electrostatic screening. *Nat Struct Mol Biol.* **19:** 991–997

CHAPTER 5: Synaptotagmin-1 Membrane Binding, the Interplay between Coordination and Electrostatics

5.1 Introduction

Syt1 is a calcium binding protein, which interacts with the lipid membrane through calcium dependent insertion of the calcium binding loops[1-4]. Syt1 is one of the many Synaptotagmins that binds to calcium. Syt1 binds to calcium through the calcium binding loops located in its tandemC2 domains, named after the homologous C2 domain in protein kinase C[5]. A C2 domain is typically composed of eight antiparallel beta-sheets attached by flexible loops length-wise[6-7]. If they are capable of calcium binding, one side of the domain contains the calcium binding loops, and the opposite side of the domain has a set of conserved helices[6-8].

Upon calcium influx, the Syt1 C2A domain binds to three calcium ions, while the C2B domain binds two[3]. These ions are coordinated mainly through the longer first and third loops of each domain. In solution the calcium affinity of each domain is low; the soluble C2A domain binds to each of the three sites at roughly 54-75 μM, 530 μM and 20 mM, respectively, and the C2B binds at 300-400 and 500-600 μM at its two binding sites (coordination geometries can be seen in *Figure 1.12* of the introduction)[9-11]. Once calcium is bound the calcium binding loops insert into charged lipid membranes to trigger fusion. In proximity to charged lipid membranes these affinities increase 100-10,000-fold, reaching 1-20 μM calcium[6].

The binding loops in the Syt1 C2A and C2B domains are known to preferentially bind to PS in the presence of calcium[12]. This binding is thought to be driven through PS coordination within the open coordination spheres of the calcium bound domains[12]. The interactions between the calcium binding loops could also, however, be driven through (or in part) by electrostatics, as the loops become positively charged when they coordinate calcium and PS is negatively charged[13]. The favorable insertion energy for placing hydrophobic residues into the hydrophobic layer of the bilayer also likely assists in membrane insertion. This is driven in part by tryptophan residues snorkeling at the bilayer interface[14,15]. These interactions are the underlying principles of the majority of mechanisms proposed for Syt1 function, however the exact contributions between them are not well understood.

Work has been performed out of the Igumenova lab on the C2α domain of protein kinase C, which reveals that C2 domains are capable of coordinating different divalent cations, such as lead (Pb^{2+}), copper (Cu^{2+}), or cadmium (Cd^{2+})[11,16,17]. Investigations of these metal ions compared to calcium using: HSQC NMR, ITC, crystallization, binding assays, and FRET have revealed that the C2α domain can incorporate these metals into the calcium binding loops, but the number of ions and coordination geometries of each metal impacts the loop structure (*Figure 5.1*)[11,16,17]. The binding affinity of each metal is also variable, which could lead to competition between cations. Lead binds two ions to the calcium binding loops at roughly 67 nM and 129 μM, respectively[16]. Cadmium binds at ~300 μM and ~4 mM Cd^{2+} which is a greater than 30-fold increase in affinity relative to calcium binding[11]. Each of these metals binds with higher affinity than calcium, can form mixed metal complexes in the loops, and at high enough concentrations cannot compete calcium for binding to the calcium binding loops[11,16,17]. This competition is concerning when binding to a protein that is calcium sensitive, as it would render the domains insensitive to calcium.

For Syt1 that would mean it could no longer fulfill its role as the calcium sensor and fusion trigger. This would imply, in part, why heavy metal toxicity impacts the nervous system so severely.

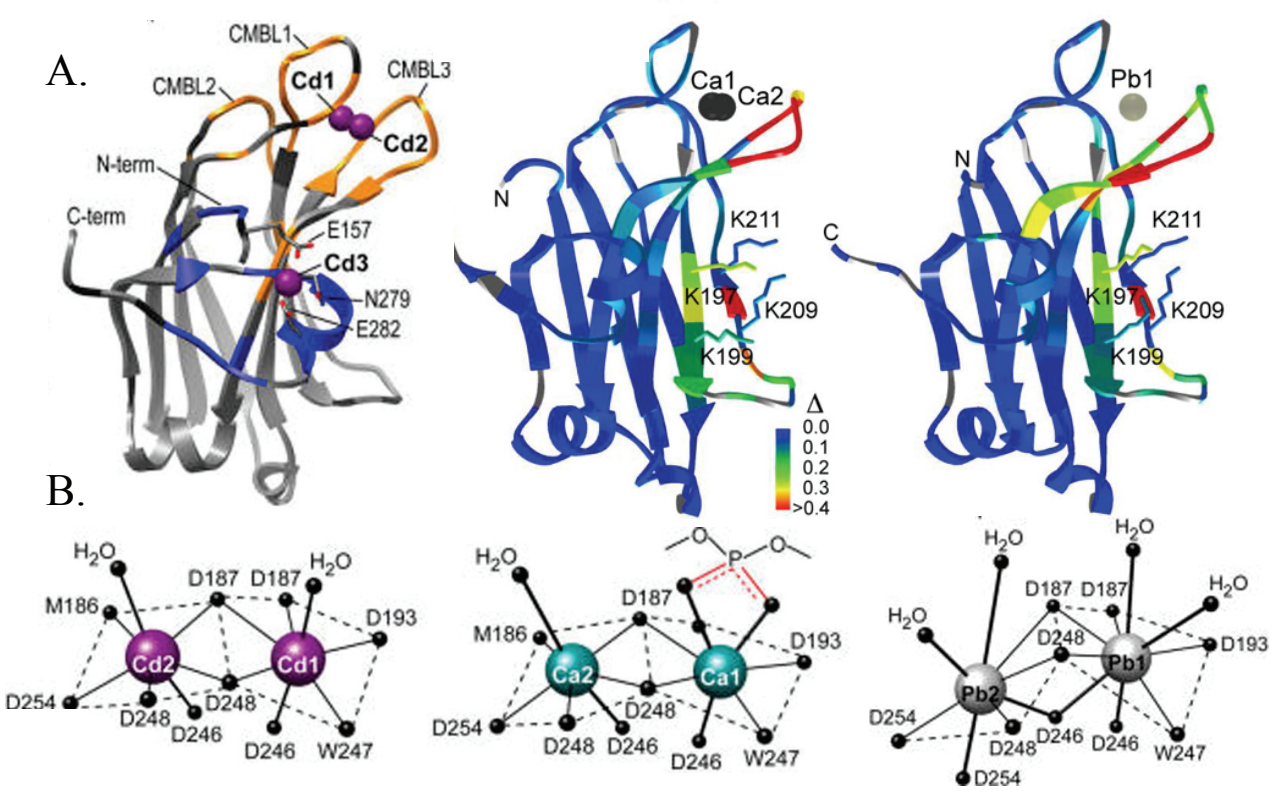

Figure 5.1: ^{15}N-^{1}H HSQC spectra and Coordination Geometry in C2α for Cd^{2+}, Ca^{2+}, and Pb^{2+}. A.^{15}N-^{1}H HSQC. B. Coordination geometry of metal ions does not correlate with their ability to mediate C2α-membrane association. Images collected from Morales and Igumenova. (2012). *Biochemistry.* **51:** 3349-3360. and Morales et al. (2016). *JACS.* **135:**12980-12983.

The next question to arise is, how do these metals function as surrogates in membrane binding? Through a combination of the same techniques, the Igumenova group was able to show that lead can actually compete with the C2α domain for binding sites to PS containing membranes, so at low concentrations of lead the lead-bound C2α domain can bind to membrane, but at high concentrations lead prevents C2α domain association[16]. Much like calcium affinities in the C2 domains of Syt1, in the presence of PIP_2, there is a synergistic enhancement of lead coordination and affinity to the domains and to the lipid membrane[11,17]. Cadmium, in contrast, can outcompete

calcium for coordination to the C2α binding loops, but it cannot associate with the membrane. This is potentially because it does not have room in the coordination sphere to accommodate PS[11]. The proposed mechanisms for the different metal interactions are then presented in the figure (*Figure 5.2*). This lack of coordination, however, could be advantageous for to determine the contributions from electrostatic interactions in the majority of mechanisms proposed for C2 domains, including Syt1 function.

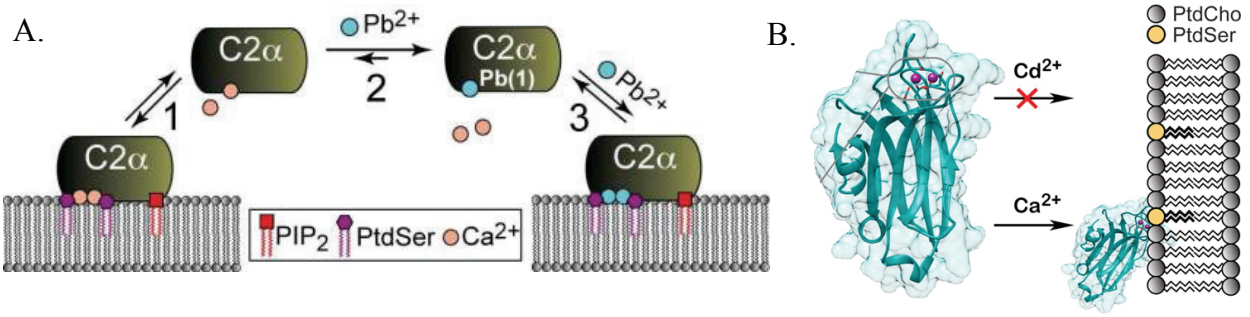

Figure 5.2: Competitive metal binding in C2α impacts the domains ability to bind to membrane. A. Pb^{2+} vs. Ca^{2+} compete through the interaction with the C2α high-affinity metal-binding site Both binding to membrane, Pb^{2+} irreversibly. B. Cd^{2+} vs. Ca^{2+} compete through the interaction with the C2α metal-binding site, but only the Ca^{2+} bound state binds to membrane. Images collected from Morales and Igumenova. (2012). *Biochemistry*. **51:** 3349-3360. and Morales et al. (2016). *JACS.* **135:**12980-12983.

This work focuses on the identifying these driving forces for membrane insertion with the expansion of work on full-length Syt1 (rather than soluble domains alone like C2α). The goal is to expand on previous work in only the soluble constructs of Syt1 and homologous C2 domains which could not fully differentiate the electrostatic and coordination-based interactions of the protein to the membrane[11,16-19]. In collaboration with the Igumenova lab (Biochemistry and Biophysics, Texas A&M University) this work highlights the use of a non-native metal ion, cadmium, in revealing the dual roles of coordination and electrostatics in Syt1 membrane interactions[13]. This is presented through a series of NMR, crystallography, sedimentation, and

fluorescence measurements performed in the Igumenova lab with a set of sedimentation assays, CW EPR, and power saturation EPR measurements performed by myself in the Cafiso lab[13]. This work is published in *Biochemistry* and titled, Non-native metal ion reveals the role of electrostatics in Synaptotagmin 1-membrane interactions[13].

5.2 Results

5.2.1 Structural Analysis and Affinities of Cadmium-Complexed C2A and C2B domains

Work out of the Igumenova lab first looked at the structure and coordination of cadmium to the C2A and C2B domains of Syt1. The first objective, which had been previously investigated in the C2α of protein kinase C, was to determine the cadmium binding sites within each C2 domain and the coordination geometry for these binding modes. Calcium ions bind to the calcium binding loops of the C2A and C2B domains through coordination with the side chains of aspartic acids in mono- and bidentate coordination modes[13]. From the crystal structures produced with cadmium bound, a single hepta-coordinated cadmium was observed in each domain with bidentate coordination to many of the side chains. The coordination geometry can be compared for both domains in the figure (*Figure 5.3, top*). The calcium binding loops of each domain are slightly altered to accommodate cadmium coordination, and particularly the third calcium binding loop, since the aspartate (232, and 365) residues which are coordinated in the presence of calcium do not coordinate to cadmium. Instead, a water molecule fills the seventh binding site for cadmium[13].

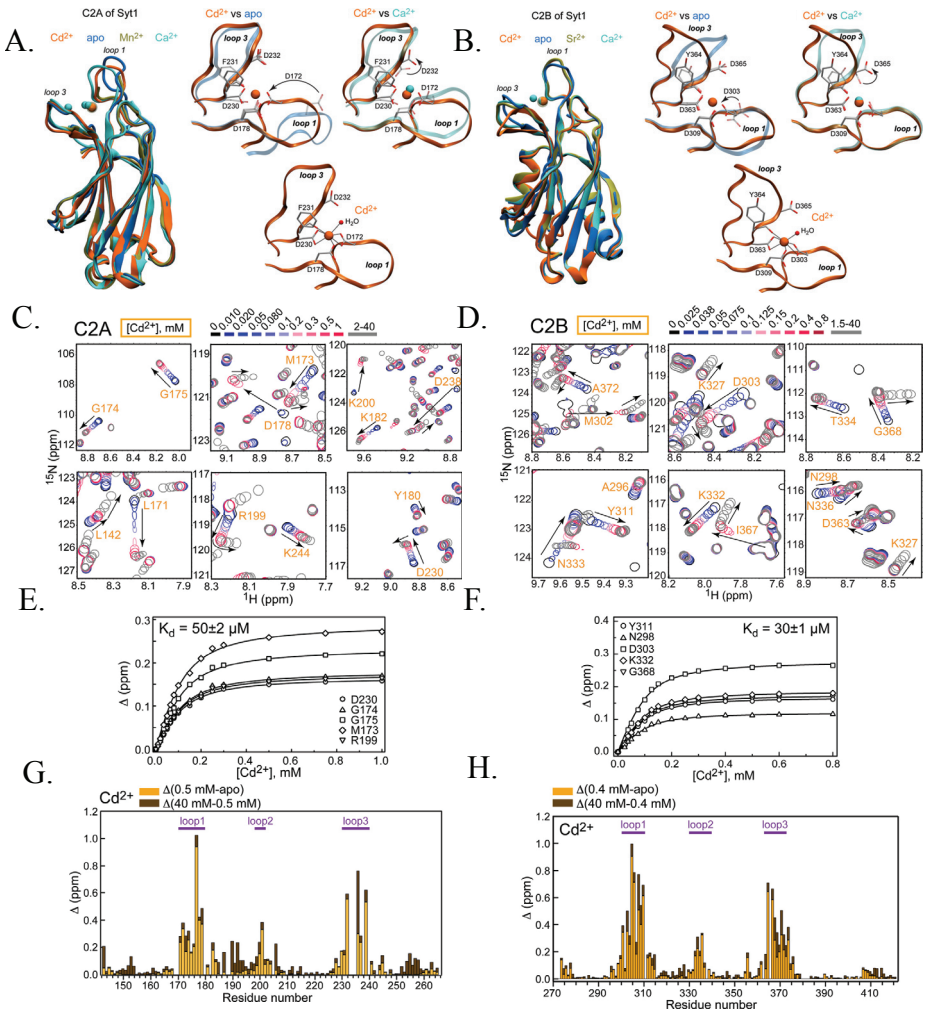

Figure 5.3: Structural analysis of Cd^{2+}-complexed C2A and C2B domains highlights Cd^{2+} binding to each domain in two populations of dramatically different affinities. Work performed in the Igumenova lab. A. crystallography, backbone superposition of four C2A structures: Cd^{2+}-complexed (orange), apo (blue), Ca^{2+}-complexed (cyan), and Mn^{2+}-complexed (tan). B. Backbone superposition of 4 C2B structures: Cd^{2+}-complexed (orange), apo mutant (blue), Ca^{2+}-complexed (cyan), and Sr^{2+}-complexed (tan). A and B. Top Right: Comparison of loop regions of Cd^{2+}-complexed with apo and Ca^{2+}-complexed highlights the differences between the loop conformations. Bottom Right: Coordination geometry of the Cd^{2+} site. Cd^{2+} has seven oxygens ligands in its first coordination sphere, six contributed by C2B and one by a water molecule. C and D: ^{15}N–^{1}H HSQC C2A spectra for the Cd^{2+} concentration range of 0-40 mM. C2A and C2B residues of the loop region respond to either one (e.g., C2A G175, Y180, K200, C2B Y311, K327, T334) or both (e.g., C2A L142, D178, R199, C2B M302, I367, G368) binding events. Peak displacement for the low and high concentration binding events is shown as a blue-red gradient and monochromatic gray, respectively. E and F. Representative NMR-detected binding curves constructed for the high-affinity Cd^{2+}sites(s). Solid lines represent the global fit of 14 residues for the high-affinity site with a K_d of 50 ± 2 μM or for C2B for 30 residues for the high-affinity site with a K_d of 30 ± 1 μM. G and H. Chemical shift perturbation plot for the low- and high-concentration regimes of Cd^{2+}. Image and caption modified from: Katti et al. (2017). *Biochemistry.* 56:3283-3295.

Next, the binding stoichiometry and affinity of cadmium relative to calcium were investigated using HSQC, NMR and FRET[13]. For NMR experiments, cadmium was titrated into solutions containing either the soluble C2A or C2B domains of Syt1 (100 μM protein) and binding was detected by chemical shift perturbation. The chemical shifts for each domain fell within fast or intermediate-fast exchange, so the binding kinetics for each site could be determined through fitting the chemical shift to a binding curve in order to quantify the binding affinity/dissociation constants (*Figure 5.3, bottom*). Both the C2A and C2B domains of Syt1 displayed two different cadmium binding events/sites, one which occurs at low concentrations (less than 1 mM) of cadmium and one which occurs at higher concentrations (1 to 40 mM) (sites are colored blue to red, or gray respectively in C and D of *Figure 5.3*).

For the C2A domain, the NMR was run in higher salt than for the previous experiments used to quantify the three bound calcium ions affinity to the calcium binding loops. This resulted in the dissociation of calcium increasing 4-5 times due to additional proton sheilding[13]. Even with the slightly different affinities for the calcium bound structure, however, there was a clear enhancement in affinity for cadmium binding to the calcium binding loops. For the low concentration binding event, a single-site binding curve was fit with a K_d of 50 ± 2 μM, which is 5 times higher affinity relative to calcium[13]. The high concentration binding site, however, could not be quantified due to its low affinity, but is probably higher than 10 mM. This would be at least 6 times lower than the second calcium binding event[13].

For the C2B domain, which was again examined at a higher salt concentration, the two bound calcium ions in the loop displayed slightly lower affinity, but the differences for cadmium binding were still clear. For the low cadmium binding event in the C2B domain, a high affinity site with K_d of 30 ± 1 μM was fit, which is over 20-fold higher affinity for cadmium over calcium[13].

The high cadmium binding event was again not fully quantifiable, but was estimated as a 50 mM dissociation constant, which is much weaker than the second calcium binding event[13].

FRET experiments between intrinsic tryptophan and luminescent terbium (an established assay to look at C2 domain binding), were then performed to compare cadmium binding affinities[13,20]. Using the C2A and C2B domains of Syt1 bound to terbium, both calcium and cadmium were individually titrated into solution with the goal of out competing terbium binding. This would decrease the detected FRET intensity and can ideally be fit to a binding curve. Both metals, when titrated into the C2 domains, displayed steady decreases in terbium luminescence that indicated displacement. Full displacement, defined as reaching the aqueous intensity of terbium, is marked as a dotted line in the figure (A and B *Figure 5.4*). For the C2A domain, FRET efficiency was low and could not quantify the binding affinities of the metals. Qualitatively, only cadmium was able to achieve full displacement of terbium. The calcium concentration to achieve half saturation/displacement of metal was also over eight times higher than cadmium, indicating a higher cadmium binding affinity in agreement with the NMR measurements[13]. For the C2B domain, the FRET efficiency was higher than that observed for the C2A domain (potentially due to the extra tryptophan in C2B), and curves could be fit to quantify metal affinity. For calcium the K_d was roughly 300-600 μM and for cadmium the K_d was 16.3 ± 1.2 μM (which is very close to the dissociation constant from NMR)[13]. These values again show that cadmium binds with higher affinity than calcium.

With these two data sets combined, the conclusion was reached that, like C2α of protein kinase C, each C2 domain in Syt1 binds to two cadmium ions[13]. One ion binds with much higher affinity than calcium, the other with lower affinity[13].

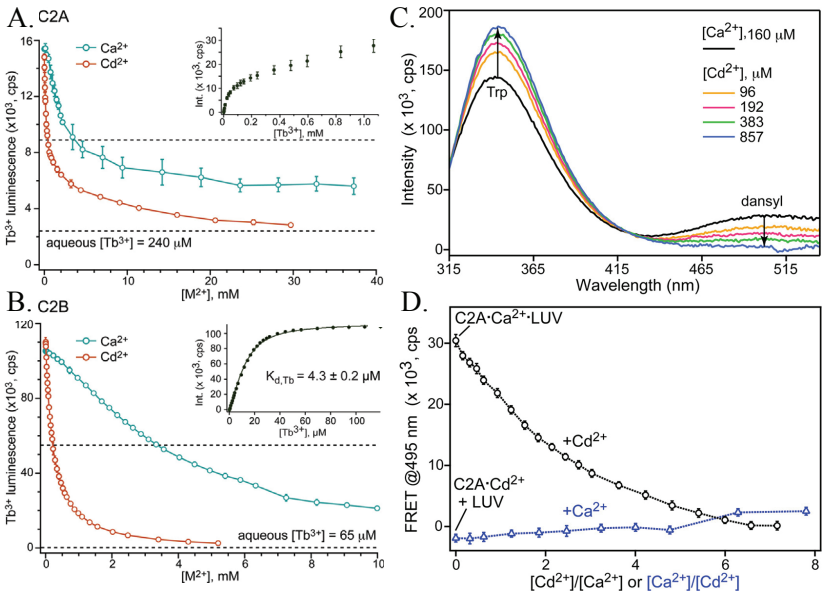

Figure 5.4: C2A and C2B domains of Syt1 bind Cd^{2+} with higher affinity than Ca^{2+} which results in dissociation from the membrane. Work performed in the Igumenova lab. A. Displacement of bound Tb^{3+} from C2A by Ca^{2+} and Cd^{2+}. C2A and Tb^{3+} concentrations are 15 and 240 µM, respectively. Inset: C2A-Tb^{3+} binding curve that has non-saturatable behavior due to comparable contributions of FRET and luminescence of free Tb^{3+} to the observed signal. B. Displacement of bound Tb^{3+} from C2B by $Ca^{2+}$and Cd^{2+}. C2B and Tb^{3+} concentrations are 15 and 65 µM, respectively. Inset: C2B–Tb^{3+} binding curve that shows saturatable behavior and produces $K_{d,Tb}$ of 4.3 ± 0.2 µM when fitted with a single-site binding model. C. Fluorescence emission spectra of C2A (0.5 µM) in the presence of LUVs (150 µM) and saturating [Ca^{2+}] (160 µM) collected at increasing [Cd^{2+}]. The intensity of the dansyl band decreases, with the concomitant increase of the intensity of the Trp emission band, indicating C2A displacement from the membrane. D. FRET-monitored competition experiments between Ca^{2+} and Cd^{2+} in the presence of LUVs. The intensity of dansyl emission band plotted as a function of Cd^{2+}/Ca^{2+} (black trace; [Ca^{2+}] = 160 µM) and Ca^{2+}/Cd^{2+} concentration ratios (blue trace; [Cd^{2+}] = 160 µM). While Cd^{2+} displaces Ca^{2+} from the protein and results in membrane dissociation, Ca^{2+} cannot displace Cd^{2+} from C2A and support membrane association. Image and caption modified from: Katti et al. (2017). *Biochemistry.* **56:**3283-3295.

The next question to address is, if cadmium binds to the calcium binding loops of the Syt1 C2 domains with higher affinity, can it displace calcium already bound to the loops. Also, can it form a mixed metal complex as in the C2α domain of protein kinase C? Again, this was examined using FRET between the intrinsic tryptophan and dansyl labeled lipid in LUVs (C and D in *Figure 5.4*). The C2A domain was first complexed with calcium, in solution. Next, charged liposomes

were added and binding was monitored by an increase in dansyl emission. Cadmium was then titrated into solution and a decrease of liposome binding was observed, demonstrating both that cadmium was binding to the C2A domain, outcompeting calcium, and that cadmium was unable to bind to membrane[13]. Next, starting from the cadmium complexed C2A domain with liposomes present but unbound in solution, calcium was titrated to excess (at values of at least 8-fold excess, from NMR estimates)[13]. Even in extreme excess of calcium, cadmium was not displaced from the C2A domain to restore membrane binding. A mixed metal bound C2A domain, however, may exist in solution, but would still be unable to bind membrane. Otherwise, the results indicate that cadmium decreases the affinity of the calcium binding sites, preventing formation of the mixed metal complex and thus membrane binding[13]. The loss in binding affinity to membrane also suggests that cadmium cannot act as a functional surrogate for calcium to mediate the interactions of Syt1 domains with anionic membranes. To investigate this observation in more depth, both the Igumenova and Cafiso labs first looked at the C2A and the C2B domains individually.

5.2.2 Isolated Cadmium-Complexed C2A does not Associate with PS-containing Membranes

To compare the ability of the C2A domain to bind to charged membrane when calcium-complexed and cadmium-complexed, FRET and co-sedimentation experiments from the Igumenova lab, as well as tryptophan emission-based sedimentation assays from the Cafiso lab were used to determine membrane binding affinities in the presence of either metal (*Figure 5.5*). FRET experiments were again performed between intrinsic tryptophans and dansyl-labeled liposomes (emission at 495 nm)[13]. Liposomes incorporated 15-20% PS to drive membrane binding. FRET measurements produced a binding curve, which when fit to the Hill equation displayed an *n*-value of 2.1 ± 0.1 μM suggesting two calcium ions were binding cooperatively to

the C2A domain and 24 ± 1 μM calcium was required for half maximal binding to liposomes[13]. Cadmium binding, however, was undetectable, as there was no increase in dansyl fluorescence, agreeing with previous measurements above (A in *Figure 5.5*). This was also seen in a FRET based co-sedimentation assay. Full membrane binding was seen for C2A in saturating calcium, but no membrane binding was observed for either 0.5 or 1 mM (B in *Figure 5.5*).

These measurements agreed with those made in the Cafiso lab, which examined the significance of electrostatics in driving membrane binding of the C2A domain. To examine if charge could screen membrane binding, sedimentation assays were performed using intrinsic tryptophan emission to measure the membrane affinity of C2A to and sucrose-loaded liposomes with 20% PS in high (300 mM) and low salt (100 mM) in the presence of calcium. (C in *Figure 5.5*). There was a significant (15-fold, 1,6 kcal/mol) decrease in binding under high salt conditions (*Table 5.1*). A positively charged lipid, DDAB (dimethyldioctadecylammonium (bromide salt)), was then added to sucrose-loaded liposomes at a 1:1 charge ratio relative to PS in order to neutralize charge on the membrane. In the presence of calcium and at physiological salt (150 mM), the C2A domain is unable to bind to the neutrally charged membrane, suggesting electrostatics contribute significantly to C2A membrane binding and not just coordination of the bound metal ion to PS. Measurements were then taken at physiological salt and PS charge in the presence of calcium and cadmium to investigate if cadmium could potentially drive membrane binding at high lipid concentrations (because cadmium binding produces a C2A domain that is more electropositive than calcium) (D in *Figure 5.5*)[13]. Cadmium was unable to promote membrane binding even in the presence of 10 mM lipid, suggesting that coordination must also contribute in some way to binding. Sedimentation assays were also performed in the absence of metal and in

the neutralized (DDAB-containing) membranes at physiological salt as controls to verify metal dependent binding and charge dependence at 15% PS.

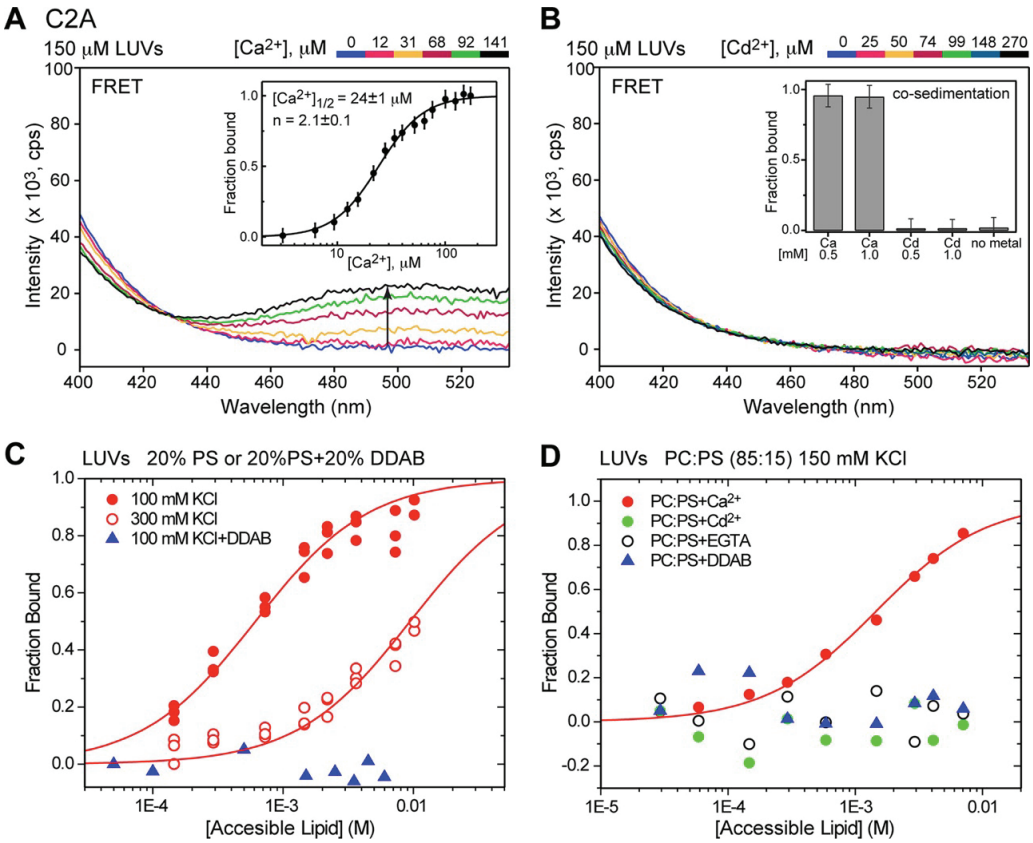

Figure 5.5: Cd^{2+}-complexed C2A domain does not associate with PS-containing LUVs. Top A and B, is work performed in the Igumenova lab. Bottom C and D is from Cafiso lab. A. Ca^{2+}-dependent fluorescence emission spectra showing an increase in the intensity of the dansyl band due to protein–membrane FRET. Inset: Ca^{2+}-dependent C2A lipid-binding curve constructed using FRET intensity at 495 nm. B. Cd^{2+}-dependent fluorescence emission spectra demonstrating that no increase in dansyl emission intensity in the C2A-LUV system is observed upon addition of Cd^{2+}. Inset: the results of vesicle sedimentation experiments that were conducted at 5 μM C2A and 1.5 mM total lipids. C. and D. C2A-lipid binding curves obtained using vesicle co-sedimentation experiments. The increase in ionic strength and neutralization of *the negative charge by DDAB significantly weakens the interaction between Ca^{2+}-complexed C2A and membranes in C. No binding of Cd^{2+}-complexed C2A to PS-containing vesicles is observed in D. In both C. and D. Ca^{2+} and Cd^{2+} are added to a concentration of 1 mM. Image and caption from: Katti et al. (2017). Biochemistry.* ***56:****3283-3295.*

Overall, these results demonstrated that cadmium may bind with higher affinity to the C2A domain in solution, but it cannot substitute as the driving force of membrane binding.

Domain		K (M^{-1})
C2A	15% PS, 150 mM KCl	810 ± 40
	20% PS, 100 mM KCl	1633 ± 113
	20% PG, 100 mM KCl	970 ± 60
	20% PS, 300 mM KCl	109 ± 3
C2B		
	15% PS, 150 mM KCl	7462 ± 950

Table 5.1: Reciprocal molar partition coefficients for the binding of Soluble C2A or C2B domains. Work performed in the Cafiso lab. Here, binding data obtained in the presence of Ca^{2+} for soluble C2A or C2B. No binding is detected with Cd^{2+}, and no binding is detected with charge-neutralized PS bilayers. Data are fit to the expression: $f_b = [L] / 1 + K[L]$, where f_b is the fraction of membrane bound domain and [L] is the concentration of accessible lipid. Table from the supplement of: Katti et al. (2017). *Biochemistry*. **56:**3283-3295.

5.2.3 Isolated Cadmium-Complexed C2B Neither Appreciably Associates with PS-containing membranes nor bridges LUVs

As with C2A, for the C2B domain a set of FRET, co-sedimentation, and dynamic light scattering experiments from the Igumenova lab were combined with sedimentation assays from the Cafiso lab to determine the membrane binding affinities for calcium and cadmium (Figure 5.6). Much like the C2A domain FRET between dansyl labeled liposomes with 15-20% PS and calcium bound C2B was observed, but cadmium bound C2B was undetectable by FRET (A in *Figure 5.6*)[13]. This also agreed with co-sedimentation measurements where liposome binding to C2B in the presence of calcium was high, but unobservable at both 0.5 and 1 mM cadmium[13]. Sedimentation assays out of the Cafiso lab confirmed the binding of C2B in calcium PS containing-liposomes in physiological salt (*Table 5.1*). Sedimentation assays showed an inhibition of binding

both when cadmium or neutralized membrane (DDAB) was present, again suggesting some kind of interplay between coordination and electrostatics.

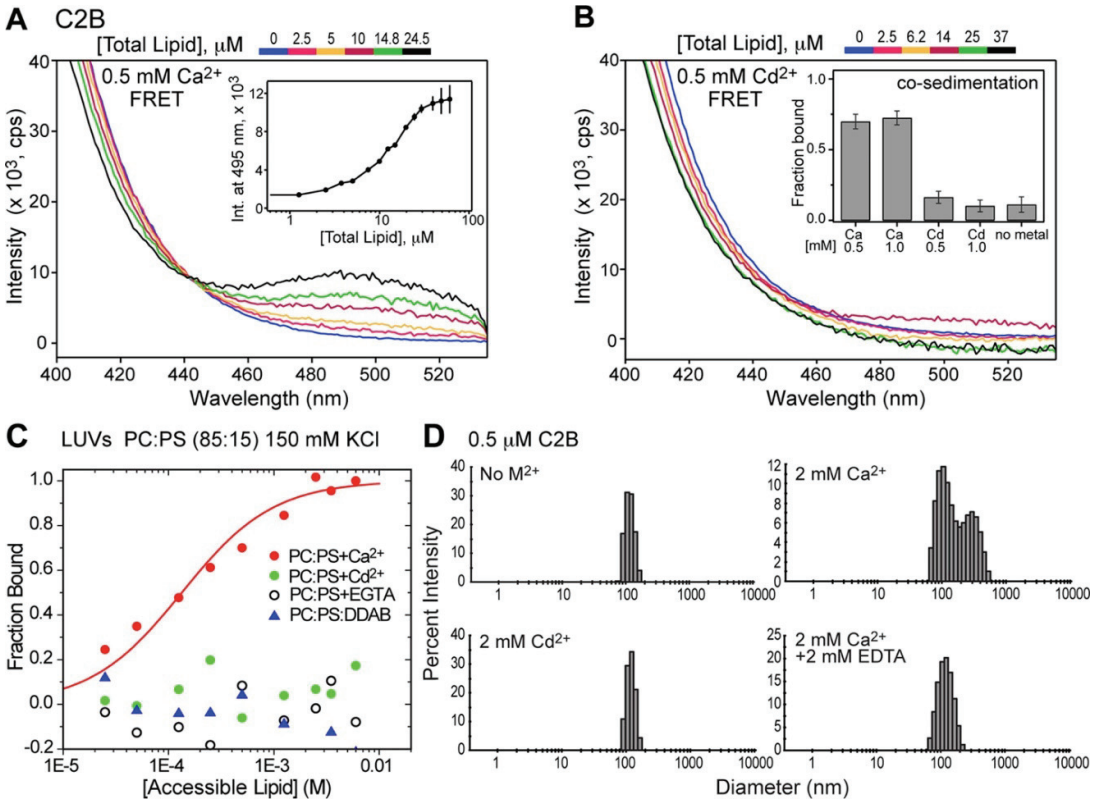

Figure 5.6: Cd^{2+}-complexed C2B domain does not appreciably associate with PS-containing LUVs. A, B and D, is work performed in the Igumenova lab. C is from Cafiso lab. A. PS-dependent fluorescence emission spectra showing an increase in the intensity of the dansyl band due to FRET between Ca^{2+}-complexed C2B and LUVs. Inset: PS-dependent C2B lipid binding curve constructed using FRET intensity at 495 nm. B. PS-dependent fluorescence emission spectra demonstrating that no significant increase in dansyl emission intensity in the Cd^{2+}-C2B system is observed upon addition of LUVs. Inset: the results of vesicle sedimentation experiments conducted at 5 μM C2B and 1.5 mM total lipids. C. C2B-lipid binding curves obtained using vesicle sedimentation experiments. The neutralization of the negative charge by DDAB abolishes the interactions between Ca^{2+}-complexed C2B and membranes. Ca^{2+} and Cd^{2+} are present at concentrations of 1 mM. D. Dynamic light scattering data show that while Ca^{2+}-complexed C2B can reversibly cluster 100 nm LUVs, the Cd^{2+}-complexed C2B cannot, due its inability to interact with the membranes through the loop regions. Image and caption from: Katti et al. (2017). *Biochemistry.* **56:**3283-3295.

The FRET experiments described above in the presence of calcium, showed light scattering effects due to calcium driven aggregation of liposomes. Thus, authors also examined the C2B

domains ability to bridge and aggregate bilayers (as mentioned in the introduction), using dynamic light scattering[13]. This aggregation again is likely driven through both sets of calcium binding loops in the C2AB fragment and in part through interaction with the arginine apex in C2AB and the C2B domain alone[13]. In the dynamic light scattering measurements, the size distribution of calcium bound C2B domains increased when bound to liposomes but failed to show an increase when the C2B domains were bound to cadmium. This indicated that the cadmium bound case prevented both membrane binding and any aggregation tendency.

Overall, this demonstrates that cadmium may bind with higher affinity to the C2B domain in solution, like the C2A domain results described above, but again it cannot substitute as the driving force for membrane binding.

5.2.4 C2AB Fragment and FL SYT Associated with membranes in the presence of Cadmium

Next, the Igumenova lab examined the C2A and C2B domains tethered in the soluble C2AB construct using FRET between intrinsic tryptophan(s) and dansyl-labeled 15-20% PS containing liposomes (*Figure 5.7*). The C2A and C2B domains have previously been observed to display a synergistic enhancement of membrane binding affinity when tethered, so the ability of cadmium binding to drive the tethered domains to the membrane was examined[21]. First, as expected calcium bound C2AB domains bound with high affinity to the liposomes, resulting in a large increase in FRET efficiency[13]. Next, cadmium bound C2AB produced an increase in FRET efficiency relative to the liposome free control, indicating some degree of membrane binding. However, in the C2AB fragment there is also some degree of calcium-independent binding driven through the polybasic face, which was observed in the metal free and metal-chelated controls. Cadmium bound C2AB binding to the membrane still produces a FRET efficiency slightly higher

than metal-independent binding, suggesting a very weak affinity contribution to insertion, but the majority of the signal is likely due to metal-independent effects[13].

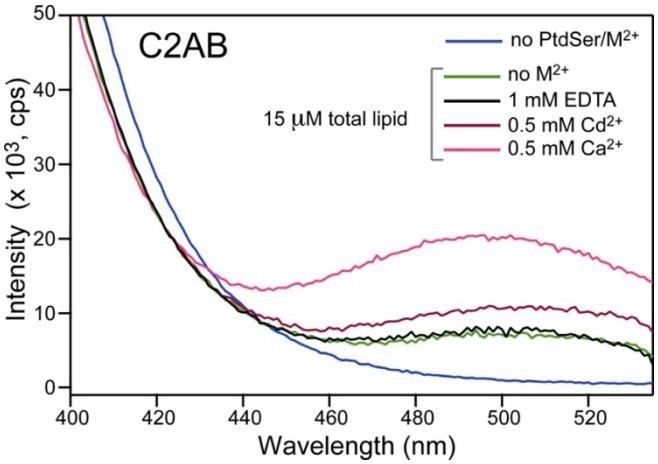

Figure 5.7: Metal-ion free and Cd^{2+}-complexed C2AB associates with PS-containing LUVs. Work performed in the Igumenova lab. Fluorescence emission spectra showing the C2AB-to-membrane FRET efficiency under different metal-ion conditions. The C2AB and total lipid concentrations are 0.5 μM and 15 μM, respectively. C2AB associates with PS-containing membranes in a metal-ion independent manner. This interaction is slightly enhanced by Cd^{2+} based on the increase in FRET efficiency. Ca^{2+} data are shown for comparison. Image and caption from: Katti et al. (2017). *Biochemistry.* **56:**3283-3295.

The Cafiso lab then used CW EPR and power saturation measurements to examine the full-length Syt1 construct tethered to PC:PS membranes (85:15) to see if tethering could enhance the weak cadmium binding observed from linking the C2A and C2B domains into the C2AB construct (*Figure 5.8).* Examining mutants in the first calcium binding loop of the C2A and the C2B domain (173R1 and 304R1 respectively), in the soluble constructs the 173R1 and 304R1 positions broaden and insert into PC:PS membrane in the presence of calcium[13,22]. Loop 1 sites were chosen over those in loop 3 in each domain to avoid changes in lineshape purely due to cadmium coordination, as seen in the crystal structure. Much like the soluble construct, the FL SYT also displays calcium dependent insertion into PC:PS membrane in the presence of calcium relative to the mobile aqueous loops (red vs. black in *Figure 5.8*). Strikingly, when cadmium is substituted into the C2

domains of the full-length constructs, both domains insert into membrane, suggesting enhancement of the electrostatic driving forces on the membrane (green vs. black in *Figure 5.8*). The tethered membrane was then neutralized with a 1:1 ratio of PS and DDAB to eliminate the electrostatic drive to the membrane and look only at coordination-based effects, and in the presence of calcium again both domains inserted into membrane. This suggests that while the effects were too weak to observe in the soluble construct, on the tethered membrane the calcium-coordination based driving force is enhanced. All membrane insertion was also verified by power saturation measurements (*Table 5.2).* The depth measurements show deepest insertion in the presence of calcium and charged membrane, because both coordination and electrostatic driving forces are contributing to insertion. Power saturation measurements also verified that membrane insertion was being driven by the presence of PS, as it did not insert into PC bilayers alone. Taken at face value the depth measurement values imply that the C2A domain insertion is driven more through electrostatic attraction to the membrane and that the C2B loops are driven more through coordination. This observation would agree with findings in the soluble construct in Chapter 3[22]. These need to be considered with caution, however, because domain orientations may also be affected when one of the two effects are neutralized, such as the C2B domain tilting the polybasic face away from the membrane in the electrostatic neutralization (DDAB), which would also agree with this trend in numbers.

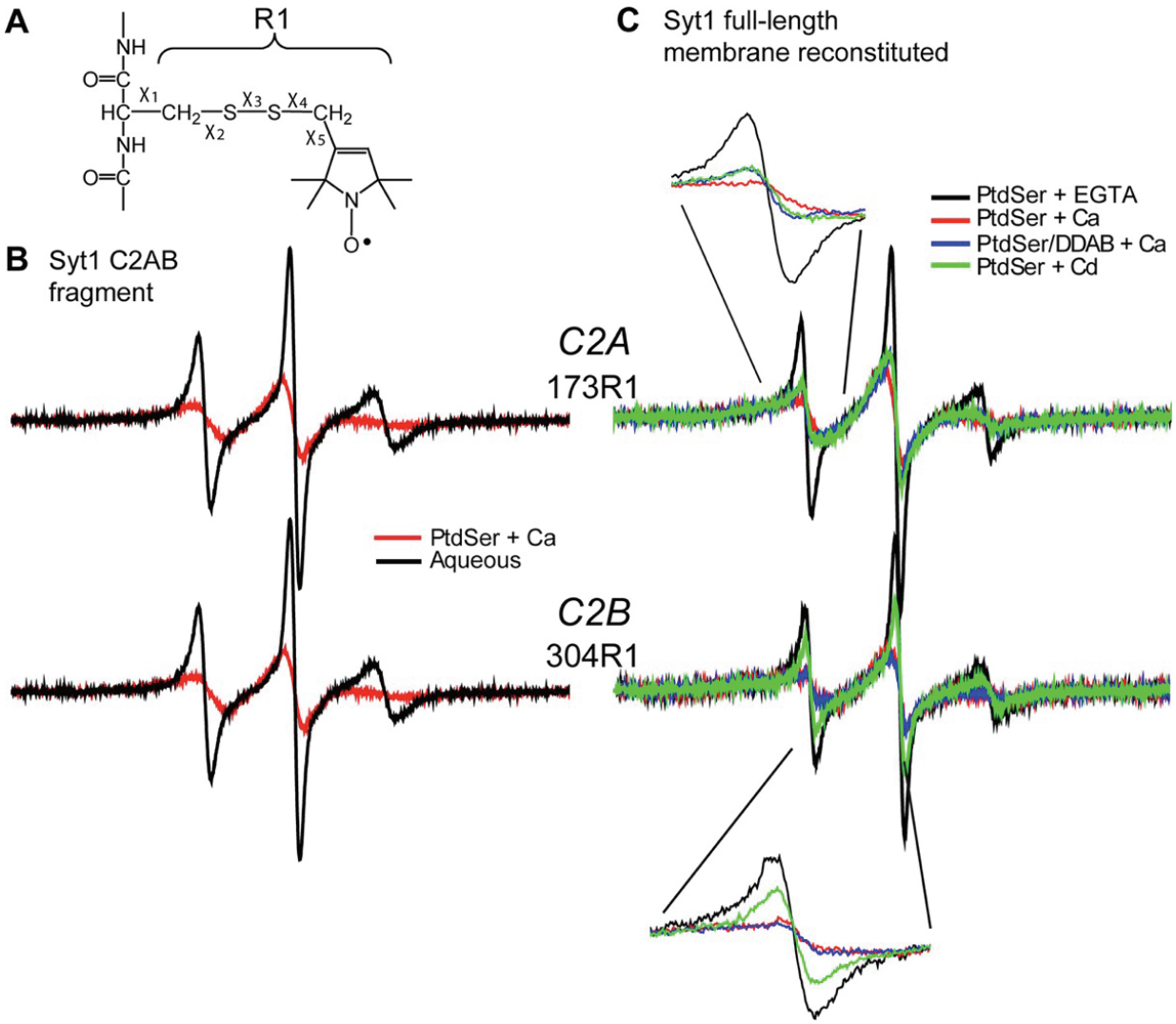

Figure 5.8: EPR spectra reveal membrane contact and insertion of the C2A and C2B domains. Work performed in the Cafiso lab. The spin labeled side chain R1 is attached to cysteines using a sulfhydryl specific MTS label. (B) EPR spectra for the Syt1 C2AB fragment with R1 at position 173 in C2A or position 304 in C2B in solution (black traces) or in the presence of Ca^{2+} and PS containing vesicles (red traces), (PC/PS = 85:15). (C) EPR spectra from R1 at sites 173 and 304 in full-length Syt1 reconstituted into PS in the absence of Ca^{2+} (black trace), in the presence of 1 mM Ca^{2+} (red trace), in the presence of 1 mM Cd^{2+} (green trace) (PC/PS = 85:15) or in the presence of 1 mM Ca^{2+} when reconstituted into charge neutralized membranes of PS and DDAB (blue trace) (PC/PS/DDAB = 70:15:15). Shown in the insets are expansions of the low-field resonance. Image from: Katti et al. (2017). *Biochemistry*. **56:**3283-3295.

protein variant	lipid conditions	metal added	depth parameter (Φ)	position from lipid phosphate (Å)
FL SYT 173R1	PC	Ca^{2+}	–1.9 ± 0.05	aqueous
	PC/PS (15%)	Ca^{2+}	1.03 ± 0.05	9.29
		Cd^{2+}	–0.6 ± 0.1	3.38
	PC/PS/DDAB (15%)	Ca^{2+}	–1.4 ± 0.2	–1.32
FL SYT 304R1	PC	Ca^{2+}	–2.0 ± 0.05	aqueous
	PC/PS (15%)	Ca^{2+}	–0.54 ± 0.05	3.53
		Cd^{2+}	–1.7 ± 0.1	–3.32
	PC/PS/DDAB (15%)	Ca^{2+}	–0.9± 0.2	1.85

Table 5.2: Depth Parameters for Full-Length Membrane Reconstituted Syt1. Work performed in the Cafiso lab. Negative depths are positioned on the aqueous side of the membrane phosphate plane; positive values are positioned toward the hydrocarbon interior. Both Ca^{2+} and $Cd^{2+}$are added to 1 mM. PC depth parameters place the spin label on the C2A or C2B binding loops in the aqueous phase 5 Å or further from the lipid phosphates. Full-length Syt1 is present at approximately 75 μM concentration with a total lipid concentration of 15 mM to yield a protein/lipid ratio of approximately 200. Table from: Katti et al. (2017). *Biochemistry.* **56:**3283-3295.

To verify the cadmium and DDAB measurements, FL SYT 173R1 and 304R1 in PC:PS were examined at very high (350 mM) and very low (45 mM) salt (unpublished data, *Figure 5.9)*. Measurements were taken in the presence or absence of calcium, and also with calcium-chelated (EGTA). First, the C2A domain as expected shows a slight enhancement of binding in low salt relative to physiological (150 mM) salt due to a decrease in electrostatic screening (blue vs. black in A of *Figure 5.9*). Then, in high salt the domain is partially shielded from the membrane, weakening the electrostatic driving force for membrane binding (red in A of *Figure 5.9).* This would indicate that when electrostatic binding of the C2A domain is inhibited, the C2A domain does not insert as strongly, which agrees with power saturation/CW EPR measurements, and also suggesting C2A is more driven by electrostatics. Next, the C2B domain in low salt is only slightly enhanced in binding when compared to physiological salt (blue vs. black in C of *Figure 5.9*). However, high salt does not significantly shield the calcium binding loops from the membrane (red in B of *Figure 5.9).* This again agrees with power saturation/CW EPR measurements,

suggesting C2B binding is more driven by coordination. Still both effects work in combination to lead to membrane binding in each domain.

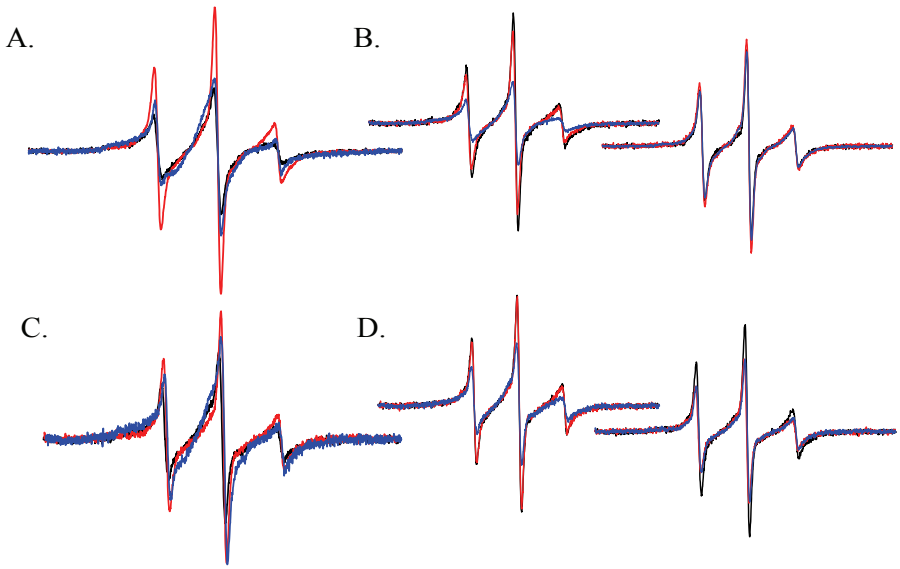

Figure 5.9: Electrostatic screening of Cadmium bound C2A and C2B domains-Membrane Binding. A. FL SYT 173R1 in low (45 mM, black), physiological (150 mM, blue), and high salt (350 mM, red). B. Left, low salt overlay of 173R1 with no metal added (black), EGTA (red), and cadmium (blue). Right, high salt overlay of 173R1 with no metal added (black), EGTA (red), and cadmium (blue). C. FL SYT 304R1 in low (45 mM, black), physiological (150 mM, blue), and high salt (350 mM, red). D. Left, low salt overlay of 304R1 with no metal added (black), EGTA (red), and cadmium (blue). Right, high salt overlay of 173R1 with no metal added (black), EGTA (red), and cadmium (blue). In low salt, both the C2A and C2B domains EPR lineshapes broaden slightly, indicating that at physiological salt there is some electrostatic screening of the membrane. At high salt, the C2A domain is slightly inhibited from membrane binding. The C2B domain is not however as affected by membrane screening, but also already binds weakly in cadmium. Overlays in B. and D. are shown to ensure high and low salt did not impact the CW lineshape, to check that salt change did not affect the state of the protein: before metal addition vs. in EGTA.

Overall, the driving forces for C2 domain membrane insertion are enhanced and observable when FL SYT is membrane tethered.

5.2.5 FL SYT binds to other Heavy Metals, including Lead

Finally, now that the soluble domains and full-length versions of Syt1 have been shown to bind to calcium, another heavy metal, lead (Pb^{2+}), was examined. Lead has previously been

suggested to bind with ~1000-fold higher affinity than calcium and to drive the protein–membrane association[13,23]. So, the Cafiso lab looked at FL SYT C2A domain, 173R1, and C2B domain, 304R1, in the presence of PC:PS (85:15) to see if lead too can substitute for calcium in the calcium binding loops (*Figure 5.10*). Like cadmium, lead can bind to the calcium binding loops of both the C2A and C2B domains of the full-length protein. Lead binding can also drive membrane insertion into PC:PS membranes, as observed through both CW EPR and power saturation (*Table 5.3*). In the C2A domain membrane insertion appears visually and through depth measurements to be very similar to the cadmium bound case. In the C2B domain, there is an additional immobile component in the presence of lead that is not observed in cadmium and the depth measurements imply deeper membrane insertion. In the previous investigations with the C2α domain, the coordination sphere for lead left two open spaces, filled by water molecules, which look very similar to the calcium coordination sphere in the figure (*Figure 5.1*). If this were the case in the C2 domains of Syt1, there is the potential that lead could coordinate a PS molecule as calcium does, due to the preference for higher coordination number ligands relative to cadmium as mentioned in previous work[13]. This would agree with the preliminary findings that in the C2A domain lead binds much as cadmium does (driven by electrostatics), and that C2B bound to lead inserts into membrane with depths intermediate between calcium and cadmium (because of an additional coordination driving effect). This is speculative until further characterization of the domains in the presence of lead takes place to determine the stoichiometry and affinity of binding, and also to look at any conformational changes that could occur due to lead coordination to the loops (potentially in collaboration with or by the Igumenova lab).

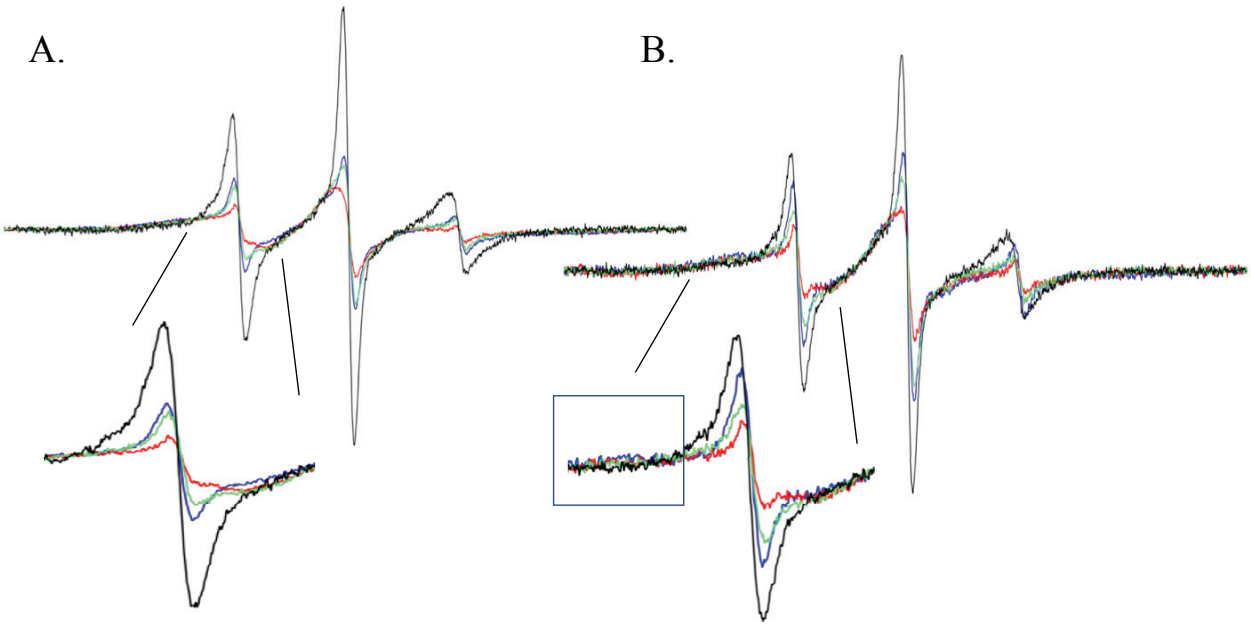

Figure 5.10: Overlay of for Cd^{2+}, Ca^{2+}, and Pb^{2+} bound to the C2A and C2B domains-interaction with membrane. A. FL SYT 173R1 in the aqueous phase, with EGTA (black), with lead bound (blue), with calcium bound (red), and with cadmium bound (green). B. FL SYT 304R1 in the aqueous phase, with EGTA (black), with lead bound (blue), with calcium bound (red), and with cadmium bound (green). Membrane for each case is PC:PS (85:15). Shown in the insets are expansions of the low-field resonance. Immobile component of lead is boxed in blue.

protein variant	lipid conditions	metal added	depth parameter (Φ)	position from lipid phosphate (Å)
FL SYT 173R1	PC/PS (15%)	Ca^{2+}	1.03 ± 0.05	9.29
		Cd^{2+}	–0.6 ± 0.1	3.38
		Pb^{2+}	–0.7±0.1	3.58
FL SYT 304R1	PC/PS (15%)	Ca^{2+}	–0.54 ± 0.05	3.53
		Cd^{2+}	–1.7 ± 0.1	–3.32
		Pb^{2+}	–1.1± 0.1	1.73

Table 5.3: Depth Parameters for Full-Length Membrane Reconstituted Syt1 with different metals bound. Negative depths are positioned on the aqueous side of the membrane phosphate plane; positive values are positioned toward the hydrocarbon interior.

5.3 Discussion

5.3.2 Conclusions

In the present work, the Igumenova and Cafiso labs examined the two C2 domains of Syt1 to determine whether the behavior of the PKC C2α domain could be generalized to other calcium-dependent C2 domains[13]. Like the C2α domain, cadmium serves as a structural surrogate for calcium in the individual C2A and C2B domains, but in solution the affinity for membrane is too weak to detect binding[13]. They also demonstrated that cadmium can drive the domains' membrane association in full-length Syt1, where the domains are directly tethered to the lipid membrane, enhancing local charge concentration and weak driving forces[13]. These results illustrate the significance and contributions of both long-range Coulombic interactions and high effective local lipid concentrations in the native protein environment (*Figure 5.12*)[13].

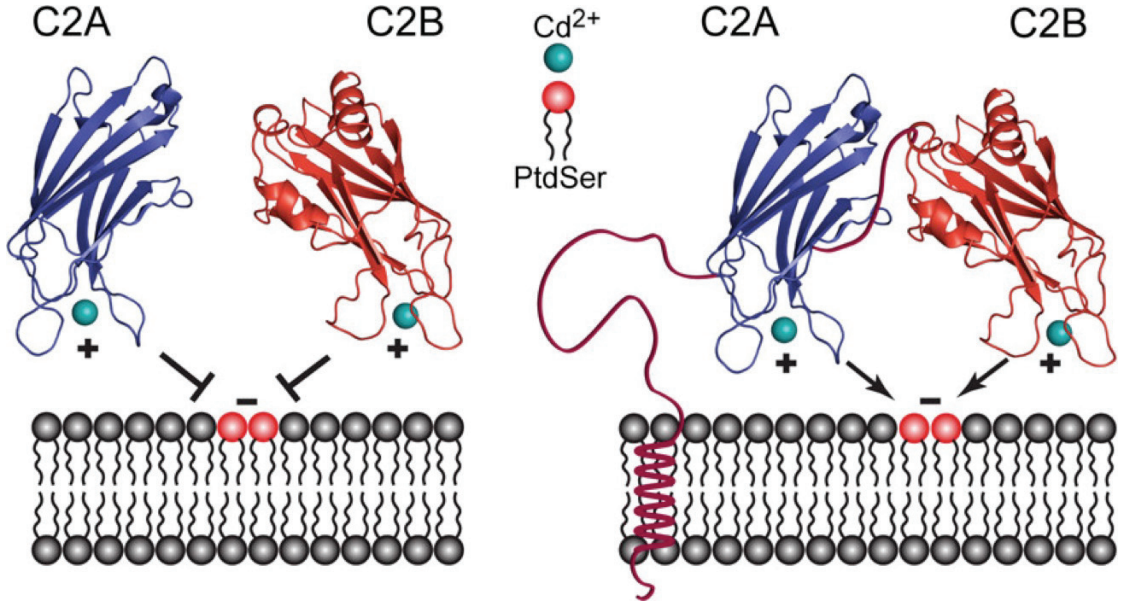

Figure 5.12: Diagram of soluble and full-length C2A and C2B domains membrane interaction in the presence calcium and cadmium.

Through the above investigations, cadmium was observed to have a very similar coordination sphere to calcium when crystalized, but only one cadmium ion binds with high affinity to the C2 domains, whereas the C2A and C2B domains are known to bind to 3 and 2 calcium ions respectively. NMR studies support these conclusions, highlighting a single high affinity cadmium binding site which binds with significantly higher affinity than the first calcium ion of each C2 domain. NMR and FRET measurements also demonstrated a potential second cadmium binding site, but this site has a much lower binding affinity than that seen for binding a second calcium ion to the C2 domains. These results are an underlying difference in metal ion binding between calcium and cadmium. The reasoning for differential binding is generalizable to the C2 domains since it agrees with the C2α observations, that meta- ligand binding and coordination depends on the acidity or softness of the cations, where cadmium prefers lower coordination numbers in its geometry[11,13].

Also, unlike calcium, cadmium ions were unable to drive the charged membrane insertion of soluble Syt1 C2 domain constructs, as was the case for C2α. This inhibition could simply be due to the decreased number of cations bound to the calcium binding loops. The calcium binding loops of C2 domains are typically negatively charged before coordination to calcium, as they must attract calcium to function[22]. When calcium binds it is thought to neutralize the loops permitting insertion of hydrophobic loops and positively charged calcium into the charged lipid membrane[22]. A single cation, in cadmiums case, may not be enough positive charge to neutralize the negatively charged calcium binding loops, or contributes to an increased energy barrier which must be overcome in some other way (such as placing the C2 domains in proximity to the membrane). If inhibition is not purely due to charge, membrane binding is likely prevented in solution because

cadmium cannot coordinate to PS on the membrane, as in the protein kinase C observations, eliminating the contributions of that driving-force[11,13].

There is the chance that in the presence of membrane the second cadmium ion could bind to the C2 domains of Syt1.Previous work has shown that the C2 domains display a significant increase in affinity for calcium when in the presence of charged phospholipid lipid membranes, where calcium affinities of the soluble domains increase 100-10,000-fold to 1-20 μM calcium[6]. If cadmium affinity increases to the C2 domains in the presence of lipid, similar to the effect observed with calcium, it would suggest that the main inhibitor of loop insertion is the lack of coordination, and not just charge repulsion.

This work also demonstrate an inhibition of membrane binding for the untethered C2 domains to negatively charged membranes in the absence of calcium in the presence of calcium the binding loops would have their negative charge neutralized, so there would be no electrostatic opposition to membrane insertion. This demonstrates that pure coordination of the domains to PS is also not sufficient to drive membrane insertion.

When the C2 domains are tethered together through the eight-residue flexible linker, a small but detectable amount of membrane binding was present for the cadmium bound case. The C2 domains were previously shown to act synergistically when linked in solution, enhancing each domains membrane affinity[21]. This demonstrates that slight enhancements or additional effects in could nucleate membrane association.

When the full-length St1 construct was used, which tethers the domains directly to the membrane, cadmium was able to drive membrane insertion. This indicates an enhancement of electrostatic driven insertion into negatively charged membrane. This again, is likely aided from closer initial membrane proximity in the full-length Syt1 which promotes the affinity of the C2

domains for cadmium. This would promote binding of the second cadmium, neutralizing the negative charge of the loops. This effect is observed due to membrane tethering limiting the distances that the C2 domains can travel away from the membrane. The close proximity then leads to the C2 domains experiencing a much higher local lipid concentration when tethered, as they would in their native environment (upward of 1 M lipid)[13]. These local concentrations exceed the lipid concentrations which can be used experimentally for the soluble domains alone or in the C2AB construct by at least 2 orders of magnitude. In solution, lipid concentrations are limited by hydration and modes of experimental detection, particularly in sedimentation assays where high lipid concentrations lead to a large amount of light scattering[13]. For these low concentrations of lipid in solution, weak interactions or driving forces (potentially on the order of membrane partition coefficients of 20 M^{-1}), would not be sufficient to observe membrane binding for the isolated domain[13]. However, when the effective local lipid concentration is very high, weak interactions would be sufficient for the domains to bind to membranes, as observed in the full-length protein[13]. Here, the substitution of cadmium or the neutralization of the membrane surface potential should individually abolish lipid-metal coordination and long-range Coulombic interactions, respectively, in the binding of these domains, helping to isolate the weak effects of both[13]. Alone, neither coordination nor Columbic interactions produce a strong C2 domain-membrane interaction, but because the free energy contributions of each effect are additive and partition coefficients multiply, both interactions when present together become significant[13]. The slightly shallower insertion of the domains with cadmium or with charge-neutralized membranes seen in the full-length protein agrees with a significantly reduced binding energy[13]. This reduction in insertion also suggests that, while driven by a combination of both weak binding forces, the contributions of electrostatic and coordination-based effects may not be generalizable for every

C2 domain, as it appears the C2A and C2B domains may be influenced more strongly by electrostatics or coordination, respectively. Linking the two domains would then take full advantage of each individually weak force.

In the PKCα domain, lead and cadmium both bind with higher affinity than calcium. They can also form mixed metal complexes in the loops and at high enough concentrations out compete calcium for loop binding[11,16,17]. This work also demonstrated the cadmium and lead can substitute and compete (due to higher binding affinity) for calcium in the C2 domains of Syt1.However, it was unclear if a mixed metal complex occurs in Syt1[11,23]. This competition between calcium and other divalent ions is concerning in a calcium sensitive protein, as interactions with lead or cadmium could render the domains insensitive to calcium. For Syt1 that would prevent the protein from fulfilling its role as the calcium sensor and fusion trigger. This would imply in part why heavy metal toxicity impacts the nervous system so severely. With no functional calcium sensors, all proteins would rely purely on asynchronous release which is much slower at signal transmission. Even asynchronous release could be halted, however, if Syt7 also binds to heavy metals with higher affinity[24]. In that case triggering would rely purely on spontaneous mini-release, which is rare and unpredictable. These aren't the only C2 domains at the site of fusion though, Munc13 for example also has C2 domains which coordinate calcium and likely play roles in regulating its function, and which could be directly involved in formation of the SNARE complex. If the SNARE complex cannot form fusion will not occur at all, which would be fatal.

5.3.2 Future Directions

Future extension of this work could be performed to better understand and characterize membrane binding in the more native environment experienced by full-length Syt. As mentioned

above, initial determination of cadmium affinity for the C2 domains in the presence of lipid would be interesting to see if increased affinity can promote binding of both cadmium ions. This, however, would only potentially be possible in the C2AB fragments, but more likely the full-length Syt1 construct due to enhancement of the weak electrostatic and coordination-based forces seen when the domains are linked together and tethered to the membrane. To compare these results, determination of the relative calcium affinity of the domains for FL SYT when tethered to charged lipid would be necessary. This would also expand upon previous observations where calcium affinity is enhanced in proximity to membrane[6]. These experiments could then also be repeated for lead and potentially for other heavy metals, including beryllium. Together, these experiments would help understand the underlying issues and contributing effects in heavy metal toxicity at the molecular level.

5.4 References

1. Chapman. (2008). How Does Synaptotagmin Trigger Neurotransmitter Release? *Annu Rev Biochem.* **77:** 615-641.
2. Jahn and Fasshauer. (2012). Molecular Machines governing exocytosis of synaptic vesicles. *Nature.* **490:** 201-207.
3. Sudhof and Rizo. (2011). Synaptic Vesicle Exocytosis. *Cold Spring Harb Perspect Biol 2011;3:a005637.*
4. Kee and Scheller. (1996). Localization of synaptotagmin-binding domains to syntaxin. *J Neurosci.* **16:** 1975-1981.
5. Perin et al. (1990). Phospholipid binding by a synaptic vesicle protein homologous to the regulatory region of protein kinase C. *Nature.* **345:** 260-263.
6. Sudhof. (2002). Synaptotagmins: Why so Many? *JBC.* **277:** 7629-7632.
7. Rizo and Sudhof. (1998). C2-domains Structure and function of a universal Ca2+ binding domain. *JBC.* **273:** 15879-15882.
8. Bai et al. (2000). Membrane-embedded Synaptotagmin penetrates cis or trans target membranes and clusters via novel mechanism. *JBC.* **275:** 25427-25435.
9. Fernandez et al. (2001). Three-dimensional structure of the C2B domain: Synaptotagmin 1 as a phospholipid binding machine. *Neuron.* **32:** 1057-1069.
10. Sugita et al. (2002). Synaptotagmins form a hierarchy of exocytotic Ca2+ sensors with distinct Ca2+ affinities. *EMBO J.* **21:** 270-280.
11. Morales et al. (2016). Cd2+ as a Ca2+ surrogate in protein-membrane interactions: isostructural but not isofunctional. *J AM Chem Soc.***135:** 12980-12983.
12. Lai et al. (2011). Synaptotagmin 1 modulates lipid acyl chain order in lipid bilayers by demixing phoshatidylserine. *JBC.* **286:** 25291-25300.
13. Katti et al. (2017). Non-native metal ion reveals the role of electrostatics in synaptotagmin 1-membrane interactions. *Biochem.* **56:** 3283-3295.
14. Park et al. (2015). Synaptotagmin-1 Binds to PIP2 containing membrane but not to SNAREs at physiological ionic strength. *NSMB.* **22:** 815-823.
15. Bai, Tucker and, Chapman. (2004). PIP2 increases the speed of response of synaptotagmin and steers its membrane-penetration activity toward the plasma membrane. *Nat. Struct. Mol. Biol.* **11**: 36–44.
16. Morales et al. (2012). Pb2+ as Modulator of protein-membrane interactions. *JACS.* **133:** 10599-10611.
17. Morales and Igumenova. (2012). Synergistic effect of Pb2+ and PIP2 on C2 domain-membrane interactions. *Biochemistry.* **51:** 3349-3360.
18. Herrick et al. (2009). Solution and Membrane-Bound Conformations of the Tandem C2A and C2B Domains of Synaptotagmin 1: Evidence of Bilayer Bridging. *J. Mol. Bio.* **390:** 913-9.
19. Guillen et al. (2013). Structural insights into the Ca2+ and PI(4,5)P2 binding modes of the C2 domains of rabphillin 3A and Synaptotagmin 1. *PNAS.* **110:** 20503-20508.
20. Walters and Johnson. (1990). Terbium as a luminescent probe of metal-binding sites in protein kinase C *J. Biol. Chem.* **265:** 4223-4226.
21. Herrick et al. (2006). Positions of Synaptotagmin 1 and the membrane interface: cooperative interactions of tandem C2 domains. *Biochemistry*. **45:** 9668-9674.

22. Perez-Lara et al. (2016) PtdInsP_2 and PtdSer Cooperate to Trap Synaptotagmin-1 to the Plasma Membrane in the Presence of Calcium, *Elife*. e15886.
23. Bouton, et al. (2001). Synaptotagmin 1 is a molecular target for lead. *Journal of Neurochemistry.* **76:** 1724-1735.
24. Bacaj et al. (2013). Synaototagmin-1 and -7 Trigger Synchronous and Asynchronous Phases of Neurotransmitter release. *Neuron.* **80:** 947-959.

CHAPTER 6: Synaptotagmin-1, a Distance Regulator for Synchronous Neuronal Exocytosis

6.1 Introduction

Synchronous neurotransmission occurs on the sub-millisecond timescale[1]. This event is triggered by calcium influx following an action potential passed along the neuron[1]. The SNARE protein complex then drives fusion and pore opening of neurotransmitter filled synaptic vesicles at the plasma membrane of the synaptic terminal, which releases the contents into the synaptic cleft to propagate signal transmission. However, the SNARE complex is not calcium sensitive, and thus the calcium sensor Synaptotagmin-1 couples depolarization and fusion events during synchronous neurotransmitter release[2]. Many mechanisms have been proposed for how Syt1 fulfills a triggering and regulatory role in the context of SNARE-dependent membrane fusion, but a consensus in the field has yet to be reached.

Syt1 is a membrane protein, which is tethered to the synaptic vesicle. Attached to the transmembrane domain is a juxta-membrane linker which connects two functional, calcium sensing C2 domains, C2A and C23[3,4]. These domains have been well studied in the soluble constructs alone (C2A and C2B) and linked (C2AB). Within these domains, the calcium binding loops on both domains have been proposed to interact with charged anionic phospholipids on the bilayer surfaces of both the vesicle membrane and the plasma membrane[1]. The polybasic face, arginine apex, and an amphipathic helix in the C2B domain are often also highlighted as additional

contact sites, potentially to the SNARE complex or the membranes to help connect Syt1 calcium binding and membrane insertion to the rest of the system[5-9]. Interactions with SNARE proteins, the membrane, or both, through the C2B critical regions and the polybasic face are likely initiated through a combination of weak driving forces including: hydrophobic insertion of the loops, electrostatic or Columbic interactions between charged regions, and metal-coordination[10-12]. These interactions in solution are nearly undetectable when isolated, but in combination function to drive fusion[12]. In the full-length construct weak interactions with the membrane, or potentially SNAREs, are likely enhanced due to membrane tethering and proximity to the charged surface and the SNARE complex[12]. *In vivo*, a complex set of the fusion machinery, regulatory proteins, and both the plasma membrane and docked synaptic vesicle membrane are within very close proximity at ~7-8 nm before calcium influx and ~2-5 nm (roughly the height of a C2 domain, or a tilted domain) after. This would mean that the weak interactions are significant, with each likely contributing to the functional system[13-15].

In the neuron, Syt1 likely interacts with the membrane surfaces directly, potentially playing a regulatory role preceding fusion. It has been shown that C2 domains can coordinate calcium, which neutralizes the initially repulsive, negatively-charged calcium binding loops, permitting hydrophobic residue insertion into the lipid bilayer[16,17]. This hydrophobic insertion is also driven by a combination of electrostatic and coordination-based attraction by the metal bound cation and negatively charged lipid on the bilayer surface[12]. On the synaptic vesicle surface, only PS contributes a negative charge, and on the plasma membrane both PS and PIP_2 contribute to negative charge density[17].

In theory, Syt1 can interact with either of the two bilayer surfaces, deemed a *cis*- interaction with the synaptic vesicle membrane, or *trans*- interaction with the plasma membrane[15]. Each

membrane has unique properties which may act to drive preferential binding of the C2 domains to one membrane over the other. Due to membrane tethering, the local charged lipid concentrations that the C2 domains could experience on the *cis* membrane are likely much higher than on the plasma membrane[12]. PS sequestering driven through domain coordination to the PS headgroup, could also enhance this local lipid concentration on the surface of the vesicle membrane[18]. *Cis* membrane binding likely plays a critical inhibitory (regulatory) role preceding fusion, by back-binding both domains to the vesicle rather than to the plasma membrane, preventing membrane fusion[15,16]. *Trans* binding of one or both C2 domains to the plasma membrane could then permit fusion to occur, potentially through additional docking and priming of the synaptic vesicle to the plasma membrane surface[15,16].

For *trans* binding to be initiated there must be a driving force large enough for at least one of the domains to prefer to interact with the *trans* membrane over the *cis* membrane. Before adding to the complexity of the full neuronal system, lipid composition on the plasma membrane alone could contribute to this force due to the presence of both PS and PIP_2 on the surface[17]. It has been shown that the polybasic face interacts strongly with negatively charged lipid clusters in a calcium-independent manner[3,4,17]. PIP_2 already possesses a bulky headgroup with higher charge density than PS and it may sit above the plane of lipid heads on the plasma membrane[19,20]. PIP_2 has also been proposed to form islands of charge, which are potentially syntaxin mediated and similar to PS clusters[10,20]. On a docked synaptic vesicle proximity to clustered PIP_2 headgroups, which could be up to ~ 0.6 nm closer to the synaptic vesicle surface, may be enough to enhance the long range electrostatic attraction and pull the C2B domain to the plasma membrane surface[19]. Once on the plasma membrane and after calcium triggering, PS and PIP_2 are shown to act synergistically to drive insertion of the calcium binding loops into the bilayer[17]. This synergy may be sufficient to

drive *trans* insertion into the plasma membrane, rather than being driven back to the *cis* membrane surface. There is also the potential that the partially zippered-SNARE complex or other regulatory proteins help to bring the synaptic vesicle surface within close enough proximity to the plasma membrane that the local concentrations on both membranes are equally competitive for C2B domain interactions.

The C2A domain could potentially insert into either bilayer in a fusion event since it does not have a (known) additional location to interact specifically with membranes or other proteins within the system. The C2A domain has shown a preferential coordination to PS membranes though, so *cis* or *trans* binding would be possible[12,21]. A driving force to pull the C2A domain off of the *cis* membrane is unknown, but potentially the short eight-residue linker attaching the C2B domain to the C2A domain would be enough driving force to pull the C2A domain toward the plasma membrane calcium-independently. From there, insertion into the PIP_2 containing plasma membrane may be enhanced due to PIP_2 increasing the C2 domains' affinity for calcium, which in turn enhances the affinity to the membrane[17,22,23]. The orientation of the C2A domain relative to the C2B domain could then potentially regulate the distances between the membrane surfaces, acting as the bilayer bridge, which would reduce the activation energy and the distance required for SNARE zippering and fusion[24].

The bilayer bridging idea has also arisen as a direct consequence of only the C2B domain, due to interactions of the arginine apex with membrane in combination with the calcium binding loops. This domain alone can bring the synaptic vesicle into ~5 nm or closer proximity. This promotes fusion, but the synergy between loop insertion of the C2A and C2B domains when C2A is present may enhance any weak forces that lead to the bridging event[4,5]. Whether the C2A domain binds to the plasma or the vesicle membrane may not be critical, since the two domains are joined

by the eight-residue flexible linker which could isolate the actions of one domain from the other? The process of both domains inserting into the same or opposite membranes likely also has the added benefit of inducing curvature strain in one or both membranes, which could promote stalk formation[15].

The enhanced membrane interactions with the membrane surface, due to tethering and increased local lipid concentrations, do not rule out any direct SNARE or regulatory protein interactions. In solution the SNARE complex has been shown to interact weakly and heterogeneously with Syt1 and this interaction is also very sensitive to the environmental salt concentration[5,15,16]. This weak, heterogeneous interaction probably explains why numerous mechanistic proposals each point to different critical domains of Syt1 as the interaction site with the SNARE complex[5-9,15,21,25-29]. However, like the membrane interactions, weak driving forces promoting interaction with the acceptor and SNARE complexes could also be enhanced when the system is within close proximity. One argument against this theory, however, is that when the *in vitro* system becomes more complex and closer to mimicking the physiological environment, these interactions are again abolished[10]. For example, the addition of charged poly-anionic compounds required for functional neurotransmission, like ATP, are thought to shield any of the weak interactions between the SNARE complex and Syt1[10]. ATP/Mg^{2+} at physiological (1-5 mM) concentrations have also been proposed to potentially regulate Syt1 *cis* and *trans* interactions with the membranes, as the C2 domains' charged attraction to ATP in solution is potentially as prevalent as the interactions of the domains with charged lipid[16,30,31].

This demonstrates that physiological charge and ion concentrations, including of: monovalent, divalent, and polyvalent ions (such as sodium and potassium, cations such as calcium and magnesium, and ATP) can hinder and shield weak charge interactions between Syt1 and either

the membrane or the SNARE complex[16]. Magnesium has been shown to hinder the C2B domains polybasic face interaction with PIP_2, and physiological salt (150 mM) blocks Syt1-SNARE binding when the C2AB construct is used[16,22]. Even sufficiently high levels of calcium can play an inhibitory role in calcium-dependent and -independent binding and fusion[58]. The question then arises, in the full-length construct (and *in vivo*) how do these charged ions hinder and promote differing states and interactions of Syt1 with the membrane or with SNAREs?

This question has in part been addressed in a set of papers from our collaborators in the Jahn lab[10,16]. Here, Park and collaborators used a combination of functional fluorescence and structural EPR techniques, and were able to show that, while present in low salt conditions, physiological salt and polyvalent ion concentrations block Syt1 interactions with the SNARE complex while permitting calcium-independent and -dependent binding to sufficiently charged PIP_2 containing membranes (*Figure 6.1*)[10]. In another paper, Park and collaborators demonstrated the potential regulation of Syt1 activity by electrostatic screening, specifically by ATP[16]. Here, *cis* and *trans* binding to various membranes were examined and the authors concluded that (unhydrolyzed) ATP inhibits *cis* binding to the PS-containing vesicle membrane, which may promote *trans* binding to the PIP_2-containing plasma membrane (*Figure 6.2*)[10,16]. Interestingly, the authors also found that the presence of ATP accelerates calcium-dependent fusion in functional assays, but this effect was dependent on the presence of PIP_2 on the target membrane[16]. However, these measurements were limited to direct (e.g. anisotropy) visualization of *cis* or *trans* binding effects in the soluble C2AB construct (which would weaken charge interactions potentially making screening easier) in combination with indirect measurements taken using the full-length protein expressed and purified in chromaffin granules[10,16]. In the following chapter, an expansion on work performed in these papers, using the full-length construct of Syt1 and direct EPR and NMR

measurements between the C2 domains and membranes, seeks to further understand this lipid-ion competition.

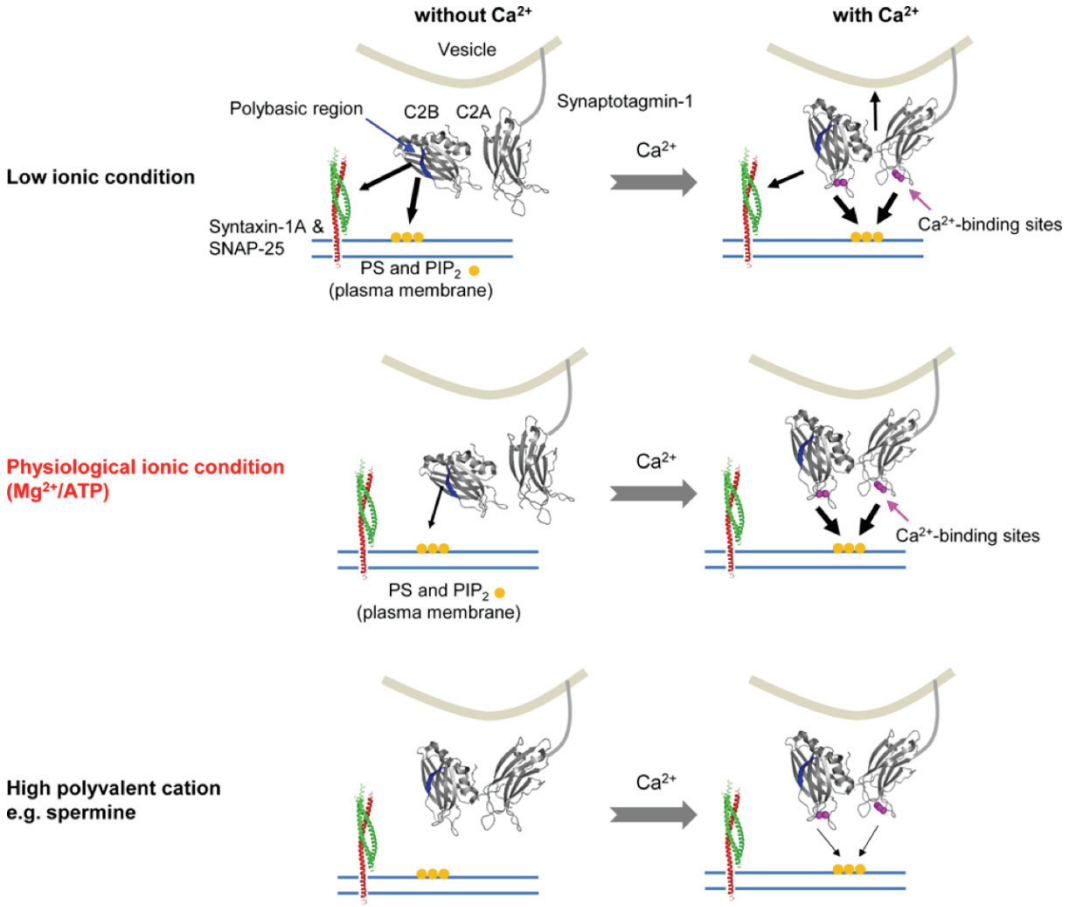

Figure 6.1 Synaptotagmin-1 binds to PIP_2-containing membrane but not to SNAREs at physiological ionic strength. The thickness of the arrows indicates the strength (affinity) of the interaction. Note that for clarity the PIP_2-clusters are depicted as being separated from the SNARE complexes which is likely not the case. The SNARE complexes are shown without synaptobrevin-2 for simplicity. Image and caption from: Park et al. (2015). *Nat Struct Mol Biol.* **22:** 815-823.

The work presented below also seeks to connect the regulatory function to a potential mechanism for FL SYT function, supporting its potential role as the distance regulator. The distance between the synaptic and plasma membranes is one of the largest energy barriers for stalk formation and bilayer fusion[32]. Syt1 could somehow regulate these distances, reducing the energy barrier for SNARE-dependent fusion. In this proposal, Syt1 binding could occur in sequence, with

initial *trans* calcium-independent binding to the plasma membrane, which would aid in docking and bringing the synaptic vesicle into the 7-8 nm distance observed preceding calcium influx[13]. Then, the C2 domains could either both insert into the plasma membrane, or one domain could insert into each membrane, with both binding modes reducing the distance between the bilayers to the length of the C2 domain, 5 nm, or even less depending on depending on the tilt angle of the C2 domain relative to the bilayer. On the low end, the separation could reach as little as 2 nm[13.33,34].

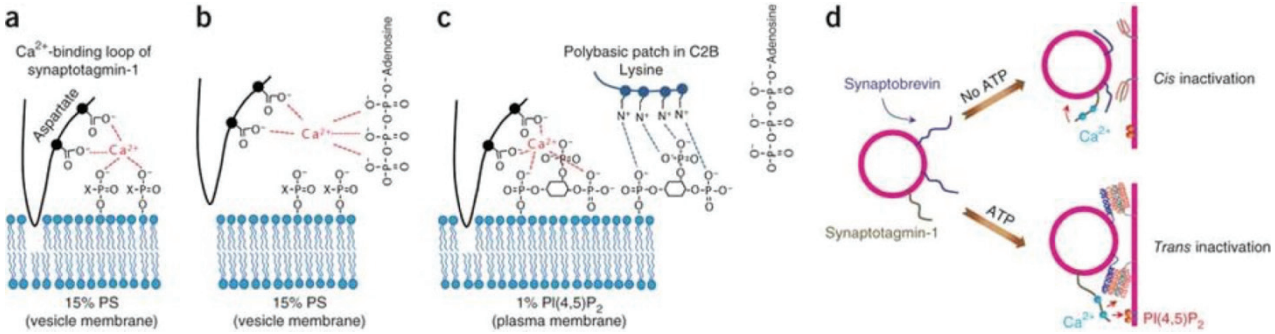

Figure 6.2: Controlling Synaptotagmin activity by electrostatic screening. A. In the absence of ATP, Syt1 binds to the vesicle membrane in a Ca^{2+}-dependent manner. Aspartate residues of the C2 domains (black balls) provide partial coordination for Ca^{2+} ions, with a more complete coordination sphere contributed by acidic membrane lipids. B. ATP, which chelates Ca^{2+} competes with Ca^{2+}-dependent membrane binding of Syt1 by shielding the coordination site of acidic phospholipids. C. In the presence of PIP_2, Ca^{2+} binding between the membrane and the C2 domains is enhanced, probably because of a polybasic patch within the C2B domain that binds PIP_2 on its own. The high Ca^{2+} affinity of C2AB binding to PIP_2-containing target membranes cannot be competed for by ATP. D. In the absence of ATP, Ca^{2+} inactivates Syt1 through cis association (binding to vesicle membrane). ATP selectively abolishes cis binding of Syt1, leaving the C2AB domains active to interact with the plasma membrane containing PIP_2, as required for Ca^{2+} triggering of exocytosis. Image and caption modified from: Park Y, et al. (2012). *Nat Struct Mol Biol.* **19:** 991–997.

Another question to address with this model would be, does the long and charged juxta-membrane linker contribute to this distance regulation? The linker has been mentioned in previous work out of the Jahn lab as likely contributing to distance regulation as simulations of Syt1 calcium-independent tethering allowed bilayer separations of up to 23 nm if the linker was fully

extended and not influenced by any charge interactions between the ionic double layers of both membranes (double layer influence is expected to shorten the linker slightly)[34]. Distance ruler experiments demonstrated the distance to be ~7 nm between bilayers for calcium-independent binding, suggesting that the linker must compress, but these experiments did not whether the linker actively contributes to binding and distance regulation[13]. The juxta-membrane linker region consists of a cysteine populated region after the transmembrane domain, which is likely palmitoylated but could also cluster Syt1[25]. The linker also has two large regions of positive and negative charge and a glycine zipper, which could potentially associate or structure to regulate distance[25,26]. While the native cysteine environment cannot be studied with EPR, as they would provide off-target sites for spin labeling, the following experiments attempt to investigate the FL SYT construct and its role as a distance regulator.

Overall, through a series of CW EPR, power saturation EPR, pulsed-EPR, HSQC-NMR, sedimentation assays and other techniques this chapter seeks to explore vesicular (*cis*) and plasma membrane binding (*trans*) of Syt1 under various physiologically relevant lipid, salt, and ion compositions to determine if Syt1 may act as a distance regulator between the vesicle and plasma membranes in SNARE-dependent fusion.

6.2 Results

6.2.1 Low concentrations of poly-electrolytes, such as ATP, can inhibit C2AB membrane-binding, but not in the presence of PIP_2

As follow-up experiments from those performed by Park and collaborators, work by Anusa Thapa and myself sought to investigate charged ion shielding, by first comparing changes in the calcium-dependent binding affinity of C2AB to PC:PS bilayers in the presence of various charged poly-electrolyte[16]. The initial work attempted to quantify the previously observed inhibition of *cis* membrane binding in the presence of various polyvalent ions. In this set of experiments a sedimentation assay involving a lipid titration of sucrose loaded PC:PS (15% charge) liposomes (mimicking the synaptic vesicle surface) was performed in the presence of 1 mM Ca^{2+} and either 1 mM ATP or 1 mM pyrophosphate ($P_2O_7^{4-}$). ATP, a triphosphate connected to corresponding nucleotide bases, was used in comparison to pyrophosphate, the diphosphate moiety of ADP, to see how differing charges shifted the binding equilibrium of C2AB in solution. Both experiments were performed in the presence of physiological levels of 2 mM Mg^{2+}. For all sedimentation assays that follow, the C2AB fragments were bodipy-FL C1-IA labeled, as mentioned in the methods, to permit detection of the amount of unbound C2AB after vesicle sedimentation. Excitation of the C2AB-fluorophore complex was performed at 480 nm and emission was detected at 510 nm to overcome the overlapping excitation wavelength range of the native tryptophans in C2AB and the absorbance of ATP, which both occur around 280 nm.

The results from the PC:PS titration display a difference in affinity between the poly-electrolyte free (control/reference) and poly-electrolyte containing cases. As expected, compared to the control case, in the presence of pyrophosphate C2AB binding affinity to PC:PS membrane

decreases roughly three-fold, from a binding constant of ~22,000 M^{-1} to a binding constant of ~ 7,400 M^{-1} (teal and magenta of A in *Figure 6.3*). The addition of ATP to the lipid titration was enough to abolish detectable binding, rendering it unquantifiable (navy of A in *Figure 6.3*). This large shift in binding affinity is consistent with an observation made by Park and collaborators using lipid mixing measurements, which demonstrated that poly-electrolyte charge affects the ability of poly-electrolytes to promote vesicle fusion[10]. The presence of vesicle fusion would indicate that *trans* binding is occurring, thus *cis* binding must be inhibited at the same rate[16]. Here, pyrophosphate promoted lipid mixing and fusion at a comparable rate to ADP, which was less effective than ATP[10].

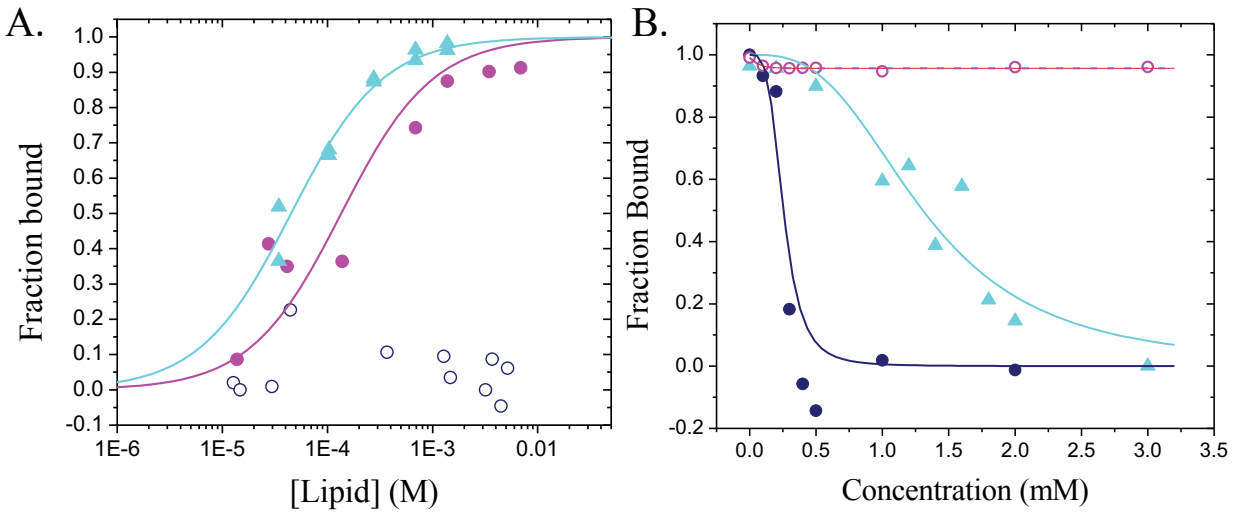

Figure 6.3: Low concentrations of poly-electrolytes can inhibit C2AB membrane-binding, but not in the presence of PIP_2. A. Vesicle sedimentation assays of C2AB titrating PC:PS (85:15) in the presence of 1 mM Ca^{2+} (teal), the addition of 1 mM pyrophosphate + 2 mM Mg^{2+} shifts affinity to PC:PS vesicles (~3 fold lower) (magenta). Addition of 1 mM ATP + 2 mM Mg^{2+} abolishes binding (navy). B. Addition of electrolytes, vesicle sedimentation assays of C2AB with constant 1 mM lipid in the presence of 1 mM Ca^{2+}. In the presence of PC:PS (85:15) a titration of pyrophosphate + Mg^{2+} (teal) decreases overall binding until abolishing it around 3 mM P_2O_7. Under the same lipid conditions, addition of ATP + Mg^{2+} rapidly hinders binding, fully blocking binding around 0.5 mM ATP (magenta). However, in the presence of PC:PS:PIP_2 (84:15:1), a titration of ATP does not alter overall binding of C2AB (navy). PIP_2 is likely able to outcompete this electrolyte driven inhibition. Pyrophosphate and PS measurements were performed by Anusa Thapa. PIP_2 measurements were performed by Sarah Nyenhuis.

In the second set of vesicle sedimentation assays, the quantity of PC:PS was held constant and pyrophosphate and ATP (with corresponding Mg^{2+}) were titrated in to quantify the amount of each poly-electrolyte required to block *cis* membrane binding (B in *Figure 6.3*). Consistent with the affinity measurements, higher concentrations (~1.5 mM) of pyrophosphate are required to block 50% of C2AB membrane binding. ATP was able to inhibit C2AB-membrane binding at a concentration lower than 0.5 mM) (teal and navy of B in *Figure 6.3*). Next, 1% PIP_2 was added to the sucrose loaded vesicles to mimic the plasma membrane in order to see if, as in the Park paper, the presence of PIP_2 can overcome ATP addition to promote *trans* binding[10]. Here, in the presence of PIP_2, there was no observed inhibition of binding over a range of 0-3 mM ATP (magenta in B of *Figure 6.3*). These results again agree with the previous observation that weak effects which promote *cis* binding to PC:PS vesicles alone in solution are screened by polyelectrolytes according to the amount of charge, but *trans* binding is possible in the presence of sufficient (1-3%) PIP_2 charge[16]. The next question to address would then be, is there a competitive contact site which promotes and inhibits the interactions of charged species, such as the polybasic face or the calcium binding loops, within C2AB?

6.2.2 IP_3 (PIP_2 headgroup) binding affinity to the C2B domain is higher than ATP, both bind competitively mainly at the polybasic face

To address, the question of interaction sites between C2AB and polyvalent species, HSQC-NMR was performed to characterize the interaction between the C2B domain and either ATP or IP_3, the PIP_2 headgroup. The NMR experiments were performed with Vanessa Bijak, under the instruction of Dr. Jeff Ellena. Anusa Thapa previously performed an initial characterization of the C2A domain in the presence of IP_3 and ATP, which showed minimal chemical shifts at the calcium

binding loops of the C2A domain (ATP data is unpublished)[17]. She also attempted to characterize the interaction with the longC2B construct. However, many follow-up and control experiments, by Vanessa and I, led to the conclusion that the additional charged residues preceding the C2B domain in the longC2B construct lead to instability at the higher temperatures required to run NMR. The interdomain linker residues may also partially (competitively) inhibit ion binding to locations on the C2B domain. Measurements performed on the shorter C2B construct display greater construct stability over time and at high temperatures. The addition of ATP leads to destabilization and accelerated precipitation of the domain, so precautions were taken: allowing the domain to run in the presence of ATP at 27 °C for no more than 2 hours and using fresh samples for each titration point. The shorter C2B domain did not display such instability in the presence of IP_3 but is still only stable for 4 hours at 27 °C, or 2 titration points. For clarity, optimization and troubleshooting of NMR experiments will not be shown.

The experimental design and setup for both ATP and IP_3were performed in the presence of constant 1 mM Mg^{2+} and buffer with 3 mM Calcium, as initially optimized by Anusa and Jeff, to best match cross peak data observed by Rizo et al. PDB ID 1K5W[35]. For ATP titrations, ATP was added over 0-5 mM concentrations and IP_3 titrations were performed over a range of 0-1 mM IP_3, until apparent saturation. C2B concentrations were 400 μM, so at least 2-fold excess of polyvalent ion was added before the end of a titration.

As Anusa previously observed, C2B and polyvalent ions interact primarily at the polybasic face with a 1:1 binding stoichiometry, and IP_3 binds with a higher affinity[17]. However, in the shorter C2B construct, chemical shifts are much less prevalent around the calcium binding loops and are more localized to the groove around the polybasic face (*Figure 6.4*). ATP contacts, however, are still less specifically localized and much lower affinity than IP_3. This indicates that

the interactions with ATP could be occasional contacts, but probably not a specific, high-affinity binding interaction.

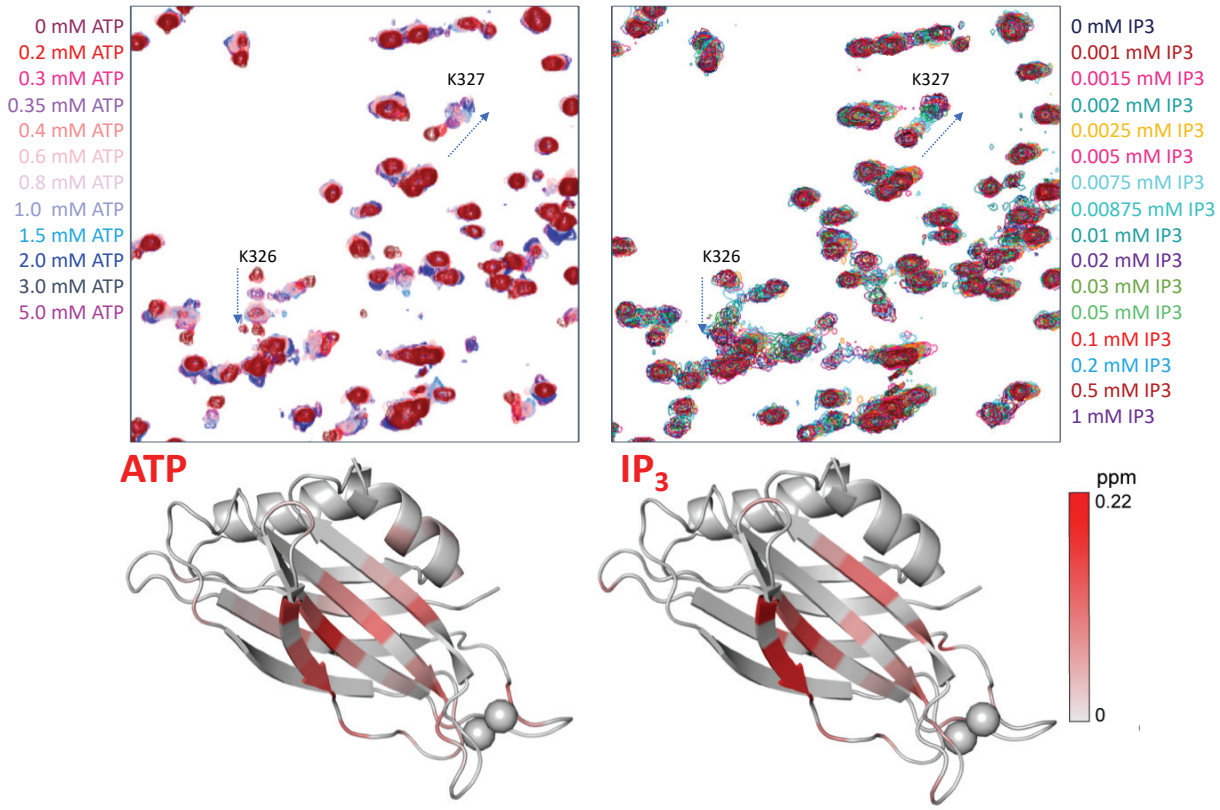

Figure 6.4: IP_3 (PIP_2 headgroup) binding affinity to the C2B domain is higher than ATP. Top: Zoomed HSQC NMR N15-short C2B titration of ATP (left) and IP_3 (right). Highlighted are shifts for K326 and K327 two key residues in the polybasic face. Bottom: Chemical shift intensities from 0 to 0.22 ppm mapped onto the C2B domain of with shifts from ATP (left) and IP_3 (right). ATP shifts map onto a larger less specific binding area than IP_3 (either due in part to bulk/size or just affinity). Measurements on the instrument were taken with Vanessa Bijak, under the instruction of Jeff Ellena.

The binding events between IP_3 or ATP and the shorter C2B domain are in general higher affinity than those observed in the longer construct. An IP_3 concentration of ~16 µM was observed for half maximal binding in short C2B versus an IP_3 concentration of 230 µM for half maximal binding of longC2B. More strikingly, however, a much higher difference was observed for the binding affinity of IP_3 to the C2B domain compared to ATP, with a 20-fold higher affinity for C2B

and IP_3 (*Figure 6.5*). This difference in binding affinity better agrees with the relative concentrations and competition between PIP_2 and ATP in the above sedimentation assays and justifies why such competition could occur in the soluble construct and potentially *in vivo*. The significant difference in affinity for IP_3 would overcome any charge shielding and permit *trans* binding in the presence of physiological concentrations of ATP.

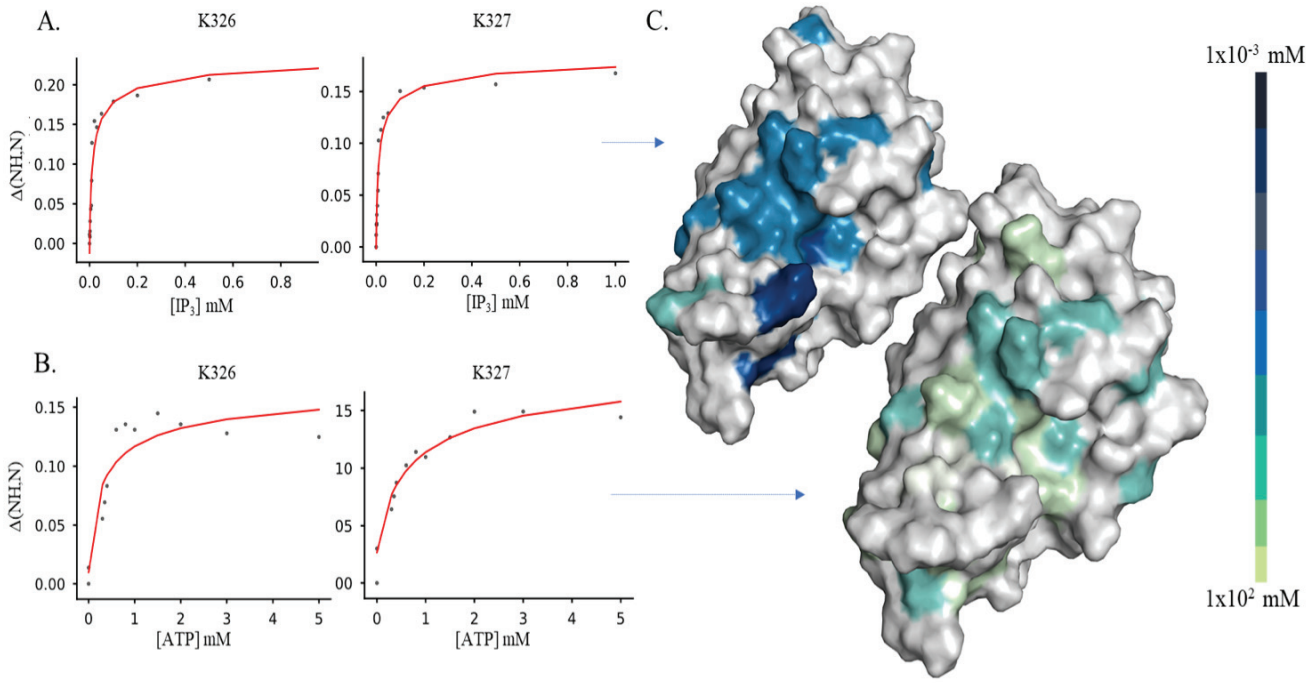

Figure 6.5: IP_3 (PIP_2 headgroup) binding affinity to the C2B domain is higher than ATP, both contact competitively mainly at the polybasic face. A. IP_3 and B. ATP titrations, the residue chemical shifts were fit to the equation: $y = A\frac{B+4x-\sqrt{(B+4x)^2-4x^2}}{4x-C}$, where y is the chemical shift, x is the ligand concentration, and A, B, and C are fitting factors. C. IP_3 (top right) vs ATP (bottom right) affinities are shown on the C2B domain (PDB 1K5W) with opaque surface renders over the binding affinity (K in mM) range where: constants are colored over a binned gradient of light green ($1x10^2$ mM) to ($1x10^{-3}$ mM dark blue), white covers no contact sites. IP_3 has a higher affinity binding site localized to the area around the polybasic face, with only a few weaker affinity contact points over the rest of the domain. ATP overall displays lower, more uniform affinity binding throughout the domain and a larger area around the polybasic face and ATP has similar affinity contact sites over the rest of the domain.

6.2.3 Charged lipid concentrations on the membrane (Cis) using EPR and FL SYT are high enough to overcome poly-electrolyte inhibition

The next step of this investigation was to move to work in the full-length Syt1 construct, to determine if any weak binding and inhibition effects could be enhanced in a more native environment. For initial measurements in the full-length construct, *cis* and *trans* membrane binding conditions were isolated to better observe effects of poly-electrolytes on each state. A series of CW EPR measurements at differing concentrations of ATP/Mg^{2+} and differing lipid compositions were then performed to compare binding, shielding, and competition effects in the full-length protein.

For *cis* back-binding, two sites in FL SYT, 173R1 in the C2A domain calcium-binding loops, and 304R1 in the C2B domain calcium binding loops were labeled and reconstituted independently, to investigate binding of both domains to membrane. These mutants were reconstituted first into charged proteoliposomes of PC:PS (85:15) alone to mimic the synaptic vesicle and then for comparison into PC:PS:PIP_2 (85:10:1.25) to compare any enhanced lipid binding to a plasma membrane mimic (schematic of design shown in A in *Figure 6.6*). Measurements were performed in the absence of calcium first, to capture the aqueous lineshape of both sites on the C2A and C2B domains (Black lines in B in *Figure 6.6*). Calcium was then added to each condition to observe calcium-dependent insertion of the calcium binding loops (Red lines in B in *Figure 6.6)*. In each domain and lipid condition, as expected, the loops inserted into membrane producing a broadened immobilized CW lineshape (verified by power saturation in the previous chapter). A concentration within the affinity range observed from sedimentation assays and NMR of 1 mM and a full excess of 5 mM ATP/Mg^{2+} was then titrated into each condition to see if *cis* membrane binding can be inhibited, as observed in the soluble construct (green then blue

lines respectively in B in *Figure 6.6*). In the full-length protein, minimal differences are observed between the calcium bound lineshape and the ATP added cases, indicating that the loops in both the C2A and C2B domain remain inserted in the *cis* membrane in the presence of ATP. The PC:PS reconstitution is counter to previous observations, though not fully surprising considering how high the local charge concentration is on the tethered membrane (~1 M), which could overcome any ATP competition within the mM affinity range[10,12].

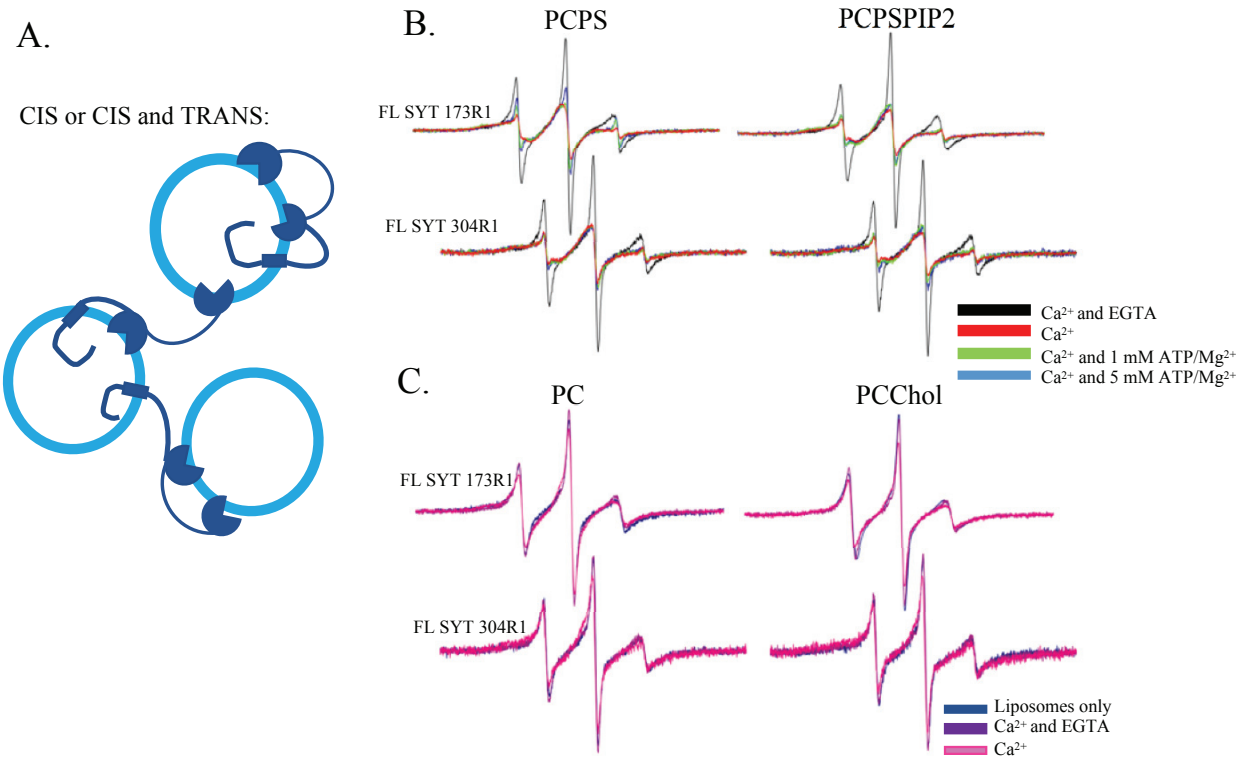

Figure 6.6: Charged lipid concentrations on the membrane (cis) using EPR and FL-Syt1 are high enough to overcome poly-electrolyte inhibition. A. Representation of FL SYT possible orientations when purely reconstituted with lipid membrane (B charged, C uncharged). B. Left C2A (173R1) and C2B (304R1) domains insert into PC:PS (85:15) upon addition of 1 mM Ca^{2+}. Right C2A (173R1) and C2B (304R1) domains also insert into PC:PS:PIP_2 (85:10:1.25) upon addition of 1 mM Ca^{2+}. For each case, titration of 1 mM and 5 mM ATP/Mg^{2+} do not affect calcium-dependent insertion. C. Controls: C2A (173R1) and C2B (304R1) domains reconstituted into PC (left) or PC:Chol (80:20) (right). In a charge free membrane, both domains remain in the aqueous phase when calcium is added.

Both FL SYT sites were also reconstituted into charge-less proteoliposomes composed of PC or PC:Chol (80:20). This isolates *trans* binding which could mimic both weaker membrane interactions observed using the C2AB construct with the synaptic vesicle (as in Park's work) or in the full-length Syt1 plasma membrane binding in the neuron. The aqueous lineshapes for each site and condition are first observed in navy (C in *Figure 6.6)*. To ensure binding to charged liposomes was not influenced by *cis* back-interactions with the charge-free surface, calcium and EGTA were added to each charge-free condition (magenta and purple respectively in C in *Figure 6.6)*. In all cases calcium did not induce membrane insertion, but did display a very small alteration in overall lineshape between PC and PC:Chol cases, to be investigated in more detail below (also verified by power saturation in the previous chapters).

6.2.4 Addition of poly-electrolytes inhibit trans FL SYT C2A binding. In the presence of PIP_2, the C2B domain can overcome this inhibition.

The next point to investigate is whether *trans* binding is permitted or enhanced in the context of the full-length protein. For this investigation CW EPR was used with the 173R1 and 304R1 sites in the C2A and C2B domains of FL SYT. These mutants were reconstituted into the PC and PC:Chol bilayers shown above, to inhibit any back-binding to the *cis* membrane. Charged liposomes of various compositions were then added to the reconstituted protein to observe any *trans* binding effects. The lack of back-binding was expected to result in slightly weaker binding, as the domains were diffusion limited, similar to using C2AB, rather than tethered to the binding membrane. To isolate lipid specific effects, PC:PS (90:10), PC:PS:PIP_2 (95:7.25:0.25) and PC:PIP_2 (95:5) (design schematic shown in A of *Figure 6.7*).

For each of these *trans* lipid additions, the aqueous lineshape is shown in black (in B and C for C2A and C2B respectively in *Figure 6.7*). The observed lineshapes for the C2A domain are very similar, as observed in the soluble constructs. For the C2B domain there is a subtle difference in lineshapes for the PIP_2 conditions that can be seen mostly in the high-field lines, due to contact from calcium independent binding of the polybasic face. This too is observed in the soluble constructs. Upon addition of calcium, for all sites and lipid conditions, the label inserts into membrane (red for C2A in B and C2B in C in *Figure 6.7*). These lineshapes also vary in intensity due to differences in the depths of insertion, which have been shown to correlate similarly to the soluble construct[17]. ATP/Mg^{2+} was again added near physiological levels to 1 mM and in far excess at 5 mM) (green and blue respectively, for C2A in B and C2B in C in *Figure 6.7)*.

In the PC:PS case, for both the C2A and C2B domains the binding equilibrium is shifted towards the unbound state at 1 mM ATP. This agrees with previous work, which also showed a decrease in binding for the soluble protein to PC:PS vesicles, which the authors interpreted as equivalent to decreased *cis* back-binding in the native system[16]. At 5 mM ATP each PC:PS case is almost fully unbound, indicating a lack of insertion. For the PC:PS:PIP_2 case the C2A domain more quickly returns to the aqueous state, potentially due to less PS being present overall if C2A insertion is driven more by coordination as previous data has suggested. Here, the C2B domain also titrates towards a more unbound state, potentially due to the low overall charge and PIP_2 concentration (0.25%, net negative 4) being unable to outcompete the high concentration of ATP. However, the aqueous/EGTA lineshape is still slightly broadened relative to PC:PS, indicating that while loop insertion appears to have been lost, the label is still hindered, probably due to membrane contacts at the polybasic face resulting from calcium independent binding. Finally, in the PC:PIP_2 case, higher overall PIP_2 is added (5%), to mimic conditions in the previously mentioned paper[10,16].

The C2A domain in this case already inserts shallowly into the PIP_2 membrane, and ATP addition restores a population of unbound loops. However, it is unclear if a small population remains inserted, potentially due to influence from the C2B domain and increased affinity in PIP_2. The C2B domain in this case shows slight deviations between PC and PC:Chol reconstitutions. For PC, ATP shifts the insertion equilibrium toward the aqueous phase more extremely than in the PC:Chol case, while still leaving the potential calcium-independent binding lineshape. PC:Chol remains mostly inserted, which would more strongly indicate promotion of *trans* binding. The differences between PC and PC:Chol binding are investigated in experiments below, however the true cause is not straightforward. The cholesterol containing condition would be more similar to the native environment and agrees with data and experimental design presented in the previous work mentioned above[10].

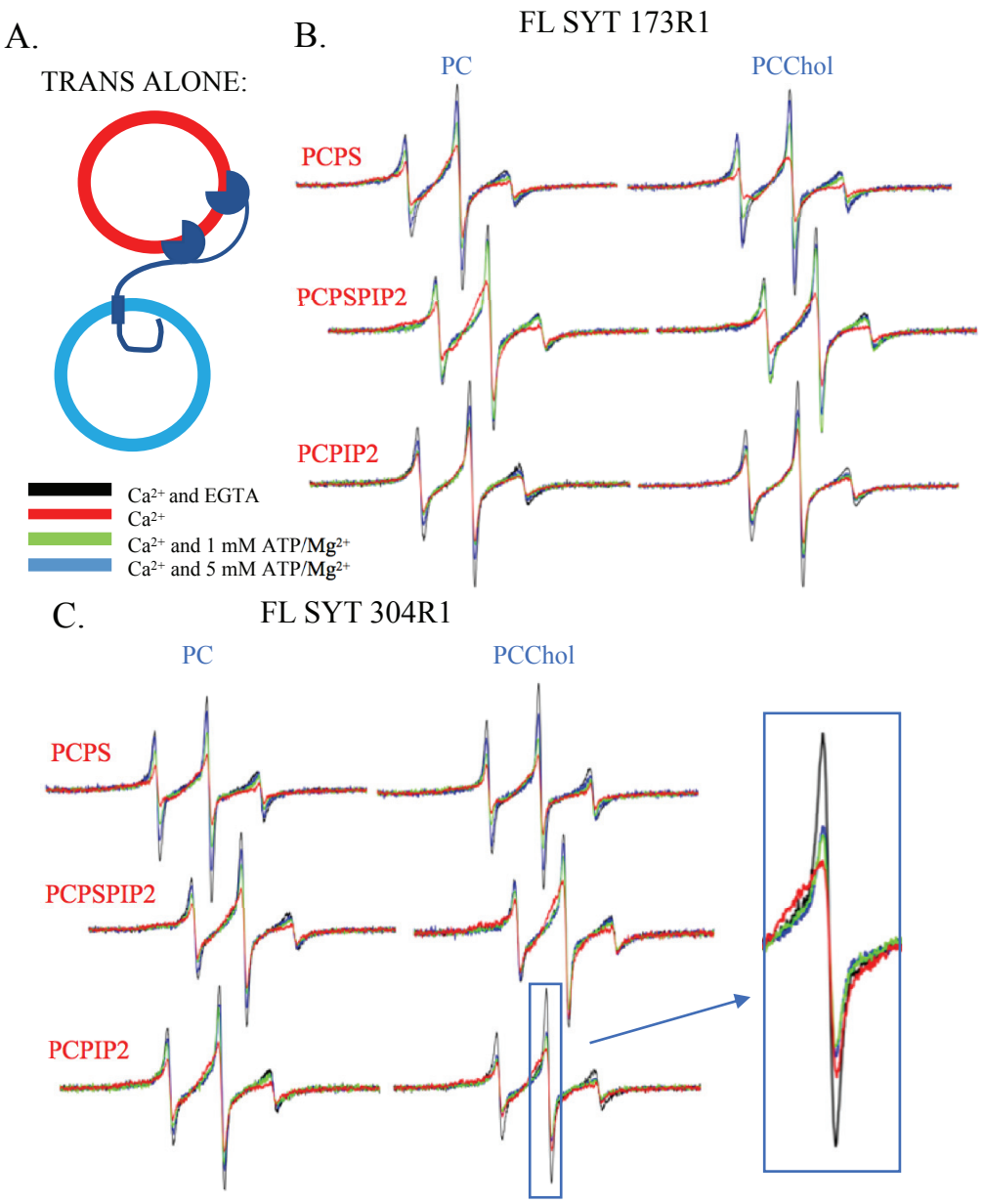

Figure 6.7: Addition of poly-electrolytes inhibit trans FL SYT C2A binding. In the presence of PIP_2 and Cholesterol, the C2B domain can overcome this inhibition. A. Representation of FL-Syt possible orientations when reconstituted into charge-free proteoliposomes (blue), extruded charged liposomes can then be added to the system. B. FL Sty 173R1 (C2A domain) was reconstituted into PC (left) alone or PC:Chol (right). Addition PC:PS (90:10) (top), PC:PS:PIP_2 (95:7.25:0.25) (middle) or PC:PIP_2 (95:5) bottom and calcium shows a shift in lineshape indicating insertion into membrane (red). Progressive titration of 1 mM and 5 mM ATP/Mg^{2+} result in shifting equilibrium of bound and unbound protein toward the aqueous phase. C. FL Sty 304R1 (C2B domain) was reconstituted into the same conditions also shows a shift in lineshape indicating insertion into membrane (red). Titration of 1 mM and 5 mM ATP/Mg^{2+} result in more slowly shifting equilibrium of bound and unbound protein toward the aqueous phase for all cases except for the PC:Chol adding PC:PIP_2 case, here the PIP_2 maintains a mostly bound state (blue box).

Next, the tethered C2A domain alone, in the ΔC2B construct, was used to isolate any influence of the C2B domain on insertion of the C2Adomain. First, charge (PC:PS, PC:PS:PIP_2) and charge-free (PC, PC:Chol) *cis* reconstitutions were performed to compare to data in *Figure 6.6* (A and B of *Figure 6.8*). Like the FL SYT construct, addition of calcium in the presence of charged liposomes drives loop insertion, and subsequent ATP addition is not able to overcome this insertion (A of *Figure 6.8*.). The strong forces driving the C2A domain to the concentrated charge on the *cis* membrane make it impossible to visualize any loss of enhancement/synergy due to the absence of the C2B domain. Also, as in the FL SYT construct, insertion is dependent on the presence of PS or PIP_2 on the membrane, allowing *trans* binding to be isolated (B of *Figure 6.8*). Finally, for the addition of PC:PS, PC:PS:PIP_2 and PC:PIP_2 alone there is a very similar trend compared to the C2A domain in FL SYT. The main difference is a larger loss of binding in the PC:PIP_2 case when reconstituted into PC, potentially due to a loss of initial calcium-independent pull to the PIP_2 membrane to localize insertion. Both PC:PS cases are largely the same, indicating that when C2B cannot mediate calcium-independent binding or repulsion to the membrane surface in the presence of ATP, C2A can still drive a small population to coordinate with the membrane. This observation is supported by preliminary measurements made in the soluble C2A domain, using vesicle sedimentation in the presence of ATP, where ATP reduces the overall binding of the domain ~25% to 55% as ATP is added from 0.5-3 mM, but does not fully abolish binding. In PC:PS:PIP_2 a similar reasoning could explain slightly enhanced binding to the membrane and no repulsive competition from the C2B domain. This effect is also enhanced in PC:Chol and PC:PIP_2, indicating some increase in affinity to the opposing membrane dependent on the reconstitution state of the protein. An attempt to examine this effect is presented below.

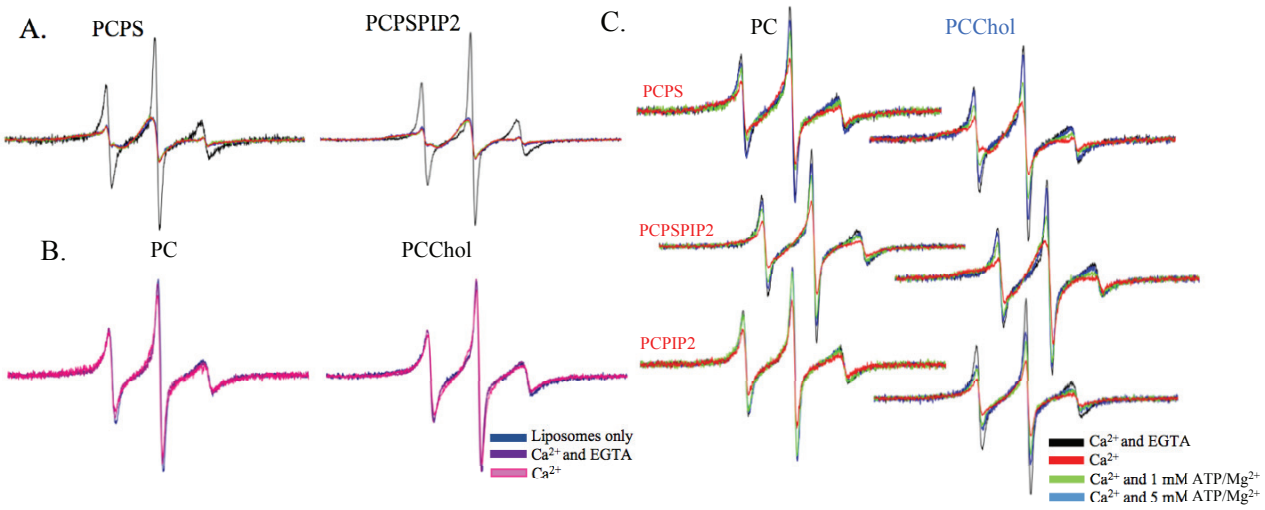

Figure 6.8: Addition of poly-electrolytes to cis and trans binding of ΔC2B trends similarly to the C2A domain in FL SYT. A. ΔC2B: membrane tethered C2A (173R1) domain alone inserts into PC:PS (85:15) upon addition of 1 mM Ca^{2+}. Right C2A (173R1) also inserts into PC:PS:PIP_2 (85:10:1.25) upon addition of 1 mM Ca^{2+}. For each case, titration of 1 mM and 5 mM ATP/Mg^{2+} do not affect calcium-dependent insertion. B. Controls: ΔC2B, C2A (173R1) domain reconstituted into PC (left) or PC:Chol (80:20) (right). In a charge free membrane, both cases remain in the aqueous phase when calcium is added. C. ΔC2B 173R1 (C2A domain) was reconstituted into PC (left) alone or PC:Chol (right). Addition PC:PS (90:10) (top) or PC:PIP_2 (95:5) and calcium shows a shift in lineshape indicating insertion into membrane (red). Progressive titration of 1 mM and 5 mM ATP/Mg^{2+} result in shifting equilibrium of bound and unbound protein toward the aqueous phase.

6.2.5 Regulation of cis or trans binding is not due to pinching, back-binding, ordering, or aggregation of the domains or the juxta-membrane linker of Syt1

The next step of the investigation was to attempt to determine any additional contributions or driving forces, other than local lipid concentration, within the full-length construct in the context of promoting *cis* and *trans* binding. Also, an attempt was made at isolating the cholesterol effect on the full-length reconstitution and its ability to enhance trans binding in the presence of PIP_2. A few hypotheses were examined here to promote differences in bridging.

First, in the CHAPs purification the C2 domains do not themselves aggregate (Shown in Chapter 3). However, from work using the soluble C2AB construct, Rothman lab has demonstrated

that in the presence of PIP_2, high charge density on the membrane, or ATP in solution, C2B domains spontaneously form ring-like oligomers of on average 17 C2B domains per ring[36-39]. In their 'washer model', ring formation, which is likely driven by charge interactions on the membrane and in the polybasic face, occurs in the absence of calcium[36]. The domains act as a regulatory washer, forcing a specific distance between the synaptic vesicle and the plasma membrane to block fusion[36]. Upon calcium influx, these rings break apart due to reorientation of the C2B domains required to accommodate insertion of the calcium-binding loops[36]. 'Clams' and 'volcano'-type formations were also observed in their earliest work, but this was performed at low (15-50 mM salt) and high (35-40%) net negative membrane charge[36]. Under more physiological salt concentrations (150 mM) and charge on the membrane (15%), the number of rings observed on an EM grid dropped significantly (from ~15 rings observed, to 3.5 rings/μm^2)[37]. The authors then demonstrated that in solution, 1 mM ATP and magnesium can also nucleate ring formation (and are insensitive to calcium), potentially meaning rings form in solution before priming of the synaptic vesicle. Then, PIP_2 out-competes the ATP interaction and promotes ring (and thus synaptic vesicle) priming to the plasma membrane[38]. These rings too, however, were on the magnitude of 4-6 rings per μm^2 on the EM grid.

Follow-up work was performed using DEER measurements on the C2B domain's calcium binding-loops (304R1) to see if ring nucleation by ATP and then formation on the PIP_2 containing bilayer could be contributing to ATP inhibiting *trans* binding to PS containing membranes, while instead promoting *trans* binding in the presence of PIP_2. Measurements were performed with the goal of comparing the relative degrees of aggregation/ring formation by comparing modulation depths (as was performed in Chapter 3). Here, ring-formation could be differentiated from generalized aggregation in the distance distribution, as the rings are separated by approximately

the length of a C2 domain, so a label on the calcium-binding loop should show a distance distribution around 45-50 angstroms. Measurements were performed on the FL SYT 304R1 site reconstituted into PC:Chol, because the strongest evidence for *trans* binding was observed under this condition. Three measurements were taken in the absence of calcium, with FL SYT reconstituted into PC:PChol bilayers alone, FL SYT reconstituted into PC:Chol bilayers in the presence of 1 mM ATP/Mg^{2+}, and then FL SYT reconstituted into PC;Chol bilayers with the addition of 1:1 PC:PIP_2 (5%) liposomes (black, blue, red respectively in *Figure 6.9*). Surprisingly, all measurements displayed little to no modulation depth (<1%), indicating that there is no significant or detectable ring-formation in the FL SYT construct. These measurements were repeated (not shown for clarity) in buffer conditions mimicking those required for EM grid experiments, with the addition of 4% trehalose, to ensure that ring formation is not nucleated by stabilizing osmolytes, but modulation depths did not change. Equivalent measurements were then taken using the soluble C2AB construct to see if this lack of ring formation was specific to the FL SYT construct. However, the C2AB 304R1 alone, with the addition of ATP and the addition of PC:PIP_2 liposomes did not display significant evidence of ring formation (black blue and red respectively in B of *Figure 6.9*). There is a potential 2% modulation depth when PIP_2 is present, so an excess of PC:PIP_2 liposomes were added to see if that could nucleate substantial ring formation, however the modulation depth did not change (green in B of *Figure 6.9*). Taken together, this indicates that the majority of Syt1 in the system is not participating in ring formation, and that rings are probably not contributing to the regulation of *cis* and *trans* binding to the membrane.

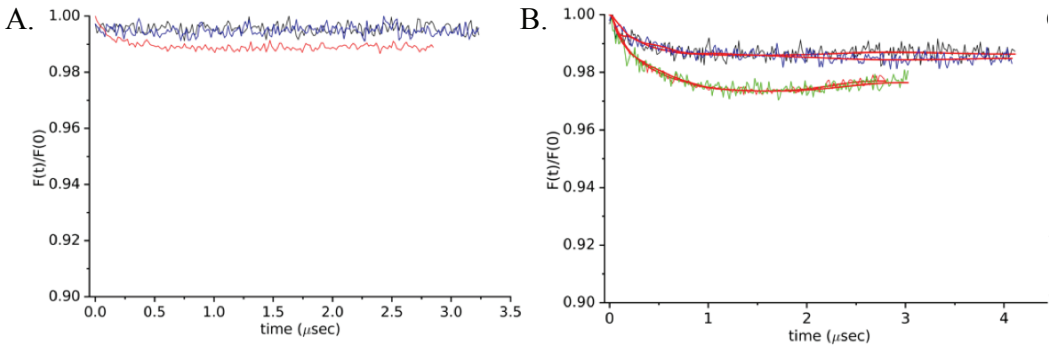

Figure 6.9: Regulation is not due to ordering or aggregation of the protein. A. FL SYT 304R1 (C2B domain) in PC:Chol does not interact with other C2B domains in the absence of calcium (black). Addition of 1 mM ATP/Mg^{2+} (blue) or extruded PC:PIP_2 liposomes (red) does not nucleate any substantial interaction. B. soluble C2AB (residues 136-421) 304R1 C2B domain, in the absence of Calcium, does not come into contact with other C2B domains in solution. Addition of 1 mM ATP/Mg^{2+} (blue) shows no increase in interactions in solution. Extruded PC:PIP_2 liposomes (green or red) increases the modulation depth to a delta of ~2%, but it is still not a large interaction.

After ruling out significant contributions from the C2 domains, this regulation was investigated from the context of the juxta-membrane linker. The hypothesis was that the juxta-membrane linker could potentially influence the C2 domains' ability and preference to bind to one membrane or another: either through distance regulation driven by pinching within two oppositely charged linker regions, direct inhibition of the C2B domain under specific lipid conditions where the polybasic face back-binds to the negatively charged linker region, or through general aggregation or structural ordering of the linker when it is reconstituted into different *cis* bilayers.

First, the linker pinching hypothesis was examined using pulsed-EPR. Sites 86 and 136 were selected within each charged region of the juxta-membrane linker in FL SYT (region is highlighted in A of *Figure 6.10*). Initially, the difference between linker pinching in PC or PC:Chol with and without calcium was examined to see if this could contribute to the stronger *trans* binding after FL SYT is reconstituted into PC:Chol (black, green, blue, and red respectively in B *of Figure 6.10*). Comparing modulation depths to look at relative populations of interacting spins, between

a 2% - 4% modulation depth is produced in all of the sample conditions. This indicates that there is a subset of interacting spins, but the majority of the linker does not pinch under these conditions. 5 mM ATP/Mg^{2+} was then added to see if this could somehow change the distribution of pinching and not-pinching populations, potentially by charge shielding or binding to the positively charged region of the linker directly. These measurements were performed in both calcium free and calcium containing cases to see if there would be a change upon calcium influx (figure C and D in *Figure 6.10*). As seen in the figure, ATP addition did not alter the modulation depths significantly. As a control, the linker mutants were run under high salt (300 mM) and low salt (45 mM) conditions to ensure charge shielding or lack thereof reduced or promoted additional linker pinching (D in *Figure 6.10*). Data is shown for PC:Chol only for clarity. As expected, in low salt, the shielding of the linker charged regions is reduced and the population of pinched-linker increases. Then, under high salt the extra ions shield the charge, reducing the population of linkers coming into contact. This verifies that the juxta-membrane linker itself is not spontaneously pinching for every FL SYT, which would reduce the distance between the two membranes. Also, ATP does not regulate any pinching that is taking place. These sites are also conveniently located within range (50 residues) to rule out any significant population of linker forming secondary structure such as a helix, within this region, which would also shorten the distance between membranes (and be observed as a short ~2.1 nm distance). This does not, however, rule out partial helix formation in different regions of the linker, which is addressed below.

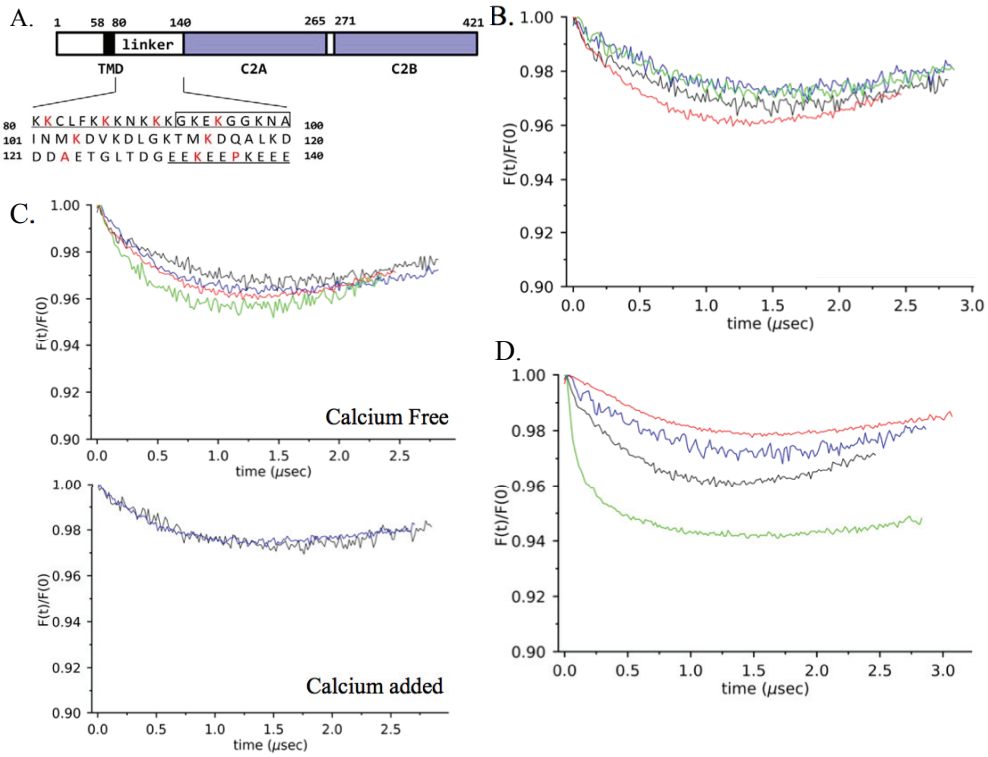

Figure 6.10: Regulation is not mediated through pinching or secondary structure changes in the linker. A. FL SYT 86-136R1 linker mutants are located in regions of positive and negative charge, which could contact and pinch the linker under differing conditions, this pinching could contribute to distance regulation. Addition of Cholesterol to the membrane does enhance minimal pinching, then addition of calcium to both cases decreases the interaction between the linker. This could be additional charge shielding or just different states of the linker or C2 domains into and out of the membrane. B. FL SYT 86-136R1 in PC with and without calcium (black and blue), and in PC:Chol with and without calcium (green and red) C. Top: FL SYT 86-136R1 linker mutant in PC (black) or PC:Chol (red) without calcium vs. addition of 5 mM ATP/Mg^{2+} respectively (blue, green). Bottom: FL SYT 86-136R1 linker mutant in PC (black) with calcium and the addition of 5 mM ATP/Mg^{2+} (blue). Under physiological salt there is little contribution to linker contacts. ATP/Mg^{2+} addition does not show significant contributions to any linker pinching or shielding. D. Charge shielding of the linker high (300 mM-red) or low (25 mM-green) salt buffer conditions shift the equilibrium between the populations of linker that are and are not pinching (shown relative to PC:Chol and PC:Chol Calcium black and blue). In PC:Chol membranes the linker pinching population decreases in high salt and increases significantly under low salt conditions. PC follows a similar trend but is not shown. A. is from Lu et al. *JBC*. 289: 22161-22171. 2014.

Next, any inhibition due to back-binding or transient contacts between the C2B domain and the negatively charged region in the juxta-membrane linker was investigated using pulsed EPR. Site 136 was again selected in the negative region of the linker and then one location on

opposing ends of the polybasic face, either 323 or 329, was added to examine contacts between the polybasic face and the juxta-membrane linker. Each set of double mutants was again reconstituted into PC or PC:Chol and run with and without calcium to see if reconstitution differentially influenced any inhibitory interactions between these regions (black, red, blue, green respectively for 136R1-329R1 and 136R1-323R1 in A and B of *Figure 6.11*). The findings for these sites display a negligible amount of contacts within the protein for site 136R1-329R1, observed again by the differences in modulation depths. However, for 136R1-323R1 there is a ~ 4-5% modulation depth, which correlates to a very close contact between these sites (C in *Figure 6.11*). This could indicate an occasional but transient interaction of the polybasic face and the negatively charged-linker region. The observation at 323R1, but not 329R1 indicates this could be location specific. 323R1 is above (nearer the arginine apex than the calcium binding loops) the main 326K, 327K residues often highlighted as the polybasic face, but lysine residues continue through residue 320 on this beta sheet, with 323 located in the middle. 329R1, however, is nearer to the calcium binding loops on the far end and is off of the beta-sheet at the transition into negatively charged calcium binding loops. This could cause charge repulsion between this region and the juxta-membrane linker, forcing the C2B domain into an orientation which pushes the loops away and putting 323 on the far end of the polybasic face in close proximity with the linker. This is still not occurring in the entire population of FL SYT though, and there are not any significant changes between PC and PC:Chol.

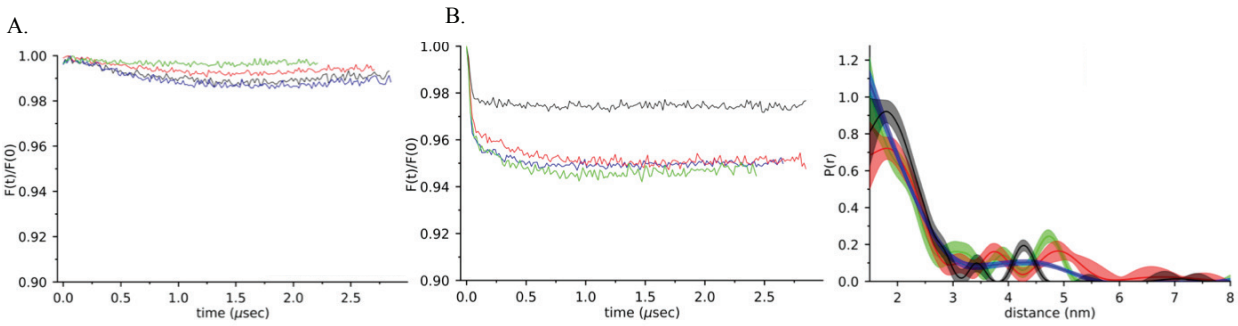

Figure 6.11: Does the C2B domain polybasic face come into contact with negatively charged regions in the linker, inhibiting binding? A. linker position 136R1 does not come into significant contact with 329R1 near the polybasic face. There is a very slight increase in populations with just the PC reconstitution with and without calcium, but still not significant. B. Linker 136R1 comes into occasional close contact with 323R1 on the other side of the polybasic face, there could be a difference in equilibrium in PC with and without calcium, but this does not explain the entire distance regulator or cholesterol effect. All figures (black equals PC no Ca^{2+}, blue equals PC with Ca^{2+}, red equals PC:Chol no Ca^{2+}, green equals PC:Chol with Ca^{2+}).

Finally, single residues throughout the linker were examined to look at linker aggregation and states relative to the *cis* membrane. Three sites were selected: site 86 near the transmembrane domain, site 90, and site 95 close to the C2A domain. These sites were selected as locations that may be in different states within the linker if present in the membrane versus the aqueous phase[26]. CW, power saturation, and pulsed EPR were performed at each site under varying conditions. Shown in this section are PC and PC:Chol reconstitutions to investigate the cholesterol effect, while in a later section charge will be introduced to the *cis* reconstituted membrane. Each site was first examined with and without calcium using CW EPR to look at any differences in lineshape and any calcium-dependent binding effects (A, C, E of *Figure 6.12*). Each CW is scaled to the same relative intensity to observe differences in lineshape in the figure (*Figure 6.12*). From this data, it is apparent that site 86R1 is broadened relative to the other two locations which appear to be flexible aqueous loops in all cases. 86 is likely interacting with the membrane due to its proximity to the transmembrane domain (data published and shown in later section)[26]. There are

very slight differences in lineshape between the PC and PC:Chol cases, but no further differences upon addition of calcium. In both the 86 and 95 locations there is a slight but apparent broadening of these sites in PC:Chol relative to PC. These differences are not apparent at 90R1, though PC:Chol is very slightly more mobile. The lineshapes in all cases are also indicative of at least two states, as they are multi-component spectra. It is unclear is these components are different modes of aggregation, or membrane interactions, and so power saturation and pulsed EPR were run to attempt to separate the two (B, D, F in *Figure 6.12* and *Table 6.1*). Site 86, shown below, and published data confirm that the site is slightly inserted into the membrane and sites 90 and 95 are in the aqueous phase for all cases (*Table 6.1 and 6.2*)[26]. There are slight differences between PC and PC:Chol in the depth measurements, but this does not fully correlate with the trend in CW lineshape, indicating some form of slight restriction or, potentially, aggregation. These measurements also cannot measure the immobile component as the power saturation measurements are overshadowed by the mobile component. The samples were then repeated in sucrose, with the goal of reducing any free tumbling of the aqueous loop to isolate the bound component, and the mobile component was subtracted from both data sets (data not shown for clarity). Sucrose did not significantly alter the lineshapes. Subtraction revealed that the mobile components all display a fairly characteristic aqueous loop lineshape and a very immobilized second component. To see if this second component was due to aggregation, pulsed EPR was run and revealed first for site 86R1 that there is no aggregation near the transmembrane region of the FL SYT construct, which is potentially inhibited due to membrane insertion. For sites 90R1 and 95R1 overall there is very little contact, again looking at modulation depths. There is a slight trend between PC and PC:Chol, where PC has an increased 0.5% - 1% modulation depth relative to the equivalent PC:Chol conditions, which in the context of 4-5% depth overall could be a significant

difference, but again is not representative of the majority of FL SYT in the experiment. (The linker will be addressed with charge again below.

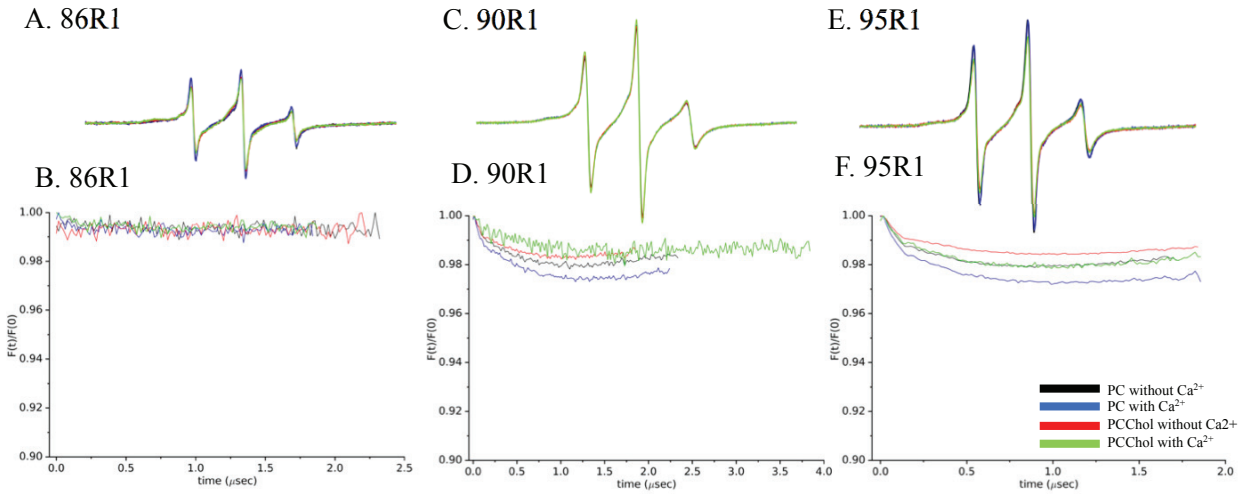

Figure 6.12: An investigation of the Juxta-membrane Linker in Charge-free liposomes. A. and B. 86R1 in the linker near the transmembrane interface CW appears broadened in all PC and PCChol cases, likely due to interactions with the membrane because there is no aggregation occurring at this site. C. and D. 90R1 is an aqueous and mobile CW in all conditions, verified by power saturation, and oligomerization is insignificant. There is again a very slight increase in aggregated population when reconstituted into PC alone. E. and F. 95R1 appear aqueous in all states, verified by power saturation, there is a slight decrease in CW mobility and depth when reconstituted just into PC liposomes and a very slight increase in aggregated populations.

Overall, there is no clear, single contribution from the above measurements which explains differences in the *trans* membrane binding affinities, but these effects could all contribute weakly to cause the observations seen for ATP and PIP_2 (and with and without cholesterol) above. The cholesterol effect could also affect the proteins' mobility throughout the membrane, and thus availability for *trans* binding, or insertion of the linker into the membrane. There is also the potential that Syt1 could be differentially sequestering cholesterol, changing the environment of the protein but not aggregating it in any way. This could alter the diffusion of Syt1 in the bilayer or act as an additional point of membrane strain and curvature induction, which could aid stalk formation during fusion. Another point to investigate, however, is whether the C2 domains binding

to a *trans* membrane alters the state of the juxta-membrane linker[1]. A full investigation of many more sites throughout the juxta-membrane linker would be an interesting future direction to see if more information could sort out this effect.

protein variant	lipid conditions	metal added	depth parameter (Φ)	position from lipid phosphate (Å)
FL SYT 90R1	PC	Ca^{2+}	–2.4 ± 0.1	aqueous
	PC	EGTA	–2.4 ± 0.2	aqueous
	PC:Chol (20%)	Ca^{2+}	–2.4 ± 0.1	aqueous
	PC:Chol (20%)	EGTA	–2.5 ± 0.2	aqueous
FL SYT 95R1	PC	Ca^{2+}	–2.3 ± 0.1	aqueous
	PC	EGTA	–2.4 ± 0.1	aqueous
	PC:Chol (20%)	Ca^{2+}	–2.7 ± 0.1	aqueous
	PC:Chol (20%)	EGTA	–2.6 ± 0.05	aqueous

Table 6.1: Depth Parameters for Full-Length Membrane Reconstituted Syt1 Linker Mutants in Charge-Free Bilayers. Negative depths are positioned on the aqueous side of the membrane phosphate plane; positive values are positioned toward the hydrocarbon interior. Ca^{2+} is added to 1 mM. Depth parameters which place the spin label 5 Å or further from the lipid phosphates are marked in the aqueous phase. Full-length Syt1 is present at approximately 75 μM concentration with a total lipid concentration of 15 mM to yield a protein/lipid ratio of approximately 200.

6.2.6 Addition of PC:PIP_2 liposomes trans presents subtle changes in the juxta-membrane linker state

The juxta-membrane linker was next examined in the context of *trans* binding, to see if tethering to two bilayers alters the state of the juxta-membrane linker. CW EPR measurements were performed on FL SYT 86R1, 90R1, and 95R1 again reconstituted into PC or PC:Chol with and without calcium. In this case, PC:PIP_2 (5%) liposomes were also added to promote *trans* binding, both calcium-independently with the polybasic face and calcium-dependently through the calcium binding loops of each C2 domain (*Figure 6.13*). There is no obvious effect or difference between PC and PC:Chol reconstitutions in all cases and the linker state in general is altered independently of calcium. The addition of PC:PIP_2 liposomes did result in subtle changes

throughout the linker, likely resulting from the interaction of C2B with the membrane before calcium addition, and then both domains after its addition. At site 86, for PC and PC:Chol below, addition of liposomes to promote *trans* binding actually immobilizes the site relative to the reconstituted state alone, potentially indicating a deeper interaction with the membrane (due to sample limitations PC:Chol *trans* binding was only performed in calcium). For site 90R1 there is not a significant change between each state, suggesting this region of the linker is not changed due to *trans* binding. At site 95R1 closer to the C2A domain, addition of PC:PIP_2 liposomes produces an increase in mobility due either to movement of the tethered domains or a more aqueous state further from the reconstituted bilayer. Depth measurements for these sites could not be performed as localization to just the *cis* membrane could not be differentiated from the *trans* bilayer (attempts to measure to just one bilayer were unsuccessful). The differences between just reconstituted lineshapes and the additional tethering to a second bilayer do show that the linker changes, being potentially pulled, strained, or compressed during *trans* binding.

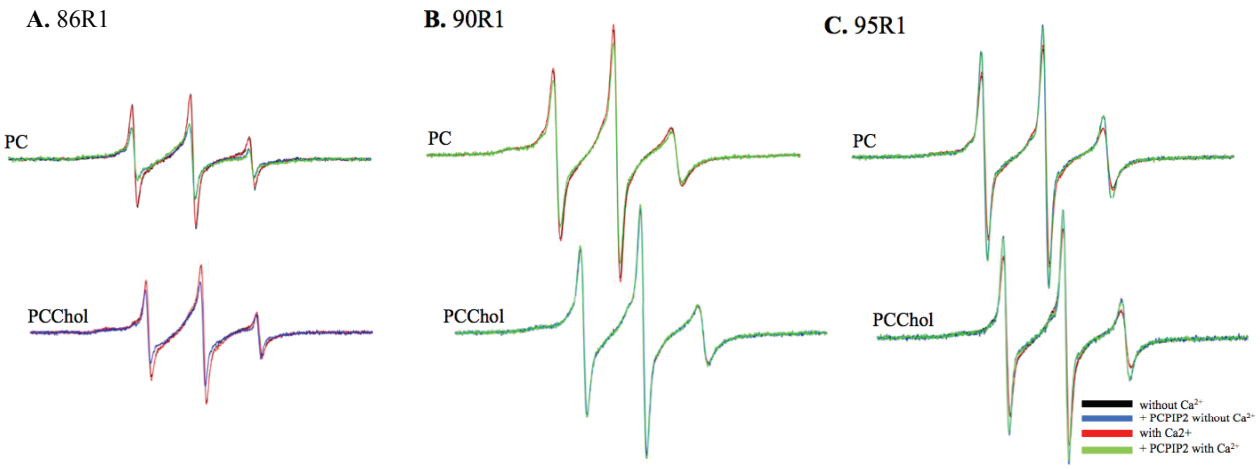

Figure 6.13: Addition of PC:PIP_2 liposomes trans presents subtle changes in the juxta-membrane linker state. A. 86R1 in PC (top) and PCChol (bottom) proteoliposomes alone (black and red without and with calcium) the CW is broadened due to insertion into the membrane. Addition of PCPIP_2 liposomes decreases the mobility of this site calcium independently, potentially pushing it further into the membrane (blue and green without and with calcium). **86R1 PC:Chol excludes PC:PIP_2 no calcium (with calcium shown in blue) B. 90R1 in PC (top) and PC:Chol (bottom) proteoliposomes alone the CW is mobile and in the aqueous phase (black and red without and with calcium). Addition of PC:PIP_2 liposomes very slightly decreases the mobility of this site in the PC case, but not the PC:Chol condition, potentially pushing the site toward one of the two membranes (blue and green without and with calcium). C. 95R1 in PC (top) and PC:Chol (bottom) proteoliposomes alone the CW is mobile and in the aqueous phase (black and red without and with calcium). Addition of PC:PIP_2 liposomes increases the mobility of this site in potentially due to tugging or strain of the linker toward one of the two membranes (blue and green without and with calcium).

6.2.7 Charge slightly increases oligomerization of the juxta-membrane linker

The next set of experiments sought to investigate if the addition of charge, to better match the physiological system, affects the state of the linker as was suggested previously[26]. The two most extreme sites, FL SYT 86R1 and 95R1 were investigated, as site 90 showed less significant changes above. Reconstitutions were performed in PC:PS (90:10) and PC:PS:PIP_2 (90:6:0.25) first to mimic the synaptic vesicle, and second to see if charge density/clustering enhances any observed effects. Measurements were again taken using CW, power saturation, and pulsed EPR and were performed with and without calcium to investigate triggering dependence. For FL SYT 86R1 and

95R1 the CW lineshape changes were independent of calcium, but a difference between the two lipid compositions was observed. In both cases, the addition of PIP_2 to the membrane slightly broadens the lineshapes relative to PC:PS alone. For FL SYT 86R1 the overall lineshapes are also slightly more-broad, with a much smaller immobile component than the charge-less reconstitutions above (A in *Figure 6.14*). FL SYT 95R1 lineshapes relative to the charge-less cases above actually sharpened the mobile component and showed a less pronounced immobile component (B in *Figure 6.14*). Power saturation measurements revealed that all FL SYT 86R1 conditions are nearly within error, inserted 1-2 angstroms into the bilayer (*Table 6.2*). FL SYT 95R1 power saturation revealed nearly aqueous measurements, which were all roughly within error of each other, and less aqueous than charge-less reconstitutions. However, it is unclear if these measurements were solely relative to the *cis* membrane, or relative to both *cis* and *trans* membranes, as the C2 domains would be tethered to other proteoliposomes under these conditions (*Table 6.2*). DEER measurements displayed an overall increase in modulation depth of between 2% - 6% for FL SYT 86R1 and between 2% - 5% for FL SYT 95R1, indicating an increase in aggregated population when the protein is reconstituted into a charged bilayer. There was no overall trend among FL SYT 86R1 DEER measurements, but 95R1 modulation depths did increase upon addition of PIP_2 and the addition of calcium, so a population of protein can indeed aggregate. With the knowledge of the above observations, measurements could then be attempted to better mimic *cis* and *trans* binding under more physiological conditions, with charge present on both membranes.

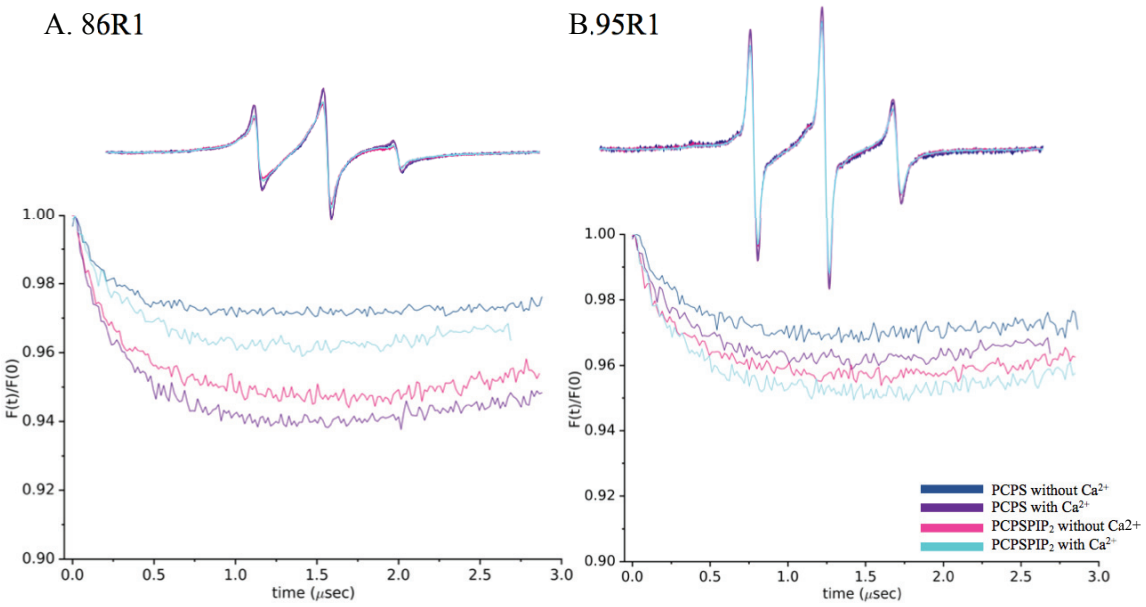

Figure 6.14: Charge increases small population of Juxta-membrane linker oligomers. A and B. 86R1 in the linker near the transmembrane interface CW appears broadened in all PC:PS and PC:PSP:PIP_2 90:6:0.25) cases, likely due to interactions with the membrane. Addition of charge to the membrane also increases aggregation occurring at this site. This slight degree of aggregation is enhanced upon addition of calcium. B. Charge at 95R1 site also enhances aggregation, but less so than 86R1. There is a slight decrease in CW mobility reconstituted just into PC:PS:PIP_2 liposomes, but PC:PS membrane result in slightly closer to the membrane power saturation measurements along with a decreased population of aggregation relative to PC:PS:PIP_2. Both aggregation populations are slightly enhanced in the presence of calcium.

protein variant	lipid conditions	metal added	depth parameter (Φ)	position from lipid phosphate (Å)
FL SYT 86R1	PC:PS (10%)	Ca^{2+}	–1.0 ± 0.1	2.24
	PC:PS (10%)	EGTA	–1.2 ± 0.1	1.09
	PC:PS:PIP_2 (6: 0.25%)	Ca^{2+}	–1.2 ± 0.2	1.37
	PC:PS:PIP_2 (6: 0.25%)	EGTA	–1.1 ± 0.2	1.82
FL SYT 95R1	PC:PS (10%)	Ca^{2+}	–2.1 ± 0.1	–4.91
	PC:PS (10%)	EGTA	–2.1 ± 0.1	–5.08
	PC:PS:PIP_2 (6: 0.25%)	Ca^{2+}	–2.1 ± 0.2	–4.94
	PC:PS:PIP_2 (6: 0.25%)	EGTA	–2.3 ± 0.2	aqueous

Table 6.2: Depth Parameters for Full-Length Membrane Reconstituted Syt1 Linker Mutants in Charged Bilayers. Negative depths are positioned on the aqueous side of the membrane phosphate plane; positive values are positioned toward the hydrocarbon interior. Ca^{2+} is added to 1 mM. Depth parameters which place the spin label 5 Å or further from the lipid phosphates are marked in the aqueous phase. Full-length Syt1 is present at approximately 75 μM concentration with a total lipid concentration of 15 mM to yield a protein/lipid ratio of approximately 200.

6.2.8 Mimicking the synaptic vesicle and plasma membrane, cis and trans binding of the C2A and C2B domain can be differentiated when there is charge on both the cis and trans membranes

Introducing charge onto both the reconstituted *cis* membrane to mimic the synaptic vesicle and *trans* membrane to mimic the plasma membrane creates a complex, but more physiologically relevant, set of conditions and set of variables which can influence C2A and C2B binding and orientation. An attempt to separate *cis* and *trans* binding was performed by a series of CW EPR measurements with and without charge, using PC:PS (90:10) on the *cis* membrane to isolate trans binding and mimic the PS on the synaptic vesicle. Then measurements were made with and without the addition of PC:PS:PIP_2 (90:6:0.25) and PC:PIP_2 (95:5) liposomes to isolate *cis* membrane interactions. Lineshape changes were then observed when *trans*, plasma membrane memetic liposomes were present. PC:PS:PIP_2 and PC:PIP_2 comparisons were both taken to better isolate differences in lineshape between PS and PIP_2 interactions. Each condition was performed first in the absence of calcium, to look at any calcium independent interactions of the domains. Measurements were then taken with calcium to see how the calcium trigger event influenced membrane insertion.

As a first comparison, both the C2A (173R1) and C2B (304R1) domains within FL SYT CW EPR were taken in PC:PS, with and without calcium and then with the addition of PC:PIP_2 (A in *Figure 6.15*). Before the addition of calcium, the addition of PC:PIP_2, *trans* vesicles does slightly alter the lineshape of the C2A site, but not significantly, and both are still characteristic of aqueous loops (B in *Figure 6.15*). The C2B site is slightly more broadened upon addition of *trans* liposomes, which is likely due to calcium-independent *trans* binding to PIP_2 (B in *Figure 6.15*). Upon addition of calcium, in all cases the C2A and C2B sites insert into the membrane. The

lineshapes for the C2A domain and the C2B domain with and without the addition of *trans* liposomes are very similar, with very slight differences in each case. This potentially indicates a mixed state of *cis* and *trans* population, although the lineshapes are not easily isolated for PS versus PIP_2 binding (C in *Figure 6.15*). 304R1 does display an increased immobile component when *trans* liposomes are present, but an easier comparison will be made in the figures below (in *Figure 6.17*).

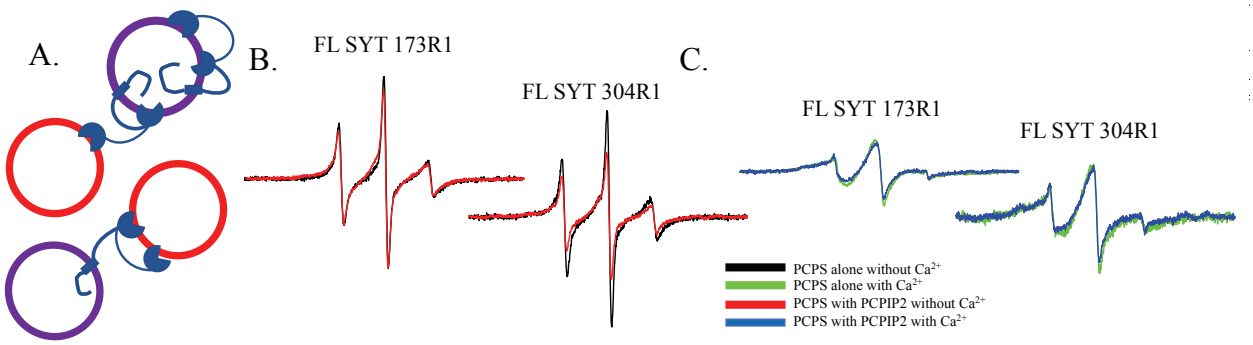

Figure 6.15: C2A and C2B domains state is altered in the full-length protein with charge on the cis membrane when trans vesicles are present. A. Representative diagram of cis vs trans binding with charge, cis purple, trans red. B. Left: FL SYT 173R1 in PC:PS alone (black) vs. the addition of PC:PIP_2 liposomes in the absence of calcium shows a slight broadening when PIP_2 is present (red). Right: FL SYT 304R1 in PC:PS alone (black) vs. the addition of PC:PIP_2 liposomes in the absence of calcium shows a more enhanced difference and broadening when PIP_2 is present (red). Potentially indicating calcium independent binding. C. Left: FL SYT 173R1 in PC:PS alone (green) vs. the addition of PC:PIP_2 liposomes (blue) in the presence of calcium shows a slight broadening when PIP_2 is present. Right: FL SYT 304R1 in PC:PS alone (green) vs. the addition of PC:PIP_2 liposomes (blue) in the presence of calcium shows a slight broadening when PIP_2 is present.

A more complex lineshape comparison can better isolate the C2A and C2B domains' preference for *cis* or *trans* membrane interaction and insertion. As seen with the soluble constructs in Chapter 3, the C2 domains insert and orient differently into PC:PS, PC:PS:PIP_2, and PC:PIP_2 membranes. These differences, which were verified with power saturation in Chapter 3, also are identifiable by differences in CW EPR lineshape. Through isolating a single characteristic lineshape, either of 173R1 in C2A or 304R1 in C2Bfor each reconstitution and the presence or

absence of calcium, the more complex interactions with charge on both membranes can be compared (overlaid) to infer which direction the C2A and C2B domains prefer to bind, *cis* or *trans*.

First, for the C2A domain, site 173R1 was compared as it was already studied for the lipid conditions used with the soluble construct. Additionally, *trans* binding had already been isolated with PC or PC:Chol reconstituted protein in the ATP inhibition experiments mentioned above. The characteristic *trans* lineshape for addition of PC:PIP_2 vs. PC:PS was first compared within *cis* membranes consisting of either PC:PS, PC or PC:Chol before and then after the addition of calcium (A and B in *Figure 6.16*). For each lipid condition the full CW spectra is overlaid, and then a zoomed region of the high field line is displayed to better highlight differences in lineshape. For 173R1 in calcium free conditions, in all conditions the lineshape appear to be nearly identical because the domain is currently in an aqueous state and not interacting with the membrane (A in *Figure 6.16*). Upon addition of calcium, each lipid condition produces a broadened lineshape, indicating calcium-binding loop insertion (B in *Figure 6.16*). Here, both PC and PC:Chol reconstituted FL SYT in the presence of PC:PIP_2 *trans* liposomes (magenta and teal) produce a less broadened lineshape than the PC and PC:Chol reconstituted FL SYT in the presence of PC:PS *trans* liposomes (maroon and light pink). In this case, when PC:PS is present on the *cis* membrane and PC:PIP_2 is added *trans* (navy), the lineshape more closely resembles the PC:PS conditions, suggesting the C2A domain prefers to insert into the PS-containing *cis* membrane rather than the PIP_2 *trans* membrane. This would agree with the C2A domain's preference for coordination driven insertion into PS over PIP_2 membranes.

Next, the characteristic lineshape for *trans* addition of PC:PS:PIP_2 vs. PC:PS were compared within *cis* membranes consisting of either PC:PS, PC, or PC:Chol before and after the addition of calcium (C and D in *Figure 6.16*). Again, for 173R1 in calcium free conditions the

lineshapes appear to be nearly identical because the domain is currently in an aqueous state and not interacting with the membrane (C in *Figure 6.16*). Upon addition of calcium, each lipid condition produces a broadened lineshape, indicating calcium-binding loop insertion (D in *Figure 6.16*). For the addition of PC:PS:PIP_2, lineshape differences between PS insertion and PS:PIP_2 insertion are not sufficiently different to determine if the C2A domain is binding *cis*, *trans*, or to both membranes. Any would be possible in if the C2A domain prefers to insert into PS-containing membranes. The higher local lipid concentration on the *cis* membrane could potentially drive *cis* insertion over trans, but with this technique it is unclear.

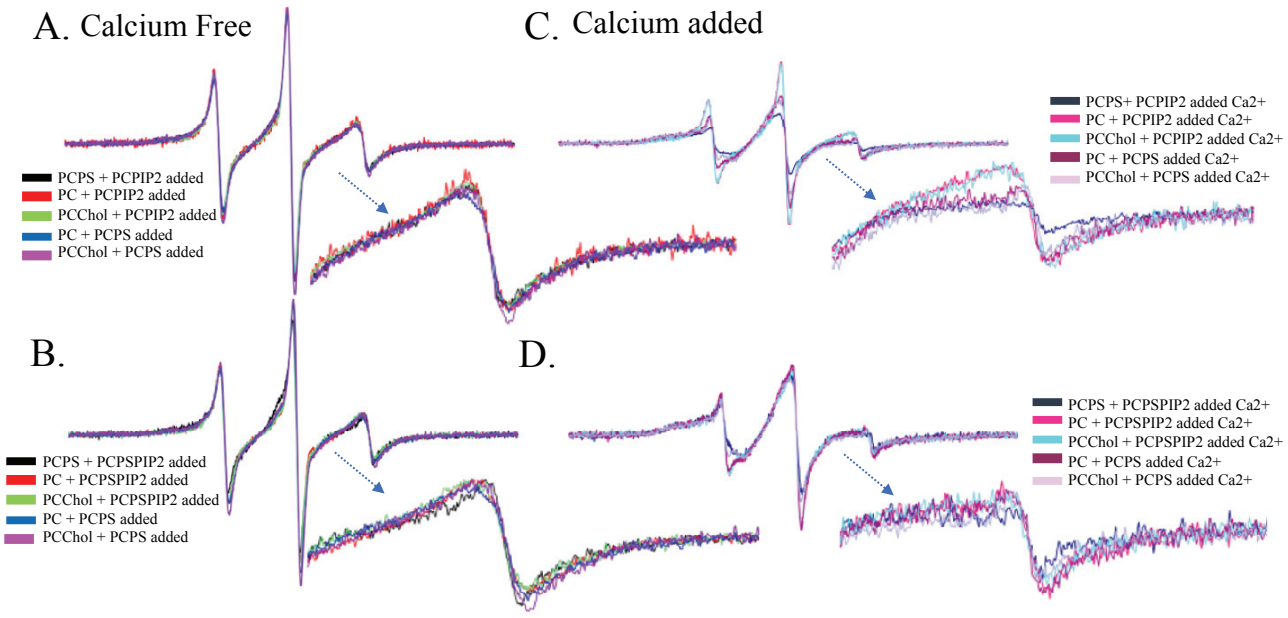

Figure 6.16: C2A domain in the full-length protein likely back-binds cis on the synaptic vesicle when charge is present on both cis and trans (plasma) membrane. Measurements taken using FL SYT 173R1. The first Calcium-binding loop of C2A under calcium-free (A and B) and calcium-containing (C and D) conditions with various lipid reconstitutions and different liposomes added trans. A and B. The calcium free state of 173R1 is in the aqueous phase when reconstituted into PC:PS (black). PC, and PC:Chol with the addition of charged PC:PS (blue and purple in A and B), PC:PIP_2 (red and green in A) or PC:PS:PIP_2 (red and green in B) does not change this lineshape. C. In the presence of calcium, 173R1 inserts into charged membrane. PC:PS membranes vs PC:PIP_2 membranes result in different lineshapes at this site. When the protein is reconstituted into charge free proteoliposomes (PC and PC:Chol), charged liposomes are added to observe these lineshapes (C. in magenta, teal, maroon and light pink). PC:PS addition is more broadened than the PC:PIP_2 addition. When the protein is reconstituted into charged PC:PS proteoliposomes and PC:PIP_2 is added the lineshape looks like the other PC:PS lineshapes. D. In the presence of calcium, 173R1 insertion into PC:PS membranes vs PC:PS:PIP_2 membranes results in similar lineshapes. The protein was reconstituted into charge free proteoliposomes (PC and PC:Chol) and then charged liposomes were added (D in magenta, teal, maroon and light pink). When the protein is reconstituted into charged PC:PS proteoliposomes and PC:PS:PIP_2 liposomes are added the lineshape looks more similar to the PC:PS lineshapes.

For the C2B domain, site 304R1 was compared as it was already studied under the lipid conditions in the soluble construct and had isolated *trans* binding with PC or PC:Chol reconstituted protein in the ATP inhibition experiments mentioned above. *Trans* addition of PC:PIP_2 vs. PC:PS was first compared within *cis* membranes consisting of either PC:PS, PC, or PC:Chol before and after the addition of calcium (A and B in *Figure 6.17*). Again, the full CW spectra is shown in addition to an overlay of the high field line. For 304R1 in calcium free conditions, the PC and PC:Chol lineshapes with addition of PC:PS vs the addition of PC:PIP_2 display differ in lineshape (A in *Figure 6.17*). These differences are due to a transition from fully aqueous domains with PC:PS present (purple and blue) to interfacial membrane interactions between PC:PIP_2 and the C2B domain's polybasic face (red and green). The PC:PS *cis* membrane with *trans* PC:PIP_2 also displays this characteristic calcium-independent binding lineshape, indicating that even with charge on the *cis* membrane, the C2B domain is primed to interact *trans*. This confirms the C2B domain's potential for docking and priming of the synaptic vesicle in the neuronal system. Upon addition of calcium, each lipid condition produces a broadened lineshape, indicating calcium-binding loop insertion (B in *Figure 6.17*). Here, both PC and PC:Chol reconstituted FL SYT in the presence of PC:PIP_2 *trans* liposomes (magenta and teal) produce only a slightly less broadened lineshape than the PC and PC:Chol reconstituted FL SYT in the presence of PC:PS *trans* liposomes (maroon and light pink). This could be due to weaker interactions with the PC:PS trans liposomes relative to the C2A domain above. When PC:PS is present on the *cis* membrane and PC:PIP_2 is added *trans* (navy), the lineshape is slightly different from both *trans* conditions, binding more tightly than both the PC:PS and the PC:PIP_2 lineshapes alone. However, after observing the *trans* calcium-independent interaction it would be more likely that the C2B domain would stay on the

trans membrane than breaking the electrostatic interactions between the domain and the membrane to bind *cis*.

Next, the *trans* addition of PC:PS:PIP_2 vs. PC:PS was compared within *cis* membranes consisting of either PC:PS, PC, or PC:Chol before and after the addition of calcium (C and D in *Figure 6.17*). For 304R1 in calcium free conditions, the PC and PC:Chol lineshapes differ after addition of PC:PS vs PC:PS:PIP_2 liposomes (C in *Figure 6.17*). These differences are again due to a transition from fully aqueous domains with PC:PS present (purple and blue) to interfacial membrane interactions between PC:PIP_2 and the C2B domain's polybasic face (red and green). The PC:PS *cis* membrane with *trans* PC:PIP_2 also displays this characteristic calcium-independent binding lineshape, indicating that even with charge on the *cis* membrane, the C2B domain is again primed to interact *trans* (C in *Figure 6.17*). Upon addition of calcium, each lipid condition produces a broadened lineshape, indicating calcium-binding loop insertion (D in *Figure 6.17*). For the addition of PC:PS:PIP_2, much like the C2A domain, the lineshape differences between PS insertion and PS:PIP_2 insertion are not different enough to determine if the C2B domain is binding *cis*, *trans*, or to both membranes. Again, the condition with charge on both membranes is slightly more bound than in either of the isolated membrane cases. It would again be more likely, however, that calcium-independent electrostatic interactions are not broken to drive the C2B domain to the *cis* membrane.

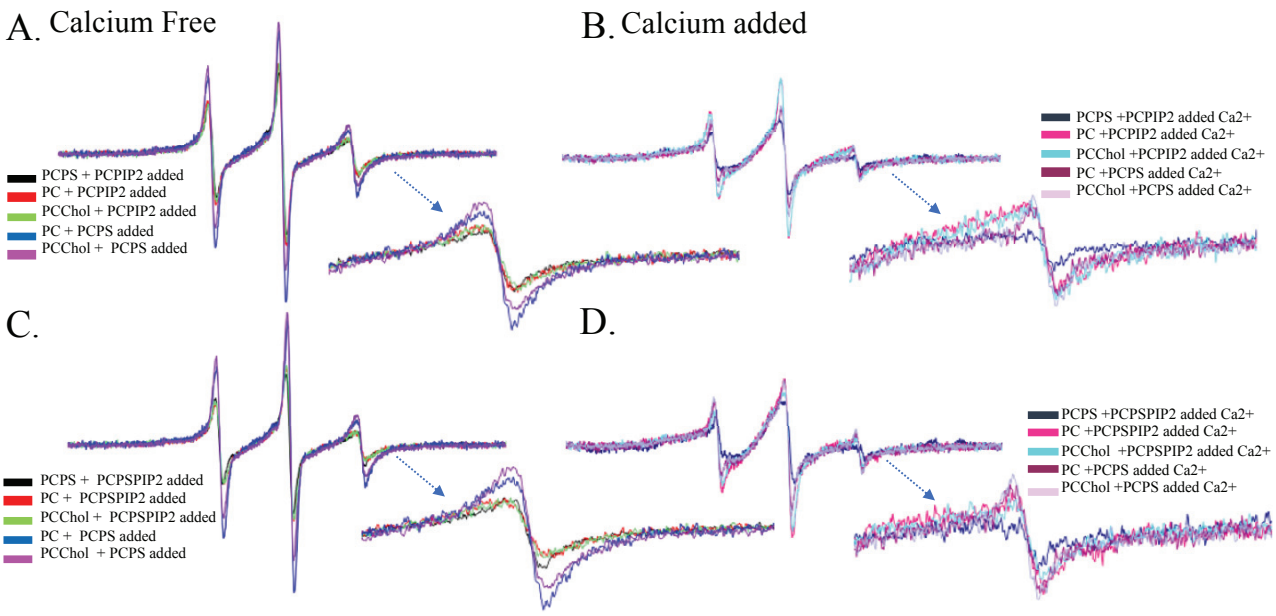

Figure 6.17: C2B domain in the full-length protein bridges trans onto the plasma membrane when charge is present on both cis (synaptic vesicle) and trans membranes. FL SYT 304R1, the first calcium-binding loop of C2B under calcium-free (A and C) and calcium-containing (B and D) conditions with various lipid reconstitutions and different liposomes added trans. The calcium free state of 304R1 is in the aqueous phase when reconstituted into PC:PS (black in A and B), PC, and PC:Chol. A and B. Addition of Charged PC:PS (blue and purple in A and B) vs. PC:PIP_2 (green and red in A) or vs. PC:PS:PIP_2 (red and green in B) liposomes display different, more broadened lineshapes when PIP_2 is present on the membrane. C. In the presence of calcium, 304R1 inserts into charged membrane. PC:PS membranes vs PC:PIP_2 membranes result in different broadened lineshapes of the R1 label at this site. When the protein is reconstituted into charge free proteoliposomes (PC and PC:Chol) and charged liposomes are added (C in magenta, teal, maroon and light pink), PCPS gives a more broadened lineshape than the PC:PIP_2 addition. When the protein is reconstituted into charged PC:PS proteoliposomes and PC:PIP_2 is added the lineshape looks slightly more-broad than both the PC:PS and PC:PIP_2 lineshapes. D. In the presence of calcium, 304R1 insert into charged membrane, and PC:PS membranes vs PC:PS:PIP_2 membranes result in nearly identical broadened lineshapes of the R1 label. The protein was reconstituted into charge free proteoliposomes (PC and PC:Chol) and charged liposomes were added (D in magenta, teal, maroon and light pink). When the protein is reconstituted into charged PC:PS proteoliposomes and PC:PS:PIP_2 is added the lineshape is more-broad than the PC:PS and PC:PS:PIP_2 lineshapes.

Next, the cholesterol effect of membrane binding was briefly explored by adding both PS and cholesterol to the *cis* membrane and continuing to analyze the CW EPR lineshape. The addition of cholesterol to the *cis* membrane had already been seen to alter the lineshape relative to PC alone, and unfortunately addition of cholesterol to the *cis* membrane also alters the lineshapes of the C2 domains shown here. For 173R1, much like the previous comparison, the calcium independent lineshapes are nearly identical for every lipid condition, again due to the domain being free in solution and not engaging in membrane interactions (A in *Figure 6.18*). The addition of calcium then broadens all of the lineshapes for PC:PS:Chol reconstitutions as does PC:PS and PC:PIP_2 trans binding. Here, PC:PS:Chol does not change in lineshape with the addition of PC:PIP_2 *trans*, however the lineshape is intermediate in broadening relative to the deeper PC:PS alone or shallower PC:PIP_2 alone cases (A in *Figure 6.18*). The similarity between PC:PS:Chol alone and the addition of *trans* liposomes likely indicates that the C2A domain prefers to insert into the *cis* membrane. The C2B domain again shows a significant change in lineshape between PC:PS and PC:PIP_2 *trans* additions, due to broadening in the PC:PIP_2 case from calcium-independent binding (B in *Figure 6.*18). The *trans* addition of PC:PIP_2 in the PC:PS:Chol reconstitution is again identical to the PC:Chol reconstitution, but unfortunately the PC:PS:Chol alone case is also quite similar. This could be solely due to the slightly different lineshapes between PC and PC:Chol or because of a potential for higher degrees of PS sequestration if cholesterol is present on the membrane. If the PS can sequester to sufficient charge density the polybasic face will also interact calcium-independently, which would inhibit some C2B domains from interacting *trans*[3]. Calcium-dependent insertion of the C2B domain again displays insertion into all charged lipid conditions (B in *Figure 6.*18). The PC:PS and PC:PIP_2 *trans* binding lineshapes are different, with PIP_2 (teal) being slightly more broadened and displaying less of a mobile component

compared to PS (magenta). PC:PS:Chol and PC:PS:Chol with PC:PIP_2 added *trans* again display similar lineshapes to each other, in this case both being more similar to PC:PIP_2 *trans* binding. In the PC:PS:Chol case alone there is a very subtle indication of a larger population of mobile component, relative to the addition of PC:PIP_2 liposomes, which is present only in PS insertion. This hint, with the knowledge that previous measurements above with charge on each membrane contributed to a less pronounced mobile component relative to charge on only the *trans* membrane, highlights a difference between the PC:PS:Chol alone and PC:PIP_2 added conditions. The domain should still preferentially insert *trans*, but again the evidence is not as strong as the previous measurements, since the lineshapes are more similar under all conditions.

After demonstrating that charge on both membranes can influence the C2 domains preference towards one membrane or the other, and that this interaction can be isolated by differences in lineshape, pulsed-EPR measurements were undertaken to see if distance distributions could also cleanly isolate *cis* or *trans* binding between the C2A and C2B domains of FL SYT.

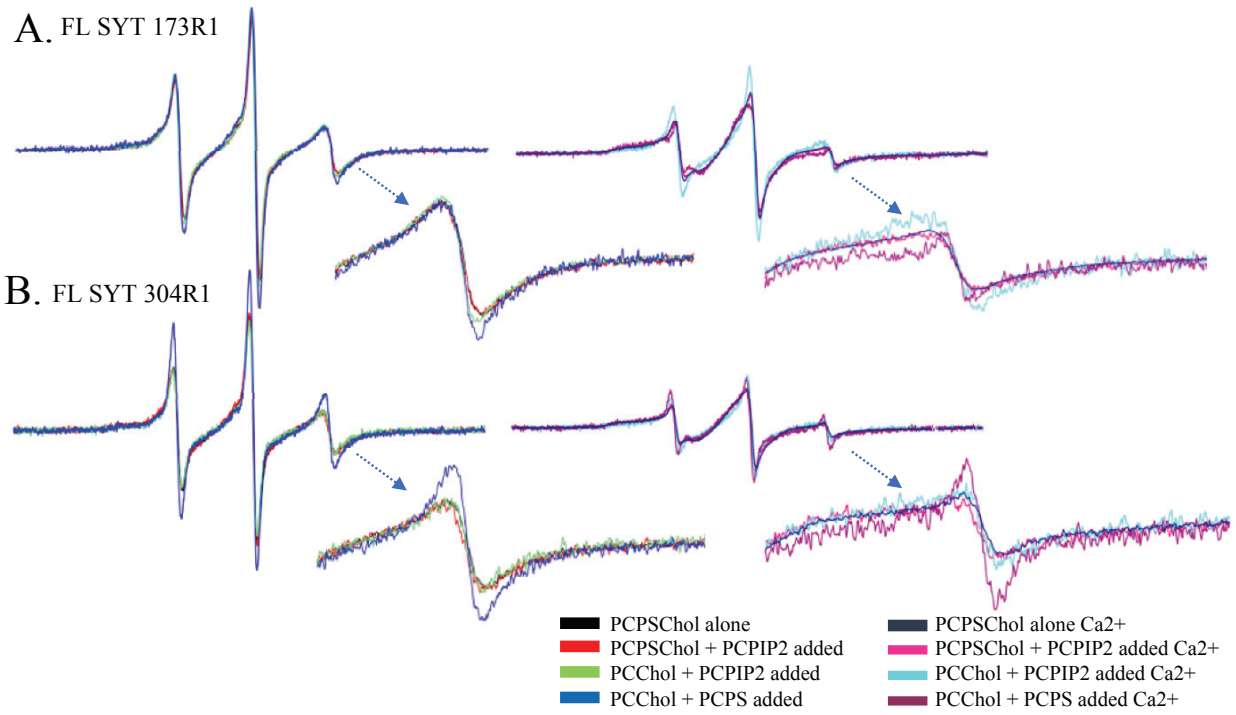

Figure 6.18: Does cis and trans binding change when there is cholesterol on the cis membrane? A. FL SYT 173R1, the first calcium-binding loop of C2A under calcium-free and calcium-containing conditions with various lipid reconstitutions and different liposomes added trans. The calcium free state of 173R1 is in the aqueous phase when reconstituted into PC:PS:Chol (black) and PC:Chol. Addition of Charged PC:PS (blue) or PC:PIP_2 (red and green) liposomes does not change this state or lineshape. Adding Calcium, 173R1 differentially inserts into these membranes resulting in different lineshapes of the R1 label at this site. When the protein is reconstituted into charge free proteoliposomes (PC:Chol), liposomes are added to observe these lineshapes (maroon vs teal). PC:PS addition trans results in a more broadened lineshape than the PC:PIP_2 addition. When the protein is reconstituted into PC:PS:Chol alone (black) the lineshape is slightly more mobile. Addition of PC:PIP_2 (pink) does not change this shape. B. FL SYT 304R1 in the first calcium-binding loop of C2B under calcium-free and calcium-containing conditions with various lipid reconstitutions and different liposomes added. The calcium free state of 304R1 is in the aqueous phase when reconstituted into PC:PS:Chol (black) and PC:Chol. Addition of PC:PS (blue) vs. PC:PIP_2 (red and green) liposomes display different, more broadened lineshapes when in the presence of PIP_2. Adding Calcium, 304R1 inserts into membrane, PC:PS (maroon) membranes vs PC:PIP_2 (teal) membranes resulting in different broadened lineshapes of the R1 label at this site. Here PIP_2 is more-broad than PS. Addition of PS to the cis membrane results in the same lineshape when PC:PIP_2 (pink) is added when compared to the PC:PS:Chol lineshape vs. PC:Chol plus PC:PIP_2 lineshape.

6.2.9 Distance measurements between C2A and C2B domains using DEER display heterogeneity in the C2A and C2B configuration

Pulsed EPR was used to examine distances between the C2A and C2B domains on FL SYT under differing lipid conditions to attempt to isolate *cis* and *trans* binding distances of FL SYT as a distance regulator. One site on the C2A domain, 173R1, was selected in combination with three sites on the C2B domain, 304R1, 323R1, and 395R in order to localize the distances and orientations of the two domains relative to each other. Samples were run in sequence, with each double mutant first reconstituted into PC:PS proteoliposomes. Measurements were taken under calcium-free conditions to look at the distribution of distances between the C2A and C2B domains freely floating in solution. Second, 1 mM calcium was added with the goal of producing full *cis* back-binding to the PC:PS proteoliposomes to which each protein is tethered. Third, PC:PIP_2 liposomes were added at a 1:1 ratio to mimic the plasma membrane in the absence of calcium (EGTA) to promote calcium-independent binding. Fourth, 1 mM calcium was again added to the system to promote insertion of the calcium binding loops, with the goal of observing *trans* binding. The data was fit to both single and double Gaussian distributions, as both fits were equally as probable. Both will be discussed below.

In single population fits, the data for each site produces a broad distribution under the varying conditions. This data is consistent with previous attempts to perform pulsed EPR and model the tandem-C2 domains in solution, in PC:PS, and in PC:PS:PIP_2[24,40]. These distributions can be compared to the soluble C2AB tandem construct which has been modeled based on restraints in previously published work[24,40]. In these data sets, power saturation and DEER measurements which were fit to a single Gaussian distribution were used as restraints to localize and model the C2A and C2B domains relative to each other and relative to a two-plane membrane

of either PC:PS or PC:PS:PIP_2 in the presence of calcium[24,40]. The tandem domains were also modeled in the absence of membrane either with restraints produced in the presence or absence of calcium or unrestrained. The resulting distances from lowest energy structures will be used as comparative distributions for FL SYT.

For FL SYT 173R1-395R1, the labels are placed in the calcium binding loops of the C2A domain and the arginine apex of the C2B domain, roughly the full 50 Å distance of each domain apart, when the two domains are oriented with each calcium binding loop on the same membrane. When the domains are oriented against each other, and thus potentially bound to opposing membranes, the distances are expected to be shorter. This distance also depends on the domains' proximity and tilt angle dictated by the 8-residue flexible linker between C2A and C2B. At these sites, both the calcium-free and calcium-containing PC:PS reconstitution alone produce a distribution centered around 50 Å with a width of about 20 Å (A in *Figure 6.19*). For the calcium free case this data does not cleanly fit a single average of DEER restrained-membrane free data from, which estimate a distance of 42 Å, but when the domains were modeled unrestrained, a 49 Å distance fits the data well. This suggests more movement or an additional orientation of the domains when attached to the flexible-juxtamembrane linker (*Table 6.3*). This could in part be due to the population of the C2B domain which can contact the charged linker region. For the calcium bound case, the broad distribution in FL SYT is likely a combination of both *cis* back-binding and *trans* binding to another membrane, as the soluble construct showed a preference for *trans* binding to accommodate the interaction between the arginine apex and the membrane. There is the chance that the domains placed in opposing orientations is a lower energy conformation, but the pull to the enhanced local lipid concentration on the *cis* membrane may be able to overcome this. If the lowest energy structures of potential *cis* and *trans* binding between the soluble constructs are

averaged, the distance would be much shorter, centering at 43 Å, but still within the distribution. However, this distance does cleanly fit the center of the *cis* modeled state at a comparative 53 Å, implying larger population of *cis* binding. This can be better represented in the two state fits below. Addition of PC:PIP_2 liposomes produces a shift to a distribution centered around 47 Å with a slightly smaller width of 18 Å. Calcium addition then lengthens the distance distribution to a center of 49 Å and a width of 22 Å. A calcium-independent binding model for the soluble domains restraining the C2B domain to the membrane without C2A tethered was unavailable to compare to (and will be interesting to model in FL SYT in the future), but a shorter distance and slight narrowing of the distribution between the two opposing sides of the C2 domains is not surprising, as the polybasic face will be the interacting surface on the *trans* membrane (as observed using CW EPR), which restricts the free rotation of the untethered domains and would prevent the additional C2B contacts with the juxta-membrane linker. Unfortunately, the tandem-C2 domains when untethered are free to move in a ~50 Å x 50 Å cube, so distances are not very restricted, but are at least slightly shorter than this estimate. The calcium bound case for t*rans* binding lengthens the observed distribution again, but it remains slightly shorter than in PC:PS. this time longer than either the single or two state distributions can model, however this is likely due to slight differences in tilting of the C2B domain between PC:PS:PIP_2 membranes and PC:PIP_2 membranes as observed with power saturation in Chapter 3. This could also be due to additional factors, such as extra strain on the tandem-linker lengthening the distance, the bulky PIP_2 pushing the domains slightly farther away from one and other, or orientation competition with the arginine apex (which will be measured as a future work relative to differing membrane conditions in FLSYT).

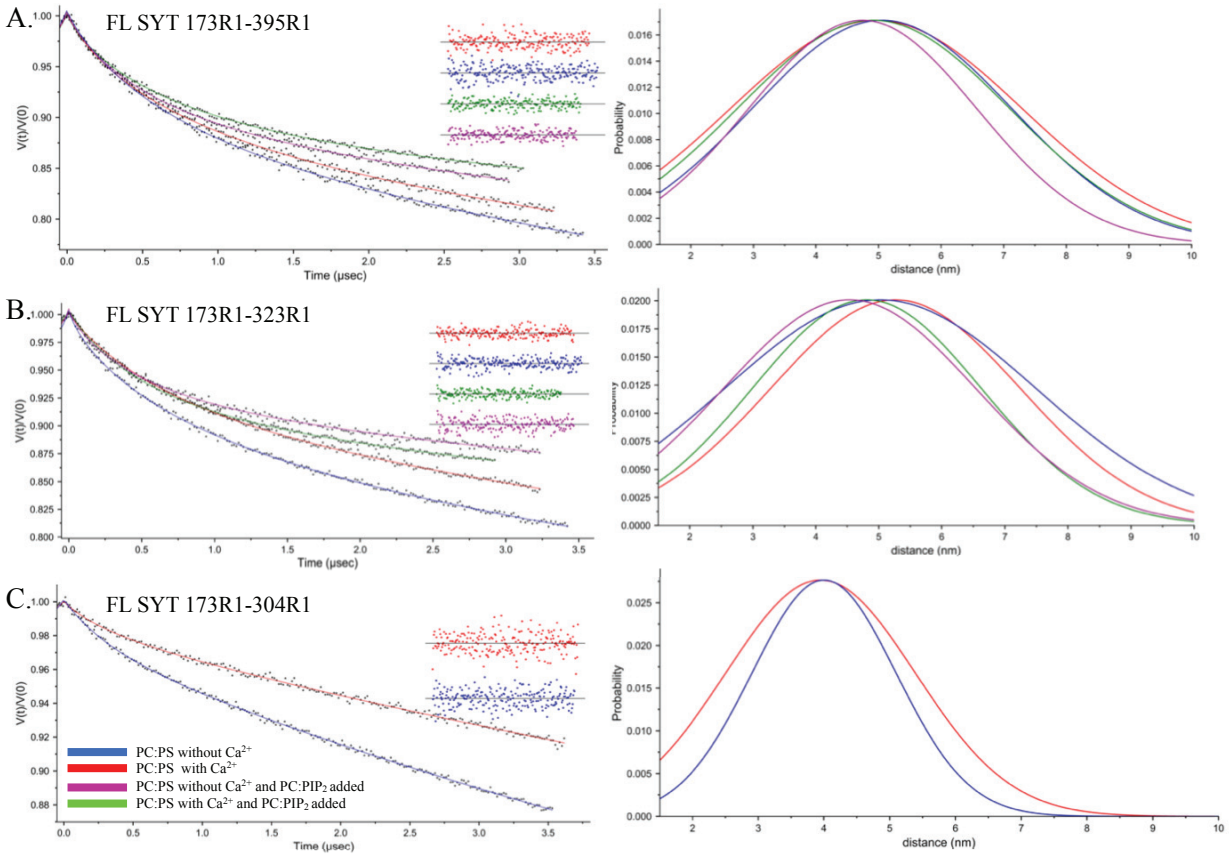

Figure 6.19: Single Population fit for distance distributions of C2A and C2B sites in FL SYT. Sites between the C2A and C2B domain were measured reconstituted in PC:PS without and with Calcium to observe relative orientations of the domains during cis interactions, preceding and post calcium influx (blue and red). PC:PIP_2 liposomes were then added to mimic trans binding both without and with calcium to look at relative domain orientations with calcium-independent binding of the polybasic face then potential trans insertion into membrane (green and magenta). FL SYT 173R1-304R1 was run for PC:PIP_2 addition, due to poor labeling efficiency resulting in small modulation depth. Analyzed in DD.

For FL SYT 173R1-332R1, the labels are placed in the calcium binding loops of the C2A domain and by the polybasic face of the C2B domain, roughly a 30 Å vertical distance apart (diagonal distance will vary), when the two domains are oriented with each calcium binding loop on the same membrane. When the domains are oriented against each other the distances are potentially shorter or longer depending on the orientation of the domains (from comparing the modeled domains), again depending on proximity and tilt angle dictated by the 8-residue flexible

linker between C2A and C2B. At these sites, the calcium-free and calcium-containing PC:PS reconstitution alone produce similar distributions centered at 50 Å with a width of about 25 Å and 52 Å with a width of about 20 Å, respectively (B in *Figure 6.19*). For the calcium free case this data does not cleanly fit a single average of DEER restrained-membrane free data, which estimates a distance of 42 Å, again suggesting more movement and pull in the FL SYT construct (*Table 6.3*). For the calcium bound case, the broad distribution in FL SYT is again likely a combination of both *cis* back-binding and *trans* binding to another proteoliposome. The averaged *cis* and *trans* binding between the soluble constructs are slightly shorter centering at 46 Å, but still within the distribution. However, this distance again fits the center of the *cis* modeled state at a comparative 50 Å, suggesting a larger population of *cis* binding. Addition of PC:PIP_2 liposomes produces a shift to a distribution centered around 45 Å with a width of 20 Å. Calcium addition again lengthens the distance distribution to a centering around 48 Å with a smaller width of 18 Å. A shorter distance is again not surprising, as the polybasic face will still be the interacting surface on the *trans* membrane, which restricts the degree of available rotation angles between the untethered domains. The calcium bound case for t*rans* binding lengthens the distribution again, but it remains slightly shorter and narrower than in PC:PS. This time, it is also slightly longer than the average of all PC:PS:PIP_2 structures, which centers around 44 Å, but near the longer population of the two-state distribution model at 52 Å. Potentially, this is due to different tandem-orienting of the C2B domain in higher densities of PIP_2 or differential insertion of the calcium binding loops under the two different lipid conditions.

protein variant	lipid conditions	metal added	1 Gauss Distance distribution (Å)	2 Gauss Distance distribution (Å)	PC:PS (25) Structures[24] or PC:PS:PIP_2 (25:1) Structures[33] (Å) (1 state)	PC:PS (25) Structures[24] or PC:PS:PIP_2 (25:1) Structures[33] (Å) (2 state)
FL SYT 173R1-395R1	PC:PS (10%)	EGTA	50 ± 21	30 ± 5 and 55 ± 16	42 ± 17 (all structures)	35 ± 15 (EGTA) 49 ± 9 (unrestrained)
	PC:PS (10%)	Ca^{2+}	50 ± 23	30 ± 7 and 55 ± 18	43 ± 25 (cis and trans)	27.5 ± 16 (trans) 52 ± 20 (cis)
	+ PC:PIP_2 (5%)	EGTA	47 ± 18	30 ± 11 and 55 ± 16	Structures unavailable	Structures unavailable
	+ PC:PIP_2 (5%)	Ca^{2+}	49 ± 22	30 ± 10 and 55 ± 11	36.5± 28 (trans PC:PS:PIP_2)	25 ± 15 and 40 ± 7 (trans PC:PS:PIP_2)
FL SYT 173R1-323R1	PC:PS (10%)	EGTA	50 ± 25	29 ± 7 and 54 ± 11	42 ± 13 (all structures)	43.5 ± 10 (EGTA) 35.5 ± 11 (unrestrained)
	PC:PS (10%)	Ca^{2+}	52 ± 20	29 ± 7 and 54 ± 13	46 ± 15 (cis and trans)	41 ± 7 (trans) 50± 15 (cis)
	+ PC:PIP_2 (5%)	EGTA	45 ± 20	29 ± 11 and 54 ± 15	Structures unavailable	Structures unavailable
	+ PC:PIP_2 (5%)	Ca^{2+}	48 ± 18	29 ± 8 and 54 ± 15	44 ± 17 (trans PC:PS:PIP_2)	35 ± 10 and 52 ± 5 (trans PC:PS:PIP_2)
FL SYT 173R1-304R1	PC:PS (10%)	EGTA	40 ± 21	**	34 ± 16 (all structures) (41 ± 13 EGTA DEER[88])	36 ± 10 (EGTA) 31± 16 (unrestrained)
	PC:PS (10%)	Ca^{2+}	39 ± 14	**	36 ± 15 (cis and trans) (38±19 PC:PS DEER[88])	39 ± 12 (trans) 28 ± 10 (cis)
	+ PC:PIP_2 (5%)	EGTA	*	*	Structures unavailable	Structures unavailable
	+ PC:PIP_2 (5%)	Ca^{2+}	*	*	44 ± 7 (trans PC:PS:PIP_2)	40 ± 5 and 46 ± 5 (trans PC:PS:PIP_2)

Table 6.3: Tabular distance distributions of C2A and C2B sites in FL SYT. Sites between the C2A and C2B domain were measured reconstituted in PC:PS without and with Calcium to observe relative orientations of the domains during cis interactions, preceding and post calcium influx. PC:PIP_2 liposomes were then added to mimic trans binding both without and with calcium to look at relative domain orientations with calcium-independent binding of the polybasic face then potential trans insertion into membrane. Distance distributions are fit to 1 or 2 Gauss as seen in Figure 6.19 and 6.20. Distance distributions are then compared to either 1 or 2 population fitting from both DEER data and modeled structures of C2AB tethered from previous work in the lab[24,33]. Distances between sites of interest were estimated using Pymol of the 5 to 10 lowest energy structures of modeled data. All structures represent the average of models fit with restraints for aqueous C2AB with calcium bound, in the presence of EGTA and unrestrained C2AB tethered. EGTA averages are restrained by EGTA data[23]. Unrestrained represents the lowest energy structures modeled without power saturation or DEER data. For PC:PS measurements cis and trans are the averages of all lowest energy structures produced. Trans are restrained by the data in the paper where the C2 domains bind to opposing membranes, dependent on power saturation of the arginine apex[88]. Cis are restrained by the data in the paper unpublished, where the 2 domains bind to the same membrane. Trans PC:PS:PIP_2 in the single Gauss represent the average of all lowest energy structures from the paper[33]. Trans PC:PS:PIP_2 in the two Gauss represent two apparent groupings of distances within the lowest energy structures from the paper[24]. **data not fit due to poor modulation depth, when attempted a population of ~1-2 nm also appeared but did not fit as reliably. *data not taken due to low labeling efficiency.

For FL SYT 173R1-304R1, the labels are placed in the calcium binding loops of the C2A domain and in the calcium binding loops of the C2B domain, close to 12 Å apart vertically (diagonal distances will vary) when the two domains are oriented with each calcium binding loop on the same membrane. When the domains are oriented against each other the distances are expected to be closer to the length of the C2 domain or slightly longer at up to 60 Å depending on orientation. At these sites, the calcium-free and calcium-containing PC:PS samples produced similar distributions centered at 40 Å with a width of about 21 Å and 39 Å with a width of about 14 Å, respectively (C in *Figure 6.19*). Here, the modulation depths for these measurements were very small, due to poor labeling of one of the two sites, so only a single component could be fit, but there was evidence in the trace for a shorter distance (below 2 nm) which was unable to be fit consistently using analysis programs. For the calcium free case this length is slightly longer than the estimated average distance of 34 Å. However, this pair has also been directly measured in the soluble construct which gave a distribution centered at 41 Å, which more closely aligns with the FL SYT data. This deviation in the soluble models highlights a potential bias in the modeled structures, as the DEER distribution falls on the farther side of averaged measurements (and will again for the calcium case). These models also are fit to only one population, which makes it easier to compare to single distributions but may not fully explain the data. For the calcium-bound case the same trend appears, where the averaged structures here estimate slightly shorter at 36 Å, but the DEER measurement is centered at 38 Å. The soluble DEER distribution is much wider and accommodates longer distances from which the models fit *trans* binding of up to 58 Å. In this pair it is more difficult to say if the distribution corresponds to larger *cis* or *trans* populations as the distribution is closer to the *trans* averaged model, but the shorter *cis*-equivalent distance could not be consistently fit.

For the two population fits for FL SYT 173R1-395R1, the centered distance for each peak highlight two locations at 30 Å and 55 Å with varying percentages and widths for the two distances under each condition. The calcium-free PC:PS reconstitution produces a distribution of 30 ± 5 Å and 55 ± 16 Å and for the calcium containing case, 30 ± 7 Å and 55 ± 18 Å (A in *Figure 6.20*). These distances fall on extreme ends of the distributions of aqueous modeled restrained and unrestrained data as seen in the table (*Table 6.3*). For the calcium-bound case these distances fit the differing distances estimated for a population of *cis* and *trans* binding to the proteoliposomes with distances of 27.5 ± 16 (*trans*) and 52 ± 20 (*cis*), reflecting a larger population of *cis* binding. Addition of PC:PIP_2 liposomes in the absence of calcium produces a population of 30 ± 11 Å and 55 ± 16 Å, where the displayed distance distribution almost appears to be a single population (magenta in A of *Figure 6.20*). The broader shorter population could be due to more intermediate distances when the orientation of the C2B domain is restricted on the *trans* membrane. Calcium addition with PC:PIP_2 liposomes moves to a larger shorter population at 30 ± 10 Å and narrows the longer distribution to 55 ± 11 Å, cutting off longer components observed in the PC:PS alone cases (which represented *cis* binding) and untethered domains. These components fit the two differing populations of low energy *trans* structures for PC:PS:PIP_2 of 25 ± 15 Å and 40 ± 7 Å. The distances modeled here surround the again increased smaller population of FL SYT.

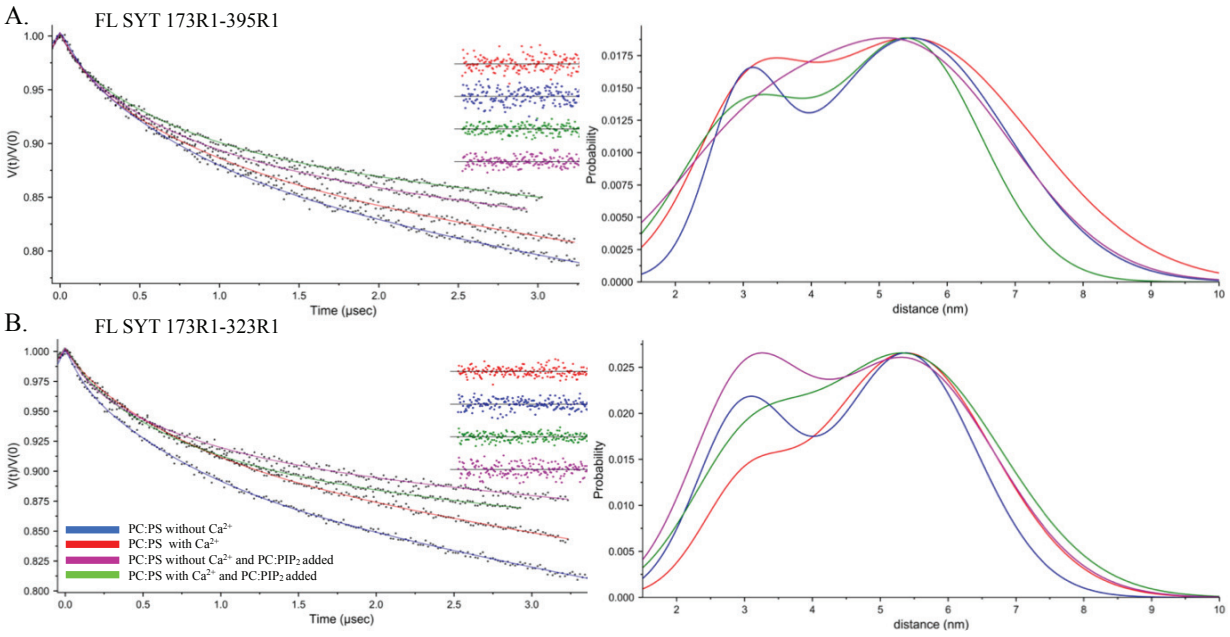

Figure 6.20: Two Population fit for distance distributions of C2A and C2B sites in FL SYT. Sites between the C2A and C2B domain were measured reconstituted in PC:PS without and with Calcium to observe relative orientations of the domains during cis interactions, preceding and post calcium influx (blue and red). PC:PIP_2 liposomes were then added to mimic trans binding both without and with calcium to look at relative domain orientations with calcium-independent binding of the polybasic face then potential trans insertion into membrane (green and magenta). FL SYT 173R1-304R1 was not fit to two gauss, due to poor labeling efficiency resulting in small modulation depth. Analyzed in DD.

For the two population fits for FL SYT 173R1-323R1, the centers of each peak are around 29 Å and 54 Å with the width and relative population of each component again varying for each condition. The calcium-free PC:PS reconstitution produces a distribution of 29 ± 7 Å and 54 ± 11 Å while the calcium containing case gives 29 ± 7 Å and 54 ± 13 Å (B in *Figure 6.20*). These distances again fall on both ends of the distributions of aqueous modeled restrained and unrestrained data as seen in the table (*Table 6.3*). For the calcium-bound case these distances better fit the estimated (modeled) distributions of a population of *cis* and *trans* binding to the proteoliposomes with distances of 41 ± 7 (*trans*) and 50 ± 15 (*cis*). The short distance population is very small in the calcium bound case, suggesting a much larger population of *cis* binding in FL

SYT. Addition of PC:PIP_2 liposomes in the absence of calcium produces a population of 29 ± 11 Å and 54 ± 15 Å, with a much larger shorter population potentially due restricted mobility of the C2A domain and the orientation of the C2B domain on the *trans* membrane. Calcium addition with PC:PIP_2 liposomes maintains but somewhat merges the two population at 29 ± 8 Å and 54 ± 15 Å but decreases the short component relative to the calcium independent case, likely due to reorientation of the C2B domain to accommodate loop insertion. Compared to the low energy *trans* structures for PC:PS:PIP_2 of 35 ± 10 Å and 52 ± 5 Å, the broadening could be due to an increase in intermediate distances which would fit the model.

Overall, either population of the pulsed EPR analysis displays a decent degree of heterogeneity between domain populations (*Figure 6.21*). This is likely due in part to the movement of the tandem-C2 domains in space relative to one another, which would continue even when the domains are membrane tethered. This heterogeneity also agrees with the small population variation present throughout the pulsed EPR measurements of the juxta-membrane-linker. The FL SYT construct could also begin in varying starting points due to additional contacts with the linker biasing the C2B domain onto a particular side of the C2A domain, potentially leading to restriction of the tandem-linker as well. To best sort out these distances and attribute them to differing orientations of the domains the FL SYT should be modeled, similarly to the soluble domains, but with a greater number of restraints (with techniques mentioned in the future directions below). Heterogeneity of the domain orientation does not mean that distances are not cleanly regulated here, as the distance between the two bilayers is still not directly known, the orientation of the C2 domains can only suggest a distance. FLIC measurements will hopefully further quantify relative distances between these surfaces. Varying orientations between C2A and C2B domains may also be of benefit to the neuronal system as other bulky regulatory proteins, the zippering-SNARE

complex and the bilayer itself are likely in constant motion around the C2 domains, which will need to move to accommodate or drive change on these surfaces, whether it is to better sequester lipid or to allow movement of other proteins nearby. The latter could include proteins such as synaptobrevin or munc13 which must enter the active zone and interact on the *trans* membrane as Syt1 helps move the synaptic vesicle closer to the plasma membrane.

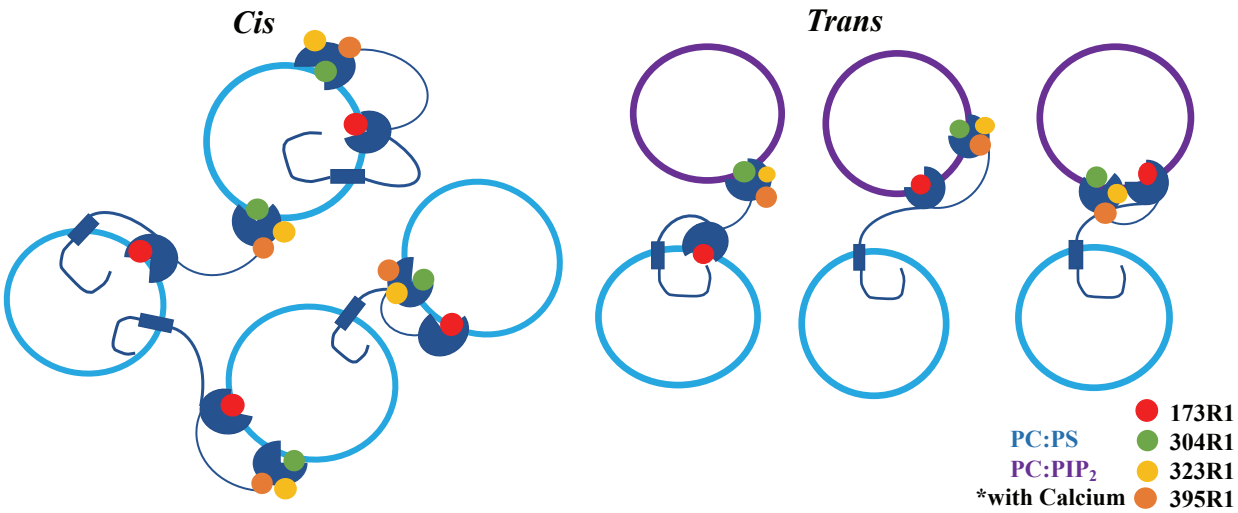

Figure 6.21: Heterogeneity of cis and trans binding between synaptic vesicle mimic, PC:PS reconstitution, and then plasma membrane mimic, the addition of PC:PIP$_2$. When reconstituted into PC:PS upon addition of calcium, the C2A and C2B domains can already bind to the same or to opposing bilayers leading to a mix of cis and trans binding. The domains are also flexible relative to each other, potentially due to the population of the C2B domain back-binding to the juxta-membrane linker, which leads to the large distribution from the DEER measurements. Upon addition of PC:PIP$_2$, the C2B domain will prefer to bind to the PIP$_2$ membrane (from CW observations). The C2A domain could bind to either membrane, likely in a mixed combination with additional heterogeneity of domain orientation relative to each other.

6.3 Discussion

6.3.1 Conclusions

The data presented above attempts to isolate the potential function of Syt1 and determine regulatory contributions from the physiological components within the system (salt and lipids) beyond protein-protein interactions. In the neuron, Syt1 interacts with the membrane surfaces directly, likely playing a regulatory role preceding and during fusion. The C2 domains coordinate calcium, and the calcium binding loops insert into charged lipid membrane through interplay between: charge repulsion neutralization, coordination, electrostatic/Columbic interactions, and hydrophobic weak driving forces[12,16]. On the synaptic vesicle surface, only PS contributes to this negative charge, and on the plasma membrane both PS and PIP_2 contribute to charge density[17].

Syt1 can interact with either of these two bilayer surfaces through either a *cis*-interaction with the synaptic vesicle membrane, or *trans*-interaction with the plasma membrane[15]. *Cis* membrane binding likely plays a critical inhibitory role preceding fusion, by back-binding the domains to the vesicle rather than to the plasma membrane to prevent membrane fusion[15,16]. *Trans* binding of one or both C2 domains to the plasma membrane likely docks and primes the synaptic vesicle to the plasma membrane surface, permitting fusion to occur[15,16]. Both the synaptic and plasma membranes have unique combinations of driving forces which likely promotes preferential binding of the C2 domains to one membrane over the other. These intrinsic properties of each membrane, combined with local charge and ion-based competition likely work together to produce Syt1 function. Each external environmental factor exposes Syt1 to a unique set of conditions in which the protein must respond and change by conformational changes in the linker and domains

to inhibit binding, bind weakly, or bind tightly to a particular membrane. This, in turn produces a protein which acts as a distance regulator between the synaptic vesicle and the plasma membrane.

As discussed in the previous chapters, a few driving forces (excluding additional forces by other proteins in the system) which could promote binding to one membrane over the other could include: Membrane tethering the local lipid concentrations the C2 domains experience on the *cis* membrane are likely much higher than any diffusion-based charge attraction on the plasma membrane[12]. PS sequestering, enhanced by domain coordination to the PS headgroup, could also enhance the local lipid concentration on the *cis* surface[18]. For *trans* binding to occur the driving force must be large enough for at least one of the domains to preferentially interact with the *trans* membrane over the enhanced *cis* membrane. *Trans* binding could overcome the *cis* proximity through the calcium-independent electrostatic interaction between the polybasic face and PIP_2[3,4,17]. If the C2B domain is in close proximity to the *trans* membrane rather than the *cis* it will likely remain on that membrane, producing calcium-dependent *trans* insertion. The synergy between PS and PIP_2 together on the plasma membrane would also promote *trans* binding[17].

Interactions between the polybasic face of the C2B domain and PIP_2 during *cis* or *trans* binding are also expected to be regulated by physiological concentrations and flux in ions and charge around the protein, particularly of poly-valent ions including ATP and Mg^{2+} [16,17,30,31]. As mentioned in the introduction, the cytosolic composition at the site of fusion is composed of a diverse set of ions which work together to maintain balance in the cell and to signal events. The ionic makeup of the aqueous environment around the synaptic cleft is ~140 mM KCl and ~10 mM NaCl, but this changes during the course of an action potential event[41]. Calcium influx also shifts resting levels of 0.1 μM to 1.5-10 μM calcium at the site of fusion. ~1.4 mM (or higher depending on estimations and the stage in vesicle cycling) ATP and magnesium are present in the cell, serving

as energy sources for neuronal exocytosis and endocytosis (ATPases, etc.)[30,31]. ATP levels are known to cycle throughout signaling events, likely through release from reserve pools at times of energy strain[30,31]. While these ions have direct roles for maintaining concentration gradients inside and outside the cell and providing energy to molecular machines, they also have indirect (and regulatory) effects on the lipids and proteins around them. Lipids adsorb ions at specific concentrations, creating an ionic double layer and altering the local ion concentration, including of calcium on the surface which could enhance Syt1 binding[31]. Charge variations, whether through salt or polyvalent ions in the aqueous environment can also shield different protein interactions[10,16].

Previous work has demonstrated the potential regulation of Syt1 activity by electrostatic competition for binding to the polybasic face of the C2B domain between the charged species PIP_2 and ATP. ATP inhibits *cis* binding to the PS-containing vesicle membrane, while potentially promoting *trans* binding to the PIP_2-containing plasma membrane[10,16]. Using vesicle sedimentation assays, the ATP inhibition of PS-containing bilayers and ATP-PIP_2 competition was quantified in the soluble C2AB construct. The measurements displayed a three-fold decrease in C2AB membrane binding to PC:PS membranes in the presence of pyrophosphate alone, and that ATP was sufficient to inhibit membrane binding, which agreed with previous observations. The concentration of ATP required to fully inhibit binding of C2AB PC:PS was found to be under 0.5 mM. However, when 1% PIP_2 is added to the membrane, even 3 mM ATP cannot fully inhibit C2AB-membrane binding.

The site of ATP and PIP_2 competition was explored in Chapter 3; the work here sought to quantify this competition (in a shorter C2B construct)[17]. HSQC-NMR was performed to characterize the interaction between ATP and IP_3, the PIP_2 headgroup. The findings demonstrate that these charged species both contact primarily at the polybasic face at a 1:1 binding

stoichiometry, and IP_3 binds with a higher affinity. The binding affinity for IP_3 to the C2B domain is ~20-fold higher affinity than for ATP. This difference in binding affinity agrees with the competition between PIP_2 and ATP in the sedimentation assays and justifies why such competition could occur in the soluble construct and in the neuronal system. Increased affinity for PIP_2 would overcome any charge shielding and permit *trans* binding in the presence of physiological concentrations of ATP.

This competition was then explored in the FL SYT construct, where *cis* and *trans* binding could occur, to see if membrane tethering alters ATP inhibition due to the increased driving forces to the tethered membrane. After verification that *cis* and *trans* binding could occur and both types of binding could be isolated, ATP was added to the system. In FL SYT *cis* binding to the surface of the tethered domains, in the presence of ATP, was strong enough to overcome previously observed *cis*-inhibition of the soluble domains regardless of lipid composition of the membrane[16]. *Trans* binding, however, showed a mixed population of bound and unbound domains which shifted to unbound as ATP was titrated into the system in the presence of PS or PS with low concentrations of PIP_2, which agrees with observations in the soluble construct[16]. Higher local concentrations of PIP_2 can outcompete ATP binding to the polybasic face of the C2B domain and promote *trans* binding. Unexpectedly, this competition is enhanced if there is cholesterol on the *cis* membrane. Affinity of PIP_2 relative to ATP (as seen in the NMR experiments) to the polybasic face alone should promote *trans* binding if the membrane is in close enough proximity, however cholesterol somehow modulates this effect.

Through investigation of varying hypotheses, the effect of cholesterol on the membrane was examined. This cholesterol effect was not due to ordering or ring formation of the C2B domains which would collect the C2B domain's polybasic faces into a single orientation,

enhancing the cluster's binding to the *trans* membrane. It also could not be fully explained by modulation of the juxta-membrane linker, by pinching of local charged regions, adoption of secondary structure, differential back-binding of the positively charged polybasic face to the negatively charged region of the juxta-membrane linker, or solely by different degrees of aggregation of the linker which could cluster the C2 domains. (Addition of charge to the *cis* reconstituted membrane though, was shown to induce slight amounts of aggregation throughout the juxta-membrane linker.) However, small populations of each hypothesized species (excluding ring formation) were present, suggesting heterogeneity of the state of the juxta-membrane linker overall. The juxta-membrane linker itself is associated partially with the *cis* membrane, but the presence of cholesterol did not significantly change the penetration of or association at the sites examined. However, the initial reconstituted lineshapes of the aqueous C2 domains did vary slightly depending on the presence of cholesterol, which could indicate a more-subtle effect of diffusion or restriction of the transmembrane domain and the protein overall.

Cholesterol is a critical component of a physiological bilayer[42]. The composition and dispersity of cholesterol is also thought to change throughout the stages of neuronal fusion, which has been proposed to regulate the oligomeric state of other key fusion proteins, including syntaxin[42]. While it is clear from the DEER measurements that cholesterol is not promoting full aggregation of FL SYT it could be promoting peripheral effects as it changes the state of the bilayer. Some protein trans-membrane domains have recognition sequences which are known to bind to cholesterol and could produce these effects, but Syt1 does not have any identified (at least traditional) binding location. Cholesterol alone is capable of sequestration which will reduce the fluidity of the bilayer. This could also promote charge sequestration or just restrict Syt1 diffusion throughout the bilayer. Limited diffusion could restrict the protein to certain regions which can

increase accessibility of populations of C2 domains to PIP_2[42]. It could also be altering the curvature of the membrane or the orientation of the transmembrane domains which in some way affects the C2 domains. Cholesterol clustering induces negative curvature, which places strain on the membrane[42]. If in some way Syt1 was modulating cholesterol sequestration rather than cholesterol modulating Syt1 (or both) this could also promote stalk formation. Syt1 can induce positive curvature, and so cholesterol would cluster and promote the negative curvature required to bridge the two bilayers as the stalk forms[1]. Overall, the effect of cholesterol on Syt1 is clearly significant, but not straightforward and *trans* binding can indeed be regulated by physiological concentrations of ATP. Still, it is unlikely that ATP inhibits *cis* binding to promote *trans* contacts as the previous model stated[16].

Cis and *trans* binding were then explored in a more physiological context to attempt to differentiate the C2 domains' insertion into either the synaptic vesicle or the plasma membrane. The C2A domains shows a strong preference to bind to a membrane which contains PS, likely due to coordination driven insertion. However, either due to heterogeneity of binding or just experimental limitations when PS is present on both the *cis* and *trans* membranes it is unclear to which bilayer C2A associates. The C2B domain shows a preference, driven by initial calcium-independent interactions, to associate with the PIP_2-containing plasma membrane mimic in varying conditions, likely then inserting into the associated membrane in the presence of calcium. C2B insertion into the plasma-membrane mimic could in at least some population force the C2A domain onto the *trans* membrane, aided by the synergy between PS and PIP_2 on that membrane as well[17].

Demonstrating a preference of the C2A and C2B domain to differing or mixed membranes, which can be regulated by the addition of physiological concentrations of ATP, suggests that Syt1

is regulating the tethering and thus distances between the synaptic vesicle and plasma membranes. Distance measurements between the FL SYT C2A and C2B domains attempted to localize and quantify the domains' relative orientations, but the measurements displayed significant heterogeneity throughout the system. While there was compelling evidence based on previously collected and modeled data, that *trans* binding is promoted when PIP_2 is present on the bilayer, as distances and distributions changed, it was not a single tight distribution. It is possible that at times the C2A domain is potentially associating with either membrane, or just that the 8-residue tandem-linker is perfectly flexible enough that the two domains can rotate around relative to each-other while tethered to either membrane. Spatially two ~25 angstrom domains attached by a short flexible linker will give the same relative distances as the height of the ~50 angstrom domains in all directions, so subtle changes in tilt and orientation will be somewhat overshadowed. Here, this heterogeneity cannot fully explain the distances which regulate fusion. Additional distance measurements cannot likely cleanly isolate this effect as the other label pairs to probe would be between the domain and sites in the juxta-membrane linker, but the linker itself is highly flexible and even sites right by the transmembrane region would likely lead to a large, heterogeneous distribution due to the C2 domains' mobility. It would then be difficult to determine if this long distance was the product of distant bilayers, with the juxtamembrane-linker stretched between the two, with the C2 domains both binding to the *trans* membrane. Alternatively, the long distance could be the product of very close bilayers, with the C2 domains interacting with opposing membranes and the linker extended away laterally from the C2 domains. Thus, future work will be performed (mentioned below) to attempt to further determine these relative distances, as the distance between the synaptic and plasma membranes is still debated and critical for promoting fusion, as it represents one of the largest energy barriers for stalk formation and bilayer fusion[43].

For SNARE-dependent fusion to occur these proteins must come into close enough proximity to zipper and fuse. Syt1 could somehow regulate these distances preceding, regulating and promoting the fusion event. In this proposal, Syt1 plasma membrane binding promotes fusion by *trans* calcium-independent binding to the plasma membrane, which can be regulated by the local composition of both the synaptic and plasma membrane as well as by ions in the system. High affinity for PIP_2 binding with the polybasic face promotes docking and brings the synaptic vesicle closer to the membrane. Then the C2 domains insert into the plasma membrane or into both the synaptic vesicle and plasma membrane, reducing the distance between the bilayers to under the length of the C2 domains, 5 nm, or shorter depending on the tilt angle of the C2 domain relative to the bilayer. A single, locked orientation of the C2A and C2B domains does not achieve this task however, as it could not maintain the motion and fluidity that is likely required to accommodate movement of additional regulatory proteins around both bilayer surfaces and in the small aqueous space between the two membranes. This flexibility also likely leads to additional movement and probing of the C2 domains on either membrane to fulfill the other potential roles of Syt1 such as charged lipid sequestration and curvature induction which will also promote fusion[18].

Overall, through a series of CW EPR, power saturation EPR, pulsed-EPR, HSQC-NMR, sedimentation assays and other techniques this chapter sought to explore vesicular (*cis*) and plasma membrane binding (*trans*) of Syt1 under various physiologically relevant lipid, salt, and ion compositions, including ATP to determine if Syt1 may act as a distance regulator between the vesicle and plasma membranes for SNARE-dependent fusion. Based on these investigations, we propose a model for Synaptotagmin-1 as the distance regulator in neuronal exocytosis.

In this model, preceding docking and priming, Syt1's juxta-membrane linker is flexible and tethered to the synaptic vesicle. This linker can stretch allowing the C2B domain to reach to

the plasma membrane. On the membrane the C2B domain's polybasic face can form charged electrostatic contacts with PIP_2 on the surface. This occurs before calcium influx which would help promote docking and priming. This process brings the synaptic and plasma membrane bilayers close together and could be regulated by ATP concentrations in the cell. Once Syt1 is close to the two bilayers the C2A domain will have the option of binding to either bilayer, but will prefer to go to PS clusters. This PS coordination is more likely to occur on the synaptic vesicle surface based on ATP measurements and characteristic binding data. Upon calcium influx, the domains will either both insert into the plasma membrane or C2A on the synaptic membrane and C2B on the plasma membrane, with C2B likely contacting the synaptic vesicle with its arginine apex. This insertion permits any lipid sequestration, curvature induction, and bilayer deformation to occur, deforming the membrane, promoting stalk formation, and overall lowering the energy barrier for SNARE-dependent fusion. All of these lipid-based alterations will in turn effect the SNARE complex and potentially other regulatory proteins in the system, by changing surface charges and packing on the membrane. One way it could do this would be isolating and moving the charge that holds syntaxin to the membrane. This series of events has the added benefit that it has brought the SNARE complex into proximity to undergo additional zippering. The heterogeneity also opens the possibility that Syt1 can not only move to either accommodate space for the other proteins in this very concentrated region but could also form additional occasional direct contacts or alter the membrane in different ways depending on what is needed in each particular situation (*Figure 6.22*).

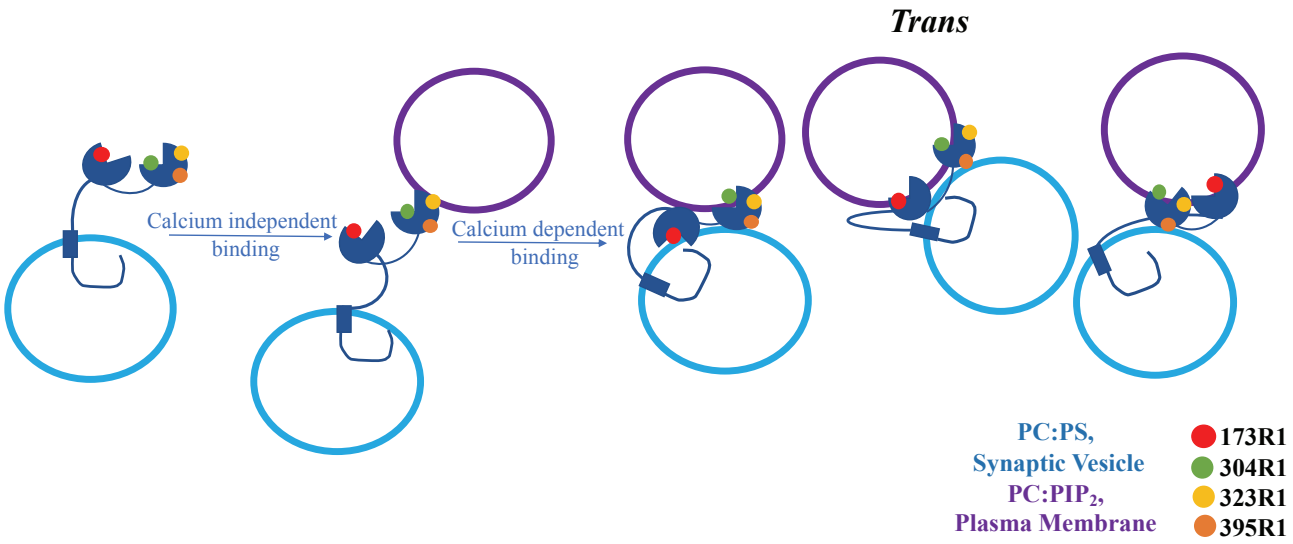

Figure 6.22: Syt1 as the Distance Regulator in Synchronous Neuronal Exocytosis. Shown far left is Syt1before docking and priming of the tethered synaptic vesicle in the active zone. In the active zone, the C2B domain polybasic face overcomes ATP interference and forms a calcium-independent binding contact with PIP_2 on the plasma membrane. Upon calcium influx, the C2B domain's calcium binding loops insert into the plasma membrane at an angle to accommodate polybasic face contact with PIP_2. The arginine apex likely then forms a contact point with lipid in the synaptic vesicle. In the presence of calcium, the C2A domain will in insert into charged PS clusters on either surface, represented here in 3 orientations either on the synaptic vesicle surface or to the left or right of the C2B domain relative to the juxta-membrane linker. This would accommodate the heterogeneity in DEER measurements and occasional contacts the C2B domain will make with the juxta-membrane linker.

6.3.2 Future Work

Future Work on this project is to combine information gained from the various CW EPR, power saturation, and DEER measurements with FLIC microscopy to produce restraints which can be used within XPLOR-NIH to model the distance regulation of FL SYT under varied lipid and ion conditions. This future work would be in collaboration with Volker Kiessling in the Tamm Lab and David Nyenhuis in the Cafiso lab. As mentioned in the methods, FLIC measurements can localize a fluorophore labels position in the Z-axis relative to the *cis* supported bilayer. This is a

powerful technique in combination with power saturation, as power saturation measures into the bilayer and in proximity (then error increases as samples become more aqueous) and FLIC measures best away from the bilayer but not in close proximity (too close to the bilayer the fluorophore is dark). For these measurements, depending on experimental setup, FL SYT can be reconstituted onto the *cis,* synaptic vesicle mimicking, supported bilayer and then plasma membrane mimicking liposomes can be titrated into the sample to which the C2 domains can bind and tether. Distance measurements away from the *cis* membrane can then localize the domains and the juxta-membrane linker relative to the plane as *trans* binding occurs. The opposite design could also be performed where FL SYT is reconstituted into proteoliposomes which mimic the synaptic vesicle and the supported bilayer mimics the plasma membrane. Then proteoliposomes are added in to detect calcium-independent docking (under varied ion conditions) and any changes in distance upon calcium addition throughout the FL SYT protein.

Work toward this goal is already in progress, ~28 FL SYT and ΔC2B sites have been grown, purified, and fluorophore labeled for use in FLIC, which is already underway. The labels selected for FLIC will attempt to localize the C2 domains and the linker regions in the Z-axis relative to the bilayer surfaces. Labels were placed on the juxta-membrane linker, the 8-residue linker between the C2 domain and then three labels per C2 domain determine orientations of the domains. FLIC, however, cannot detect labels in close proximity to the *cis* bilayer surface, as when the label is too close to the surface it will not fluoresce. Fortunately, any dark label will still represent proximity or in the case of the C2 domain, *cis* binding, or indicate that the juxta-membrane linker is contacting the surface. Here, power saturation measurements for site 86R1, 90R1 and 95R1 can localize the juxta-membrane linker's transition out of the *cis* bilayer. Power saturation at sites 173R1 and 304R1 can also be used when the domains are inserted into the *cis*

membrane and orient the C2B domain onto the *trans* membrane (from soluble measurements). Additional measurements will be taken in the future in collaboration with an undergraduate student in Cafiso lab, Nakul Karandikar, to add additional restraints to determine the proximity and orientation of the arginine apex relative to differing membrane conditions. These measurements in combination with the DEER restraints (including many null restraints throughout the linker and actual distance distributions between the C2 domains) will attempt to localize the protein in 3D space and produce a model of Syt1 function.

With this collection of data from various techniques, information and insight toward local changes within the juxta-membrane linker and the C2 domains that likely contributes to distance regulation will be modeled to better understand and visualize subtle changes during Syt1 function. An initial model will show any changes in Syt1 orientation before and after calcium influx, to show how docking and priming may promote distance regulation. Next, poly-valent ions and lipid compositions (heads and tails) can be varied to examine how *cis* and *trans* binding/Syt1 distance regulation is promoted or regulated by the environment under different physiological conditions.

6.4 References

1. Jahn and Fasshauer. (2012). Molecular Machines governing exocytosis of synaptic vesicles. *Nature.* **490:** 201-207.
2. Sudhof and Rizo. (2011). Synaptic Vesicle Exocytosis. *Cold Spring Harb Perspect Biol 2011;3:a005637.*
3. Kuo et al. (2010). The calcium-dependent and calcium-independent membrane binding of synaptotagmin 1: 2 modes of C2B binding. *J Mol Bio.* **387:** 284-294.
4. Herrick et al. (2006). Positions of Synaptotagmin 1 and the membrane interface: cooperative interactions of tandem C2 domains. *Biochemistry*. **45:** 9668-9674.
5. Xue et al. (2008). The Janus-faced nature of the C2B domain is fundamental for synaptotagmin-1 function. *NSMB.* **15:** 1160-1168.
6. Wang et al. (2016). Synaptotagmin-1 C2B domain interacts simultaneously with SNAREs and membrane to promote membrane fusion. *eLife.*, eLife 2016;5:e14211.
7. Loewen et al. (2006). C2B polylysine motif of synaptotagmin facilitates a calcium independent stage of synaptic vesicle priming in vivo. *Mol biol. Cell.* **17:** 5211-5266.
8. Ubach et al. (2001). The C2B domains of Synapototagmin 1 is a ca2+-binding module. *Biohem.* **40:** 5854-5860.
9. Wu, Z. & Schulten, K. (2014). Synaptotagmin's Role in Neurotransmitter Release Likely Involves Ca (2+)-induced Conformational Transition. *Biophys J* **107**: 1156-66.
10. Park et al. (2015). Synaptotagmin-1 Binds to PIP2 containing membrane but not to SNAREs at physiological ionic strength. *NSMB.* **22:** 815-823.
11. Morales et al. (2016). Cd2+ as a Ca2+ surrogate in protein-membrane interactions: isostructural but not isofunctional. *J AM Chem Soc.***135:** 12980-12983.
12. Katti et al. (2017). Non-native metal ion reveals the role of electrostatics in synaptotagmin 1-membrane interactions. *Biochem.* **56:**3283-3295.
13. Lin et al. (2014). Control of membrane gaps by Synaptotagmin-Ca2+ measured with a novel membrane distance ruler. *Nature communications.* **5:** doi:10.038/ncomm6859.
14. Yavuz et al. (2018). Arrest of trans-SNARE zippering uncovers loosely and tightly docked intermediates in membrane fusion. *JBC.* **Doi:** 10.1074/jbc.RA118.003313.
15. Vennekate et al. (2012). Cis- and trans- membrane interactions of Synaptotagmin-1. *PNAS.* **109:** 11037-11042.
16. Park Y, et al. (2012). Controlling synaptotagmin activity by electrostatic screening. *Nat Struct Mol Biol.* **19:** 991–997.
17. Perez-Lara et al. (2016) $PtdInsP_2$ and PtdSer Cooperate to Trap Synaptotagmin-1 to the Plasma Membrane in the Presence of Calcium, *Elife*. e15886.
18. Lai et al. (2011). Synaptotagmin 1 modulates lipid acyl chain order in lipid bilayers by demixing phoshatidylserine. *JBC.* **286:** 25291-25300.
19. Li et al. (2009). Molecular Dynamics simulations of pip2 and pip3 in lipid bilayers determination of ring orientation and the effects of surface roughness on a Poisson Boltzmann description. *Biophys J.* **97:** 155-163.
20. Honigann et al. (2012). Phosphatidylinositol 4,5-bisphosphate clusters act as molecular beacons for vesicle recruitment. *NSMB.* **20:** 679-686.
21. Kee and Scheller. (1996). Localization of synaptotagmin-binding domains to syntaxin. *J Neurosci.* **16:** 1975-1981.

22. Li et al. (2006). Phosphatidylinositol bisphosphates as co-activators of Ca2+ binding to C2 domains of Synaptotagmin 1. *JBC.* **281:** 15845-15852.
23. Van den Bogaart et al. (2012). Phosphatidylinositol 4,5-bisphosphate increases Ca2+ affinity of Synaptotagmin-1 by 40-fold. *JBC.* **287:** 16447-16453.
24. Herrick et al. (2009). Solution and Membrane-Bound Conformations of the Tandem C2A and C2B Domains of Synaptotagmin 1: Evidence of Bilayer Bridging. *J. Mol. Bio.* **390:** 913-9.
25. Vrljic et al. (2011). Post translational modifications and lipid binding profile of insect cell expressed full length mammalian synaptotagmin 1. *Biochem.* **50:** 9998-10012.
26. Lu et al. (2014). The Juxtamembrane linker of full length synaptotagmin 1 controls oligomerization and calcium dependent membrane binding. *JBC.* **32:** 22161-22171.
27. Vrljic M, et al. Molecular mechanism of the synaptotagmin-SNARE interaction in Ca2+-triggered vesicle fusion. *Nature structural & molecular biology*. 2010; 17:325–331.
28. Zhou et al. (2017). The primed SNARE-complexin-synaptotagmin complex for neuronal exocytosis. *Nature.* **548:** 420-425.
29. Lai et al. (2011). Synaptotagmin 1 and SNAREs form a complex that is structurally heterogeneous. *J Mol Bio.* **405:** 696-706.
30. Sperlagh and Vizi. (1996). Neuronal Synthesis, storage, and release of ATP. *Seminars in neuroscience.* **8:** 175-186.
31. Rangaraju et al. (2014). Activity Driven local ATP synthesis is required for synaptic function. *Cell.* **156:** 825-835.
32. Risselada et al. (2012). How SNARE molecules mediate membrane fusion: Recent insights from molecular simulations. *Current opinion in structural biology.* **22:** 187-196.
33. Kuo et al. (2011). Phosphatidylinositol 4,5-bisphospate alters synaptotagmin 1 membrane docking and drives opposing bilayer closer together. *Biochemistry.* **50:** 2633-2641.
34. Van den Bogaart et al. (2011). Synaptotagmin-1 may be a distance regulator acting upstream of SNARE nucleation. *NSMB*. **18:** 805-812.
35. Ubach et al. (2001). The C2B domain of Synaptotagmin 1 is a Ca2+ binding module. *Biochemistry.* **40:** 5854-5860.
36. Wang et al. (2014). Calcium sensitive ring-like oligomers forms by synaptotagmin. *PNAS.* **11:** 13996-13971.
37. Zanetti et al. (2016). Ring-like oligomers of Synaptotagmins and related C2 domain proteins. *Elife.* 2016;5:e17262 DOI: 10.7554/eLife.17262
38. Wang et al. (2017). Circular oligomerization is an intrinsic property of synaptotagmin. *Elife.* 2017;6:e27441 doi: 10.7554/eLife.27441
39. Rothman et al. (2017). Hypothesis – buttressed rings assemble, clamp, and release SNAREpins for synaptic transmission. *FEBSPress.* **591:** 10.1002/1873-3468.12874.
40. Rizo J, Chen X, Arac D. Unraveling the mechanisms of synaptotagmin and SNARE function in neurotransmitter release. *Trends in cell biology*. 2006; 16:339–350.
41. Reichardt and Kelly. (1983). A molecular description of the nerve terminal function. *Annu Rev Biochem.* **52:** 871-926.
42. Yang et al. (2016). The role of cholesterol in membrane fusion. *Chemistry of physics and lipids*. **199:** 136-143.
43. Risselada et al. (2012). How SNARE molecules mediate membrane fusion: Recent insights from molecular simulations. *Current opinion in structural biology.* **22:** 187-196.

CHAPTER 7: Significance and Future Directions

7.1 Summary and Significance

This body of work aimed to contribute to the determination of the elusive function of Synaptotagmin-1 as well as neuronal exocytosis as a whole. The chapters presented above aimed to step through an investigation of Sytnaptotagmin-1 as the membrane binding protein and calcium sensor in neuronal exocytosis. Each chapter added complexity to the system, moving from work on the soluble construct to the full-length protein, and then to investigating Synaptotagmin-1's function in increasingly complex, more physiological conditions. Future work should aim to continue to add to the *in vitro* system piece-by-piece in an attempt to understand how each component, whether is it lipid diversity, cholesterol, or added proteins, functions and changes within the system.

The first major aim of this work focused on the interplay and influence of different lipid headgroups on the insertion and orientation of the soluble Syt1 construct, C2AB. For this work EPR CW and power saturation measurements were taken throughout the calcium binding loops of the C2A and C2B domains and areas near the polybasic face. This investigation, in collaboration with work from members in the Cafiso and the Jahn labs (Max Plank Institute for Biophysical Chemistry, Germany) overall used a combination of different structural and functional techniques to identify a synergy between PIP_2 and PS, which cooperate to trap Syt1 to the plasma membrane in the presence of calcium[89].

The second aim of this work focused on the transition to the full-length construct of Syt1 and optimization and characterization of the construct's purification. A series of CW EPR and pulsed-EPR measurements were used to compare the resulting protein from purification in either OG or CHAPs. Overall, this chapter highlights the idea that different purifications can produce different final protein states when reconstituted into membrane[90]. Additional characterization of the CHAPs procedure using CW EPR, power saturation EPR and TIRF, compared to the soluble domains, was then presented as reasoning to proceed with the CHAPs protocol[90].

The third aim of this thesis focused on the driving forces for FL SYT membrane insertion. Experiments on the soluble C2A, C2B, and C2AB constructs, including ultracentrifugation sedimentation assays, were combined with CW and power saturation experiments on the full-length Syt1 to identify the contributions of weak driving forces which promote Syt1-membrane binding. In collaboration with the Igumenova lab (Biochemistry and Biophysics, Texas A&M University) this work highlighted the use of a toxic metal ion, cadmium, and the dual roles of coordination and electrostatics in Syt1 membrane interactions[87].

The fourth aim of this work attempted to examine regulatory roles for the membrane and polyvalent ions in solution for Syt1 function and to propose Syt1's function as a distance regulator. A series of CW EPR, power saturation EPR, pulsed-EPR, HSQC-NMR and other experiments explored vesicular (*cis*) and plasma membrane binding (*trans*) of Syt1. Various physiologically relevant lipid, salt, and ion composition were used to characterize the competition between ATP and PIP_2 binding to the polybasic face and show how that may influence and promote *trans* binding. Charge was then added to both *cis* and *trans* membranes to determine if Syt1's C2A and C2B domains could be identified to bind to either membrane based on lipid headgroup specificity. This headgroup specificity and varied lipid compositions in the plasma membrane when compared

to the vesicle membrane likely play a key role in Syt1 activating fusion by promoting Syt1 function potentially as a distance regulator between the vesicle and plasma membranes to promote SNARE-dependent fusion.

All of these aims contribute to the work to determine how Syt1 functions as the calcium sensor and trigger in neuronal exocytosis and how this influences all of the other regulatory and fusion machinery in the system. This work also aims to highlight that the membrane itself is a key contributor to fusion and exocytosis. If the complex system can be dissected to gain full understanding, then not only will it become clearer how the body and brain communicates, but also it will become evident what is occurring on the molecular level when the nervous system misfunctions, which triggers a wide array of diseases and pain, all of which are currently poorly understood.

7.2 Additional Future Directions

7.2.1 The Cholesterol Effect

As mentioned in Chapter 6, the addition of cholesterol affects the ability of FL SYT to bind to *trans* membranes and has minor effects on the state of the protein's juxta-membrane linker. However, the cause for this cholesterol effect is still unclear. Additional work using the soluble C2AB domains of Syt1 also demonstrates a cholesterol dependent shift in binding affinity to charged lipid membranes (*Figure 7.1*). Here, only the C2B domain is sensitive to cholesterol addition. Future work to attempt to determine how cholesterol alters the state of the protein and

influences membrane insertion would provide insight for how cholesterol and its frequently changing concentrations on both the plasma and synaptic membranes throughout exocytosis may contribute to the neuronal system. Localizing this effect to a location on Syt1 could also lead to a better understanding of Syt1 membrane interactions.

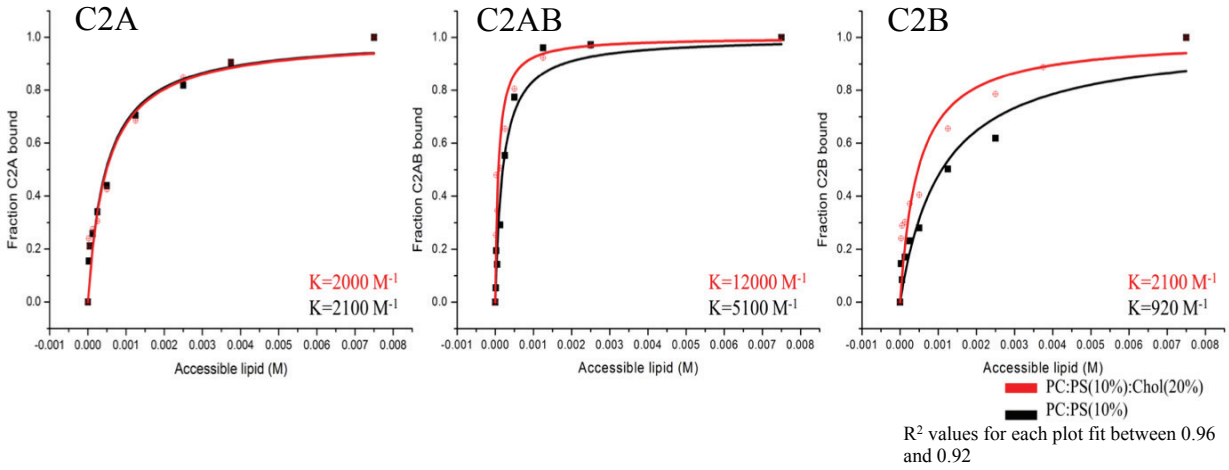

Figure 7.1: Presence of cholesterol enhances the binding affinity of the C2B domain to charged membrane. Left: Vesicle sedimentation assay of the C2A domain alone in either PC:PS (10%) or PC:PS:Chol (10:20) in the presence of calcium using intrinsic tryptophan fluorescence. Binding affinity of the C2A domain to membrane is not altered upon addition of cholesterol Middle: the C2AB construct under the same conditions displays a slight increase in affinity in the presence of cholesterol. Right: The C2B domain alone shows a significant increase in binding affinity in the presence of cholesterol.

7.2.2 The Arginine Apex

The arginine apex, much like the calcium binding loops, has been identified as a contact point for the C2B domain with the membrane. This to some degree has been characterized in the soluble domain, but no work has been performed on the full-length construct or under varying lipid conditions to determine if this region may influence the C2B domains preference to bind *cis* to the synaptic vesicle or *trans* to the plasma membrane. CW and Power saturation measurements could also determine if in the full length construct the arginine apex contributes to distance regulation

(*Figure 7.2*). Power saturation measurements could also be used as additional restraints for modeling the full-length protein, as previously mentioned in the future directions in Chapter 6. Work is in progress for generating cysteine mutations to examine locations around the arginine apex, including 285C, 349C, and 350C. A stepwise neutralization of the arginine apex (R398R399, R398QR399, R398QR399Q) will also attempt to better highlight its affinity and binding relative to the membrane.

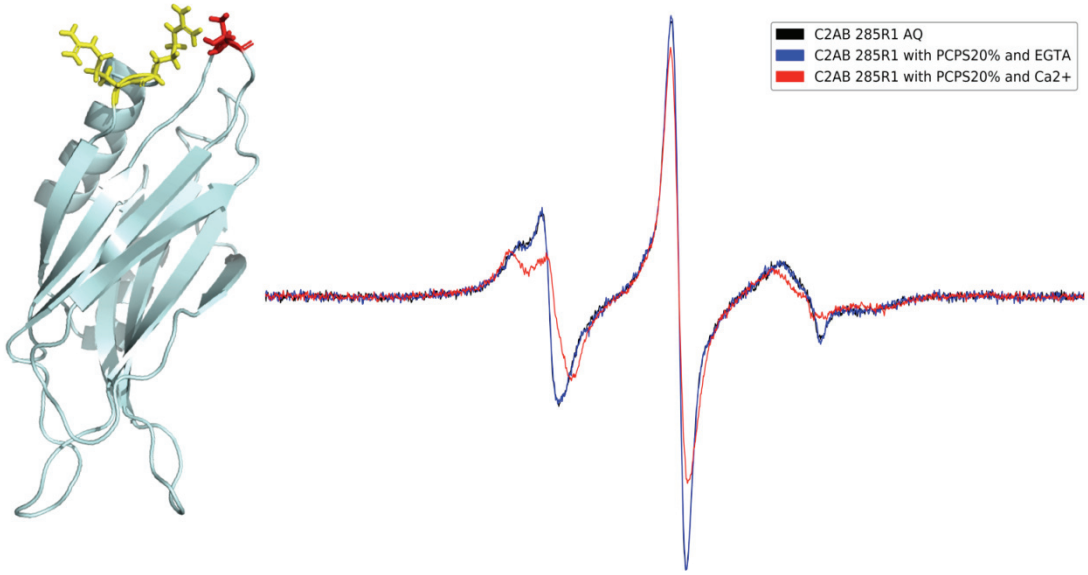

Figure 7.2: Representative CW EPR Spectra for the Arginine Apex. Calcium addition influences the state of the arginine apex in the presence of PC:PS (25%), highlighted by a shifting lineshape in the low-field line due to the spin-label experiencing different polarity within its environment. This investigation will move to the full-length protein using CW and power saturation to determine the proximity of the arginine apex to both a plasma membrane mimicking membrane and a synaptic vesicle mimic. Sites will be probed at 349, 350, and 285 with a progressive knockout of the arginine apex, R398R399, R398QR399, R398QR399Q. These restraints will add to the modeling of FL SYT mentioned in the future directions of Chapter 6.

7.2.3 Lipid Tails Influence on Syt1 Binding Affinity

A body of work with the Tamm lab, has identified a lipid tail saturation and ordering dependence for calcium/Syt1-triggered exocytosis[1]. This investigation couples the function of the SNARE complex with effects caused by Synaptotagmin-1 binding and through changes which occur within the membrane. Preliminary work beyond the paper used a set of vesicle sedimentation assays to examine lipid specific binding, here not of the lipid headgroups, but of the acyl chain composition. The acyl chains within the neuronal system are a diverse set of lengths and saturations which may affect membrane binding. Here, this work highlighted large differences in Syt1 binding to varying saturation acyl chains and ordering, which demonstrates a potential preference for Syt1 calcium binding loop insertion into more disordered membranes. These preliminary measurements were limited by the protein concentrations required for detection using intrinsic tryptophan emission, which were too high relative to the lipid concentrations to properly fit to binding curves. Future work to investigate this observation in more detail should occur. First, measurements using fluorescent tags will be used to achieve lower protein concentrations to perform these measurements, and then in the future potentially more sophisticated measurements will be taken to investigate this effect in more detail.

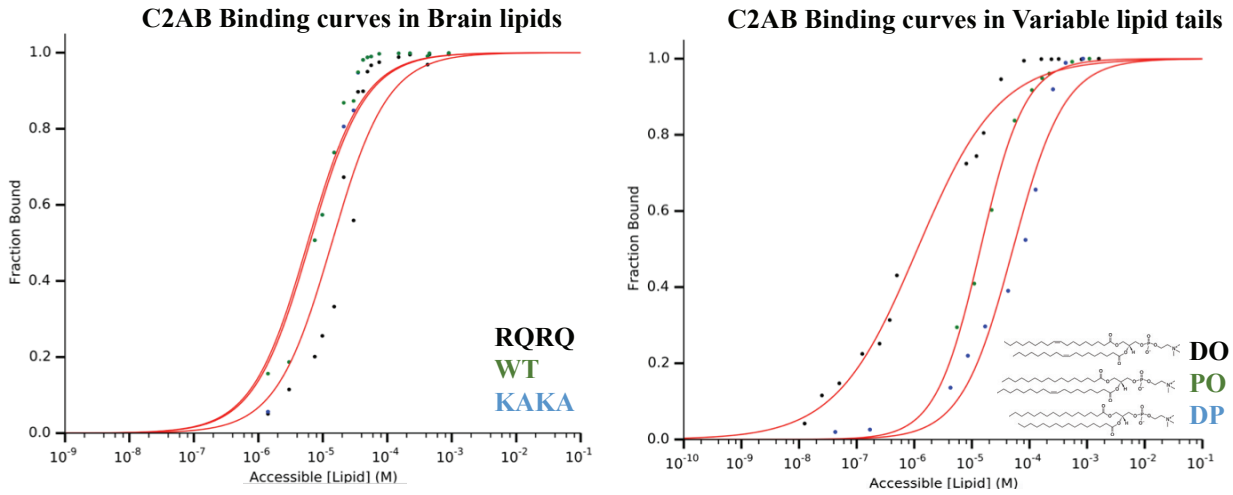

Figure 7.3: Lipid tail composition and saturation affect Syt1 binding affinity. Left: Vesicle sedimentation assay of the C2AB construct in a mixture of brain lipids mimicking the plasma membrane: PC:Chol:PE:PS:PIP_2 (34:20:30:15:1) in the presence of calcium using intrinsic tryptophan fluorescence. Mutants abolishing the function of the polybasic face: K326AK327A, and Arginine Apex: R398QR399Q are shown and binding affinity shifts from:C2AB WT in Brain PM Mix where the value of K is: $1.358 \times 10^5\ M^{-1}$, C2AB RQRQ in Brain PM Mix where the value of K is: $1.285 \times 10^5\ M^{-1}$, to C2AB KAKA in Brain PM Mix where the value of K is: $5.747 \times 10^4\ M^{-1}$. Right: Vesicle sedimentation assay of the C2AB construct in a mixture of varying lipids tail saturations mimicking the plasma membrane: PC:Chol:PE:PS:PIP_2 in the presence of calcium using intrinsic tryptophan fluorescence. *16:0/18:1* PO (1-palmitoyl-2-oleyol), *di-18:1* DO (1,2-dioleoyl), (Brain left), and *di-16:0* DP (1,2-dipalmitoyl) were used which show a decrease in affinity as lipid tail saturation changes from: C2AB WT DO PM Mix where the value of K is: $8.811 \times 10^5\ M^{-1}$, C2AB WT PO PM Mix where the value of K is: $7.131 \times 10^4\ M^{-1}$, to C2AB WT DP PM Mix where the value of K is: $1.943 \times 10^4\ M^{-1}$.

7.3 References

1. Kiessling et al. (2018). A molecular mechanism for calcium/synaptotagmin-triggered exocytosis. *NSMB*. Accepted, but not yet published.